8-2016

INVESTIGATING THE ROLES OF ΔNP63 AS A SUPPRESSOR OF MIGRATION, INVASION, AND METASTASIS

Ramon E. Flores Gonzalez

INVESTIGATING THE ROLES OF ΔNP63 AS A SUPPRESSOR OF MIGRATION, INVASION, AND METASTASIS

By

Ramón Edgardo Flores González, M.D.

APPROVED:

_____
Elsa R. Flores, Ph.D.
Advisory Professor

_____
Don L. Gibbons, M.D., Ph.D.

_____
Sendurai Mani, Ph.D.

_____
Kenneth Y. Tsai, M.D., Ph.D.

_____
Jeffrey Rosen, Ph.D.

APPROVED:

_____
Dean, The University of Texas
Graduate School of Biomedical Sciences at Houston

INVESTIGATING THE ROLES OF ΔNP63 AS A SUPPRESSOR OF MIGRATION, INVASION, AND METASTASIS

A

DISSERTATION

Presented to the Faculty of

The University of Texas

Health Science Center at Houston

and

The University of Texas

MD Anderson Cancer Center

Graduate School of Biomedical Sciences

in Partial Fulfillment

of the Requirements

for the Degree of

DOCTOR OF PHILOSOPHY

By

Ramón Edgardo Flores González, M.D.

Houston, Texas

August, 2016

Dedication

To my family, who I can always count on and have always encouraged a sense of wonder in me.

Acknowledgments

First of all, I would like to thank my family, for giving me their unconditional love and support. I also would like to thank my girlfriend, Claritsa Santos Malavé, the love of my life, who has been instrumental in helping get through the final hurdles of completing my Ph.D. I would also like to thank all my friends who made the task of moving to Houston and pursuing a Ph.D. much easier.

I would like to thank my mentor Dr. Elsa R. Flores, for giving me the opportunity to work in her laboratory and for her guidance and support throughout my Ph.D. career.

I would like to thank committee members: Dr. Jeffrey Rosen for his feedback regarding the mammary gland project, Dr. Kenneth Y. Tsai, for his help and feedback with the wound healing model, and Dr. Sendurai Mani and Dr. Don L. Gibbons for their feedback throughout these five years of research.

I would like to thank other members of the Flores Lab, particularly Dr. Marco Napoli for his mentoring all his help with the mammary gland project, Ngoc Bui for her help with staining for the wound healing experiment characterization, Brooke Meyers for tissue culture support, Kunal Jain for helping me manage my mouse colony, and Dr. Hussein Abbas for his help with the bioinformatics analysis.

Finally I would like to thank my other collaborators: Dr. Christian Coarfa for additional bioinformatics support, Dr. Kevin Roarty and Yang “Daisy” Lu from the Rosen lab for all their help with troubleshooting mammary protocols and for teaching me everything I know regarding mammary mouse surgeries, and Jodie Polan for microscopy support.

Investigating the Roles of ΔNp63 as a Suppressor of Migration, Invasion and Metastasis

By

Ramón Edgardo Flores González

Supervised by

Elsa R. Flores, Ph.D.

Abstract

Cancer is one of the leading causes of death and disease in the world. Considerable resources are spent to study and understand cancer, with the hope of developing new treatments and eventually cures that will help millions of people. Efforts to understand cancer are hindered by its inherent complexity and instability. Nonetheless, understanding the basics of tumor development and progression are the key to focused on studying the role of ΔNp63 in cancer, a p53 family member known to be involved in epithelial development, microRNA biogenesis, and stem cell maintenance. Using the strength of *in vivo* mouse models, we found that ΔNp63 is capable of modulating tumor development by regulating the epithelial mesenchymal transition. ΔNp63 does this through its role regulating microRNAs, in this case, miR-98 and miR-34a, which in turn regulate known EMT transcription factors Twist1 and Lef1. Alterations of ΔNp63 led to the development of various tumor types, among them mammary adenocarcinomas that were aggressive and highly metastatic. Focusing on this tumor type, we investigated ΔNp63's role regulating mammary gland development. We found a striking phenotype where ΔNp63 loss led to increased proliferation in mammary epithelial cells but stunted gland growth and promoted structural disorganization. We complemented these findings with sequencing results; where we were able to identify several pathways such as EMT, cell polarity, ER signaling, and IGF signaling

that are also altered upon ΔNp63 loss and could potentially explain both of the developmental and tumor phenotypes observed. In the end, shed light on the role of ΔNp63 as a modulator of cancer progression and on the pathways through which it could be doing this function. This information could potentially be used to identify novel targets and develop novel targeted cancer therapies that would greatly improve the lives of patients.

Table of Contents

List of Figures

List of Tables

Chapter 1

Chapter 1: Introduction

Cancer remains one of the leading causes of death and disability around the world. In the United States cancer is the second leading cause of death and it is estimated that there will be around 1,600,000 new cases and 600,000 deaths due to cancer in 2016 alone (1). Most of the burden of cancer is due to its spread throughout the body, a process called metastasis. In metastasis, cells from the original primary tumor invade through adjacent tissues, get into the circulation, and travel to seed distant organs (2, 3). Metastasis can cause a variety of problems in patients ranging from metabolic deficiencies and cognitive difficulties to organ failure depending on the sites where the tumors were seeded. It is because of this burden and the many deleterious effects of cancer in our society that considerable efforts have been done to understand it and to develop ways to manage, treat and eventually cure it.

In the decades that have passed since cancer was first described, our understanding of the disease has come a long way. Cancer can present in many forms and be caused by environmental factors, familial susceptibility, or occur spontaneously but they all have one common element: genomic instability. It is the intrinsic instability of tumor cells that drives their continued mutation and provides tumors their characteristic properties of uncontrolled growth, immune system evasion, metabolic reprograming, invasion of adjacent tissues, and spread to distant organs (4, 5). It is this genomic instability as well that has made it difficult to discover the key to treating and curing cancer. Cancer research has been focused on understanding the mechanisms and ramifications of genomic instability, the physiologic mechanisms that our cells have to deal with it, and how these mechanisms become altered leading to tumorigenesis.

The processes of cell division and DNA replication have many instances where mutations can occur. Normally there are proofreading mechanisms, cell cycle checkpoints, and DNA repair mechanisms that look for mistakes in DNA replication that could lead to

harmful mutations and either repair the damage or program cell death if the damage is to severe. One of the most important molecules in these repair pathways is p53. Often called the guardian of the genome, p53 is a transcription factor that plays an essential role as a tumor suppressor in many pathways such as senescence and apoptosis among others that protect cells from the harmful effects of mutations. It is no wonder that in many cancers, inactivation of p53 through mutations, silencing, or other methods is one of the initial insults that start the tumorigenic cascade.

Research in the p53 field has shed light in its many functions as a protector from cancer although this has not translated into new therapeutic modalities due to the physiological importance of tight p53 regulation. Systemic activation of p53 can lead to unforeseen side effects that can potentially cause the patients more harm than good. This is why focus has shifted into studying other molecules such as p53 binding partners, downstream effectors, and other p53 family members in order to be able to develop more nuanced, targeted therapies that only alter the p53 functions that have lead to a specific tumor while leaving the p53 physiologic function in the remaining normal tissues untouched. Our lab focuses on studying the p53 family members p63 and p73 with the ultimate goal of developing novel therapies to treat cancer.

p63 and p73 are transcription factors that share structural homology with p53 mainly in their DNA binding domain (6). Although similar, the differences in the structure allow p63 and p73 to regulate expression of their own sets of genes, as well as share some targets with p53 (7). To complicate matters further, both p63 and p73 have two different isoform families that arise from separate promoters: The TA isoforms, which contain a transactivation domain and the ΔN isoforms, which have a truncated transactivation domain. Both sets of isoform families have distinct functions and targets. Our lab has been one of the pioneers characterizing the different roles of the TA and ΔN isoform subfamilies, and the

interactions and cross talk between TA and ΔN p63 and p73 isoforms and p53. My focus has been particularly in understanding the roles of the ΔNp63 subfamily.

In normal tissues, p63 plays important roles in, stem cell maintenance, cell differentiation, and microRNA biogenesis, among others (6, 8-15). TAp63 is essential for the maintenance of the stem cell compartments in the skin and regulates cellular aging, cellular energetics, and the processing of precursor microRNAs into mature microRNAs through regulation of Dicer (9-12). ΔNp63 on the other hand, is expressed in the basal layer of the skin and regulates differentiation into more specialized cell types. It is also involved in microRNA processing by regulating DGCR8, which is part of the enzyme complex that processes the primary transcript into the characteristic stem loop structure of the precursor microRNAs. In most tissues, ΔNp63 is the dominant isoform and also functions as a dominant negative by suppressing TAp63 and even p53.

Besides their physiological roles, both TAp63 and ΔNp63 have been found to be involved in the tumorigenesis process (9, 13-19). TAp63 is commonly thought of as a tumor suppressor similar to p53 and has been found to suppress metastasis through Dicer regulation, regulate adult stem cells and aging, and regulate cellular energetics and metabolism. The picture for ΔNp63 on the other hand is more complex. ΔNp63 is used as a marker for epithelial tumors such as mammary adenocarcinoma and lung adenocarcinoma. This is due to its expression in the putative cells of origin for these tumor types. Beyond its use as a biomarker, some studies have found that ΔNp63 can exhibit both oncogenic and tumor suppressive functions (6, 13, 15-19). It appears that its function is context and tissue dependent, and perhaps even varies throughout different stages of the tumorigenic and metastatic cascades. Recently, ΔNp63 has been found to regulate multipotency (8), which could have implications in its role in cancer stem cells. Loss of ΔNp63 has also been associated with increased invasion and migration and with stimulation of an epithelial mesenchymal transition (EMT) *in vitro* (16-18, 20). Other studies have found that ΔNp63 can

promote tumor growth by inactivating TAp63, TAp73, and p53, at least in some tissues (13). Some of the conflicting evidence regarding the role of ΔNp63 in cancer is due to lack of knowledge regarding its physiologic role in many tissues. Loss of ΔNp63 in the embryonic stage results in craniofacial abnormalities, limb agenesis, and problems with development of the epidermal skin layer, which ultimately results in newborn pups dying within a day after birth (8). Because of this, a conditional knockout mouse model is necessary to study the physiologic roles of ΔNp63 in its biological context beyond the first day of life. In our lab we generated this model and have used it to better understand both the physiologic and pathologic functions of ΔNp63.

The purpose of this project was to use our available mouse models to better understand the role of ΔNp63 in tumorigenesis. My hypothesis was that ΔNp63 can function as a tumor and metastasis suppressor through microRNA mediated regulation of migration, invasion, and transition into a mesenchymal phenotype. We also wished to corroborate whether the functions and mechanisms found to be regulated by ΔNp63 in previously published and our own *in vitro* data held up with the added complexity of a complete biological organism. To test this hypothesis, we used ΔNp63 knockout ($\Delta Np63^{-/-}$) mice, ΔNp63 heterozygous ($\Delta Np63^{+/-}$) mice, and ΔNp63 conditional knockout mice generated in our lab. The project was divided into three parts. First, enhance our basic understanding of the role of ΔNp63 in tumor development and metastasis. For this part, we used $\Delta Np63^{+/-}$ mice crossed to mice with various p53 status backgrounds and compared their tumor spectrum and characteristics. We discovered that $\Delta Np63^{+/-}$ status shifted the tumor spectrum and promoted aggressive metastatic tumors in these mice, which suggested that it might function as a tumor suppressor in some tissues. Second, elucidate the molecular mechanisms through which ΔNp63 exerts is functions in tumorigenesis and metastasis within an *in vivo* system. To this end we used ΔNp63 conditional knockout mice and a wound-healing assay as a surrogate for some of the processes involved in cancer and

metastasis. Using this system we discovered that ΔNp63 loss promotes a mesenchymal phenotype and its absence seems to prevent a full transition back into an epithelial phenotype, which suggests that ΔNp63 is an essential regulator of the epithelial mesenchymal transition. We also found evidence that ΔNp63 exerts this role through its regulation of specific microRNAs. And finally, combine the first and second parts together to understand the role of ΔNp63 in a specific tumor type. For this part, we chose to focus on breast cancer since it is a cause of significant morbidity and death every year. To fully understand the role of ΔNp63 in breast cancer it was necessary to study its role in normal mammary gland development and function. We used ΔNp63 conditional mouse models combined with transplantation procedures for this final part of the project. We also sequenced RNA and microRNA from primary mammary epithelial cells to obtain a broad, unbiased picture of how ΔNp63 loss affects overall gene and microRNA expression in the mammary gland. Together, these techniques gave us an idea of the essential pathways regulated by ΔNp63 in the developing mammary gland and how their potential alterations can lead to cancer.

In the end, this project managed to shed light on the physiologic and pathologic functions of p63 within the context of an *in vivo* system. The results of these studies will be detailed in the upcoming chapters.

Chapter 2

Chapter 2: Materials and Methods

2.1 Mouse genotypes

Table 1. Information for mice used in various experiments

Genotype	Description	Uses
$\Delta Np63^{+/-}$	ΔNp63 heterozygous mice	Used to generate $\Delta Np63^{-/-}$ primary mouse keratinocytes Used for tumor studies
$\Delta Np63^{+/-}$, $p53^{-/-}$	ΔNp63 heterozygous, p53 knockout mice	Used for tumor studies
$\Delta Np63^{+/-}$, $p53^{+/-}$	ΔNp63 and p53 double heterozygous mice	Used for tumor studies
$p53^{-/-}$	p53 knockout mice	Used for tumor studies
$p53^{+/-}$	p53 heterozygous mice	Used for tumor studies
$TAp63^{-/-}$	TAp63 knockout mice	Used to generate $TAp63^{-/-}$ keratinocytes
$\Delta Np63^{fl/fl}$, $Rosa^{M/M}$, $K14^{Cre\ ER+}$	ΔNp63 conditional knockout, Rosa mTmG fluorescent reporter mice with Tamoxifen inducible Cre under the control of the K14 promoter	Used for the *in vivo* wound healing experiment
$\Delta Np63^{fl/fl}$, $Rosa^{M/M}$	ΔNp63 conditional knockout, Rosa mTmG fluorescent reporter mice	Used to isolate Mammary Epithelial Cells for mammary gland transplantations, RNA and miRNA sequencing, validation and 3D culture experiments Used for Adenoviral Cre Intraductal Injections
$\Delta Np63^{fl/fl}$, $BRCA1^{fl/fl}$ $Rosa^{M/M}$	ΔNp63 conditional knockout, BRCA1 conditional knockout, Rosa mTmG reporter mice	Used for Adenoviral Cre Intraductal Injections
$TAp63^{fl/fl}$, $Rosa^{M/M}$	TAp63 conditional knockout, Rosa mTmG fluorescent reporter mice	Used for Adenoviral Cre Intraductal Injections
$TAp63^{fl/fl}$, $BRCA1^{fl/fl}$, $Rosa^{M/M}$	TAp63 conditional knockout, BRCA1 conditional knockout, Rosa mTmG fluorescent reporter mice	Used for Adenoviral Cre Intraductal Injections
$BRCA1^{fl/fl}$, $Rosa^{M/M}$	BRCA1 conditional knockout, Rosa mTmG fluorescent reporter mice	Used for Adenoviral Cre Intraductal Injections

2.2 Mouse husbandry and tumor analysis

Mice heterozygous for ΔNp63 isoforms ($\Delta Np63^{+/-}$) with intact TAp63 isoforms in a C57BL/6 background were generated as previously detailed (Chakravarti, *et. al.*, 2014). A subset of these mice was crossed with $p53^{-/-}$ or $p53^{+/-}$ for the tumor study. Mice were aged until moribund for up to 24 months. Distressed or visibly sick mice were euthanized by asphyxiation using carbon dioxide and subsequent cervical dislocation following IACUC guidelines. Necropsies were performed and soft tissues were kept in 10% neutral buffered formalin overnight and then switched to 70% ethanol, while bones were placed in Bouin's fixative solution for 3 weeks and then switched to ddH_2O. Tissues were then submitted to the MD Anderson Cancer Center Research Histology Core Laboratory for processing and embeddeding in paraffin blocks. The blocks were then sectioned onto slides. Slides were stained with hematoxylin and eosin at the core and histopathological analysis was performed for each tissue.

2.3 Primary mouse keratinocyte isolation

To obtain primary mouse keratinocytes, we set up crosses using $TAp63^{-/-}$ mice, $\Delta Np63^{+/-}$ mice and wild type mice. All the crosses were set up between the same genotypes. To time the gestation period, the females were monitored the morning after set up (no more than15 hours after setting up the cross) for the presence of plugs that suggested that copulation had taken place. Embryos were harvested at the 18.5-day of gestation. Epidermal cells were isolated from skin of embryos at day 18.5 by treatment with Dispase II (Roche) as previously detailed (Su *et. al.*, 2009). Each pregnant female was euthanized using carbon dioxide asphyxiation and cervical dislocation. Their abdominal cavity was opened and the uterus taken out, placed on a 10 cm dish with PBS, and transferred to the sterile tissue culture hood. Then the uterus was opened and the individual embryos were

taken out. The head, tail and four limbs for each embryo were removed and the skin was peeled off from the remaining torso using sterile forceps. The skin was then placed in Dispase II in a culture tube and placed on the 4°C refrigerator for 16 hours. The cut tails of the pups were stored at -20°C for confirmatory genotyping. After the overnight incubation, the separated epidermis was minced using straight blades and incubated at 37°C in 0.25% trypsin/EDTA (Corning) for 20 minutes. Cells were plated on collagen-coated flasks (50 µg/ml) collagen type I (BD Biosciences) in defined K-SFM medium (GIBCO). After the cultures reached 70% confluence in about 5 days, the cells were passaged into new flasks. Once the secondary passage cells reached 70% confluence, they were frozen down in media with 10% DMSO (Corning) and stored in liquid nitrogen until needed. Keratinocytes were isolated from wild type, $\Delta Np63^{-/-}$, and $TAp63^{-/-}$ mice.

2.4 *In vitro* scratch assay

Primary mouse keratinocytes were plated on 6 well plates on top of J2 3T3 feeder cells. Once the keratinocyte colonies were big enough any remaining feeders were removed using 0.02% EDTA before starting the assay. Using a 200µl sterile pipette tip, a scratch was made through the colony and the progress of the gap closure was monitored over a 24-hour period using time-lapse microscopy. Time-lapse images were taken every 10 min. For the analysis, individual cells were followed using the time-lapse images and their path lengths were quantified and compared.

2.5 *In vitro* Boyden Chamber assay

Primary murine keratinocytes harvested as previously detailed were resuspended in 500 µl of F media (8) with 2% FBS (3×10^4 cells/insert) and added to the top of each chamber

containing BD BioCoat cell culture inserts (354578; BD Biosciences) or Matrigel Invasion Chamber (354480; BD Biosciences). 750 µl of media with 20% FBS was added to the bottom chamber. The cells were fixed and stained with Diff-Quik kit (Siemens). Non-invasive cells were removed from the upper chamber using a cotton swab. The remaining cells were counted with a Zeiss AxioObserver A1 inverted microscope.

2.6 *In vivo* wound healing assay

ΔNp63 conditional knockout mice ($\Delta Np63^{fl/fl}$) were crossed to $Rosa^{M/M}$ mice, and $K14^{CreER+}$ mice to generate the $\Delta Np63^{fl/fl}$, $Rosa^{M/M}$, $K14^{CreER+}$ mice used for the in vivo wound healing studies. 15 mice per condition were used, for a total of 30 mice. Mice were anesthetized using inhaled isoflurane. The backs of the mice were shaved and treated with Nair for of 90 seconds the day before starting the experiment. Proper rinsing of the Nair under running water and application for no more than 90 seconds are essential to prevent burn wounds that would affect the experiment. On Day 1, a 1 cm wound constrained to the epidermis was made using DXB compound. DXB is a detergent compound that selectively dissolves the epidermis. To induce the wound, a vacuum seal was created in the shaved mouse back using a plastic seal chamber. The skin rises inside the chamber when a proper seal is established. A proper seal is required to prevent leakage of DXB solution beyond the intended wound site. Once a seal was established, 250 µl of DXB solution were added and the area was sheared using an electric drill file for 40 seconds. After 40 seconds, the solution with the sheared cells was removed and the area cleaned. 200 µl of Tamoxifen (100mg/mL in 100% Ethanol) was applied topically using a cotton swab for three consecutive days following wound induction to induce recombination in the experimental mice. For the control mice, an equivalent volume of 100% Ethanol was applied instead. Up to three mice were housed together, and subsets were euthanized at days 1, 4, and 8 after

induction, Three at day 1 for each group, and 6 at days 4 and 8 for each group. One half of the epithelium was fixed in 10% formalin and the other frozen in OCT medium (Tissue Tek). Frozen sections were used to assess recombination status. Formalin fixed sections were embedded in paraffin and sectioned onto slides by the MD Anderson Cancer Center Research Histology Core Laboratory. Slides were stained with hematoxylin and eosin and the wound sizes were measured and analyzed. To measure the wound size, the hematoxylin and eosin stained sections were measured using the Olympus IX83, 10x objective, and the CellSense software. Unstained slides were used for immunofluorescence and immunohistochemical analysis.

2.7 Immunohistochemistry

Paraffin embedded tissue sections were prepared as previously described (7). Sections were incubated with anti-ΔNp63 (619002, Biolegend, 1:1000), Twist1 (sc-81417, Santa Cruz, 1:100), or Lef1 (2230S, Cell Signaling, 1:200) antibodies overnight at 4°C in a humid chamber followed by incubation with horseradish peroxidase conjugated-secondary antibody in the ImmPRESS kit (Vector lab) for 45 minutes at room temperature, then followed by the DAB kit (Vector lab). Images were taken using the Olympus IX83 microscope, using objectives 10x and 40x)

2.8 Immunofluorescence

Paraffin embedded tissue sections were prepared as previously described (7). Sections were incubated with anti-GFP (ab13970, Abcam, 1:1000), Ki67 (ab15580, Abcam, 1:250), Cytokeratin 5 (ab53121, Abcam, 1:500), E-Cadherin (ab76319, Abcam, 1:200), Vimentin (ab92547, Abcam, 1:200) Aquaporin 5 (178615, Calbiochem, 1:100), , Cytokeratin 14 (LS-C22637, LifeSpan Biosciences, 1:500), Sox9 (Ab5535, Millipore, 1:100), Slug (SC-

10437, Santa Cruz, 1:100), Laminin (L9393, Sigma, 1:125), Cytokeratin 18 (Sigma, SAB4501665, 1:200), Smooth Muscle Actin (SMA) (A2547, Sigma, 1:250), and RFP (600-401-379, Rockland, 1:200) primary antibodies. For secondary antibodies, Alexa Fluor 568 goat anti-mouse (Life Technologies 1:500), Alexa Fluor 568 goat anti-rabbit (Life Technologies, 1:500), Alexa Fluor 633 goat anti-rabbit (Life Technologies, 1:500), FITC goat anti-guinea pig (Jackson ImmunoResearch, 1:500), or Alexa Fluor 488 donkey anti-chicken (Jackson ImmunoResearch, 1:500) antibodies were used. DAPI was used to stain the nuclei of all immunofluorescence samples when mounting the slides (Vector). An Olympus IX83 fluorescent microscope or Olympus FV1000 confocal microscope was used to take images, using the 10x, 20x, and 40x objectives.

2.9 SYBR Green qRT-PCR assays

Total RNA was isolated from human and mouse keratinocytes by using TRIzol Reagent (Invitrogen) or from mouse primary mammary epithelial cells using TRIzol reagent (Invitrogen) with the PureLink RNA isolation kit (Ambion) modified to enrich for small RNAs. Complementary DNA was synthesized from total RNA using SuperScript First-Strand Synthesis System (Invitrogen) and followed by qRT-PCR with the 7500 Fast real-time PCR System using Power SYBR Green PCR Master Mix (Kapa Biosystems) in accordance with the manufacturers' protocols. The following primers were used: human Twist1: 5'-GGAGTCCGCAGTCTTACGAG-3' (forward) and 5'-TCTGGAGGACCTGGTAGAGG-3' (reverse), human Lef1: 5'-CGGGTACATAATGATGCCAA-3' (forward) and 5'-TCACTGTAAGTGATGAGGGGG-3' (reverse), murine Twist1: 5'-GCCGGAGACCTAGATGTCATTG-3' (forward) and 5'-CACGCCCTGATTCTTGTGAA-3' (reverse), murine Lef1: 5'-CCCACACGGACAGTGACCTA-3' (forward) and 5'-TGGGCTCCTGCTCCTTTCT-3' (reverse), murine Igfp5 5'-

AGATGGCTGAAGAGACCTACTCC-3' (forward) and 5'-GCTTTCTCTTGTAGAATCCTTTG-3' (reverse), murine Tgfbr3: 5'-CCCTGCATCTGAACCCCATT-3' (forward) and 5'-ACCACAGAACCCTCCGAAAC-3' (reverse), murine Cnp: 5'-TACTTCGGCTGGTTCCTGAC-3' (forward) and 5'- GCCTTCCCGTAGTCACA-3' (reverse), murine Cdh2: 5'-AGGGTGGACGTCATTGTAGC-3' (forward) and 5'-CTGTTGGGGTCTGTCAGG-3' (reverse), murine Hif1A: 5'-TGGTGCTAACAGATGACGGCGA-3' (forward) and 5'-CCCGTGCAGTGAAGCACCTTCC-3' (reverse), murine Cald1: 5'-CGCCAGAAGATGCCAGAAGATG-3' (forward) and 5'-TTGGAGACTATTGCTGCTTG-3' (reverse), murine Pten: 5'-CATGACAGCCATCATCAAAGAGA-3' (forward) and 5'-TGCTTTGAATCCAAAAACCTTACT-3' (reverse), and murine Cdkn1A: 5'-TCAGAGTCTAGGGGAATTGGA-3' (forward) and 5'-AATCACGGCGCAACTGCT-3' (reverse). Human GAPDH: 5'-TCTCTGCTCCTCCTGTTC-3' (forward) and 5'-GCCCAATACGACCAAATCC-3' (reverse), and murine GAPDH: 5'-TCACCACCATGGAGAAGGC-3' (forward) and 5'-GCTAAGCAGTTGGTGGTGCA-3' (reverse) were used as internal controls. Each sample was run in triplicate. C_t values for each gene were calculated and normalized to C_t values for GAPDH.

2.10 TaqMan RT-PCR assays

TaqMan mRNA and TaqMan miRNA assays from Applied Biosystems were used to quantify mRNA and mature miRNAs, respectively using looped-primer real-time PCR. Total RNA were isolated from human and mouse keratinocytes using TRIzol Reagent (Invitrogen) or from mouse primary mammary epithelial cells using TRIzol reagent (Invitrogen) with the PureLink RNA isolation kit (Ambion) modified to enrich for small RNAs. Total RNA (500 ng)

was used to synthesize complementary DNA with the Two-Step TaqMan MicroRNA Assay kit (Applied Biosystems) in accordance with the protocol. qRT-PCR was performed with the 7500 Fast real-time PCR System, TaqMan PCR master mix (Applied Biosystems), and TaqMan primers for murine Nrip1 (ID: Mm01343437_m1, Applied Biosystems), murine Itga7 (ID: Mm00434400_m1, Applied Biosystems), hsa-miR-34a-5p (ID: 000426, Applied Biosystems), hsa-miR-98-3p (ID: 472125_mat, Applied Biosystems), mmu-miR-98* (ID: 462189_mat, Applied Biosystems), mmu-miR-592 -5p (ID: 002017, Applied Biosystems), hsa/mmu-miR-150-5p (ID: 000473, Applied Biosystems), hsa/mmu-miR-33-3p (ID: 002136, Applied Biosystems), hsa/mmu-miR-146b-5p (ID: 001097, Applied Biosystems), hsa/mmu-miR-10b-5p (ID: 002218, Applied Biosystems), mmu-miR-147-5p (ID: 463997_mat, Applied Biosystems), hsa/mmu-miR-193b-5p (ID: 002366, Applied Biosystems), mmu-miR-205-3p (ID: 464195_mat, Applied Biosystems), and hsa/mmu-miR-147-3p (ID: 002262, Applied Biosystems). Each sample was run in triplicate. C_t values for mRNAs and miRNAs were calculated and normalized to C_t values for either human RNU6B (ID: 001093, Applied Biosystems) or murine snoRNA234 (ID: 001234, Applied Biosystems).

2.11 ChIP assay

ChIP was performed with nuclear extracts from NHEK-WT and NHEK-shΔNp63 as previously described (12). Briefly, cells were grown to 90% confluence. Cellular proteins were crosslinked to DNA using 1% formaldehyde. Samples were sonicated on ice to obtain 500-1000bp DNA fragments. 2μg of either ΔNp63-specific antibody (sc-8609, Santa Cruz) or control IgG (sc-2027, Santa Cruz) was added to each sample and incubated overnight at 4°C. Then, protein-DNA complex was precipitated using protein A agarose beads/Salmon sperm DNA (Millipore). qRT-PCR was performed with the following primer sequences

specific for p63-binding sites: human Twist1: 5'-CGCTCTTCTCCTCTGCCC-3' (forward) and 5'- TCTTCCTCGCTGTTGCTCAG-3' (reverse), human Lef1: 5'-GCGTTGGTGACGGACTTTTT-3' (forward) and 5'- TGGAACCCTAATCCCCGAGA-3' (reverse). Primer sequences for non-specific binding sites were as follows: human Twist1 promoter: 5'-AATTCTAGAGGCACCCAGGAG-3' (forward) and 5'-GCCCTCTGAATACCAAACTGGA-3', human Lef1 promoter: 5'-GCAGAGGCAACAAGGACTGA-3' (forward) and 5'-TGGCTTCCTCTTGCTCACTG-3' (reverse).

2.12 Western blot analysis

Total cell lysates were prepared from cell pellets of WT keratinocytes or ΔNp63$^{-/-}$ keratinocytes. 50μg of total protein were electrophoresed on 10% SDS-PAGE gel and transferred to PVDF membrane as previously described (12). Blots were probed with anti-ΔNp63 (619002, Biolegend, 1:500), E-cadherin (3195, Cell Signaling, 1:1000), Vimentin (ab92547, Abcam, 1:1000), Twist1 (sc-81417, Santa Cruz, 1:250), Lef1 (2230S, Cell Signaling, 1:1000), Snail (3879S, Cell Signaling, 1:1000) and Zeb1 (sc-10572, Santa Cruz, 1:500) overnight at 4^{o}C. Horseradish peroxidase conjugated- secondary antibodies against murine, rabbit, or goat IgG (Jackson lab) were incubated with the blots for 1 hour at room temperature. Actin (A5060, Sigma) or Hsp90 (ab13495, Abcam) was used as loading control. Detection was performed using ECL Plus Kit (Amersham).

2.13 Lentiviral infection

Lentivirus-based vectors (3 μg) overexpressing mmu-miR-34a (SBI), mmu-miR-98-3p (Sigma) or an empty vector (as a control) were transfected into 293T cells along with 3 μg of each vector required for lentivirus packaging (pCMV-VSVG and pRSV-REV) using X-tremeGENE HP (Roche) in accordance with the manufacturer's protocol. After 48 hours post-transfection, supernatants containing the lentivirus were collected, filtered and added to $\Delta Np63^{-/-}$ keratinocytes for 48 hours in the presence of 8 μg/ml Polybrene (Santa Cruz). 2 μg/ml of purmocyin was added to the media 48 hours after infection for 2 days. Cells were then changed to fresh media for further analysis. Infected cells were analyzed by miRNA TaqMan assay to determine the level of miRNA overepxression. These cells were further analyzed for migration and invasion capacity using the Boyden chamber assay described above.

2.14 siRNA transfection

1×10^6 $\Delta Np63^{-/-}$ keratinocytes were plated in 10-cm dishes. siTwist1 (SASI_Mm01_00043025, Sigma) or siLef1 (SASI_Mm01_00158789, Sigma) was transfected into the cells at 40 nM using Lipofectamine RNAi Max (Invitrogen) according to manufacturer's protocol. The cells were collected 48 hours post-transfection for further analysis. Infected cells were analyzed by western blot to determine knockdown efficiency. These cells were further analyzed for migration and invasion capacity using a Boyden chamber assay as described above.

2.15 Generation of a single cell suspension of primary mammary epithelial cells

To generate a single cell suspension of primary mammary epithelial cells, the #4 pair of mammary glands from the donor mice was isolated. The donor mice were females between

the ages of 8 and 12 weeks. The glands were placed on a previously weighed 50 ml conical tube containing 30 ml of Hank's Buffered Saline Solution (HBSS) (Corning). The tube containing the glands was then weighed again and the weight subtracted from the original weight. For every 1 g of tissue, 10 ml volume of digestion media was used. The digestion medica consisted of 1mg/ml Type 1 Collagenase (GIBCO) in HBSS with calcium and magnesium. 10% Pen/Strep was added. After weighing the glands, they were placed on a glass Petri dish and the tissue was minced using two feather scalpels (size #21 until it resembled a paste. Individual pieces of the minced tissue should be ~1mm in diameter. This step is imperative and will determine the efficiency of the digestion. After mincing, the tissue was digested Digest tissue in the calculated volume of digestion media in a clean, autoclaved 125 ml Erlenmayer flask with beveled bottom and covered with a foil lid. Digestion occurs for 2 hours in a 37°C incubator set to rotate at 125rpm. Every 30 minutes, the mixture was pipetted up and down to break any aggregated clumps. After 2 hours, the digest should not have any undigested pieces remaining. After the digestion was completed, the digested sample was transferred to a 15 ml conical tube (or multiple tubes if the digestion volume was more than 15 ml) and centrifuged at 450g for 5 minutes. After the initial centrifugation, the supernatant was aspirated and the remaining pellet resuspended in 10 ml 1x HBSS. If there were multiple tubes, the pellets were combined and resuspended in 10 ml total. 3 short centrifugation steps were then performed on this suspension to enrich for mammary organoids. These steps were done in PBS. Each of this steps was done by centrifuging the suspension at 450g for 7 seconds, removing the supernatant, resuspending in fresh PBS, and repeating the steps, two more times until a clear supernatant was observed. Upon completion of these steps, the pellet would be enriched for mammary organoids. At this stage you should have enriched for mammary epithelial organoids in the pellet. After enriching for mammary organoids, the pellet was washed once with PBS (5 minutes at 450g), resuspended in 2 ml pre-warmed 0.25% Trypsin EDTA (Corning), and

transferred to a single well of a 6 well tissue culture dish. This step is to dissociate mammary organoids into a single cell suspension. The suspension was then placed in a 37°C incubator for 5 minutes, pipetting up and down every 2 minutes using a 1 ml pipette. The disassociation of the organoids was monitored under a microscope. Once complete dissociation was observed, the trypsin was neurtralized using mammary epithelial cell growth media (DMEM/F-12 50:50, 10% FBS, 5ug/ml Insulin, 1ug/ml Hydrocortisone, 10 ng/ml EGF, and 10% Pen/Strep) and filtered through a 40 µm cell strainer into a 50 ml conical tube. After transferring the filtered cell suspension into a 15 ml conical tube, it was centrifuged at 300g for 5 minutes and the resulting pellet was washed two times with growth media. The final pellet was then resuspended in 4 ml of growth media and the cells were counted using a hemocytometer or Cellometer before proceeding to the desired application. The final yield was approximately 2 million cells per mouse.

2.16 Adenovirus Transduction of Primary Mammary Epithelial Cells

For adenovirus transduction of primary mammary epithelial cells in suspension, adenovirus Cre (Ad-Cre) and adenovirus Empty (Ad-Empty) were purchased from the Baylor Vector Development Laboaratory. Cre virus stock concentration: 5 x10^{12} particles per ml, Cre virus particle functional units (pfu): 2 x 10^{11} pfu/ml. Empty virus stock concentration: 5 x 10^{12} particles per ml, Empty virus pfu: 1.3 x 10^{11}pfu/ml. To transduce the mammary epithelial cells, Ad-Cre or Ad-Empty virus was added to 2 ml of growth media with cells in 50 ml conical tubes at Multiplicity of Infection (MOI) of 50. 50 ml tubes were used because they provide a larger surface area. The tubes with the cell suspensions with the virus were paced at 45° angle in a 37° C and incubated for 1 hour. Every 15 minutes, the tubes were taken out and mixed, at the 15 and 45 minute time points the tubes were gently agitated to mix, while at the 30 minute time point the suspensions were my by gently pipetting up and down.

Once the incubation period was completed, the cell and virus suspensions were transferred to 15 ml conical tubes and the volume brought up to 15 ml using HBSS. The suspensions were centrifuged at 300g for 5 minutes to remove any unbound virus and. The resulting cell pellets were washed once more with HBSS at 300g for 5 minutes and then resuspended in the appropriate media for the downstream applications.

2.17 Mammary Gland Transplantation

In this procedure Adenovirus treated primary mammary epithelial cells or pieces of mammary outgrowths were transplanted into the cleared fat pads of 3 week old female SCID mice. The primary mammary epithelial cells were obtained as detailed above. Mice were harvested 5 or 10 weeks after injection to check growth of the transplanted cells into mammary ductal trees. The recipients were 3-week-old virgin female SCID mice. For primary transplantations, cell suspensions were prepared fresh before each injection: 100,000 cell suspension in 20 µl 50:50 Growth Factor Reduced (GFR) matrigel (BD Biosciences 354230)/HBSS solution per injection. The matrigel needed to be placed overnight on ice in the 4°C refrigerator to liquefy. Thawing at higher temperatures caused the matrigel to polymerize prematurely. A glass syringe with 50 µl capacity and a fixed 12° beveled-ended, 22 gage, ½ inch long needle was used to deliver the cells (Hamilton). For secondary transplantations, the 4^{th} mammary fat pads of mice previously transplanted 10 weeks before were harvested and kept on PBS. The pads were then imaged using a fluorescent stereomicroscope to assess the percent of the fat pad covered mammary gland. Once the glands were visualized, fine forceps, scissors, and scalpels were used to dissect the mammary gland out. 1 mm diameter pieces of mammary gland were then placed on 1.5 ml microcentrifuge tubes with PBS and kept on ice until transplantation. The mice were

anesthetized using a Ketamine/Xylazine mixture (10 mg ketamine and 1 mg xylazine per kg of body weight) administered intraperitoneally. Buprenorphine (0.1 mg per kg of body weight) was used for analgesia, administered intraperitoneally as well. The anesthetized mice were then shaved and tagged and placed on an impervious board for the surgery. Sterile strips were used to immobilize the mouse limbs. The surgical area in the mouse was then cleaned using 70% ethanol and betadyne, after which a Y-incision was made on the abdomen to allow the skin covering the inguinal mammary fat pads to be peeled back to expose the inguinal (4^{th}) gland. The connection between the 4^{th} and 5^{th} mammary glands was then carefully severed. The vessels in the area were cauterized to prevent bleeding. To clear the fat pad, a cautery pen was used to cut at the level of the visible lymph node, at a Y shaped intersection of three vessels. Each vessel was cauterized to prevent blood loss. The connection of the fat pad to the nipple area was also cauterized off. For primary transplantations, 20 µl of the cell suspension was injected into each mammary fat pad. The injections were done parallel to the mammary fat pad while being careful to avoid piercing the skin. Ad-Cre infected cells were injected into the left 4^{th} mammary fat pad while Ad-Empty infected cells were injected into the right 4^{th} mammary fat pad of the same mouse. For the secondary transplantations, a small pocket was cut into the cleared fat pad and the piece of donor tissue was placed in it. Pieces coming from knockout donor tissue were transplanted into the left mammary fad pad while pieces coming from control donor tissue were transplanted into the right mammary fat pad of the same mouse. The skin flaps were re-positioned normally and held together with wound clips. Wound clips were removed 2 weeks after the procedure. The mice were housed together, up to 5 mice per cage. They were closely monitored for 72 hours after the surgery for sings of distress and additional analgesia was administered as needed. They were monitored every other day throughout the remainder of the experiment. After the conclusion of the experiment the 4^{th} mammary glands were harvested and fixed using 4% PFA. Fixed tissues were then submitted to the

MD Anderson Cancer Center Research Histology Core Laboratory for processing and embedding in paraffin blocks. The blocks were then sectioned onto slides. Slides were stained with hematoxylin and eosin at the core and histopathological analysis was performed for each gland. Unstained slides were used for immunofluorescence analysis.

2.18 Characterization of Transplanted Mammary Glands

The outgrowths arising from transplanted mammary epithelial cells were characterized as follows. To determine the fat pad coverage, the glands were dissected and placed between two glass slides to flatten the gland and imaged using a fluorescence stereomiscroscope. Pictures were taken for the red and green fluorescence channels and imported into Photoshop, where using the measurement tool, the area covered by the gland outgrowth was divided by the total area of the fat pad. The average percentage of the fat pad covered for the knockout condition was compared to the average percentage of the fat pad covered for the control condition at both 5 weeks and 10 weeks after transplantation.

To assess the number of terminal end buds for each sample analyzed, the number of terminations per gland was counted directly from the whole mount fluorescent images. The average number of terminal end buds for the knockout condition was compared to the average number of terminal end buds for the control condition at both 5 weeks and 10 weeks.

To assess the organization of the luminal and a basal layers, paraffin embedded slides were cut and stained with cytokeratin 18, to stain the luminal layer, SMA, to stain the basal layer, GFP to stain recombined cells that had lost ΔNp63 expression, and RFP to stain unrecombined cells. The stained slides were then imaged using an Olympus FV1000 confocal microscope with a 20x objective. A high-low filter was used to optimize the image. 20 1 μm stacked images were used to create the composite image used for quantification.

The number of ducts per sample with SMA staining, the number of ducts with 2 or more clearly visible luminal layers, and the number of ducts with stacked basal layers were quantified.

To assess proliferation, slides were stained for Ki67 and GFP and the number of Ki67 positive nuclei and the number of total nuclei per duct were counted. The slides were imaged using the Olympus IX83 fluorescent microscope with a 40x objective. The average percentage of Ki67 positive nuclei in the knockout condition was compared to the average percentage of Ki67 positive nuclei in the control condition at both 5 weeks and 10 weeks. Prism software, version 6 was used to plot graphs for all of these counts.

2.19 Primary Mammary Epithelial Cell 3D Cultures

For the primary mammary epithelial cell 3D cultures, a previously published method for the 3D culture of normal and malignant mammary epithelial cells (21) was modified. $\Delta Np63^{fl/fl}$, $Rosa^{M/M}$ mammary epithelial cells were isolated and infected them to induce recombination as previously detailed. During the final steps of the infection procedure, chamber slides were coated with 40 µl of GFR matrigel (BD Biosciences) and set to dry in a 37° C incubator for 15 to 30 minutes, being careful not to over dry the slides. Once the infection was complete, the cells were counted and resuspended directly in matrigel at a concentration of 667 cells per µl. 150 µl of the cell mix was added to each well, so that there would be 100,000 cells per well. The slides were then placed for another 15 to 30 minutes in the 37° C incubator to polymerize the matrigel after which 200 µl of mammoshpere growth media (DMEM/F12 50:50, 5% Horse Serum, 5µg/ml Insulin, 1µg/ml Hydrocortisone, 20 ng/ml EGF, 100 ng/ml cholera toxin, 1% Pen/Strep) were added. Media was replaced every other day for the two-week duration of the culture. Once the culture period was complete, the spheres were fixed in 4% PFA as detailed in the published protocol for whole culture fixation. The number of

spheres per condition and the size of those spheres was assessed. The size of the spheres was measured using an Olympus IX83 fluorescent microscope, 10x objective, and the CellSense software. Finally, the spheres were stained for GFP(abcam, 1:1000) and SMA (Sigma, 1:250) following the published protocol as well.

2.20 Intraductal Adenovirus Injections

In this procedure Adenovirus-Cre was injected intraductally through the nipple into 6-week-old conditional knockout female mice to induce recombination and knockout expression of desired genes in the mammary ducts. The mice were aged for up to 18 months to assess for the development of tumors. Recipients were 6-week-old virgin female mice. Virus suspensions were prepared fresh before injection of adenovirus. A 30-gauge glass syringe with 50µl capacity and a blunt-ended ½ inch needle (Hamilton) was used to deliver the virus. The mice were anesthetized using a Ketamine/Xylazine mixture (10 mg ketamine and 1 mg xylazine per kg of body weight) administered intraperitoneally. Buprenorphine (0.1 mg per kg of body weight) was used for analgesia, administered intraperitoneally as well. The anesthetized mice were then shaved and tagged and placed on an impervious board for the surgery. Sterile strips were used to immobilize the mouse limbs. The surgical area in the mouse was then cleaned using 70% ethanol and betadyne, after which a Y-incision was made on the abdomen to allow the skin covering the inguinal mammary fat pads to be peeled back to expose the inguinal (4^{th}) gland. Using a stereomicroscope to visualize the nipple, the nipple of the inguinal gland was held using angled fine forceps (FST, 9cm, cat# 11063-07) and snipped using Wecker spring scissors (FST, 11cm, 7mm blades, cat# 15010-11) so that the needle could be directly inserted through the nipple into the primary duct. Two thirds of the nipple was snipped in this step. 20 µl of virus PBS solution (with 0.1% trypan blue) containing virus at 1.3×10^5 pfu/µl is injected. The injected liquid was visually

detected in the duct to confirm successful injection. Ad-Cre virus was injected into the left 4th mammary gland while Ad-Empty virus was injected into the right 4th mammary gland. The skin flaps were re-positioned normally and held together with wound clips. Wound clips were removed 2 weeks after the procedure. The mice were housed together, up to 5 mice per cage. They were closely monitored for 72 hours after the surgery for sings of distress and additional analgesia was administered as needed. They were monitored once a week throughout the remainder of the experiment, up to 2 years. After the conclusion of the experiment the 4th mammary glands were harvested and fixed using 4% PFA. Fixed tissues were then submitted to the MD Anderson Cancer Center Research Histology Core Laboratory for processing and embedding in paraffin blocks. The blocks were then sectioned onto slides. Slides were stained with hematoxylin and eosin at the core and histopathological analysis was performed for each gland.

2.21 Statistical Analysis

Unpaired t-test with equal variances was used to test for statistical significance. The Prism software, version 6 was used to perform all statistical tests.

Chapter 3

Chapter 3: Using Mouse Models to further understand the role of ΔNp63 in tumorigenesis.

Mouse models have helped to significantly increase our knowledge of genetics. Although, cell culture and other *in vitro* experiments can provide useful information regarding the functions and pathways regulated by specific genes, they lack the complexity and biological context of a full organism, which limits the information we can obtain. Using knockout mouse models, we can specifically address this, and paint a picture of all the essential functions of a specific gene within the context of a whole organism.

As previously mentioned, ΔNp63 knockout ($\Delta Np63^{-/-}$) mice have a striking phenotype of craniofacial abnormalities, limb deformities and, impaired epidermal development (8). $\Delta Np63^{-/-}$ pups have a discontinuous and disorganized epidermis due to problems in terminal differentiation of epidermal cells that impairs the skin's barrier function and regulation of water transport ultimately resulting in their death within the first day after birth. Because $\Delta Np63^{-/-}$ pups die so soon, we need alternative approaches to study adult biological processes such as cancer in the absence of ΔNp63 *in vivo*. One such approach is to use $\Delta Np63^{+/-}$ mice instead of the full knockout. $\Delta Np63^{+/-}$ mice have a grossly normal phenotype and can grow into adulthood. They have reduced levels of ΔNp63, which do not seem to affect development but could lead to a tumor phenotype later on. To this end, we used mice heterozygous for ΔNp63 isoforms with intact TAp63 isoforms in a C57BL/6 background generated as previously detailed (8).

To understand the roles of ΔNp63 in tumor development, we crossed $\Delta Np63^{+/-}$ mice to of various p53 backgrounds p53 wild type ($p53^{WT}$), p53 heterozygous ($p53^{+/-}$), or p53 knockout ($p53^{-/-}$) mice and followed them for a period of up to two and a half years looking for the development of tumors. Crossing the $\Delta Np63^{+/-}$ mice to others with various p53 backgrounds that have been fully characterized previously (9, 13) allowed us to compare

any differences in tumor characteristics. Distressed or visibly sick mice were euthanized by asphyxiation using carbon dioxide and subsequent cervical dislocation following IACUC guidelines. We performed necropsies and fixed soft tissues with 10% neutral buffered formalin, while bones were fixed in Bouin's fixative solution for 3 weeks, after which soft tissues were switched to 70% ethanol and bony tissues to deionized distilled water (ddH_20) before processing, embedding in paraffin and sectioning onto slides. Finally, slides were stained with hematoxylin and eosin (H&E) to perform histopathological analysis of each tissue.

Our first significant finding was that crossing $\Delta Np63^{+/-}$ mice into various $p53^{-/-}$ or $p53^{+/-}$ backgrounds shifted the tumor spectrum towards increased carcinomas. On a $p53^{-/-}$ background, $\Delta Np63^{+/-}$ increased the percentage of carcinomas from 0% to 8%, while at the same time reducing lymphomas from 90% to 57%. The percentages of sarcomas increased as well, from 10% to 29%. There were 6% of $\Delta Np63^{+/-}$, $p53^{-/-}$ mice that did not present any tumors (Figure 1). Similarly, in a $p53^{+/-}$ background, the percentage of carcinomas also increased from 0% to 32%, while both lymphomas and sarcomas decreased from 80% to 29% and from 20% to 18%, respectively. There were 21% of $\Delta Np63^{+/-}$, $p53^{+/-}$ mice that did not present any tumors (Figure 1). Moreover, 67% of $\Delta Np63^{+/-}$ mice in a wild-type p53 background developed tumors, which were exclusively carcinomas.

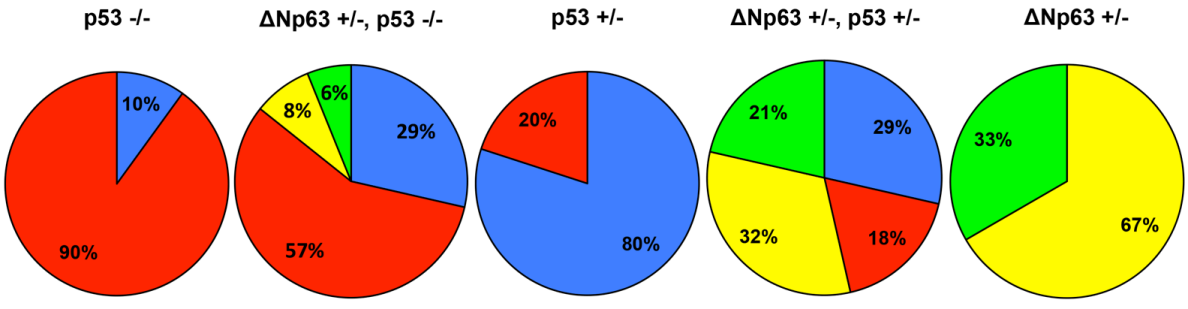

Figure 1. Pie charts representing the mouse tumor spectrums. For $p53^{-/-}$ (N = 100), $\Delta Np63^{+/-}$ $p53^{-/-}$ (N = 49), $p53^{+/-}$ (N = 100), $\Delta Np63^{+/-}$ $p53^{+/-}$ (N = 28), or $\Delta Np63^{+/-}$ (N =

24) genotype mice. Red represents lymphomas, blue represents sarcomas, yellow represents carcinomas, and green represents no tumor.

The types of tumors identified among the different genotypes were varied and included thymic lymphomas, osteosarcomas, squamous cell carcinomas, lung adenocarcinomas, mammary adenocarcinomas, pancreatic adenocarcinomas, and ovarian adenocarcinomas among others (Table 2).

Table 2. Tumor spectrum for mice mutant for p53 and ΔNp63

Genotype	Tumor Type	% mice
p53 -/-	thymic lymphoma	65%
	lymphoma NOS	25%
	angiosarcoma	0%
	histiocytic sarcoma	0%
	osteosarcoma	0%
	rhabdomyosarcoma	0%
	sarcoma NOS	10%
	lung adenocarcinoma	0%
	squamous cell carcinoma	0%
	testicular adenocarcinoma	0%
	mammary adenocarcinoma	0%
	pancreatic adenocarcinoma	0%
	ovarian adenocarcinoma	0%
	gastric adenocarcinoma	0%
	salivary adenocarcinoma	0%
	carcinoma NOS	0%
	hemangioma	0%

Genotype	Tumor Type	% mice
p53 +/-	thymic lymphoma	0%
	lymphoma NOS	20%
	angiosarcoma	0%
	histiocytic sarcoma	0%
	osteosarcoma	0%
	rhabdomyosarcoma	0%
	sarcoma NOS	80%
	lung adenocarcinoma	0%
	squamous cell carcinoma	0%
	testicular adenocarcinoma	0%
	mammary adenocarcinoma	0%
	pancreatic adenocarcinoma	0%
	ovarian adenocarcinoma	0%
	gastric adenocarcinoma	0%
	salivary adenocarcinoma	0%
	carcinoma NOS	0%
	hemangioma	0%

Genotype	Tumor Type	% mice
ΔNp63 +/-; p53 -/-	thymic lymphoma	44%
	lymphoma NOS	5%
	angiosarcoma	10%
	histiocytic sarcoma	7%
	osteosarcoma	5%
	rhabdomyosarcoma	5%
	sarcoma NOS	5%
	lung adenocarcinoma	2%
	squamous cell carcinoma	2%
	testicular adenocarcinoma	2%
	mammary adenocarcinoma	2%
	pancreatic adenocarcinoma	0%
	ovarian adenocarcinoma	0%
	gastric adenocarcinoma	0%
	salivary adenocarcinoma	10%
	carcinoma NOS	0%
	hemangioma	2%

Genotype	Tumor Type	% mice
ΔNp63 +/-; p53 +/-	thymic lymphoma	14%
	lymphoma NOS	9%
	angiosarcoma	0%
	histiocytic sarcoma	0%
	osteosarcoma	14%
	rhabdomyosarcoma	0%
	sarcoma NOS	18%
	lung adenocarcinoma	5%
	squamous cell carcinoma	5%
	testicular adenocarcinoma	5%
	mammary adenocarcinoma	14%
	pancreatic adenocarcinoma	0%
	ovarian adenocarcinoma	18%
	gastric adenocarcinoma	0%
	salivary adenocarcinoma	0%
	carcinoma NOS	5%
	hemangioma	0%

Genotype	Tumor Type	% mice
ΔNp63 +/-	thymic lymphoma	0%
	other lymphoma	0%
	angiosarcoma	0%
	histiocytic sarcoma	0%
	osteosarcoma	0%
	rhabdomyosarcoma	0%
	other sarcoma	0%
	lung adenocarcinoma	25%
	squamous cell carcinoma	0%
	testicular adenocarcinoma	6%
	mammary adenocarcinoma	38%
	pancreatic adenocarcinoma	31%
	ovarian adenocarcinoma	13%
	gastric adenocarcinoma	6%
	salivary adenocarcinoma	6%
	Carcinoma NOS	31%
	hemangioma	0%

Besides shifting the tumor spectrum, $\Delta Np63^{+/-}$ status also resulted in more metastatic tumors, independent of the p53 background: 22.9% of $\Delta Np63^{+/-}$, $p53^{-/-}$ metastasized while none of the $p53^{-/-}$ tumors did while the percentage of metastatic tumors increased from 5% for $p53^{+/-}$ mice to 10% for $\Delta Np63^{+/-}$, $p53^{+/-}$ mice. In the case of $\Delta Np63^{+/-}$ mice with a p53 wild-type p53 background, 88% of the observed tumors metastasized (Figure 2).

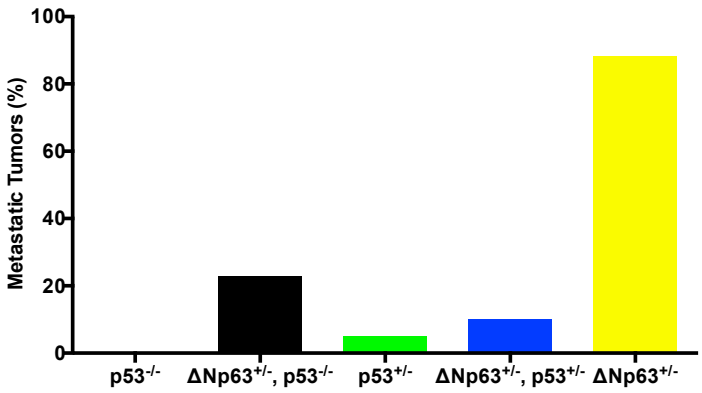

Figure 2. Percentage of metastatic tumors for $p53^{-/-}$, $\Delta Np63^{+/-}$ $p53^{-/-}$, $p53^{+/-}$, $\Delta Np63^{+/-}$ $p53^{+/-}$, or $\Delta Np63^{+/-}$ mice.

The most common observed metastatic site for tumors that arose in $\Delta Np63^{+/-}$ mice irrespective of their p53 status was the liver upon analysis of hematoxylin and eosin (H&E) stained formalin fixed paraffin embedded (FFPE) sections (Figure 3A-F). Mammary adenocarcinoma was the most common tumor in $\Delta Np63^{+/-}$ mice, and H&E analysis showed all the tumors observed in this background were highly metastatic (Figure 4), not only to the liver but the lung as well (Figure 3G-I). Some of these tumors were poorly differentiated, but the specific subtypes of mammary adenocarcinomas observed still need to be determined.

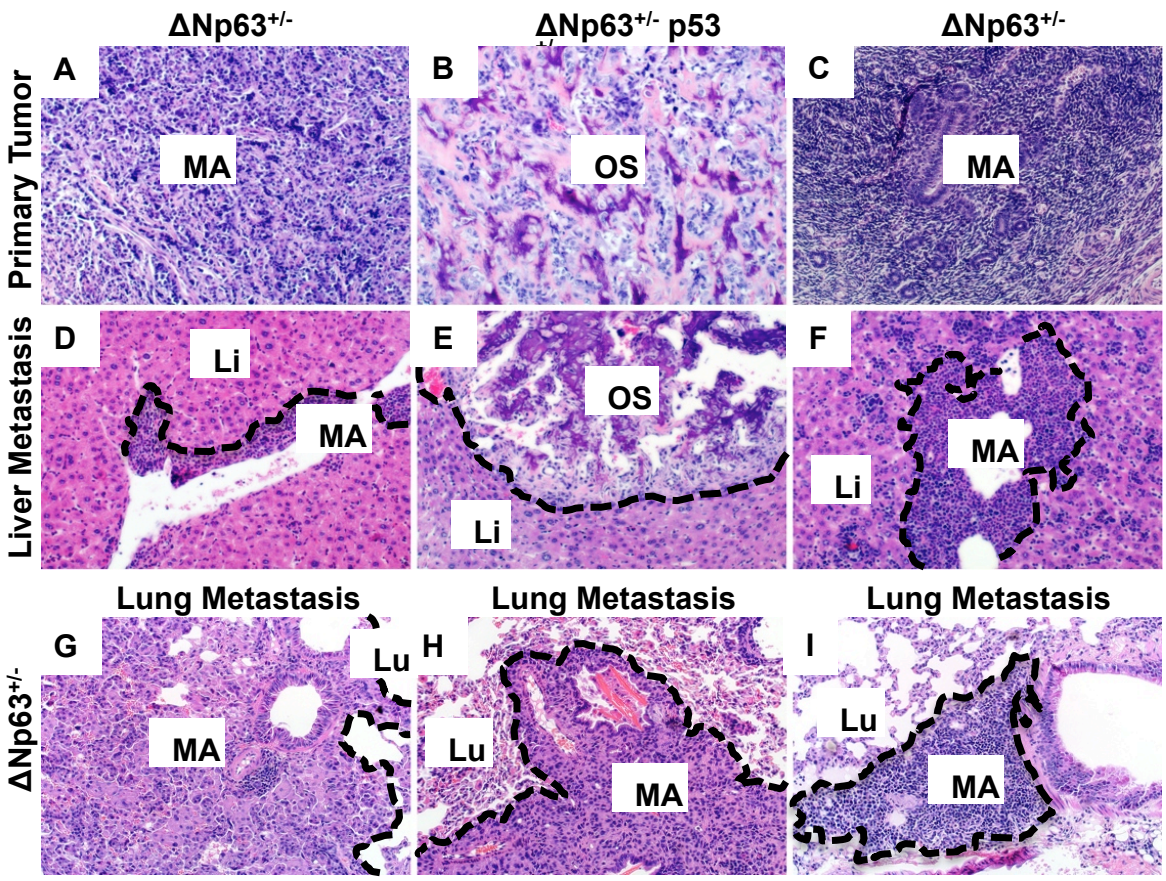

Figure 3. H&E stained cross sections of mouse primary tumors and metastases. H&E stained cross sections of primary tumors (A-C) and liver metastases (D-F) from ΔNp63$^{+/-}$ p53$^{-/-}$, ΔNp63$^{+/-}$ p53$^{+/-}$, or ΔNp63$^{+/-}$ mice. MA: Mammary Adenocarcinoma, OS: Osteosarcoma, Li: Liver. G-I. H&E stained cross sections of ΔNp63$^{+/-}$ mice tumor lung metastases. Lu: Lung

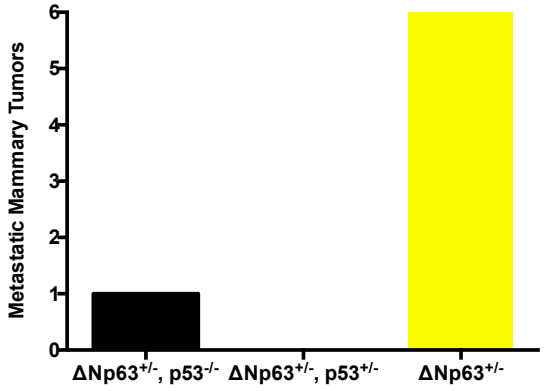

Figure 4. Number of metastatic mammary adenocarcinomas for ΔNp63$^{+/-}$ p53$^{-/-}$, ΔNp63$^{+/-}$ p53$^{+/-}$, or ΔNp63$^{+/-}$ mice

Finally, we compared the tumor free survival of these cohorts. ΔNp63$^{+/-}$ status did not affect tumor free survival in the cases p53$^{+/-}$, or p53$^{-/-}$, only the tumor spectrum. However, ΔNp63$^{+/-}$ status alone significantly reduced survival when compared to wild type (WT) (Figure 5).

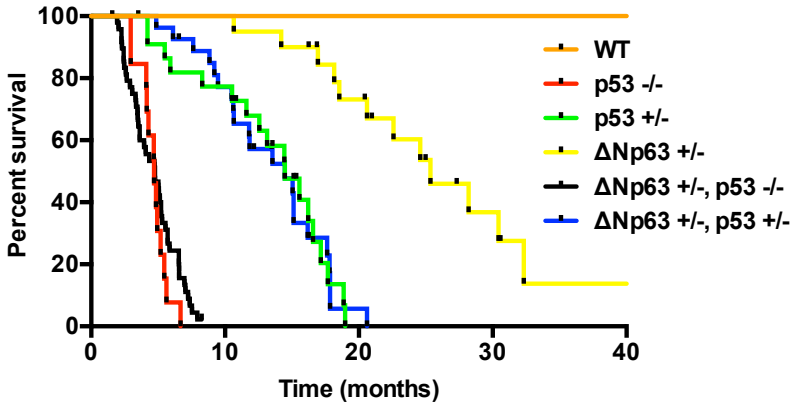

Figure 5. Tumor free survival curve for Wild type (WT), p53$^{-/-}$, ΔNp63$^{+/-}$ p53$^{-/-}$, p53$^{+/-}$, ΔNp63$^{+/-}$ p53$^{+/-}$, or ΔNp63$^{+/-}$ mice.

Taken together, these data provide evidence that alterations in ΔNp63 could lead to the formation of tumors, specifically carcinomas. There is some evidence for ΔNp63's putative role as a tumor and metastasis suppressor, at least in certain tissues. This function could be due to loss of heterozygosity or alterations ΔNp63 dependent pathways. Nonetheless, questions remained regarding the mechanism through which ΔNp63 exerts its tumor and metastasis suppressive functions, which were sought to address in other sections of this work.

Chapter 4

Chapter 4: Using a conditional knockout mouse model to understand the mechanism for ΔNp63 mediated tumor suppression

The $\Delta Np63^{+/-}$ tumor cohort study gave us *in vivo* evidence that ΔNp63 plays a role in the processes of tumor development and metastasis. Our next step was to push forward to understand the mechanisms through which ΔNp63 plays such a role. Previous studies have shed some light on what are some of the functions of ΔNp63 in the context of cancer. Venkatanarayan *et al.* (2015) showed that ΔNp63 promotes lymphoma growth *in vivo* by affecting glucose metabolism, cellular energetics and suppressing p53, TAp63, and TAp73 and their tumor suppressive functions (13). This effect was also observed in several cancer cell lines. Chakravarti *et al.* (2014) found that loss of ΔNp63 in keratinocytes causes dysregulation of the microRNA transcriptome, interferes with terminal differentiation, and confers properties of stem cells such as self renewal and the capacity to contribute to multiple tissues in chimeras and to form teratomas when transplanted in immune compromised mice (8). These properties are similar to those present in cancer stem cells. Other studies such as Tran *et al*. (2013) also showed that ΔNp63 can regulate the epithelial mesenchymal transition (EMT) (17). EMT is a process through which epithelial cells lose cell-cell contacts and acquire mesenchymal properties (22-27). This morphological change is usually accompanied by decreased expression of epithelial markers such as E-Cadherin and increased expression of mesenchymal factors such as Vimentin. EMT is an important process in development, wound healing, and metastasis (22-26, 28-32). Taking these data as a starting point, we proceeded to develop new methods and models to understand the role of ΔNp63 in cancer development and metastasis.

One of the issues with our current understanding of the role of ΔNp63 in cancer is that it is mostly based on *in vitro* assays using cancer cell lines. Cancer cell lines have many additional mutations that may confound any results obtained. With this in mind, our aim was

to reassess these findings using primary cell lines obtained from the ΔNp63$^{-/-}$ mice and to develop an *in vivo* system to study the mechanisms through which ΔNp63 regulates cancer.

4.1 Loss of ΔNp63 promotes a mesenchymal phenotype in cultured primary mouse keratinocytes

To generate primary keratinocytes, epidermal cells were isolated from skin of embryos at day 18.5 by treatment with Dispase II (Roche) as previously detailed (Su *et. al.*, 2009). The separated epidermis was minced and incubated in 0.25% trypsin/EDTA (Corning) for 20 minutes. Cells were plated on collagen-coated flasks (50 µg/ml) collagen type I (BD Bioscience) in defined K-SFM medium (GIBCO). Cells were fed every other day and grown until 60% - 80% confluent and passaged into a secondary culture. The secondary culture was grown until 60% to 80% confluence as well under the same condition. Once the desired confluence was achieved, the keratinocytes were trypsinized and frozen culture freezing media with 10% DMSO. Keratinocytes were isolated from wild type, ΔNp63$^{-/-}$, and TAp63$^{-/-}$ mice. For the experiments, the cells were grown on top of J2-3T3 feeder cells using F-media (8).

We first analyzed the morphology of the primary keratinocytes in culture. ΔNp63$^{-/-}$ knockout keratinocytes no longer grew in colonies or required feeder cells to grow in culture and exhibited an elongated mesenchymal-like phenotype when compared to wild type (Figure 6).

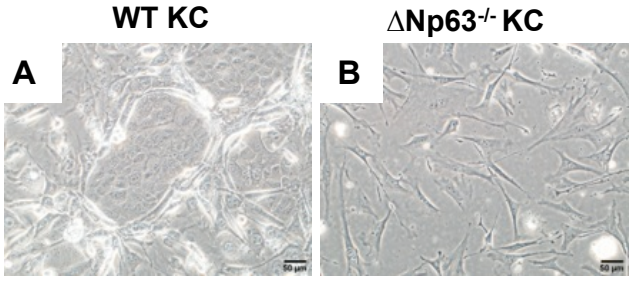

Figure 6. ΔNp63$^{-/-}$ mouse keratinocytes exhibit mesenchymal morphology. Cell morphology of Wild-type (WT) (A) and ΔNp63$^{-/-}$ mouse keratinocytes (KC) (B).

These morphological changes were accompanied by changes in protein expression consistent with a transition towards a mesenchymal phenotype: decreased E-cadherin and increased Vimentin. Protein levels of the transcription factors associated with EMT Lef1, Snail, Twist1, Zeb1 were also increased (Figure 7).

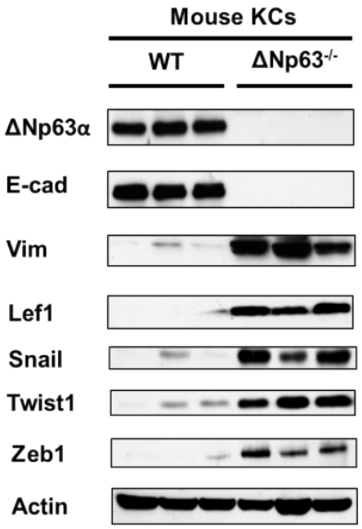

Figure 7. Comparison of protein expression in WT and ΔNp63$^{-/-}$ KCs. Western blot analysis for expression of EMT-related factors in WT and ΔNp63$^{-/-}$ KCs derived from three independent embryos using the indicated antibodies. Actin was used as loading control.

Next we tested whether ΔNp63 knockout keratinocytes had changes in their functional properties to accompany their mesenchymal-like appearance and protein expression profile. Increased migratory and invasive capabilities are essential aspects of the mesenchymal phenotype and we used an *in vitro* scratch assay and an *in vitro* Boyden Chamber assay to test for changes in migration an invasion. For the scratch assay, primary mouse keratinocytes were plated on 6 well plates on top of J2 3T3 feeder cells. Once the keratinocyte colonies were big enough, any remaining feeders were removed using 0.02%

EDTA before starting the assay. Using a 200 µl pipette, we made a scratch was across the center the colony and the progress of the gap closure was monitored over a 24-hour period using time-lapse microscopy. Time-lapse images were taken every 10 min. For the analysis, individual cells were followed using the time-lapse images and their path lengths were quantified and compared. For the Boyden Chamber assay we used a BioCoat Matrigel Invasion Chamber (Corning). Matrigel invasion inserts were used together with 24 well plates. The inserts had two chambers separated either by a Matrigel coated porous membrane, to assess invasion or just a membrane, to assess migration. Primary mouse keratinocytes were plated on the upper compartment. F-media was used in both chambers. No nutrient gradient was established in order to determine so that we could observe the base migratory and invasive potential of the cells. After a 24-hour period, the membranes were removed, fixed, and stained and the numbers of cells that migrated through the membrane or invaded through the Matrigel were counted using bright field microscopy and a 10x objective. Migrating cells per field and invading cells per field were quantified and compared. We found that knocking out ΔNp63 significantly increased migration in both assays (Figure 8, Figure 9, Figure 10A) as well as invasion in the Boyden Chamber assay (Figure 10B). For comparison, TAp63$^{-/-}$ keratinocytes were also used in these assays as TAp63 had been previously implicated as a regulator of tumor migration and invasion (reference).

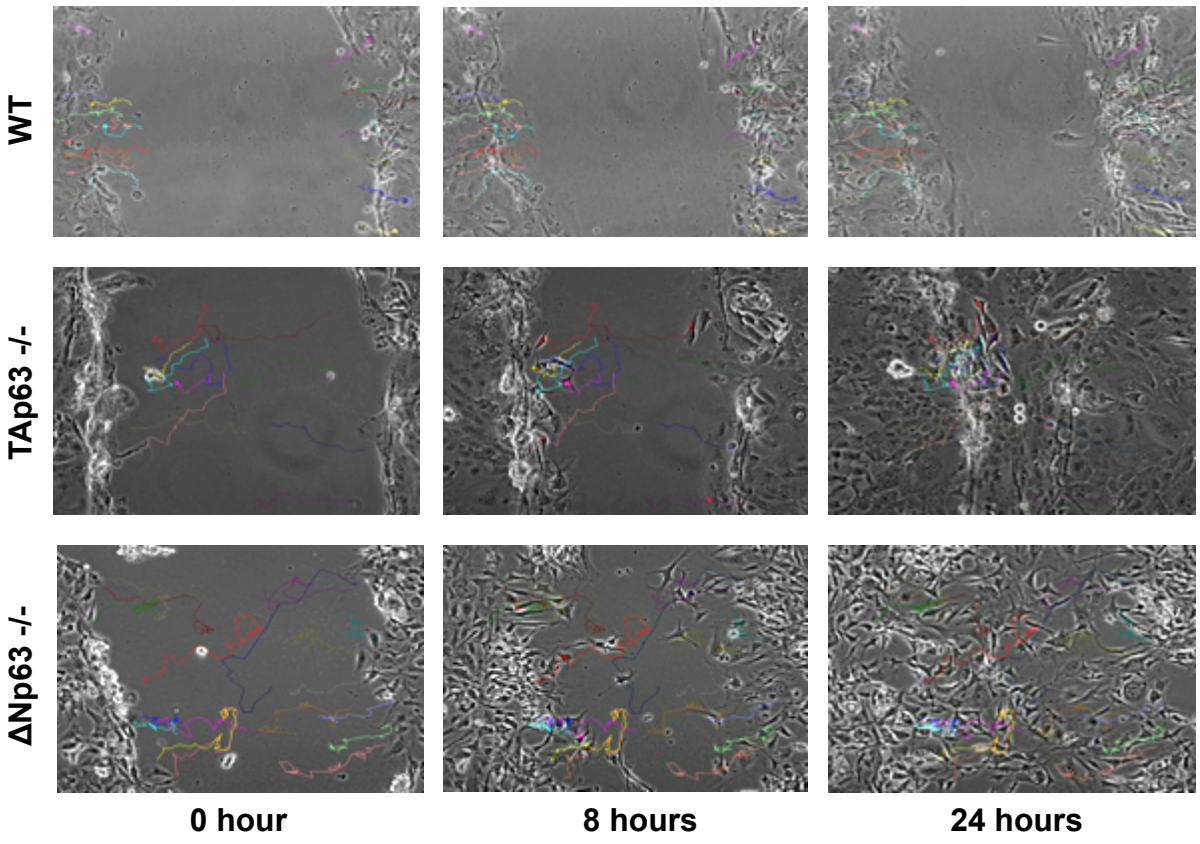

Figure 8. Images from *in vitro* scratch assay using WT, ΔNp63$^{-/-}$, and TAp63$^{-/-}$ KCs. Time points for 0 hours, 8 hours, and 24 hours are shown.

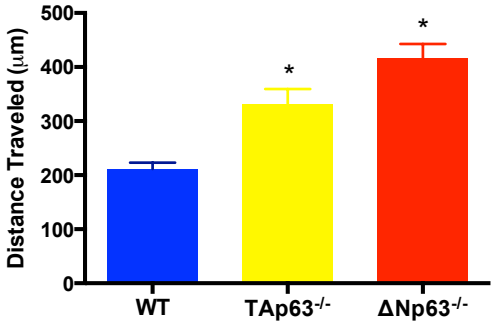

Figure 9. *In vitro* scratch assay quantification. Measurements of distance traveled by WT, ΔNp63$^{-/-}$, and TAp63$^{-/-}$ KCs in the *in vitro* scratch assay shown in figure 8. Asterisks, p ≤0.0003

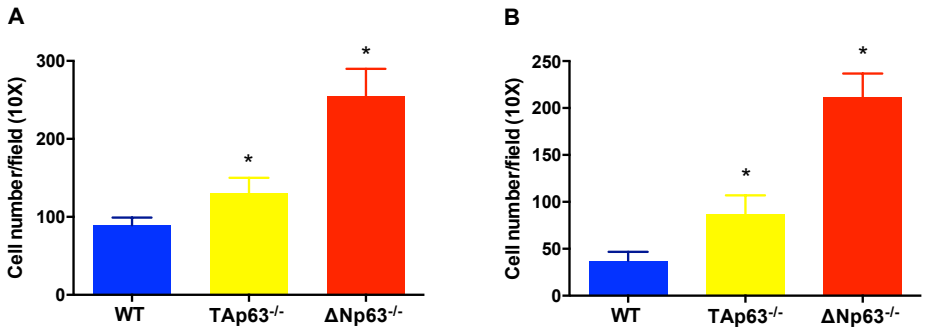

Figure 10. Boyden Chamber Assay Migration and Invasion Results. Migration (A) and invasion (B) assay of WT, ΔNp63$^{-/-}$, and TAp63$^{-/-}$ KCs. Asterisks, p < 0.0001.

Moreover, when we analyzed the behavior of individual ΔNp63$^{-/-}$ cells in the scratch assay, we saw that their cell contacts had been lost, and they migrated individually and more erratically (Figure 8). In contrast, TAp63$^{-/-}$ cells, they still retain their cell contacts and migrate as a unit even though overall migration is increased. We followed the paths that individual cells and quantified their traveled distance and saw that ΔNp63$^{-/-}$ cells also traveled a significantly longer distance than WT or TAp63$^{-/-}$ cells (Figure 9). These results further evidence that loss of ΔNp63 promotes a mesenchymal phenotype, as their migration patterns closely mirror those of mesenchymal cells.

Taken together, these data provide evidence that ΔNp63 loss in keratinocytes promotes a transition from an epithelial to a mesenchymal phenotype. ΔNp63$^{-/-}$ keratinocytes lose expression of E-cadherin and cell-cell contacts typical of epithelial cells while at the same time acquire expression of Vimentin and other EMT related transcription factor typical of mesenchymal cells. Besides expression changes, the transition into a mesenchymal phenotype affected the functional properties of ΔNp63$^{-/-}$ making them more migratory and invasive, as observed in the *in vitro* assays. ΔNp63$^{-/-}$ keratinocytes also appear to migrate individually and in an erratic manner, suggesting that they have little communication with surrounding cells. With this in mind, we sought to address the question

as to whether ΔNp63 loss leads to EMT and increased migration and invasion with the added complexity of an *in vivo* system.

4.2 Loss of ΔNp63 promotes an epithelial to mesenchymal transition *in vivo*.

To investigate how ΔNp63 regulates the epithelial to mesenchymal transition *in vivo*, we developed an *in vivo* cutaneous wound-healing assay. p63 has been previously shown to play a role in normal cutaneous wound healing through mostly through its function as a regulator of skin stem cell compartments (12, 33). The process of cutaneous wound healing shares many similarities and molecular pathways with tumor development and metastasis (34-40). Many of the pathways that are involved in cutaneous wound healing are also present in an unregulated way during cancer and metastatic progression. For example, cell proliferation and migration are important to repopulate the wound site and heal it while in cancer, uncontrolled proliferation leads to tumor growth and migration and invasion through tumor adjacent stroma are essential parts of metastasis. EMT is another important process common between cutaneous wound healing and cancer progression. In cutaneous wound healing, epidermal cells at the wound edge partially lose cell-cell adhesions, alter their cell morphology, and acquire mesenchymal properties that allow them to migrate and close the wound gap (29, 32, 41-44). A similar process takes place during metastasis. The cutaneous wound healing mouse model allows us to study proliferation, migration, invasion and EMT in a shorter and more controlled time frame and also using the power of genetically engineered conditional knockout mice.

For the cutaneous wound healing mouse model, ΔNp63 conditional knockout mice ($\Delta Np63^{fl/fl}$) were crossed to reporter $Rosa^{M/M}$ mice (45) and to mice expressing a tamoxifen inducible Cre under the K14 promoter ($K14^{CreER+}$) mice (46) to generate $\Delta Np63^{fl/fl}$, $Rosa^{M/M}$, $K14^{CreER+}$ mice. The mice were anesthetized using inhaled isoflurane and a 1 cm wound

constrained to the epidermis was made using DXB compound. DXB is a proprietary detergent solution provided by one of our collaborators that selectively dissolves the epidermis to generate the wound. This allows us to solely focus on the processes involved in epidermal repair. Tamoxifen (100 mg/mL 100% Ethanol) was applied topically to the mice backs for three consecutive days following wounding to activate Cre and induce recombination. Mice were housed together, and subsets were euthanized at days 1, 4, and 8 after induction (Figure 11).

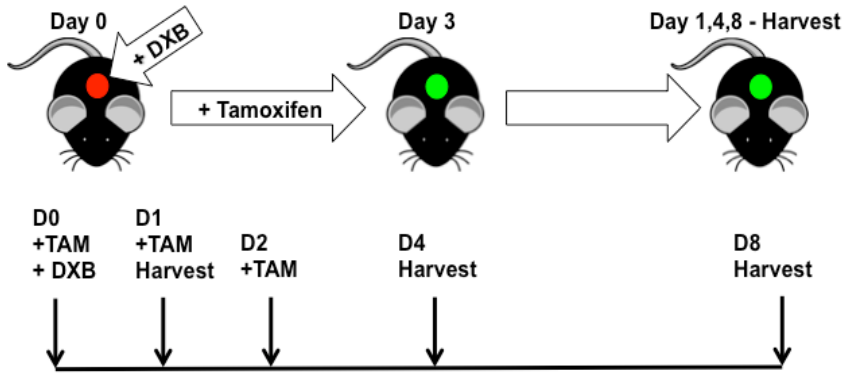

Figure 11. Experimental design for *in vivo* wound healing experiment. ΔNp63$^{fl/fl}$, Rosa$^{M/M}$, K14^{CreER+} mice in a C57Bl/6, 129 background were treated topically with DXB compound to create 10 mm epidermal wounds and with Tamoxifen for 3 consecutive days to induce recombination constrained to the epidermis. Wounds were assessed on days 1, 4, and 8 after wound induction

One half of the epithelium was fixed in 10% formalin and the other frozen in OCT medium (Tissue Tek). Frozen sections were used to assess recombination status. Due to the Rosa$^{M/M}$ reporter, the recombined tissues would express GFP and fluoresce green as shown in this representative image (Figure 12).

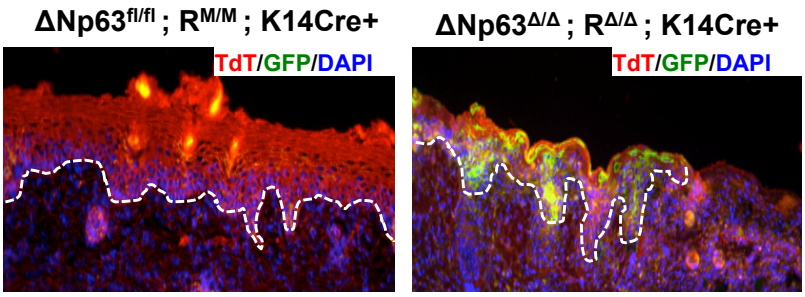

Figure 12. Assessment of recombination efficiency. *In vivo* recombination efficiency of unrecombined ($\Delta Np63^{fl/fl}$) and recombined ($\Delta Np63^{\Delta/\Delta}$) wound sites was assessed after three days of Tamoxifen by imaging frozen sections using fluorescence microscopy. R, Rosa mutant. Red, TdTomato. Green, GFP. Blue, DAPI.

Formalin fixed sections were embedded in paraffin and sectioned onto slides. These slides were stained with hematoxylin and eosin and the wound sizes were measured and analyzed. Unstained paraffin embedded tissue sections were dewaxed in xylene and rehydrated in a graded series of ethanol following standard protocols (7). Slides were incubated with primary antibodies for ΔNp63 (rabbit, BioLegend 1:100), Twist1 (rabbit, 1:100) from Santa Cruz, Lef1 (rabbit, 1:200) from Cell Signaling, GFP (chicken 1:1000), Ki67 (rabbit 1:100), Cytokeratin 5 (rabbit 1:500), E-Cadherin (rabbit 1:300), and Vimentin (rabbit 1:200) from Abcam, and cytokeratin 14 (guinea pig 1:500) from LifeSpan Biosciences. For immunohistochemical detection, Vectastain ABC Kit (Vector Lab) was used. For immunofluorescence detection, Alexa Fluor 568 goat anti-rabbit (Life Technologies, 1:500), FITC goat anti-guinea pig (Jackson ImmunoResearch 1:500), or Alexa Fluor 488 donkey anti-chicken (Jackson ImmunoResearch 1:500) secondary antibodies were used.

We confirmed that for all $\Delta Np63^{fl/fl}$, $Rosa^{M/M}$, $K14^{CreER+}$ samples treated with tamoxifen, the recombination efficiency was 100% after the third day and was constrained to the epidermis (Figure 12). At day 1, only about 20% of the epidermis showed recombination in the tamoxifen treated samples. We then analyzed H&E stained formalin fixed paraffin

embedded (FFPE) sections of the wound site and found that while the control wounds were completely reepithelialized by the fourth day, the ΔNp63 knockout wounds remained open even after the eighth day (Figure 13).

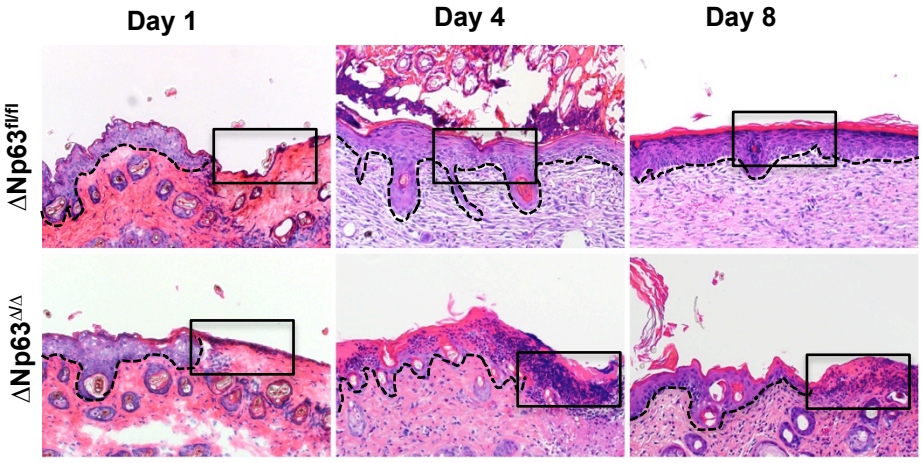

Figure 13. H&E-stained cross sections of ΔNp63$^{fl/fl}$ and ΔNp63$^{Δ/Δ}$ skin. Samples were collected on days 1, 4, and 8 after wounding. The dotted line marks the epidermal border and the box marks the wound site.

Staining for cytokeratin 5 (K5), which is only present in the epidermis, to ddeliniate the epidermal layer confirmed that control wounds had completely healed after 4 days while ΔNp63 knockout wounds remained open up to eight days after induction (Figure 14).

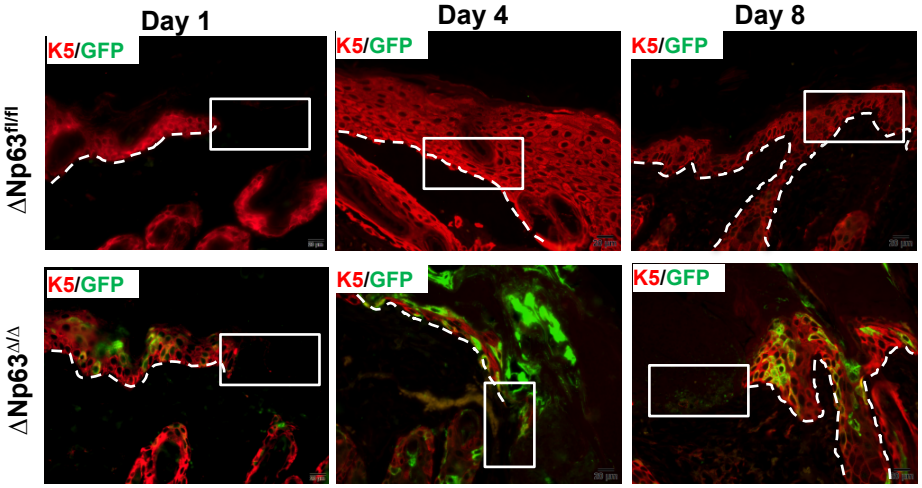

Figure 14. Staining of wound sites for cytokeratin 5 to delineate the epidermis. Double immunofluorescence staining of ΔNp63$^{fl/fl}$ and ΔNp63$^{Δ/Δ}$ wound sites on days 1, 4, and 8 after wounding for cytokeratin 5 (red) and GFP (green).

To quantify this, we measured the wound gap sizes at the different time points of the experiment and found the size of ΔNp63 knockout wounds to be significantly bigger across the eight-day duration of the experiment (Table 3, Figure 15).

Table 3. Wound Gap Measurements for Various Time Points

Sample	Experiment Group	Time Point	Wound Size (mm)
G992	Control	Day 1	7.8
G1013	Control	Day 1	6.9
G1014	Control	Day 1	6.7
G1000	Knockout	Day 1	10.4
G1001	Knockout	Day 1	9.9
G669	Control	Day 4	0
G696	Control	Day 4	0
G668	Knockout	Day 4	4.7
G695	Knockout	Day 4	2.6
G700	Knockout	Day 4	4
G671	Control	Day 8	0
G698	Control	Day 8	0
G666	Knockout	Day 8	2.6
G667	Knockout	Day 8	3.1
G701	Knockout	Day 8	4

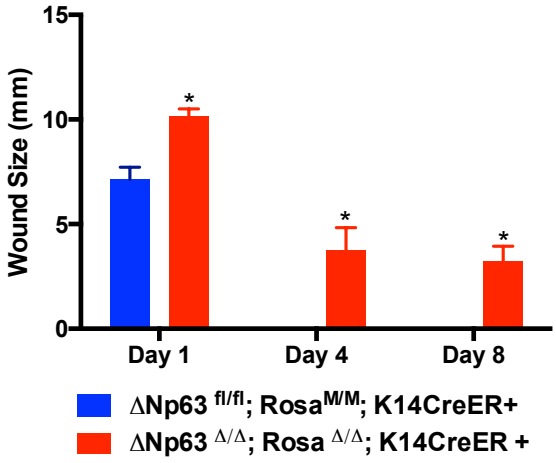

Figure 15. Wound size quantification. Quantification of the size of the wound site on days 1, 4, and 8 after wounding. n = 3, $p < 0.05$

Although, the wound gap in the ΔNp63 knockout condition decreased throughout the duration of the experiment, the wound never fully healed. Our intention was to continue the experiment beyond eight days to observe if the wound eventually healed but we had to stop at the eighth day time point due to health concerns brought up by our animal facility veterinarians.

To test whether ΔNp63 knockout wounds failed to re-epithelialize due to a defect in proliferation, we performed immunofluorescence staining on FFPE sections of the wound site with Ki67. We observed comparable Ki67 staining in both ΔNp63 knockout wounds 1 day after induction and significantly increased Ki67 staining on days four and eight for ΔNp63 knockout wounds when compared to control (Figures 16, 17).

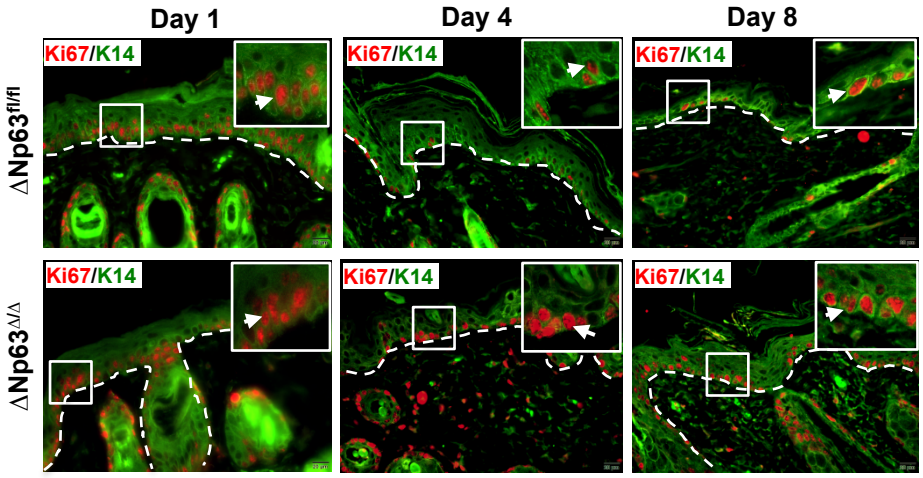

Figure 16. Ki67 staining at the wound sites to assess proliferation. Double immunofluorescence staining of ΔNp63$^{fl/fl}$ and ΔNp63$^{Δ/Δ}$ wound sites on days 1, 4, and 8 after wounding for cytokeratin 14 (green) and Ki67 (red).

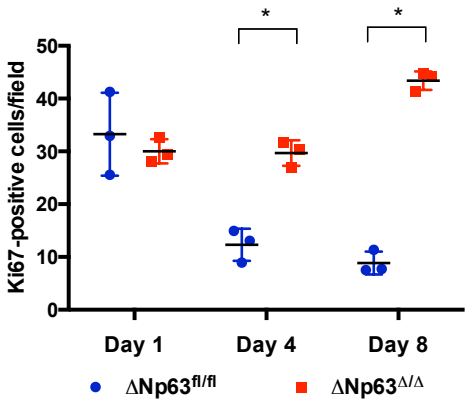

Figure 17. Quantification of proliferation in wound healing samples. Quantification of Ki67-positive cells on days 1, 4, and 8 post-wounding. n = 3, p < 0.0002.

This suggests that epidermal cells in the wound edges continue to proliferate in the absence of ΔNp63 while the wound remains open. Taken together these data show that ΔNp63 knockout in the epidermis delays wound healing but it is not due to a defect in proliferation.

Since ΔNp63 knockout epithelial cells continued to proliferate as expected, we decided to look at other processes that could explain the impaired re-epithelialization observed in ΔNp63 knockout wounds. Based on our *in vitro* experiments and its importance in normal epithelial wound healing, we set our sights on the EMT process and how changes due to loss of ΔNp63 could explain the observed wound-healing defect. We performed E-cadherin and Vimentin staining and saw E-cadherin loss (Figure 18A) upon ΔNp63 deletion while expression of Vimentin increased in the epidermal compartment (Figure 18B).

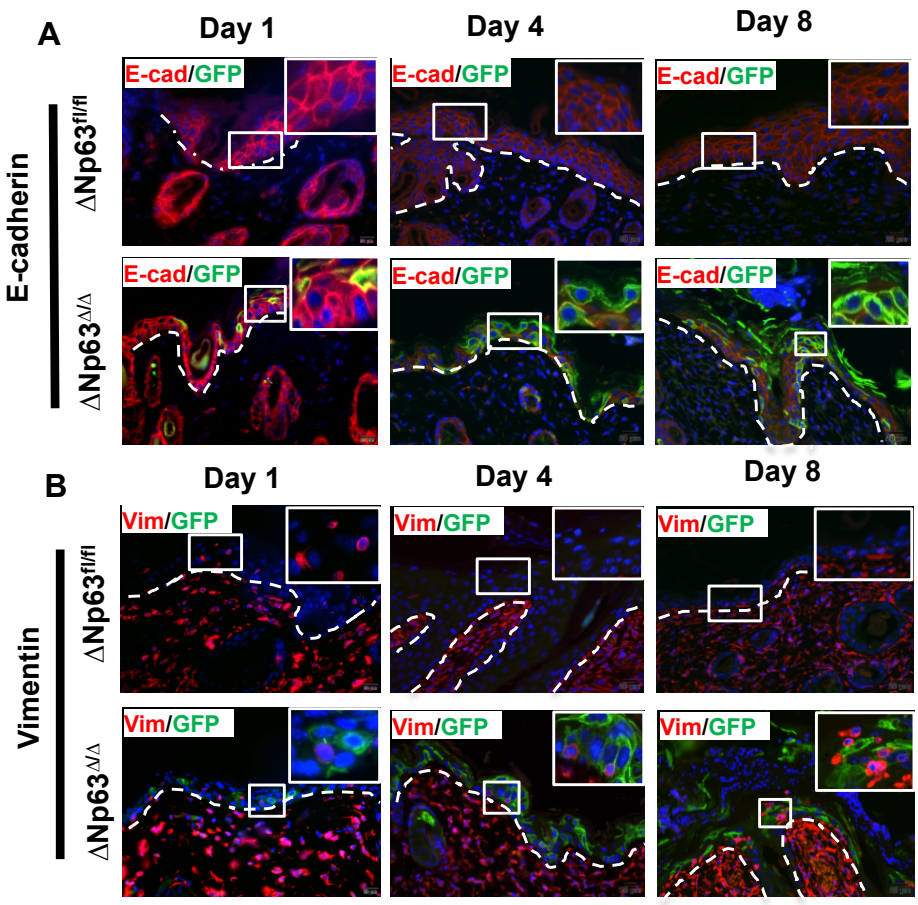

Figure 18. E-cadherin and Vimentin expression at the wound sites. Double immunofluorescence staining of ΔNp63$^{fl/fl}$ and ΔNp63$^{Δ/Δ}$ wound sites on days 1, 4, and 8 post-wounding for E-cadherin (red) and GFP (green) (A), or Vimentin (red) and GFP (green) (B).

These changes were present throughout the duration of the experiment during which the ΔNp63 knockout wounds failed to heal. In contrast, E-cadherin expression persisted even as Vimentin increased during wound healing in the control condition, as observed in the day one staining. This suggested that epidermal cells that lose ΔNp63 undergo a different kind of EMT and go further into a mesenchymal phenotype. To test this we performed immunohistochemistry for known EMT related transcription factors and found that Twist1 (Figure 19A) and Lef1 (Figure 19B) expression increased upon ΔNp63 deletion.

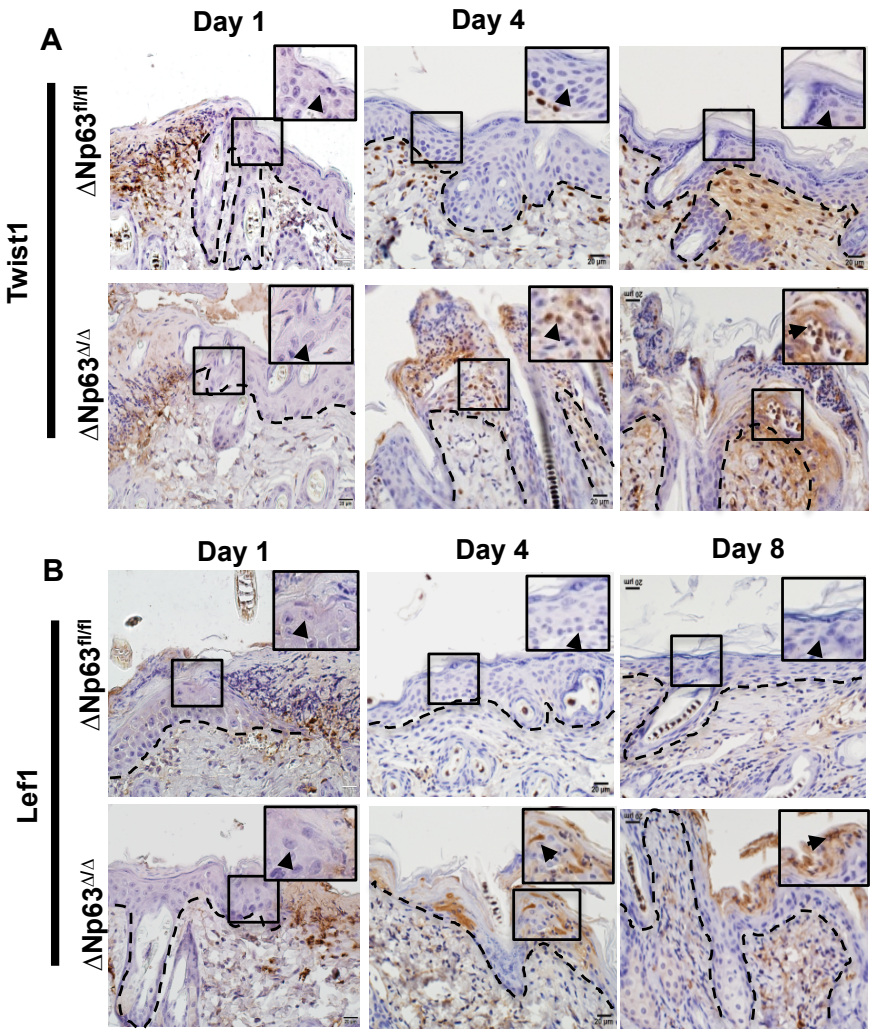

Figure 19. Twist1 and Lef1 immunohistochemistry staining at the wound sites. Immunohistochemical staining of ΔNp63$^{fl/fl}$ and ΔNp63$^{Δ/Δ}$ wound sites on days 1, 4, and 8 after wounding for Twist1 (C) and Lef1 (D).

This persisted throughout the eight-day duration of the experiment during which the wounds did not heal. In contrast, Twist1 and Lef1 expression never increased in the control condition, even during the first day when the wound was still in the process of healing. This suggests that the EMT program activated in the absence of ΔNp63 could be different than the one observed in conventional wound healing: The transcription factors Twist1 and Lef1 become activated in the absence of ΔNp63 but not when it is still expressed

To tie the results from the *in vivo* model to the tumor phenotype observed on the ΔNp63$^{+/-}$ mice we performed immunohistochemistry on the tumors collected from ΔNp63$^{+/-}$ mice and the same reciprocal relationship between ΔNp63 and Twist1 and Lef1 levels at both the primary tumors and liver metastases. In well-differentiated primary tumors, ΔNp63 continued to be expressed while Twist1 and Lef1 expression was low. In poorly differentiated primary tumors, ΔNp63 expression was decreased while Twist1 and Lef1 expression was increased, pushing the tumors towards a more migratory and invasive phenotype. In the metastases, the inverse was true: ΔNp63 expression was restored and Twist1 and Lef1 expression was decreased, suggesting a reversion to the epithelial phenotype essential to seed the target metastatic organ (Figure 20). These stains also suggest that at least some of the tumors observed in the ΔNp63$^{+/-}$ mice are not due to loss of heterozygosity since ΔNp63 continues to be expressed in well differentiated tumors and in the metastases.

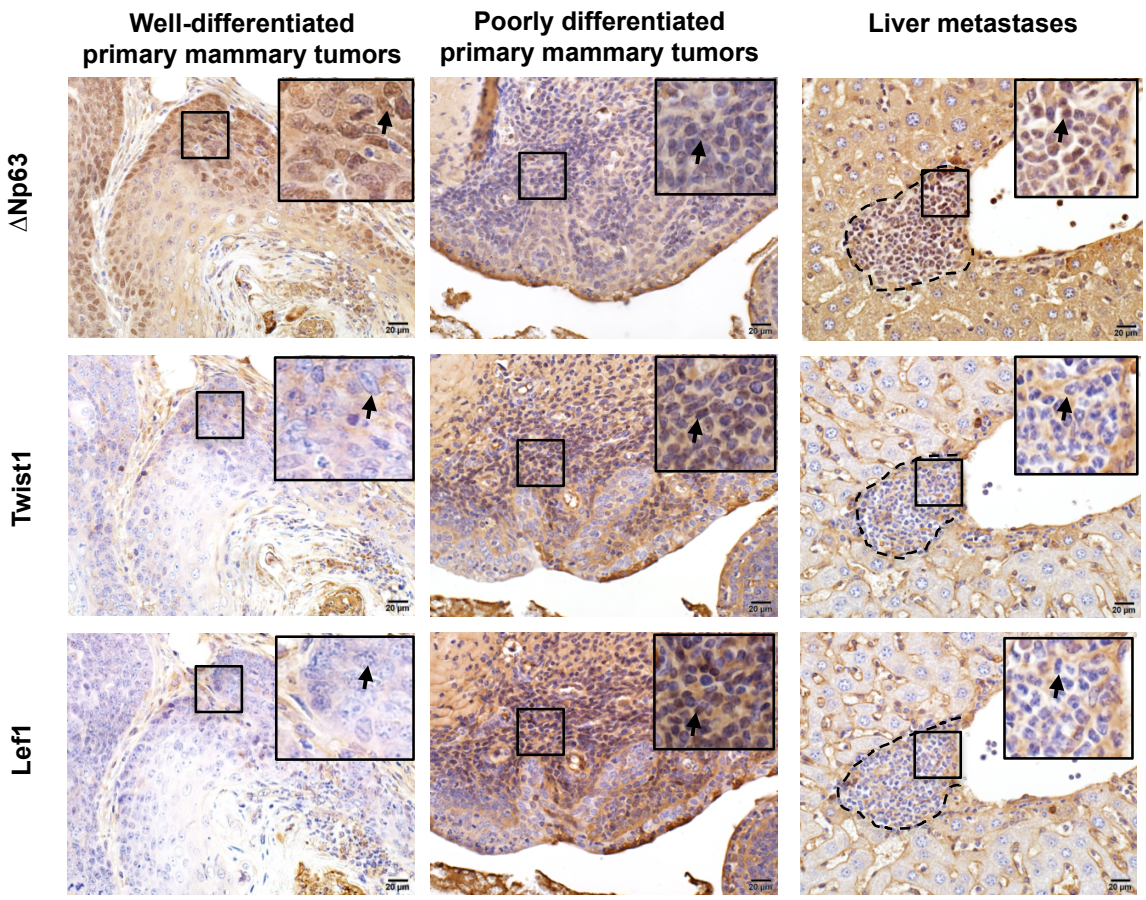

Figure 20. ΔNp63, Twist1 and Lef1 expression in tumors from ΔNp63$^{+/-}$ mice. ΔNp63 expression inversely correlates with Twist1 and Lef1 expression in primary mammary tumors and metastases from ΔNp63$^{+/-}$ mice. Immunohistochemical staining for ΔNp63, Twist1, and Lef1 in well-differentiated or poorly differentiated primary mammary tumors and liver metastases.

Taken together these data show that ΔNp63 loss appeared to promote a different EMT program and mesenchymal phenotype *in vivo* from the EMT program observed with wild type ΔNp63. In this program, E-cadherin loss was observed as Vimentin expression increased rather than what is observed in the typical wound healing process where E-cadherin expression persists even as Vimentin increases. Furthermore, Twist1 and Lef1 are two EMT associated transcription factors that are typically not activated in the partial EMT found in wound healing, yet they were activated in the EMT program observed in the absence of ΔNp63, which further differentiates it. Finally, the tumors and metastases from

the ΔNp63$^{+/-}$ cohort presented the same reciprocal relationship between ΔNp63 and Twist1 and Lef1, which suggested that the same EMT program could be activated in these tumors.

4.3 ΔNp63 modulates invasion, migration, and EMT through regulation of microRNAs

To build on our *in vivo* findings we designed *in vitro* experiments using ΔNp63$^{-/-}$ primary keratinocytes to understand mechanism through which ΔNp63 could modulate migration. The first step was to address whether the relationship between ΔNp63, Twist1, and Lef1 observed *in vivo* could be recapitulated in an *in vitro* system. To this end, we used siRNA to knockdown expression of Twist1 and Lef1 (Figure 21) and performed a Boyden Chamber assay to test for reversion of the migration and invasion phenotypes observed in the absence of ΔNp63.

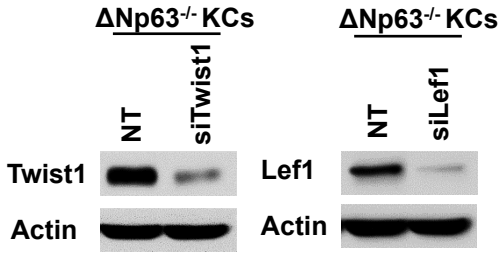

Figure 21. Western blot analysis for knockdown efficiency of either Twist1 or Lef1 in ΔNp63$^{-/-}$ KCs.

We saw that knockdown of either Twist1 or Lef1 in ΔNp63$^{-/-}$ primary keratinocytes decreased migration and invasion when compared to the non-targeting control (Figure 22A-B) confirming that the migration and invasion phenotype observed upon loss of ΔNp63 is partly due to its regulation of Twist1 and Lef1.

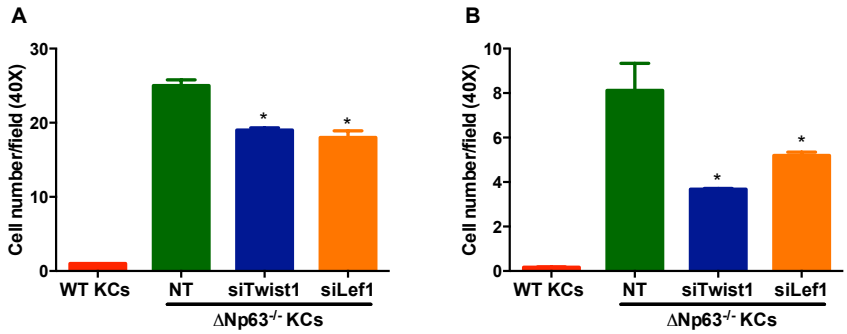

Figure 22. Migration (A) and invasion (B) assay of WT KCs and ΔNp63$^{-/-}$ KCs transfected with either siTwist1 or siLef1. Asterisks, p ≤ 0.0006.

We also performed qRT-PCR to determine if the mRNA levels of Twist1 or Lef1 were affected upon loss of ΔNp63. We found that ΔNp63$^{-/-}$ keratinocytes had increased levels of Twist1 (Figure 22A) and Lef1 (Figure 22B). We also confirmed that this phenomenon can be recapitulated when deleting ΔNp63 in normal human epidermal keratinocytes (NHEKs) (Figure 22A-B).

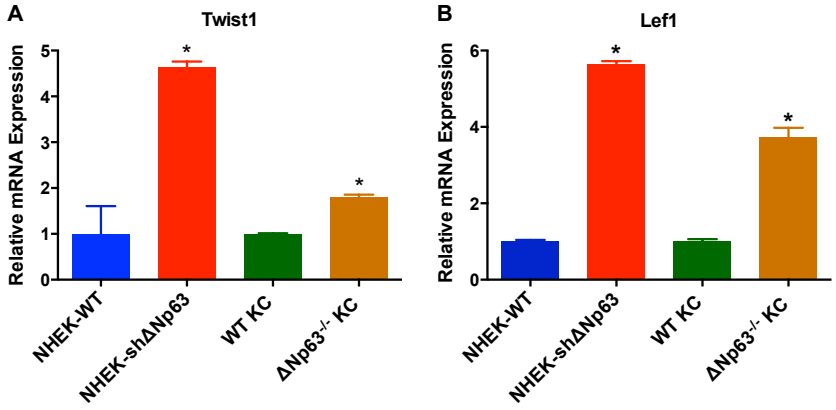

Figure 22. Relative Twist1 and Lef1 expression in keratinocytes upon loss of ΔNp63. qRT-PCR of human and mouse Twist1 mRNA (A) and Lef1 mRNA (B) in NHEK-WT, NHEK-shΔNp63, WT KCs and ΔNp63$^{-/-}$ KCs. Asterisks, p < 0.0005.

Finally we performed a CHIP assay to determine if ΔNp63 directly bound to the Twist1 or Lef1 promoters and regulated their transcription but found no significant evidence that this was the case (Figure 23A-B).

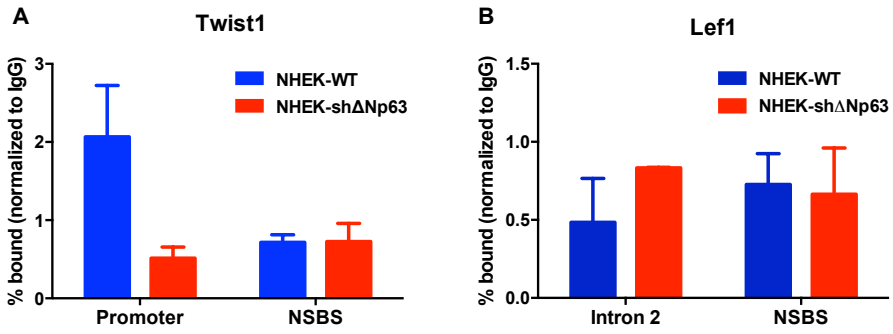

Figure 23. ChIP assay for human Twist1 (A) and Lef1 (B) in NHEK-WT and NHEK-shΔNp63. NSBS, non-specific binding sites.

Overall these data show that the mesenchymal phenotype observed in ΔNp63$^{-/-}$ keratinocytes and ΔNp63 knockdown NHEKs is partly due to its repression of Twist1 and Lef1. However, ΔNp63 does not directly bind to either the Twist1 or Lef1 promoters, which suggests that it regulates their expression through indirect pathways.

Since ΔNp63 did not directly regulate Twist1 or Lef1 transcription, we decided to focus on ΔNp63's role in microRNA biogenesis as an indirect pathway through which ΔNp63 could regulate their expression. Using mRNA and microRNA sequencing data previously published by our lab (8), we did a functional pair analysis looking at candidate microRNAs that regulate Twist1 or Lef1 whose levels are affected by ΔNp63 (Figure 24).

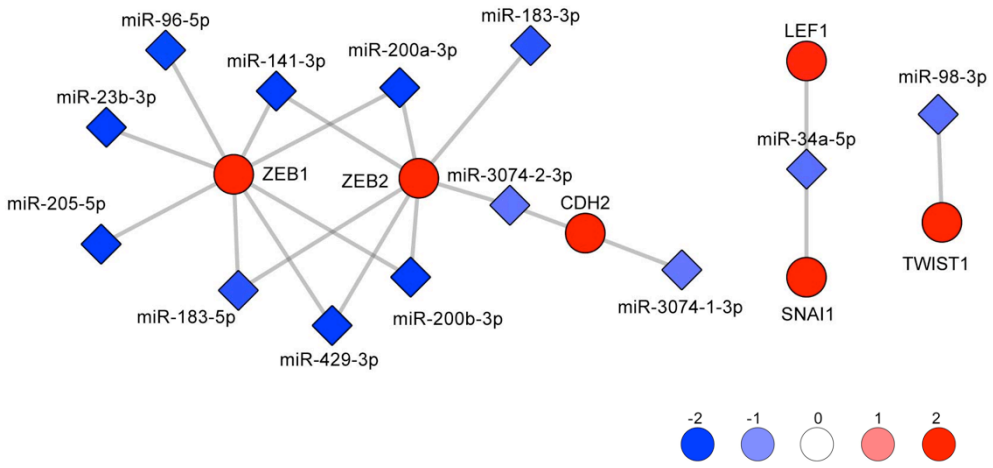

Figure 24. Functional pair analysis using ΔNp63$^{-/-}$ mRNA and microRNA sequencing. MicroRNA-RNA functional pair analysis for genes associated with EMT upon the depletion of ΔNp63 in KCs. Expression down (blue), expression up (red)

We found two candidates: miR-98 and miR-34a. Both of these microRNAs are DGCR8 dependent (8). Using Taqman qRT-PCR, we confirmed that there was significantly reduced expression of both miR-98 (Figure 25A) and miR-34a (Figure 25B) upon loss of ΔNp63 in both keratinocytes and NHEK.

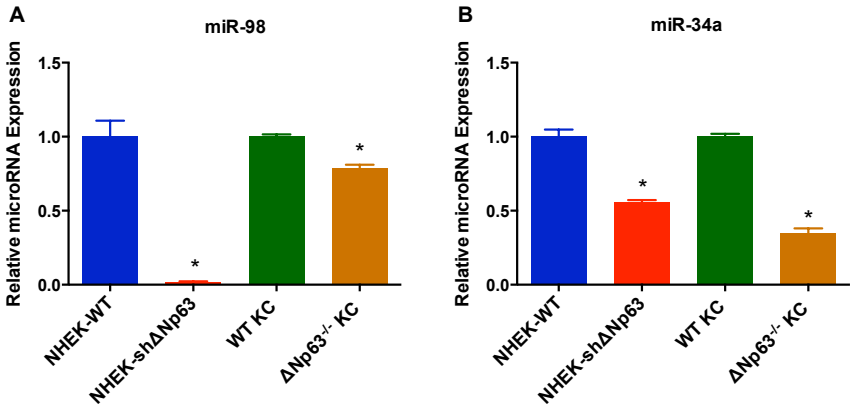

Figure 25. miR-98 and miR-34a expression upon loss of ΔNp63. Taqman qRT-PCR of miR-98-3p (miR-98) (A) and miR-34a-5p (miR-34a) (B) in NHEK-WT, NHEK-shΔNp63, WT KCs and ΔNp63$^{-/-}$ KCs. Asterisks, p ≤ 0.0001.

We then proceeded to re-introduce and overexpress these microRNAs to ΔNp63$^{-/-}$ keratinocytes (Figure 26A-B) and assess whether they were enough to reverse the effects of loss of ΔNp63$^{-/-}$.

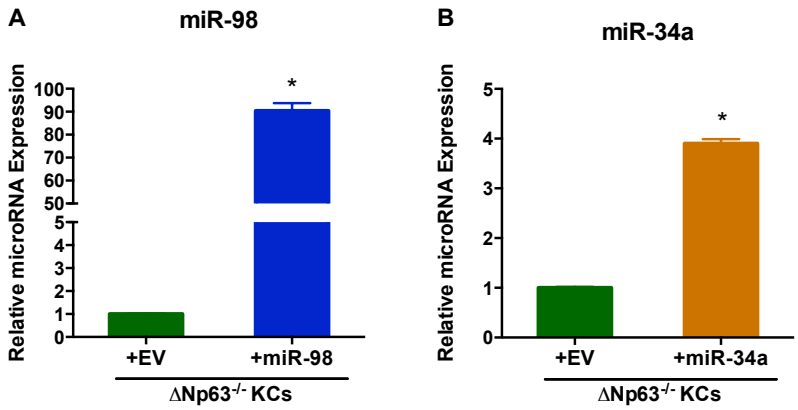

Figure 26. Confirmation of reintroduction and expression of miR-98 or miR-34a into ΔNp63$^{-/-}$ KCs. Taqman qRT-PCR of miR-98 (A) and miR-34a (B) in ΔNp63$^{-/-}$ KCs overexpressing either miR-98 (A) or miR-34a (B). Asterisks, p < 0.0001.

We saw that upon overexpression of miR-98, Twist1 protein levels were significantly reduced (Figure 27A) and upon overexpression of miR-34a, Lef1 protein levels were significantly reduced (Figure 27B).

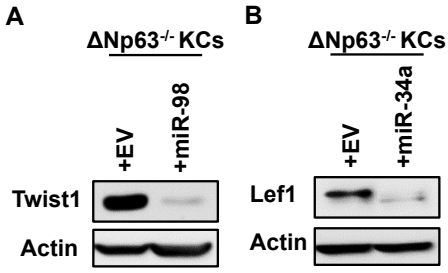

Figure 27. Change in Twist1 and Lef1 protein levels upon reintroduction of miR-98 or miR-34a. Western blot analysis of Twist1 (A) and Lef1 (B) expression levels in ΔNp63$^{-/-}$ KCs overexpressing either miR-98 (A) or miR-34a (B).

Finally, using a Boyden Chamber assay, we observed that overexpression of miR-98 or miR- 34a in ΔNp63$^{-/-}$ primary keratinocytes decreased migration and invasion thus partially reversing the phenotype observed after loss of ΔNp63 (Figure 28A-B).

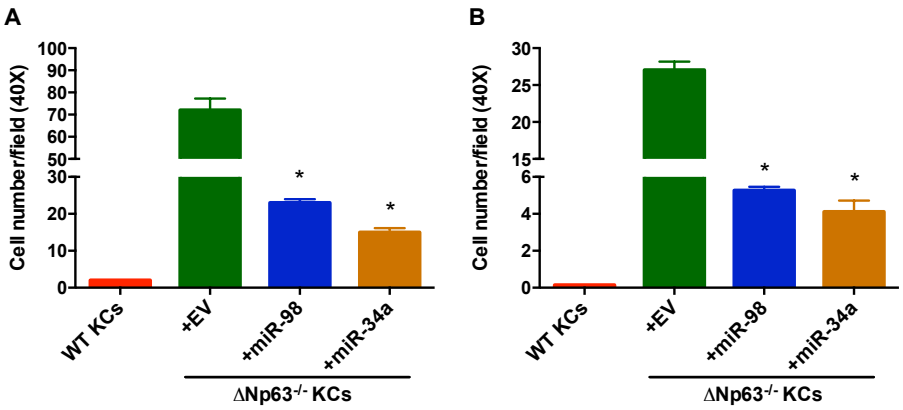

Figure 28. Migration (A) and invasion (B) assay of WT KCs and ΔNp63$^{-/-}$ KCs infected with either miR-98, miR-34a, or an empty vector. Asterisks, p < 0.0006.

Taken together, these data give evidence that ΔNp63 can modulate migration, invasion, and EMT by indirectly regulating Twist1 and Lef1 through miR-98 and miR-34a regulation, respectively.

In summary, we used *in vivo* mouse models and primary cells to explore mechanisms through which ΔNp63 could suppress tumor development and metastasis. We found that ΔNp63 loss leads to loss of epithelial characteristics and cell-cell contacts, and increased migration and invasion *in vitro*. This migration is erratic, as it appears that the cells are not coordinating well with each other. Using mouse models, we found evidence that an EMT program happens in the absence of ΔNp63 where levels of Twist1 and Lef1 are increased and cells could their cell-cell contacts and ability to coordinate, which could lead to the observed inability to close a wound gap. ΔNp63 appears to regulate Twist1 and Lef1 indirectly, in part through its role as a regulator of microRNA biogenesis. These findings suggest a potential mechanism that could explain the tumor phenotype observed in ΔNp63$^{+/-}$ mice.

Chapter 5

Chapter 5: Role of ΔNp63 in mammary gland development and tumorigenesis

The most common tumors present in $\Delta Np63^{+/-}$ mice were mammary adenocarcinomas. Breast cancer is the second cause of cancer related death among women, only behind lung cancer. In 2016 alone, approximately 250,000 cases of breast cancer will be diagnosed in the United States alone. Some of these tumors will respond to surgery, hormone therapy or other targeted therapies such as anti Her2 receptor therapy. However, significant subsets of tumors termed triple negative breast cancers have limited response to chemotherapy but no effective targeted therapies. These tumors tend to be poorly differentiated, aggressive, and metastatic, characteristics they share with the mammary tumors observed in $\Delta Np63^{+/-}$ mice. Because of these similarities, we sought to understand better what is the role of ΔNp63 in the mammary gland in the context of development as well as in breast cancer.

In the clinic, p63 is used in conjunction with a panel of cytokeratins as a biomarker to stage breast tumors. In this immunohistochemical stain, p63 is expressed in normal basal cells and gives information of whether a tumor has progressed beyond carcinoma in situ and is invading into the stroma (47, 48). Even though a total p63 antibody is used for this test, the main p63 isoform expressed in the basal cells is ΔNp63. Studies have confirmed that replacing the total p63 antibody with a ΔNp63 specific antibody produces comparable results (49). Beyond its use as a clinical biomarker, the role of ΔNp63 in breast cancer is not very clear. There are a number of contradicting reports that argue that ΔNp63 can function as an oncogene or as a tumor suppressor: some studies report that ΔNp63 functions oncogene by regulating stem cell properties, differentiation, and proliferation in basal type breast cancer (50-52), while others show that ΔNp63 can function as a tumor suppressor by working together with Brca1 and by modulating sensitivity to chemotherapy (53, 54). Even ΔNp63's role in mammary gland development is not well understood. Recent studies have shown that ΔNp63 is can promote mammary stem cells through the Wnt pathway (50) and

that it can control the process of lactogenesis (55). Still many questions remain. We sought to use our ΔNp63 conditional knockout mouse model to further understand the role of ΔNp63 in normal mammary gland development and answer some of these questions. This would enable us to learn about the role ΔNp63 plays in breast cancer by understanding better its physiological role. Our approach consisted of three main parts. First, we characterized mammary transplants of primary recombined ΔNp63 knockout mammary epithelial cells. Second, we sequenced RNA and microRNA isolated from the primary recombined ΔNp63 knockout mammary epithelial cells to obtain a global and unbiased picture of expression changes due to loss of ΔNp63 in this tissue. And finally, we sought to develop a new mouse model that would more closely represent the evolution and metastatic profile of human tumors.

5.1 Lack of ΔNp63 impairs ductal growth and branching in the developing mammary gland

Mammary gland development mostly occurs after birth and can be divided into four distinct phases. First, pubertal development starts once an organism reaches puberty, which is around 3 weeks in mice, and includes ductal elongation, tunneling of the terminal end buds through the mammary fat pad, and branching to form the final mammary ductal tree. Second, during pregnancy, the ducts undergo rapid proliferation to form terminal alveoli that are used in milk production. Third, after delivery, the luminal cells in the alveoli begin milk production, which will continue until nursing stops. And fourth, once the infants have been weaned off milk, the glands undergo a process called involution in which they revert to a pubertal state. Since $\Delta Np63^{-/-}$ mice die shortly after birth, we need to use alternative approaches to study the role of ΔNp63 in postnatal mammary development. To this end, we chose to take advantage of the ΔNp63 conditional knockout mouse.

To study the role of ΔNp63 in early pubertal mammary gland development, our approach was to transplant harvested mammary epithelial cells into the cleared fat pads of Severe Combined Immune Deficiency (SCID) mice and then study the resulting outgrowths (Figure 29).

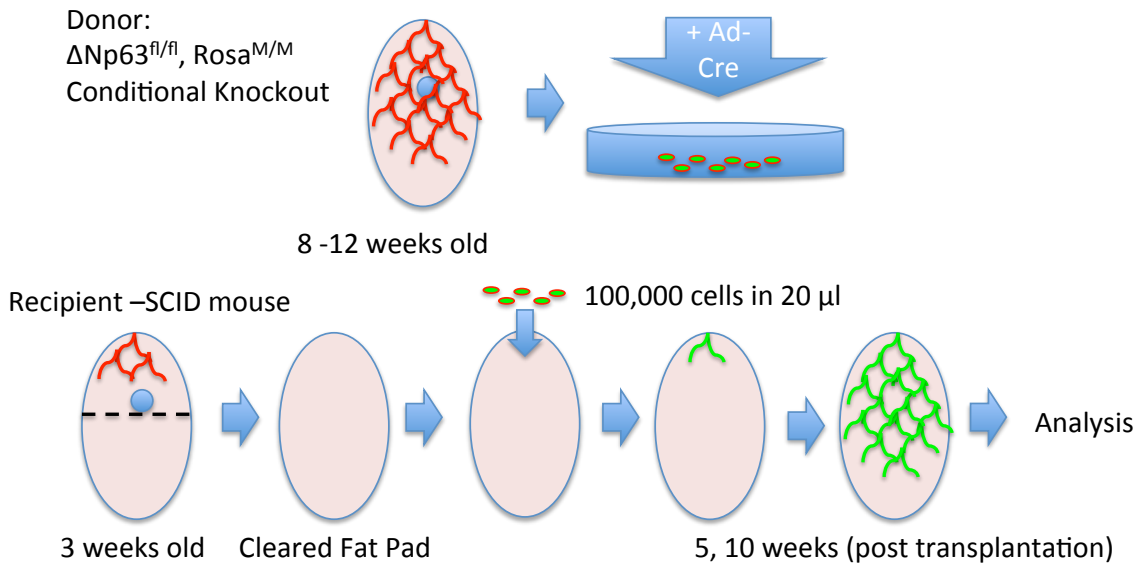

Figure 29. Mammary Transplantation Procedure Diagram.

The mammary epithelial cells were harvested from ΔNp63$^{fl/fl}$, Rosa$^{M/M}$ mice, which contain a reporter that turns the cells fluorescent green once recombination has happened. The protocol to obtain single mammary epithelial cells was as follows. We harvested the number 4 mammary glands from 8 week old ΔNp63$^{fl/fl}$, Rosa$^{M/M}$ mice, recorded their total weight, and minced the glands into 1 mm^3 portions for subsequent digestion. The digestion was done using a 1mg/ml collagenase solution for 2 hours, pipetting every 30 minutes to properly mix. A minimum of 10 ml of solution was used per 1 g of gland. Once the digestion was done, we washed the suspension with Hank's Buffered Saline Solution (HBSS) and performed 3 short 7-second centrifugation steps at 450g to enrich for mammary organoids. The organoids were then trypsinized with 1 ml 0.25% Trypsin/EDTA for up to 10 minutes,

pipetting every 2 minutes until a single cell suspension was observed under the microscope. Finally, the suspension was run through a 40 µm cell strainer to remove debris and resuspended on fresh mammary epithelial cell growth media (DMEM/F12 50:50, 10% FBS, 5µg/ml Insulin, 1µg/ml Hydrocortisone, 10 ng/ml EGF, 1% Pen/Strep) and counted to set up the recombination step. To induce recombination, we infected the harvested mammary epithelial cells in suspension with Adenovirus-Cre or Adenovirus-Empty as a control at a multiplicity of infection (MOI) of 50 for a total of 1 hour at 37°C, mixing the suspension every 15 minutes. The recombination efficiency after infection was consistently 95-100%. After infection, the cells were resuspended in a 50:50 HBSS:Growth Factor Reduced (GFR) Matrigel (Corning) mix, with 0.1% Trypan Blue. The Trypan Blue helped visualize the cells when transplanted. For the transplantation surgeries, 3 week-old SCID mice were anesthetized using intraperitoneal ketamine/xylazine (10mg/1mg per 10 g weight). We then proceeded to clear their 4th mammary fat pads of native gland and transplanted 100,000 cells in a 20 µl suspension. We transplanted the Adenovirus Cre treated cells ($\Delta Np63^{\Delta/\Delta}$) in the right side and the control Adenovirus Empty treated cells ($\Delta Np63^{fl/fl}$) on the left side of each mouse. The mice were monitored for a period of 5 or 10 weeks at which point the transplants were harvested and characterized.

The first step to characterize the transplants was to image the whole mounts upon harvest. Since the transplanted cells had the Rosa reporter, we used a fluorescent stereomicroscope to image the glands and record their fat pad coverage. There was a lot of variability from mouse to mouse. For the knockout ($\Delta Np63^{\Delta/\Delta}$) outgrowths, the maximum fat pad coverage was 13%, the minimum was 0% and the average was 1.9% at 5 weeks, while the maximum fat pad coverage was 29%, the minimum 0% and the average 7.6% at 10 weeks. For the control ($\Delta Np63^{fl/fl}$) outgrowths, the maximum fat pad coverage was 93%, the minimum was 1% and the average was 36.8% at 5 weeks, while the maximum fat pad coverage was 100%, the minimum 5% and the average 58.9% at 10 weeks. Overall, the

knockout outgrowths covered a significantly smaller percentage of the mammary fat pad when compared to the control outgrowths at both 5 and 10 weeks (Figures 30-31, Table 4).

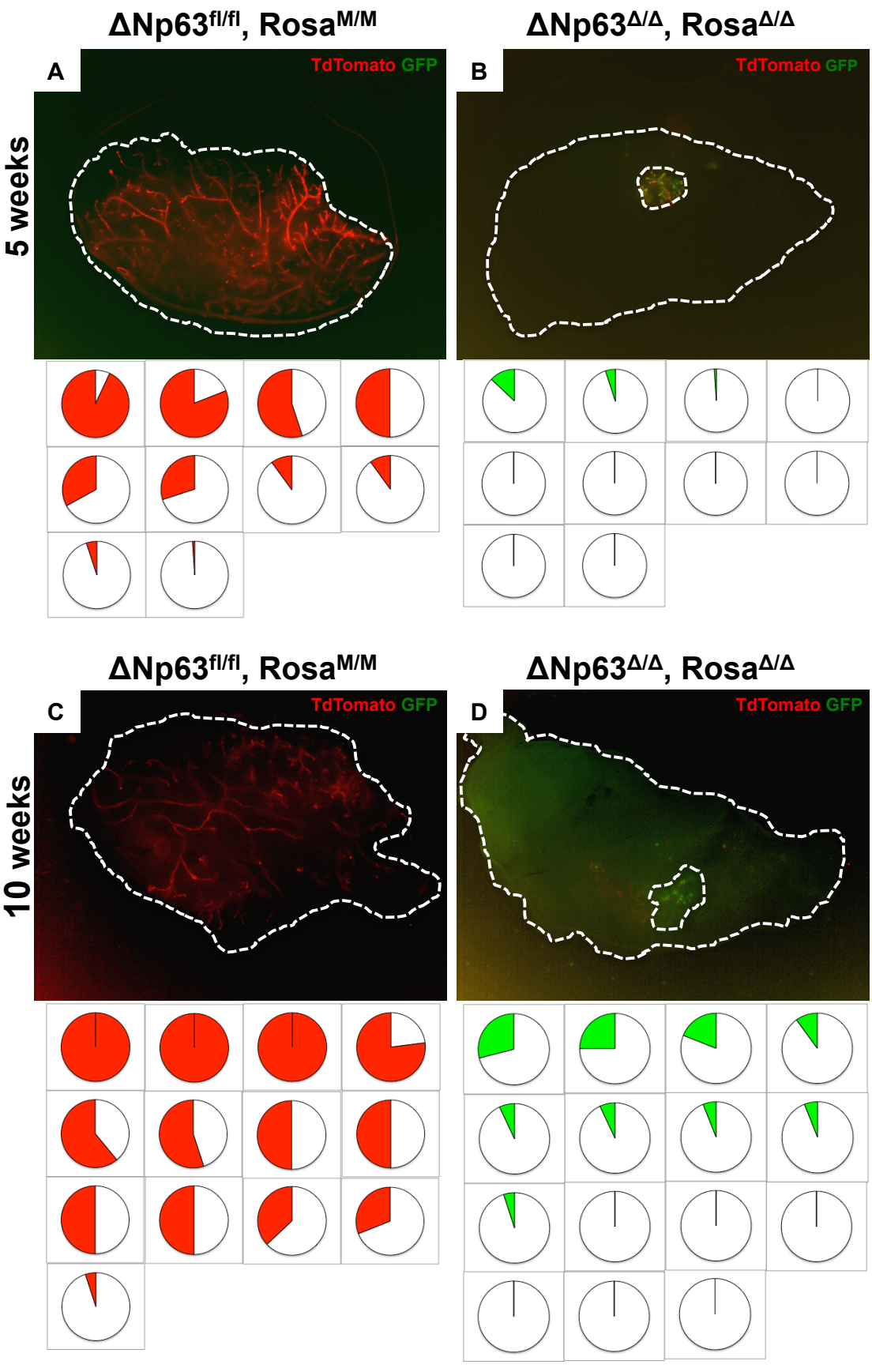
ΔNp63fl/fl, RosaM/M
ΔNp63Δ/Δ, RosaΔ/Δ
A
B
C
D
TdTomato GFP
5 weeks
10 weeks

Figure 30. Fluorescent whole mounts for 5 weeks and 10 weeks ΔNp63 mammary epithelial cell transplantations. The pie charts represent the percentage of the fat pad covered for each sample. ΔNp63$^{fl/fl}$, Rosa$^{M/M}$ outgrowths (Red), ΔNp63$^{Δ/Δ}$, Rosa$^{Δ/Δ}$ outgrowths (Green)

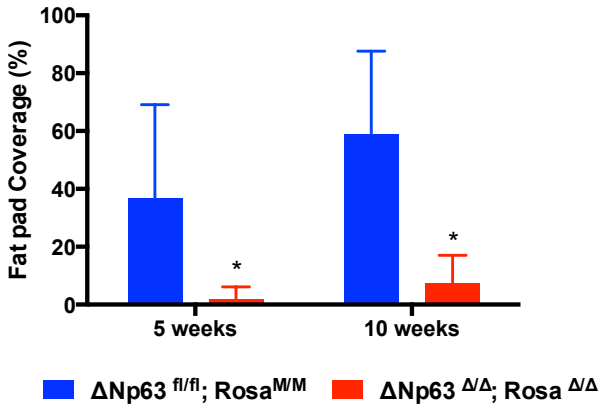

Figure 31. Percentage of fat pad coverage. Asterisks, for 5 weeks time point: p = 0.003, ΔNp63$^{fl/fl}$, Rosa$^{M/M}$ n = 10, ΔNp63$^{Δ/Δ}$, Rosa$^{Δ/Δ}$ n = 10. For 10 weeks time point: p < 0.0001 ΔNp63$^{fl/fl}$, Rosa$^{M/M}$ n = 13, ΔNp63$^{Δ/Δ}$, Rosa$^{Δ/Δ}$ n = 15.

Table 4. Percentage of mammary fat coverage for each knockout and control sample analyzed at the 5 week and 10 week time points.

5 week - ΔNp63 fl/fl, Rosa M/M		
Sample	**Percent Coverage**	
G848-RE	0% GFP	30% TdT
G920-LE	0% GFP	55% TdT
G921-LE	0% GFP	81% TdT
G922-LE	0% GFP	33% TdT
G924-LE	0% GFP	93% TdT
G1275-LE	0% GFP	1% TdT
G1277-LE	0% GFP	5% TdT
G1279-LE	0% GFP	10% TdT
G1310-LE	0% GFP	10% TdT
G1312-LE	0% GFP	50% TdT

5 week - ΔNp63 Δ/Δ, Rosa Δ/Δ		
Sample	**Percent Coverage**	
G848-LC	13% GFP	0% TdT
G920-RC	0% GFP	0% TdT
G921-RC	0% GFP	0% TdT
G922-RC	5% GFP	0% TdT
G924-RC	0% GFP	0% TdT
G1275-RC	1% GFP	1% TdT
G1277-RC	0% GFP	10% TdT
G1279-RC	0% GFP	0% TdT
G1310-RC	0% GFP	0% TdT
G1312-RC	0% GFP	0% TdT

10 week - ΔNp63 fl/fl, Rosa M/M		
Sample	**Percent Coverage**	
G591-RE	0% GFP	55% TdT
G847-RE	0% GFP	37% TdT
G976-LE	0% GFP	77% TdT
G977-LE	0% GFP	61% TdT
G980-LE	0% GFP	31% TdT
G1264-LE	0% GFP	50% TdT
G1265-LE	0% GFP	5% TdT
G1266-LE	0% GFP	50% TdT
G1267-LE	0% GFP	50% TdT
G1269-LE	0% GFP	100% TdT
G1270-LE	0% GFP	100% TdT
G1271-LE	0% GFP	100% TdT
G1273-LE	0% GFP	50% TdT

10 week - ΔNp63 Δ/Δ, Rosa Δ/Δ		
Sample	**Percent Coverage**	
G591-LC	19% GFP	32% TdT
G594-RC	29% GFP	0% TdT
G847-LC	6% GFP	0% TdT
G976-RC	6% GFP	6% TdT
G977-RC	5% GFP	5% TdT
G979-RC	7% GFP	7% TdT
G980-RC	7% GFP	7% TdT
G1264-RC	0% GFP	0% TdT
G1265-RC	25% GFP	25% TdT
G1266-RC	10% GFP	10% TdT
G1267-RC	0% GFP	0% TdT
G1269-RC	0% GFP	0% TdT
G1270-RC	0% GFP	0% TdT
G1271-RC	0% GFP	0% TdT
G1273-RC	0% GFP	0% TdT

The number of terminal end buds was significantly lower in the knockout outgrowths as well (Figure 32, Table 5).

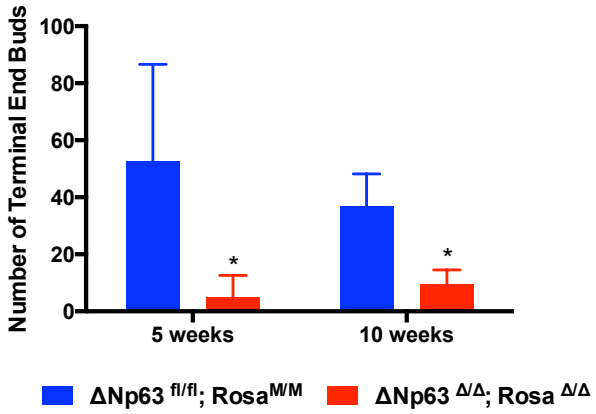

Figure 32. Number of terminal end buds per outgrowth. Asterisks, for 5 weeks time point: p = 0.015, ΔNp63$^{fl/fl}$, Rosa$^{M/M}$ n = 5, ΔNp63$^{Δ/Δ}$, Rosa$^{Δ/Δ}$ n = 5. For 10 weeks time point: p = 0.0002 ΔNp63$^{fl/fl}$, Rosa$^{M/M}$ n = 5, ΔNp63$^{Δ/Δ}$, Rosa$^{Δ/Δ}$ n = 7.

Table 5. Number of Terminal End Buds (TEBs) for each knockout and control sample at the 5 week and 10 week time points

5 week - ΔNp63 fl/fl, Rosa M/M	
Sample	**Number of TEBs**
G848-RE	95
G920-LE	82
G921-LE	25
G922-LE	41
G924-LE	20

5 week - ΔNp63 Δ/Δ, Rosa Δ/Δ	
Sample	**Number of TEBs**
G848-LC	18
G920-RC	0
G921-RC	0
G922-RC	6
G924-RC	0

10 week - ΔNp63 fl/fl, Rosa M/M	
Sample	**Number of TEBs**
G591-RE	38
G847-RE	40
G976-LE	18
G977-LE	49
G980-LE	39

10 week - ΔNp63 Δ/Δ, Rosa Δ/Δ	
Sample	**Number of TEBs**
G591-LC	6
G594-RC	12
G847-LC	5
G976-RC	5
G977-RC	16
G979-RC	7
G980-RC	16

Next we compared the histology of knockout and control outgrowth using hematoxylin and eosin (H & E) stained slides. We noticed that some of the knockout ducts were more disorganized and had an increased number of layers (Figure 33).

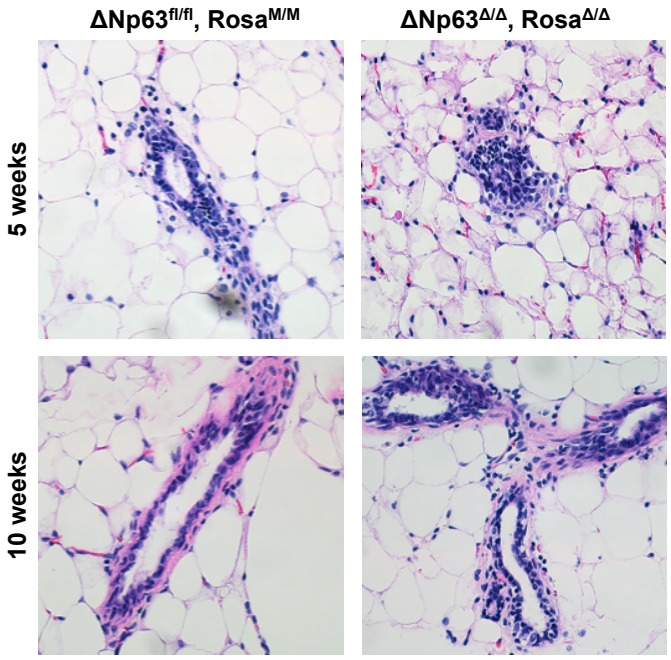

Figure 33. H&E staining of 5 week and 10 week post transplantation mammary outgrowths.

The normal mammary structure has two layers: a myoepithelial or basal layer adjacent to the stroma and a luminal layer that faces the lumen. To assess this further, we did immunofluorescence staining using anti - cytokeratin 18 antibody (rabbit 1:200) from Sigma to stain the luminal layer, anti- smooth muscle actin (SMA) antibody (mouse 1:250) from Sigma to stain the basal myoepithelial layer, and anti-GFP antibody (chicken 1:1000) to stain recombined cells to check for structural differences (Figures 34-35). We observed that there were in fact multiple luminal layers in the ΔNp63 knockout outgrowths at both the 5 week (Figure 34) and 10 week (Figure 35) time points and that the basal layer was disorganized in some of the 10-week ΔNp63 knockout samples (Figure 35).

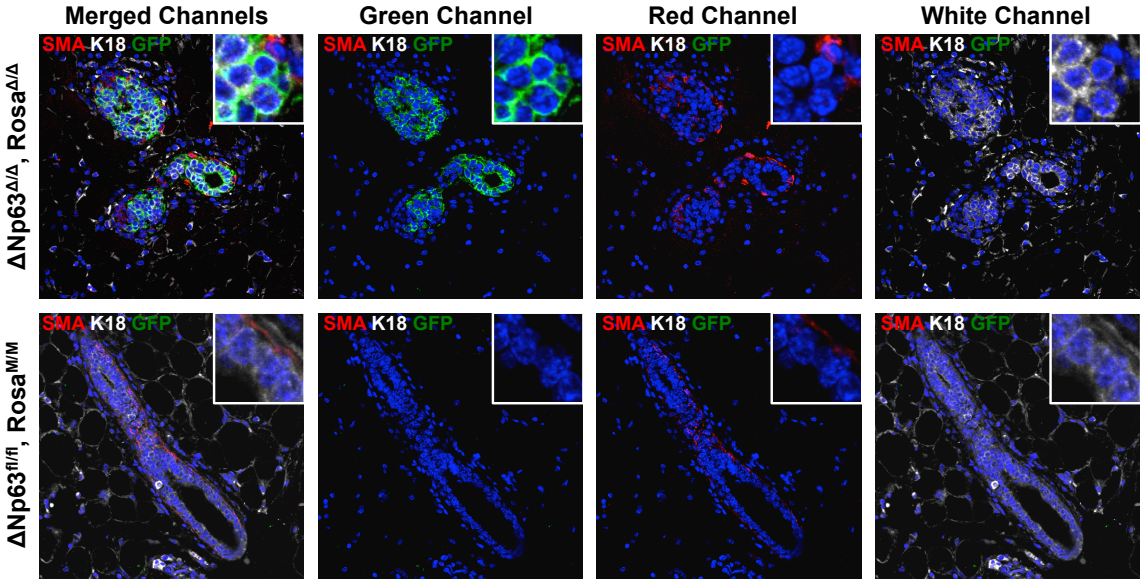

Figure 34. SMA and K18 expression in transplant outgrowths at 5 weeks. SMA (red), GFP (green), K18 (white), DAPI (blue). ΔNp63$^{fl/fl}$, Rosa$^{M/M}$ n = 5, ΔNp63$^{Δ/Δ}$, Rosa$^{Δ/Δ}$ n = 3

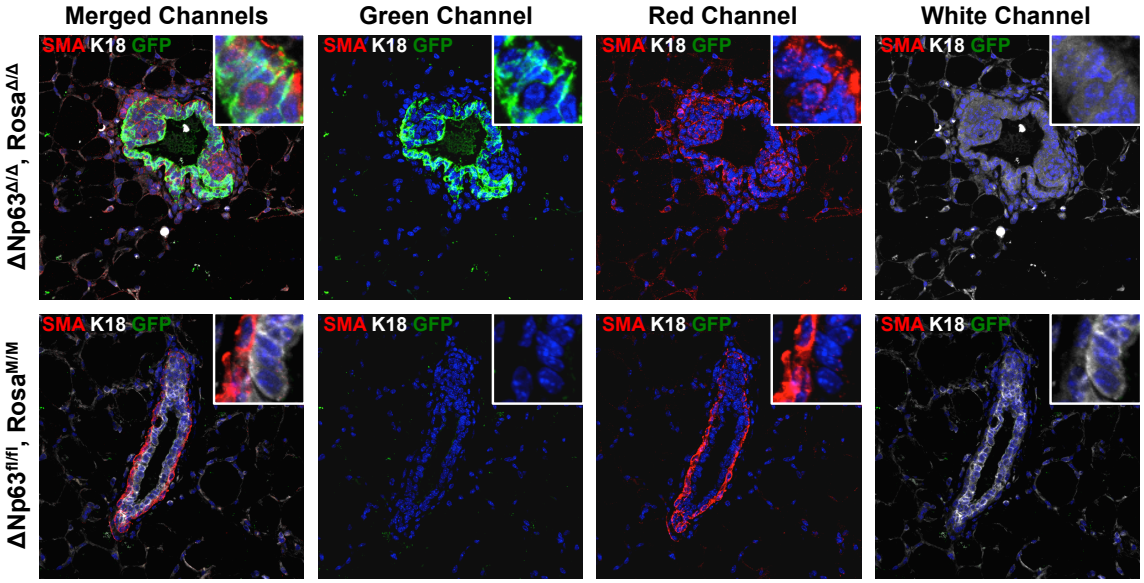

Figure 35. SMA and K18 expression in transplant outgrowths at 10 weeks. SMA (red), GFP (green), K18 (white), DAPI (blue). ΔNp63$^{fl/fl}$, Rosa$^{M/M}$ n = 6, ΔNp63$^{Δ/Δ}$, Rosa$^{Δ/Δ}$ n = 8

We quantified the disorganization and found that 5 weeks after surgery 69% of the observed knockout ducts had multiple luminal layers while none of the control ducts did. 10 weeks after surgery 72% of the observed knockout ducts had multiple luminal layers compared to only 8% of the observed control ducts (Figure 36, Table 6).

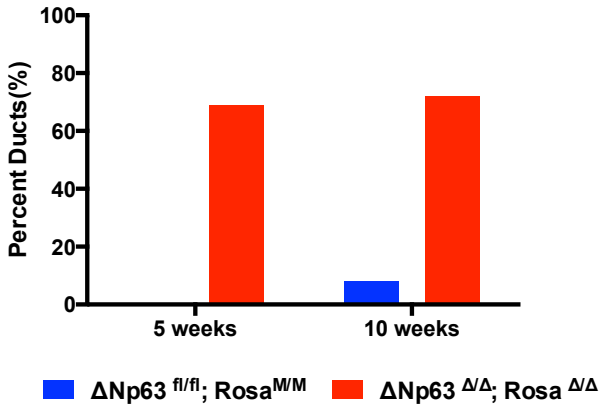

Figure 36. Percentage of ducts with multiple luminal layers. For 5 weeks time point: ΔNp63$^{fl/fl}$, Rosa$^{M/M}$ n = 5, ΔNp63$^{Δ/Δ}$, Rosa$^{Δ/Δ}$ n = 5. For 10 weeks time point: ΔNp63$^{fl/fl}$, Rosa$^{M/M}$ n = 5, ΔNp63$^{Δ/Δ}$, Rosa$^{Δ/Δ}$ n = 7.

56% of the knockout ducts appeared to have a discontinuous basal layer at the 5-week post surgery time point evidenced by lack of SMA signal around the ducts (Figure 37, Table 6).

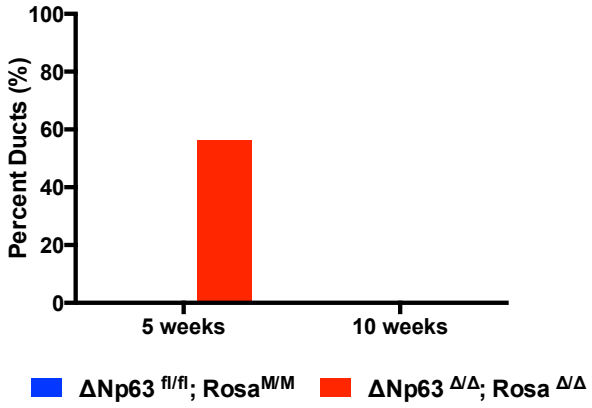

Figure 37. Percentage of ducts with a discontinuous basal layer evidenced by lack of SMA staining. For 5 weeks time point: ΔNp63$^{fl/fl}$, Rosa$^{M/M}$ n = 5, ΔNp63$^{Δ/Δ}$, Rosa$^{Δ/Δ}$ n = 5. For 10 weeks time point: ΔNp63$^{fl/fl}$, Rosa$^{M/M}$ n = 5, ΔNp63$^{Δ/Δ}$, Rosa$^{Δ/Δ}$ n = 7.

44% of the knockout ducts appeared to have a disorganized basal layer as well at the 10-week post surgery time point (Figure 38, Table 6).

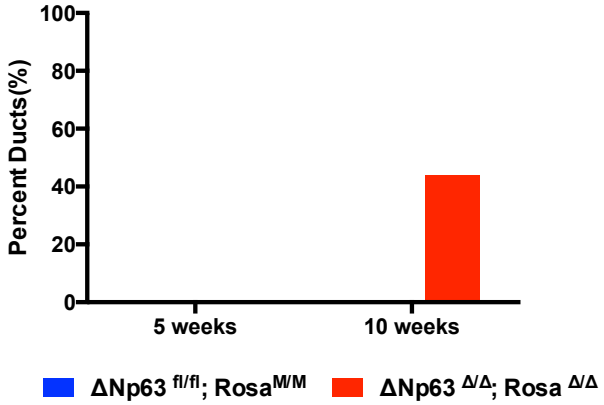

Figure 38. Percentage of ducts with a disorganized basal layer. For 5 weeks time point: ΔNp63$^{fl/fl}$, Rosa$^{M/M}$ n = 5, ΔNp63$^{Δ/Δ}$, Rosa$^{Δ/Δ}$ n = 5. For 10 weeks time point: ΔNp63$^{fl/fl}$, Rosa$^{M/M}$ n = 5, ΔNp63$^{Δ/Δ}$, Rosa$^{Δ/Δ}$ n = 7.

Table 6. Number of ducts with structural abnormalities per sample analyzed for the 5 week and 10 week time points

5 week - ΔNp63 fl/fl, Rosa M/M - Total Ducts: 5			
Sample	**Luminal Layer Thickening**	**Basal Layer Disorganization**	**Ducts without SMA staining**
G848-RE	0	0	0
G920-LE	0	0	0
G921-LE	0	0	0
G922-LE	0	0	0
G924-LE	0	0	0

5 week - ΔNp63 Δ/Δ, Rosa Δ/Δ - Total Ducts: 16			
Sample	**Luminal Layer Thickening**	**Basal Layer Disorganization**	**Ducts without SMA staining**
G848-LC	5	0	3
G920-RC	0	0	0
G921-RC	0	0	0
G922-RC	6	0	6
G924-RC	0	0	0

10 week - ΔNp63 fl/fl, Rosa M/M - Total Ducts: 12			
Sample	**Luminal Layer Thickening**	**Basal Layer Disorganization**	**Ducts without SMA staining**
G591-RE	0	0	0
G847-RE	1	0	0
G976-LE	0	0	0
G977-LE	0	0	0
G980-LE	0	0	0

10 week - ΔNp63 Δ/Δ, Rosa Δ/Δ - Total Ducts: 18			
Sample	**Luminal Layer Thickening**	**Basal Layer Disorganization**	**Ducts without SMA staining**
G591-LC	0	0	0
G594-RC	3	0	0
G847-LC	0	0	0
G976-RC	0	0	0
G977-RC	10	7	0
G979-RC	0	0	0
G980-RC	0	1	0

To get to the root of this phenotype, we planned a set of immunofluorescence experiments to look at changes in EMT, polarity, or stem cell properties as potential explanations.

One of the theories we had regarding the ductal disorganization was that, similarly to what we previously observed in culture and in the wound-healing model, ΔNp63 loss could le leading to unregulated EMT and affecting ductal development. We proceeded to stain the transplants for E-cadherin, but we were not able to detect any gross differences between E-

cadherin expression and localization between knockout and control glands at either 5 weeks (Figure 39) or 10 weeks (Figure 40).

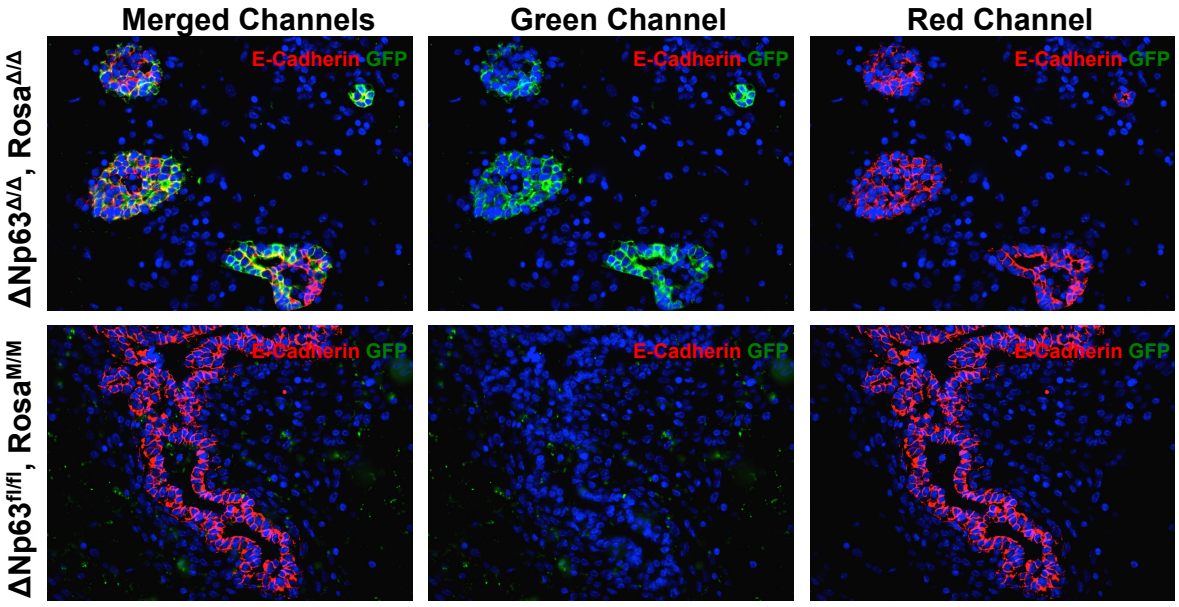

Figure 39. E-cadherin expression in transplant outgrowths at 5 weeks. E-cadherin (red), GFP (green), DAPI (blue). ΔNp63$^{fl/fl}$, Rosa$^{M/M}$ n = 3, ΔNp63$^{Δ/Δ}$, Rosa$^{Δ/Δ}$ n = 2.

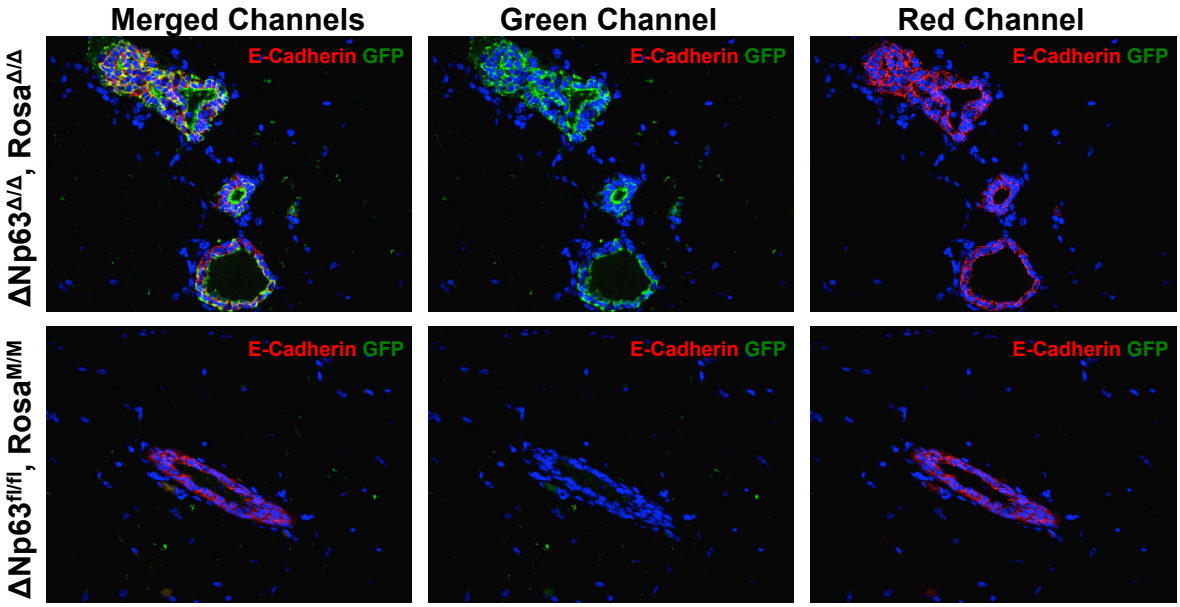

Figure 40. E-cadherin expression in transplant outgrowths at 10 weeks. E-cadherin (red), GFP (green), DAPI (blue). ΔNp63$^{fl/fl}$, Rosa$^{M/M}$ n = 5, ΔNp63$^{Δ/Δ}$, Rosa$^{Δ/Δ}$ n = 7.

This lead us to believe that the ΔNp63-regulated pathways leading to the observed phenotype could be different than those observed in the skin.

The next possibility we tested was whether a defect in polarity might be the cause for the observed disorganization. To test this, we performed immunofluorescence stains with Laminin (Rabbit 1:125, Sigma) antibody to look at the integrity of the basal membrane (Figure 41) and with Aquaporin 5 (AQP5) (Rabbit 1:100, Calbiochem) antibody to look at the orientation of the luminal cells regarding the lumen (Figures 42- 43).

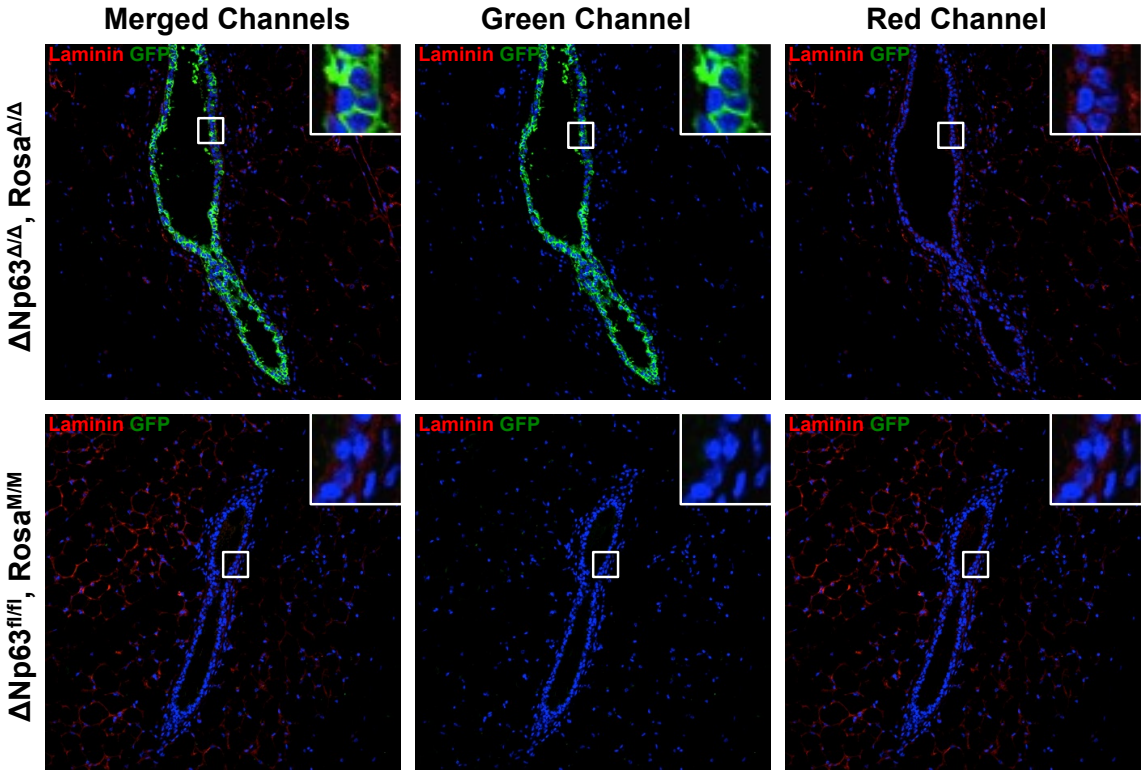

Figure 41. Laminin expression in transplant outgrowths at 10 weeks. Laminin (red), GFP (green), DAPI (blue). ΔNp63$^{fl/fl}$, Rosa$^{M/M}$ n = 2, ΔNp63$^{Δ/Δ}$, Rosa$^{Δ/Δ}$ n = 3.

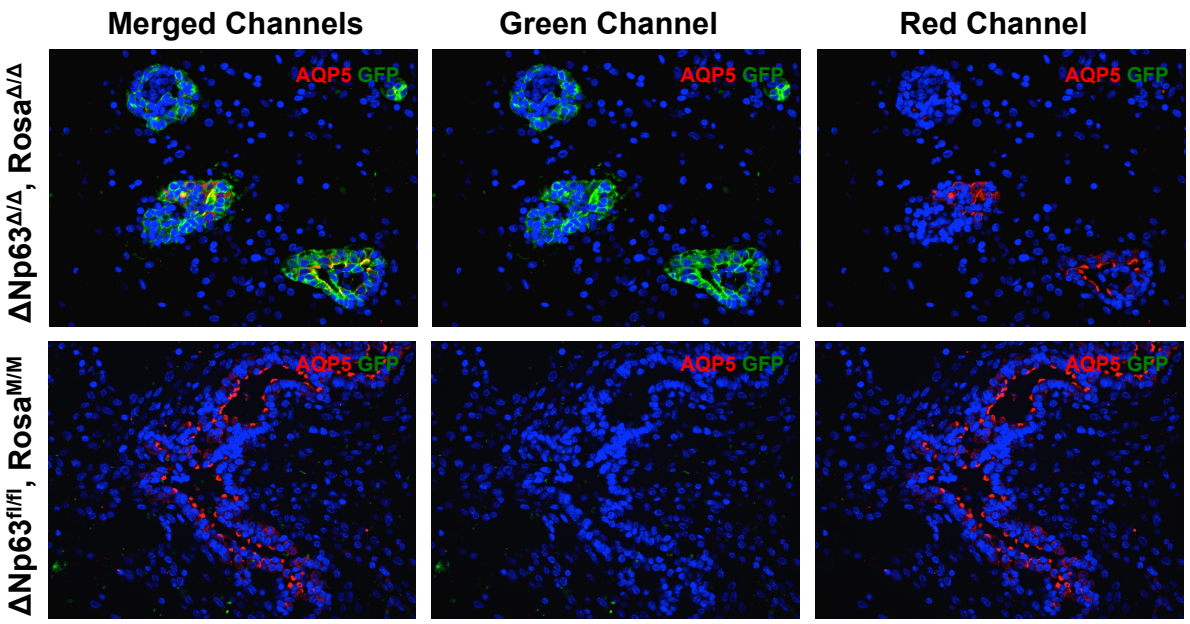

Figure 42. AQP5 expression in transplant outgrowths at 5 weeks. AQP5 (red), GFP (green), DAPI (blue). ΔNp63$^{fl/fl}$, Rosa$^{M/M}$ n = 2, ΔNp63$^{Δ/Δ}$, Rosa$^{Δ/Δ}$ n = 2.

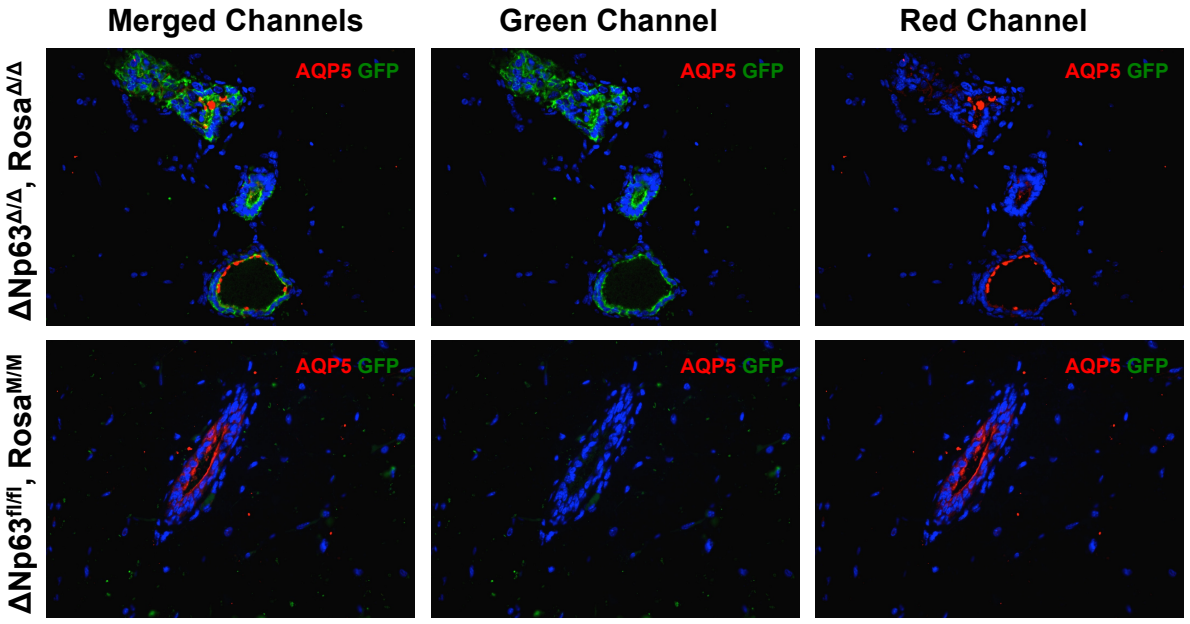

Figure 43. AQP5 expression in transplant outgrowths at 10 weeks. AQP5 (red), GFP (green), DAPI (blue). ΔNp63$^{fl/fl}$, Rosa$^{M/M}$ n = 4, ΔNp63$^{Δ/Δ}$, Rosa$^{Δ/Δ}$ n = 5.

We did not notice any differences in laminin expression, however we noticed that in 30% of the knockout ducts observed at 5 weeks and 10% of the knockout ducts observed at

10 weeks, AQP5 appeared to be mislocalized and not clearly delineating a lumen (Figure 44, Table 7).

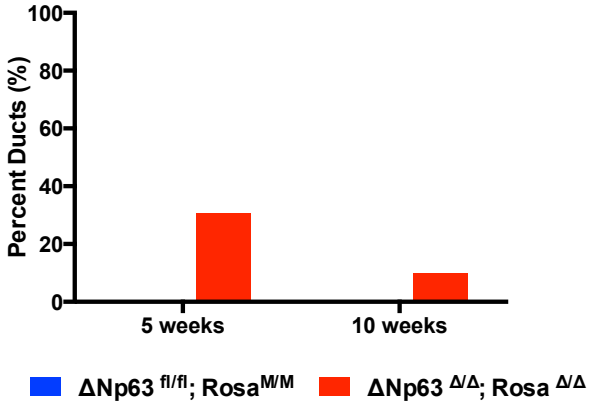

Figure 44. Percentage of ducts with AQP5 mislocalization. For 5 weeks time point: ΔNp63$^{fl/fl}$, Rosa$^{M/M}$ n = 2, ΔNp63$^{Δ/Δ}$, Rosa$^{Δ/Δ}$ n = 2. For 10 weeks time point: ΔNp63$^{fl/fl}$, Rosa$^{M/M}$ n = 4, ΔNp63$^{Δ/Δ}$, Rosa$^{Δ/Δ}$ n = 5

Table 7. Number of ducts with AQP5 mislocalization per sample analyzed for the 5 week and 10 week time points

5 week - ΔNp63 fl/fl, Rosa M/M - Total Ducts: 8		
Mouse ID	**Normal AQP5 Distribution**	**Mislocalized AQP5**
G848-RE	2	0
G922-LE	6	0

5 week - ΔNp63 Δ/Δ, Rosa Δ/Δ - Total Ducts: 13		
Mouse ID	**Normal AQP5 Distribution**	**Mislocalized AQP5**
G848-LC	1	2
G922-RC	8	2

10 week - ΔNp63 fl/fl, Rosa M/M - Total Ducts: 16		
Mouse ID	**Normal AQP5 Distribution**	**Mislocalized AQP5**
G847-RE	6	0
G976-LE	2	0
G977-LE	7	0
G1266-LE	1	0

10 week - ΔNp63 Δ/Δ, Rosa Δ/Δ - Total Ducts: 20		
Mouse ID	**Normal AQP5 Distribution**	**Mislocalized AQP5**
G594-RC	4	1
G847-LC	3	0
G977-RC	10	0
G979-RC	0	1
G1266-RC	1	0

This suggested that apical basal polarity may be affected in the knockout outgrowths, however the small number of 5 and 10 week knockout samples we had to analyze did not allow us to reach a definitive conclusion. More samples need to be collected to properly assess this potential phenotype.

The final possibility we tested for was whether the phenotype observed was due to a stem cell or differentiation defect. Previous studies in keratinocytes demonstrated that ΔNp63 regulates differentiation and its loss causes cells to acquire stem cell properties such as self-renewal (8). We performed two stains to test for stem cells: a Slug (goat 1:100, Santa Cruz) and Sox9 (Rabbit 1:100, Millipore) co-stain to identify mammary stem cells (reference) and a Ki67 (Rabbit 1:250, abcam) stain for active proliferation, one of the properties of cells with capacity for self-renewal. We did not find any Slug and Sox9 double stained cells (Figure 45).

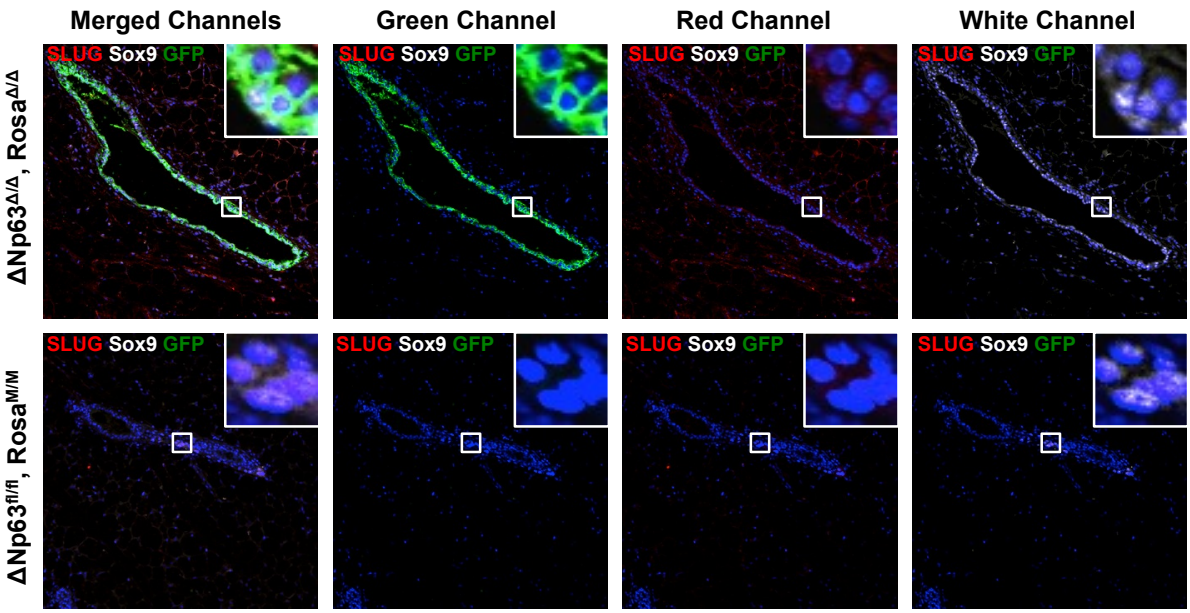

Figure 45. Slug and Sox9 co-expression in transplant outgrowths at 10 weeks. Slug (red), GFP (green), Sox9 (white), DAPI (blue). ΔNp63$^{fl/fl}$, Rosa$^{M/M}$ n = 2, ΔNp63$^{Δ/Δ}$, Rosa$^{Δ/Δ}$ n = 3.

The low total number of ducts we observed in our transplants together with the fact that stem cells marked by Slug and Sox9 double staining are only present in a small fraction of normal mammary ducts could explain why we failed to see any double positive nuclei in our samples. The results from the Slug and Sox9 staining were inconclusive so we could not draw any conclusions regarding ΔNp63's role in mammary stem cells. On the other hand, Ki67 staining demonstrated that cells in knockout ducts proliferate (Figure 46).

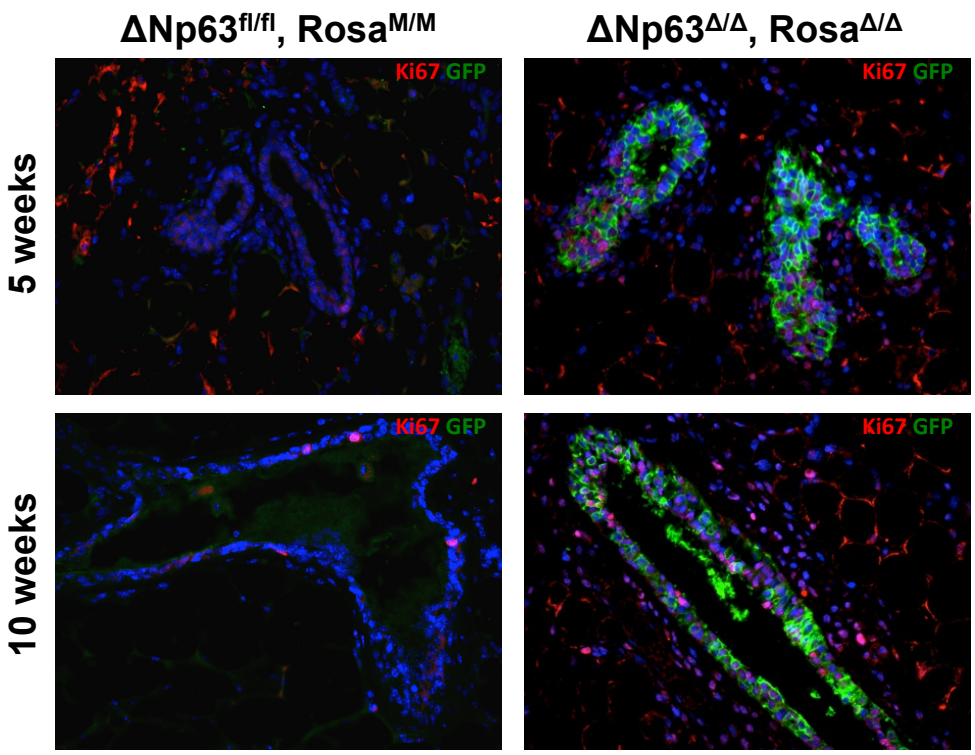

Figure 46. Assessment of proliferation in the ducts using Ki67 staining. Ki67 (Red), GFP (Green), DAPI (Blue). For 5 weeks time point: ΔNp63$^{fl/fl}$, Rosa$^{M/M}$ n = 15, ΔNp63$^{Δ/Δ}$, Rosa$^{Δ/Δ}$ n = 8. For 10 weeks time point: ΔNp63$^{fl/fl}$, Rosa$^{M/M}$ n = 15, ΔNp63$^{Δ/Δ}$, Rosa$^{Δ/Δ}$ n = 13

We proceeded to quantify the proliferation in the knockout and control ducts by counting the Ki67 positive nuclei and dividing by the total number of nuclei. Table 8 shows counts of Ki67 positive nuclei and total DAPI stained nuclei for each of the ducts quantified.

Table 8. Quantification of total nuclei (DAPI stain) and proliferating nuclei (Ki67 stain) in knockout and control ducts 5 and 10 weeks after transplantation.

5 week - ΔNp63 fl/fl, Rosa M/M			
Sample	**DAPI**	**Ki67+**	**Percent Positive**
G922-LE-1	300	109	36.33
G922-LE-2	130	67	51.54
G922-LE-3	100	60	60.00
G922-LE-4	76	1	1.32
G922-LE-5	214	99	46.26
G922-LE-6	255	35	13.73
G848-RE-1	99	6	6.06
G848-RE-2	116	0	0.00
G848-RE-3	150	14	9.33
G848-RE-4	42	4	9.52
G848-RE-5	226	51	22.57
G848-RE-6	179	31	17.32
G848-RE-7	120	23	19.17
G848-RE-8	86	34	39.53
G848-RE-9	45	17	37.78
Total			**24.70**
St dev			**19.16**

5 week - ΔNp63 Δ/Δ, Rosa Δ/Δ			
Sample	**DAPI**	**Ki67+**	**Percent Positive**
G922-RC-1	194	95	48.97
G922-RC-2	237	149	62.87
G922-RC-3	80	50	62.50
G848-LC-1	360	186	51.67
G848-LC-2	310	130	41.94
G848-LC-3	128	62	48.44
G848-LC-4	133	73	54.89
G848-LC-5	91	51	56.04
Total			**53.41**
St dev			**7.18**

10 week - ΔNp63 fl/fl, Rosa M/M			
Sample	**DAPI**	**Ki67+**	**Percent Positive**
G847-RE-1	85	15	17.65
G847-RE-2	156	18	11.54
G847-RE-3	184	24	13.04
G847-RE-4	97	6	6.19
G847-RE-5	168	4	2.38
G847-RE-6	132	17	12.88
G847-RE-7	124	27	21.77
G847-RE-8	123	24	19.51
G976-LE-1	52	4	7.69
G976-LE-2	72	8	11.11
G977-LE-1	218	5	2.29
G977-LE-2	143	4	2.80
G977-LE-3	118	5	4.24
G977-LE-4	45	5	11.11
G977-LE-5	112	3	2.68
Total			**9.79**
St dev			**6.47**

10 week - ΔNp63 Δ/Δ, Rosa Δ/Δ			
Sample	**DAPI**	**Ki67+**	**Percent Positive**
G847-LC-1	49	20	40.82
G847-LC-2	42	20	47.62
G847-LC-3	110	48	43.64
G591-LC-1	47	19	40.43
G591-LC-2	150	14	9.33
G591-LC-3	70	13	18.57
G591-LC-4	46	10	21.74
G977-RC-1	100	25	25.00
G977-RC-2	198	18	9.09
G977-RC-3	126	10	7.94
G594-RC-1	224	95	42.41
G594-RC-2	190	49	25.79
G594-RC-3	195	122	62.56
Total			**30.38**
St dev			**17.14**

In fact, it appeared that proliferation may be significantly increased upon ΔNp63 loss in the mammary gland (Figure 47). This appeared to contradict earlier findings where we saw that the knockout mammary ductal trees grew to cover significantly smaller portions of the mammary fat pad than the control glands, although it offers a potential explanation for the observed expansion of the luminal layer and disorganization of the basal layer. One possibility was that increased cell death or apoptosis accompanied the increased proliferation, but we were unable to perform a suitable apoptosis assay in our samples to test this theory. This is something that should be tested in the future.

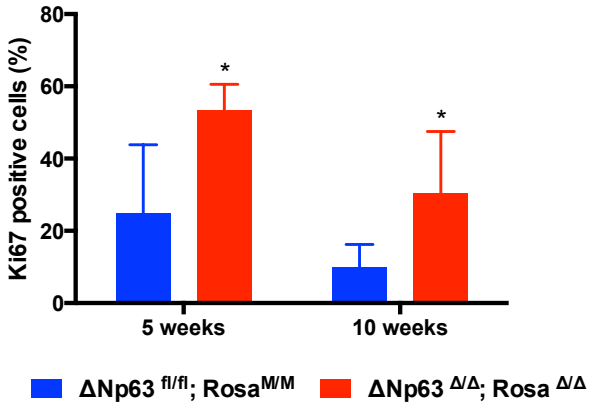

Figure 47. Quantification of proliferation cells per duct. Percentage of Ki67 positive cells per duct. For 5 weeks time point: p = 0.0006, ΔNp63$^{fl/fl}$, Rosa$^{M/M}$ n = 15, ΔNp63$^{Δ/Δ}$, Rosa$^{Δ/Δ}$ n = 8. For 10 weeks time point: p = 0.0002, ΔNp63$^{fl/fl}$, Rosa$^{M/M}$ n = 15, ΔNp63$^{Δ/Δ}$, Rosa$^{Δ/Δ}$ n = 13.

To expand on this, we designed a secondary transplantation experiment to more directly test the self-renewal capacity of ΔNp63 knockout mammary epithelial cells. We harvested mammary gland tissue from SCID mice transplanted with ΔNp63$^{Δ/Δ}$ and ΔNp63$^{fl/fl}$ mammary epithelial cells following the same protocol detailed previously and transplanted them into 3-week-old SCID mice. To obtain the donor tissue, we imaged the fat pads harvested from the primary transplants under a fluorescent stereomicroscope and used a #11 blade scalpel and fine forceps to isolate 1 mm^3 pieces of the glands for transplant. The

pieces were placed on HBSS and stored on ice until transplantation. We transplanted the mammary gland pieces by first clearing the fat pad and then placing the piece of donor mammary gland into a pocket within the remaining fat pad. $\Delta Np63^{\Delta/\Delta}$ donor glands were transplanted into the right side and control $\Delta Np63^{fl/fl}$ donor glands onto the left side of each mouse. 10 weeks after the surgeries, we harvested the secondary transplants and prepared fluorescent whole mounts. All of the $\Delta Np63^{fl/fl}$ secondary transplantations grew out to varying degrees. In contrast, none of the $\Delta Np63^{\Delta/\Delta}$ secondary transplantations grew out. The only visible signal under the fluorescent microscope corresponded to the transplanted donor piece (Figure 48, Table 9).

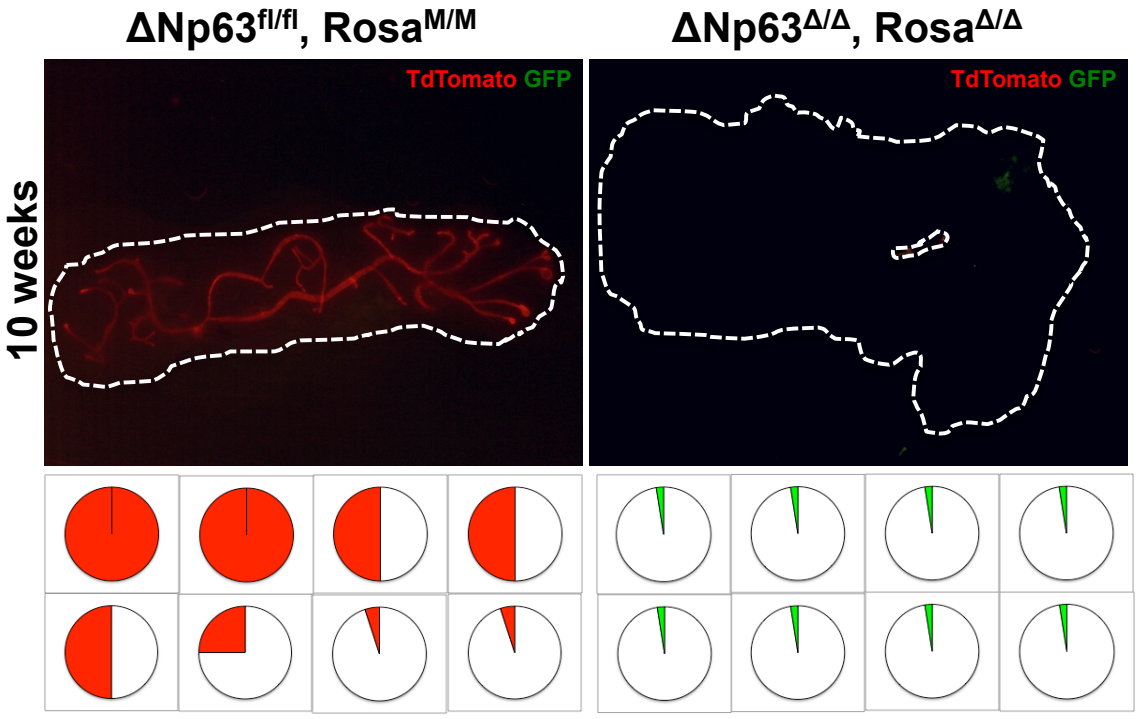

Figure 48. Fluorescent whole mounts for 10 weeks ΔNp63 secondary mammary transplantations. The pie charts represent the percentage of the fat pad covered for each sample. $\Delta Np63^{fl/fl}$, $Rosa^{M/M}$ outgrowths (Red), $\Delta Np63^{\Delta/\Delta}$, $Rosa^{\Delta/\Delta}$ outgrowths (Green)

Table 9. Percentage of mammary fat coverage for each knockout and control sample analyzed for the secondary Mammary Transplantations.

2ry Transplant - ΔNp63 fl/fl, Rosa M/M		
Mouse ID	**Percent Coverage**	
G1349-LE	0% GFP	100% TdT
G1350-LE	0% GFP	100% TdT
G1351-LE	0% GFP	50% TdT
G1352-LE	0% GFP	50% TdT
G1353-LE	0% GFP	50% TdT
G1354-LE	0% GFP	25% TdT
G1355-LE	0% GFP	5% TdT
G1356-LE	0% GFP	5% TdT

2ry Transplant - ΔNp63 Δ/Δ, Rosa Δ/Δ		
Mouse ID	**Percent Coverage**	
G1349-RC	2.5% GFP	2.5% TdT
G1350-RC	2.5% GFP	2.5% TdT
G1351-RC	2.5% GFP	2.5% TdT
G1352-RC	2.5% GFP	2.5% TdT
G1353-RC	2.5% GFP	2.5% TdT
G1354-RC	2.5% GFP	2.5% TdT
G1355-RC	2.5% GFP	2.5% TdT
G1356-RC	2.5% GFP	2.5% TdT

This suggests that ΔNp63 loss adversely affects the mammary stem cell population's capacity to self renew.

In summary, although we observed that transplanted ΔNp63 knockout mammary epithelial cells are able to grow into mammary ducts, the ducts that grow out have aberrant morphology. ΔNp63 knockout ducts have reduced fat pad coverage, reduced number of terminal end buds, and expanded luminal and basal layers. Further staining did not show any changes in E-cadherin, Laminin, or AQP5 expression or localization, which suggests that in the context of mammary gland development, ΔNp63 does not appear to regulate EMT or polarity. The ΔNp63 knockout ducts did not co express Slug and Sox9 which could

mean that ΔNp63 loss does not affect the stem cell population in the ducts, although it is not conclusive. On the other hand, secondary transplantation experiments demonstrated that ΔNp63 loss appears to impair the self-renewal capacity of the mammary epithelial cells, which could mean that the stem cell population is decreased or affected in some other way. Finally, proliferation was significantly increased in the ΔNp63 knockout ducts, even though this additional proliferation did not translate into ductal growth. This initial characterization presented a clear phenotype upon los of ΔNp63, but questions still remained regarding the pathways involved. We explored next whether the presence of ΔNp63 expressing cells could account for the phenotype involved and give us an idea of what might be happening.

5.2 ΔNp63 epithelial mammary epithelial cells have a competitive growth advantage when transplanted together with ΔNp63 knockout cells.

Previous publications had suggested that ΔNp63 was essential for mammary gland development. However, no definitive *in vivo* studies had been done to confirm this. Our data seems to suggest that ΔNp63 is essential for normal mammary gland development, but disorganized mammary ducts can grow in its absence. As detailed before, even in the apparent absence of ΔNp63, there were some ducts that retained the expected normal structure. We speculated this might be due to the presence of cells that had not undergone recombination and thus continued to express ΔNp63. To test this, we performed an immunofluorescence stain using RFP antibody (Rabbit 1:200, Rockland) to stain unrecombined cells in conjunction with GFP antibody to stain recombined cells and SMA antibody to stain the myoepithelial basal cells, which delineate the mammary ducts. We found out that at 5 weeks, all the observed ducts from knockout cell transplants appear to solely contain unrecombined basal cells (Figures 49, 51, Table 10).

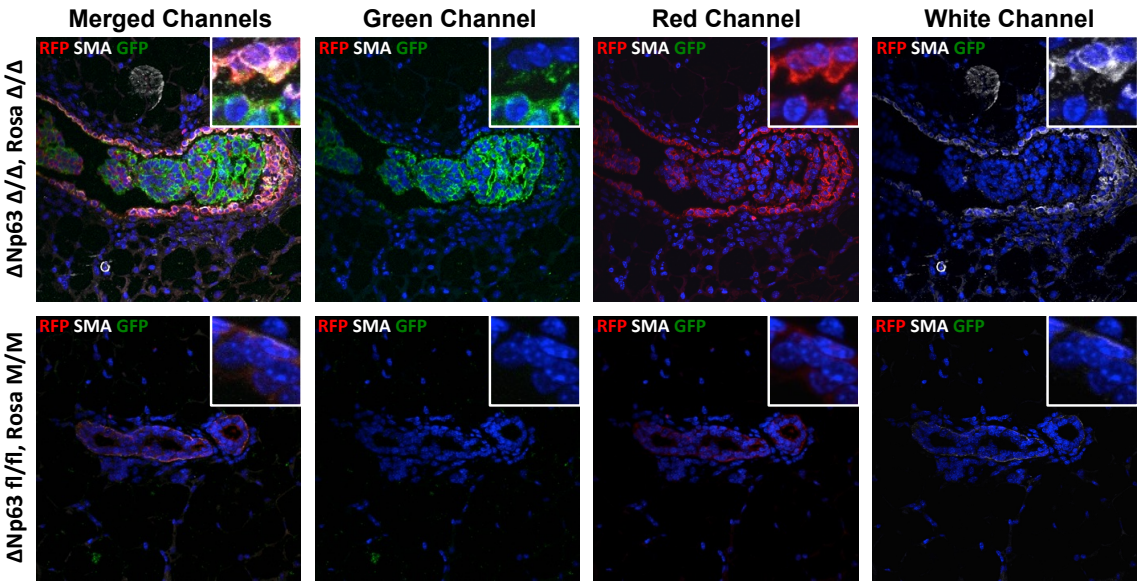

Figure 49. RFP, GFP and SMA co-expression in transplant duct outgrowths at 5 weeks. RFP (red), GFP (green), SMA (white), DAPI (blue). ΔNp63$^{fl/fl}$, Rosa$^{M/M}$ n = 2, ΔNp63$^{Δ/Δ}$, Rosa$^{Δ/Δ}$ n = 2 (17 ducts analyzed).

However, at 10 weeks, 41.66% of the observed ducts from knockout cell transplants contained only recombined basal cells (Figures 50, 51, Table 10).

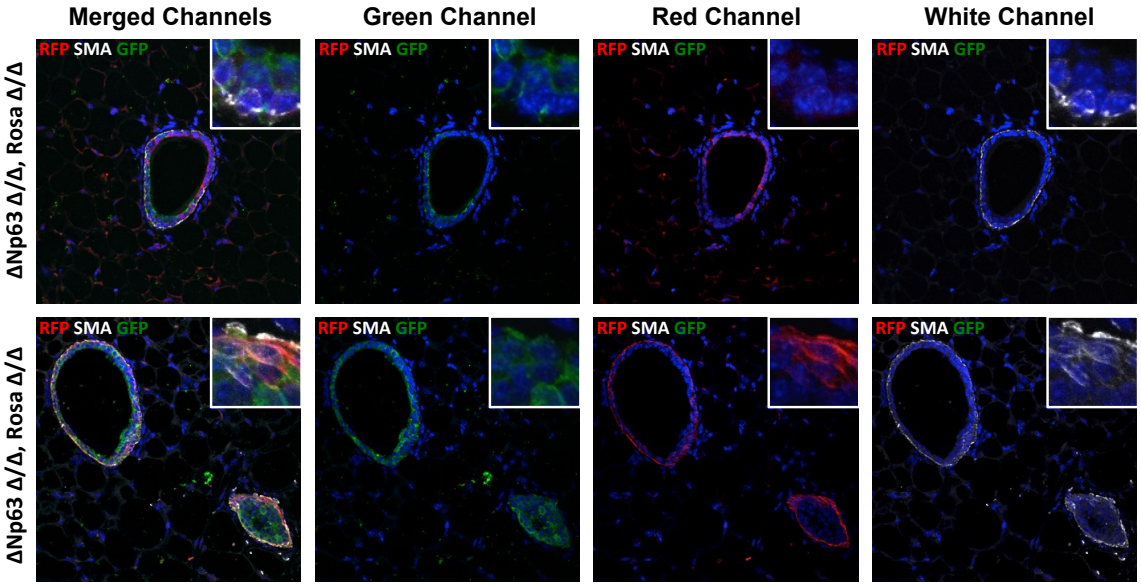

Figure 50. RFP, GFP and SMA co-expression in transplant duct outgrowths at 10 weeks. RFP (red), GFP (green), SMA (white), DAPI (blue). ΔNp63$^{Δ/Δ}$, Rosa$^{Δ/Δ}$ n = 2 (12 ducts analyzed).

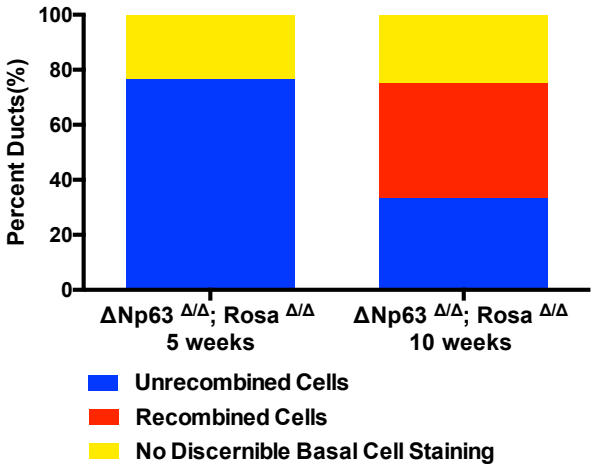

Figure 51. Quantification of the composition of the basal layer for 5 week and 10 week ΔNp63 transplantations. For 5 week old transplantations, 76.47% of ducts had basal layers composed solely of unrecombined cells, while for 10 week old transplantations, 41.66% of the ducts had basal layers composed solely of recombined basal cells, while 33.33% of the ducts had basal layers composed solely of unrecombined basal cells.

Table 10. Quantification of the composition of the basal layers per sample analyzed for the 5 week and 10 week time points.

5 week - ΔNp63 Δ/Δ, Rosa Δ/Δ - 17 total ducts			
Sample	**Only RFP+ basal layer**	**Only GFP+ basal layer**	**No Basal Layer Staining**
G848-LC	3	0	0
G922-RC	10	0	4

10 week - ΔNp63 Δ/Δ, Rosa Δ/Δ - 13 total ducts			
Sample	**Only RFP+ basal layer**	**Only GFP+ basal layer**	**No Basal Layer Staining**
G594-RC	1	4	0
G847-LC	3	1	3

This suggests that although cells that express ΔNp63 have a growth advantage, transplanted ΔNp63 knockout cells are still capable to grow into ducts although it might take longer for the ducts to grow out.

To further assess the apparent growth advantage of ΔNp63 expressing cells, we designed a transplantation experiment where known ratios of recombined and unrecombined cells would be transplanted to evaluate competition between ΔNp63 knockout and control mammary epithelial cells in a controlled *in vivo* environment. We transplanted 4 different combinations: 50% knockout cells with 50% control cells (50:50 $\Delta Np63^{\Delta/\Delta}$:$\Delta Np63^{fl/fl}$), 90% knockout cells with 10% control cells (90:10 $\Delta Np63^{\Delta/\Delta}$:$\Delta Np63^{fl/fl}$), 10% knockout cells with 90% control cells (10:90 $\Delta Np63^{\Delta/\Delta}$:$\Delta Np63^{fl/fl}$), and 100% knockout cells (100% $\Delta Np63^{\Delta/\Delta}$). These combinations would allow us to assess whether the knockout or the control cells have a competitive advantage and whether the disadvantaged cell group can overcome the disadvantage with increased cell numbers. The cells were transplanted in the same manner as detailed above: 100,000 cells in 20 µl 50:50 HBSS:GFR Matrigel mix, with the known ratios of cells transplanted on the right side, 100% control cells transplanted of the left. Glands were harvested 10 weeks after surgery. Unfortunately, only a few of the glands grew out so we could only draw some preliminary conclusions. For the 50:50 $\Delta Np63^{\Delta/\Delta}$:$\Delta Np63^{fl/fl}$ group, three of the transplants grew out: one of them had a 50% fat pad coverage with mixed growth (ducts were double positive for GFP (recombined cells) and Tomato (unrecombined cells)) while the other two only had unrecombined growth (Figure 52).

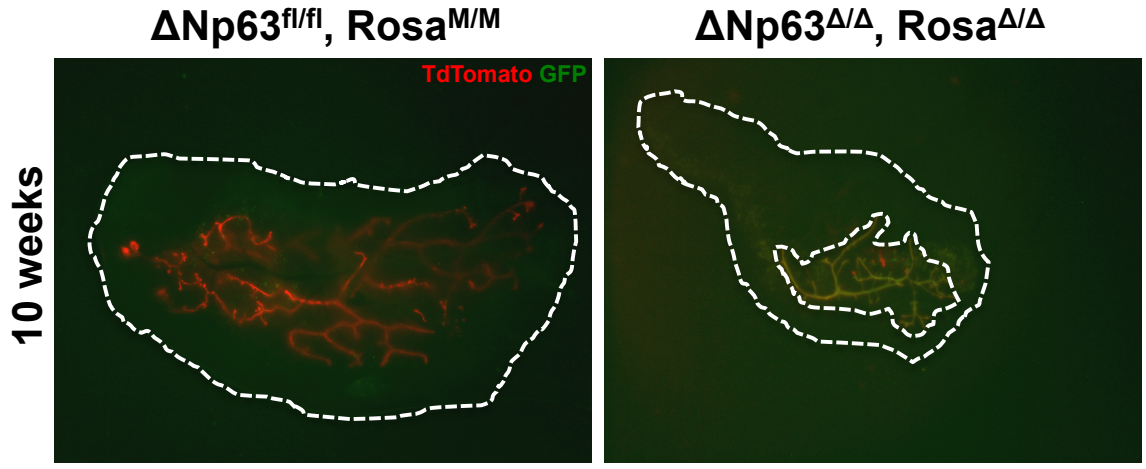

Figure 52. Fluorescent whole mounts for 10 weeks 50:50 ΔNp63$^{Δ/Δ}$:ΔNp63$^{fl/fl}$ mammary transplantations. ΔNp63$^{fl/fl}$, Rosa$^{M/M}$ outgrowths (Red), ΔNp63$^{Δ/Δ}$, Rosa$^{Δ/Δ}$ outgrowths (Green)

For the 90:10 ΔNp63$^{Δ/Δ}$:ΔNp63$^{fl/fl}$ group, three transplants grew out as well: one had 95% unrecombined cells and 5% recombined cells while the other two had only unrecombined cells (Figure 53).

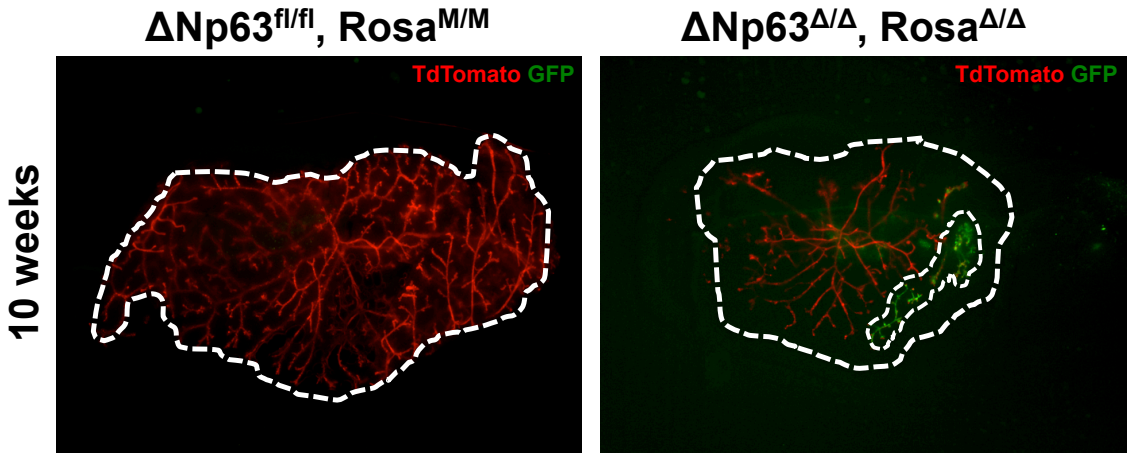

Figure 53. Fluorescent whole mounts for 10 weeks 90:10 ΔNp63$^{Δ/Δ}$:ΔNp63$^{fl/fl}$ mammary transplantations. ΔNp63$^{fl/fl}$, Rosa$^{M/M}$ outgrowths (Red), ΔNp63$^{Δ/Δ}$, Rosa$^{Δ/Δ}$ outgrowths (Green)

For the 10:90 ΔNp63$^{Δ/Δ}$:ΔNp63$^{fl/fl}$ group, only two transplants grew out and both had only unrecombined cells. Taken together, these data suggest that control mammary epithelial cells that express ΔNp63 have a growth advantage that is not handily overcome by ΔNp63 knockout cells.

In summary, we demonstrated that mammary epithelial cells that express ΔNp63 have a competitive growth advantage and the presence of ΔNp63 expressing myoepithelial basal cells could promote the organization of ΔNp63 into ducts. A small percentage of unrecombined cells that continued to express ΔNp63 even after the infection could be the

reason we saw the ΔNp63$^{\Delta/\Delta}$ outgrowths stall. Still, this does not fully explain the observed phenotype, particularly because we did observe ducts that only had recombined basal cells.

Because we were not able to account for a mechanism to explain the mammary gland development phenotype observed in the absence of ΔNp63, we decided to sequence the mRNA and microRNA of ΔNp63 knockout and wild type mammary epithelial cells, to obtain a more complete, unbiased picture of expression changes due to loss of ΔNp63 in the mammary gland.

5.3 mRNA and microRNA sequencing of ΔNp63 knockout and wild type mammary epithelial cells presents a complex network of pathways affected upon ΔNp63 loss.

Biological systems are very complex and interconnected. Advances in sequencing and bioinformatics have helped us make considerable inroads understanding complex biological interactions. RNA and microRNA sequencing allows us to obtain a comprehensive picture of the gene and microRNA expression profile of a specific cell type. It also allows us to establish correlations with sequencing data from human tumors and determine common elements that could give an idea of how a gene is involved in cancer. In our case, sequencing coupled with bioinformatic analysis allowed us to compare the expression profiles of knockout mammary epithelial cells with wild type mammary epithelial cells profiles, determine which pathways and mechanisms are altered, and how they relate to the observed phenotype.

To obtain mammary epithelial cells for sequencing, we harvested the 4th mammary gland pair from wild type mice and from ΔNp63$^{fl/fl}$, Rosa$^{M/M}$ mice and isolated the mammary epithelial cells following the protocol outlined before. To generate ΔNp63 knockout (ΔNp63$^{\Delta/\Delta}$) cells, we infected ΔNp63$^{fl/fl}$, Rosa$^{M/M}$ with adenovirus Cre following the same infection protocol as the transplants as and plated them in monolayer culture without feeders for 3 days. We used EpiCult B-Basal Medium (Stem Cell Technologies) for these cultures.

After 3 days, the recombination was complete, evidenced by GFP signal under the microscope. The cells were then harvested and we performed RNA extraction. In order to obtain enough material to extract the RNA, pools of 3-4 mice were plated together. At least five 10 cm dishes per sample were required in order to be able to harvest enough RNA for sequencing. The RNA extraction was done using Trizol and the PureLink RNA extraction kit (Ambion), modified to collect small RNAs, which gave us the best combination of yield and quality. We checked the yield and purity with a Nanodrop spectrophotometer and did an RT-PCR for ΔNp63 to confirm knockout (Figure 54). Although there was variability in the ΔNp63 mRNA expression among the three different $\Delta Np63^{\Delta/\Delta}$ samples, their levels were reduced when compared to the wild type samples so they were all sent for sequencing. We were unable to test protein expression because we only obtained enough material to send for sequencing.

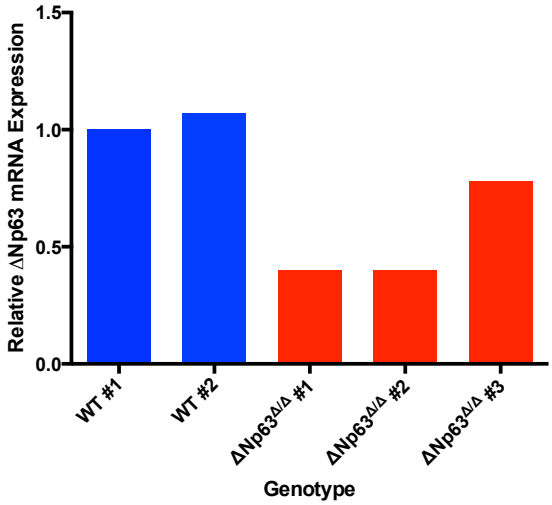

Figure 54. Relative expression of ΔNp63 in the sequencing samples. qRT PCR to verify knockout of ΔNp63 in the mammary epithelial cell sequencing samples after infection. WT, wild type.

Once we handed the samples to the sequencing core, they tested the quality and yield of the RNA once more, found it to be optimal, and sequenced the samples. Once the

sequencing was completed, the data was analyzed. Three independent pools of $\Delta Np63^{\Delta/\Delta}$ samples and two wild-type samples were used for the analysis.

We set the criteria for significance at a fold change of 1.5 with a p value equal or less than 0.05 between $\Delta Np63^{\Delta/\Delta}$ and wild type samples. Based on these criteria we identified 1247 genes that were differentially expressed when comparing $\Delta Np63^{\Delta/\Delta}$ to wild type, 691 whose expression was decreased and 556 whose expression was increased (Appendix Table 1).

For microRNAs, we identified 34 microRNAs that were differentially expressed when comparing $\Delta Np63^{\Delta/\Delta}$ to wild type, 12 that were down regulated and 22 that were up regulated (Appendix Table 2).

We performed unsupervised hierarchical clustering of the results and for both the mRNA and microRNA sequencing, the three $\Delta Np63^{\Delta/\Delta}$ samples clustered together and were different from the two wild type samples that clustered together as well (Figures 55-56).

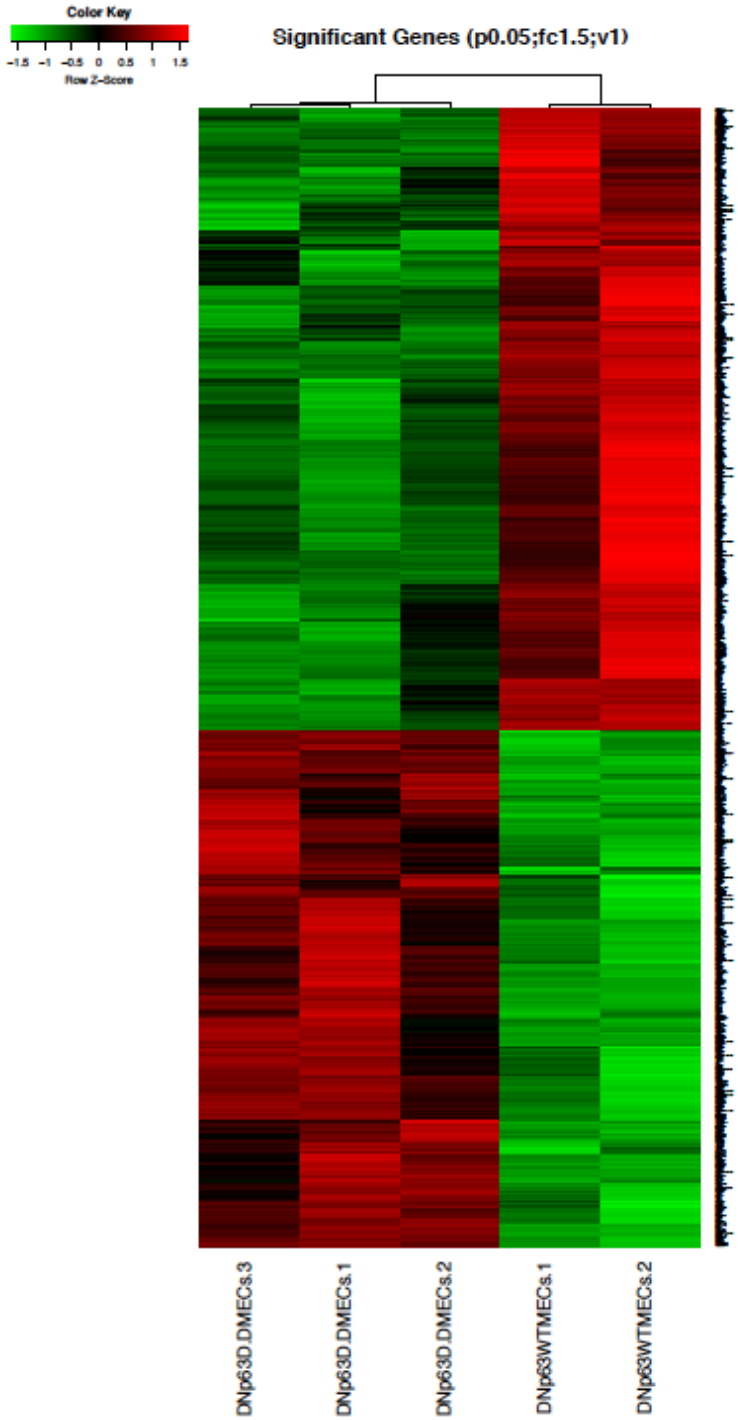

Figure 55. Unsupervised hierarchical clustering of mRNA sequencing results from ΔNp63 knockout and wild type mammary epithelial cells. DNp63D.DMECs = $\Delta Np63^{\Delta/\Delta}$ mammary epithelial cells, DNp63WTMECs = wild type mammary epithelial cells.

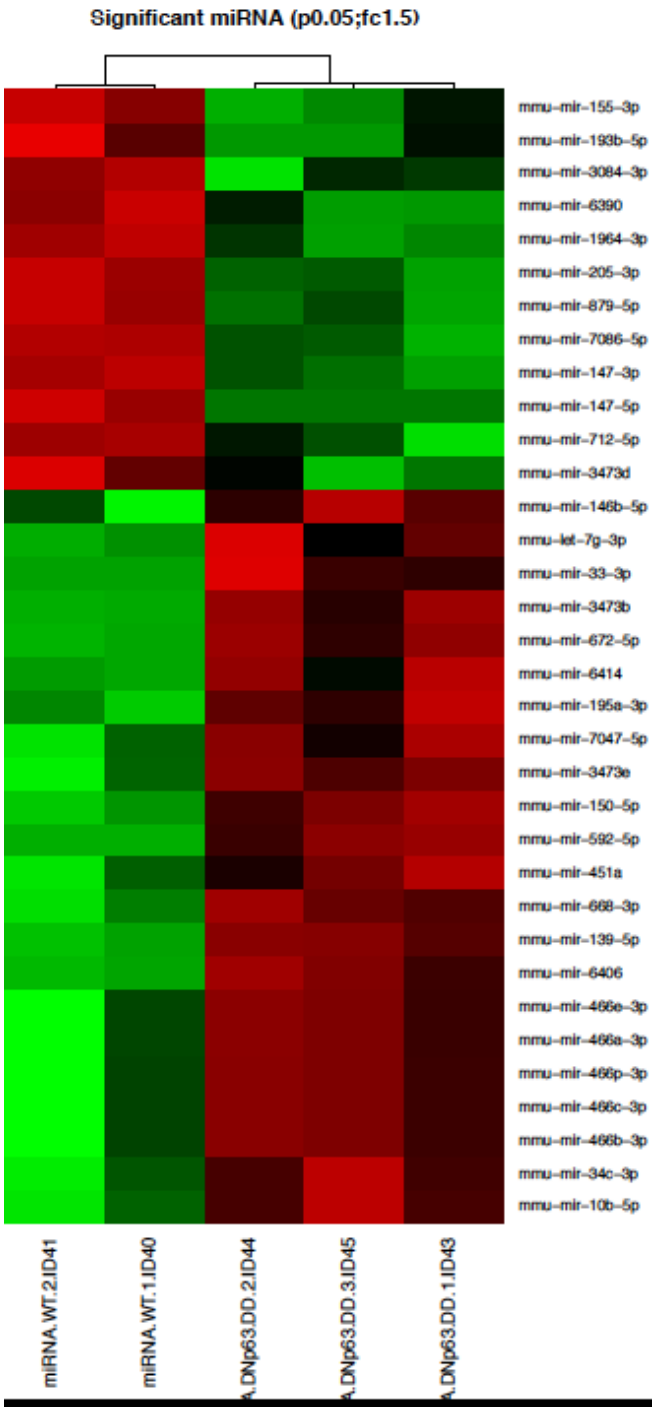

Figure 56. Unsupervised hierarchical clustering of microRNA sequencing results from ΔNp63 knockout and wild type mammary epithelial cells. A.DNp63DD = $\Delta Np63^{\Delta/\Delta}$ mammary epithelial cells, miRNAWT = wild type mammary epithelial cells.

To understand the role of these differentially expressed genes, we did pathway analysis and identified 553 pathways that were significantly altered upon loss of ΔNp63.

Finally, we did functional pair analysis using the mRNA and microRNA sequencing data to understand the relationship between the identified microRNAs and genes, and found 6 microRNAs whose targets were decreased while they were increased and 3 microRNAs whose targets were increased while they were decreased (Appendix Table 3).

This preliminary analysis gave us the big picture regarding the expression changes that occur in mammary epithelial cells upon loss of ΔNp63. Our next step was to validate these sequencing results. To this end, we developed an algorithm to narrow down the list of genes and microRNAs and select a relevant subset to begin the validation.

To select genes and microRNAs for validation, we developed an algorithm that takes into account, the sequencing results, the phenotype we observed with our *in vivo* transplantation experiments, and the current published literature regarding genes of interest (Figure 57).

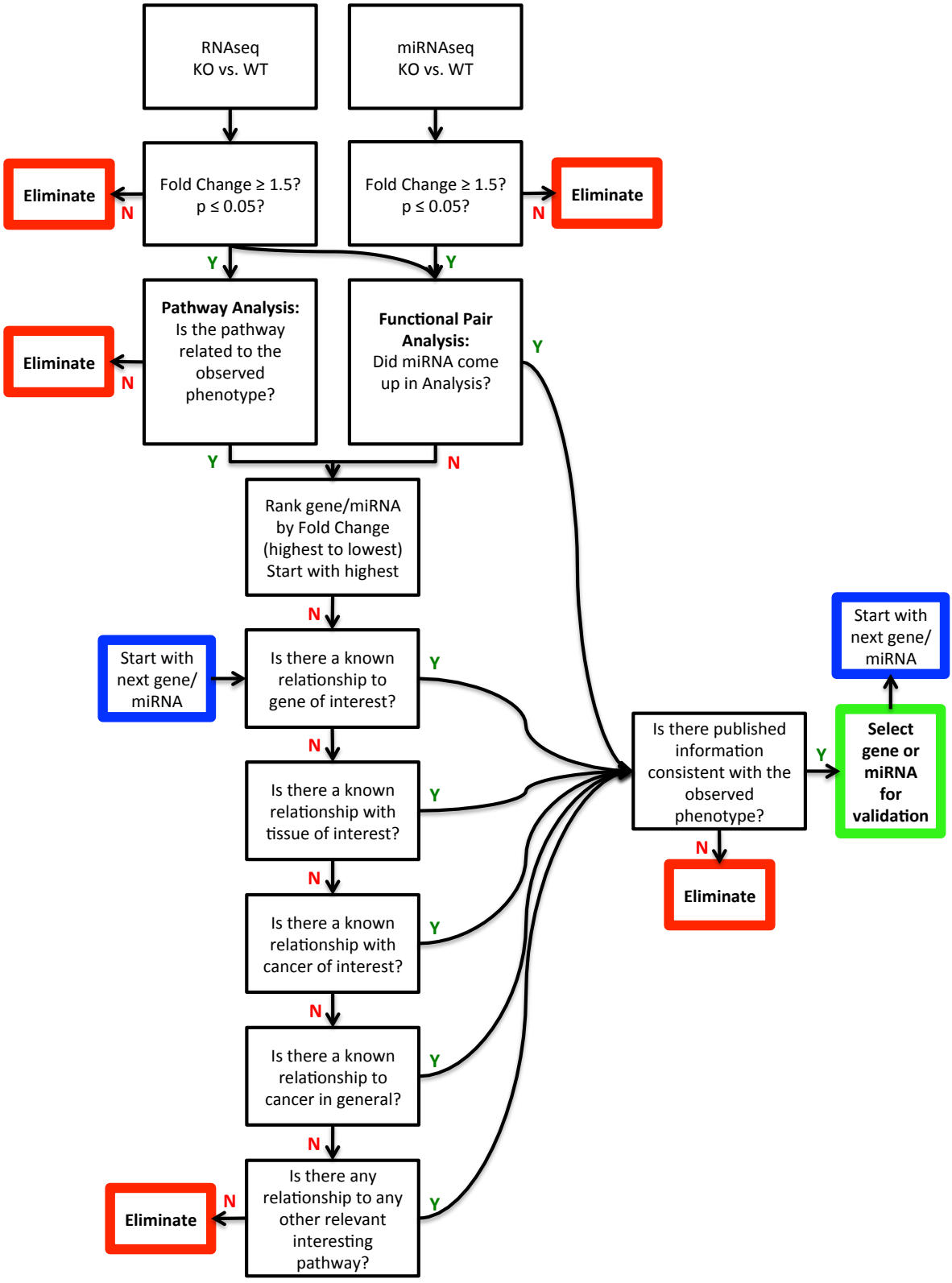

Figure 57. Algorithm used to narrow down sequencing results and select candidates for validation.

We first focused pathways that came up on the pathway analysis could potentially explain the phenotype observed in our previous *in vivo* experiments. The pathways we identified were apical junction, cell adhesion, cell fate commitment, cell junction organization, cell migration, cell proliferation, EMT, estrogen response, focal adhesion, gap junctions, actin cytoskeleton regulation, small GTPase signal transduction, TGF-β signaling, and pathways in cancer. There were a total of 114 genes in these pathways, which we then ran through our algorithm to narrow them further down (Table 11).

Table 11. Differentially expressed genes in selected pathways.

Gene	**Pathway**	**fold change**	**p value**
ldlrap1	Apical Junction	1.67	0.024
mapk11	Apical Junction	1.81	0.001
nrtn	Apical Junction	1.63	0.029
adam10	Cell Adhesion	0.53	0.023
lgals7	Cell Adhesion	0.17	0.007
rasa1	Cell Adhesion	0.49	0.024
esam	Cell Adhesion	3.31	0.045
l1cam	Cell Adhesion	1.81	0.002
ifrd1	Cell Fate Commitment	0.55	0.041
notch4	Cell Fate Commitment	1.69	0.016
cldn5	Cell Junction Organization	5.64	0.017
col17a1	Cell Junction Organization	0.27	0.005
pvrl2	Cell Junction Organization	1.65	0.005
tesk1	Cell Junction Organization	1.82	0.003
clic4	Cell Migration	0.6	0.011
trip6	Cell Migration	1.56	0.016
abi1	Cell Proliferation	0.58	0.018
bmpr2	Cell Proliferation	0.55	0.011
cdh13	Cell Proliferation	2.62	0.017
cdkn2d	Cell Proliferation	1.6	0.042
cul5	Cell Proliferation	0.49	0.036
cxcr2	Cell Proliferation	2.14	0.02
jag2	Cell Proliferation	2.9	0.032
krt4	Cell Proliferation	1.75	0.025
mxd4	Cell Proliferation	1.98	0.008
nap1l1	Cell Proliferation	0.62	0.037

Gene	Pathway	fold change	p value
prkrir	Cell Proliferation	0.54	0
sertad1	Cell Proliferation	1.85	0.048
tbx3	Cell Proliferation	0.48	0.006
tnfrsf11a	Cell Proliferation	0.45	0.035
tnfsf15	Cell Proliferation	0.55	0.044
aplp1	EMT	2.23	0.033
cald1	EMT	0.58	0.038
calu	EMT	0.64	0.003
cdh2	EMT	0.66	0.042
cdh6	EMT	0.44	0.041
col11a1	EMT	0.51	0.001
eln	EMT	2.42	0.001
igfbp2	EMT	0.58	0.038
il6	EMT	0.31	0.044
inhba	EMT	0.60	0.031
itgav	EMT	0.57	0.006
nt5e	EMT	0.62	0.027
pmp22	EMT	0.59	0.03
pvr	EMT	0.66	0.022
tgfbr3	EMT	2.45	0.034
thbs1	EMT	0.51	0.012
vcam1	EMT	0.58	0.047
vegfa	EMT	0.32	0.030
add3	Estrogen Response	0.59	0.037
aldh3b1	Estrogen Response	1.75	0.004
dcxr	Estrogen Response	2.61	0.003
dhrs3	Estrogen Response	0.42	0.007
faim3	Estrogen Response	2.90	0.045
fasn	Estrogen Response	1.56	0.020
gale	Estrogen Response	1.65	0.015
hr	Estrogen Response	1.67	0.045
isg20	Estrogen Response	1.84	0.028
kdm4b	Estrogen Response	1.55	0.035
ltf	Estrogen Response	3.14	0.035
nrip1	Estrogen Response	0.44	0.043
pkp3	Estrogen Response	1.56	0.038
sult2b1	Estrogen Response	0.33	0.031
tpd52l1	Estrogen Response	1.85	0.000
tsta3	Estrogen Response	1.66	0.037
ugcg	Estrogen Response	0.66	0.025

Gene	Pathway	fold change	p value
bcl2	Focal Adhesion	0.6	0.048
birc3	Focal Adhesion	0.46	0.045
crk	Focal Adhesion	0.66	0.011
flnc	Focal Adhesion	1.51	0.047
fyn	Focal Adhesion	0.64	0.019
itga7	Focal Adhesion	1.78	0.025
itgb8	Focal Adhesion	0.36	0.042
pdgfb	Focal Adhesion	0.41	0.034
pdgfd	Focal Adhesion	0.41	0.044
pik3ca	Focal Adhesion	0.56	0.047
ppp1cb	Focal Adhesion	0.53	0.007
pten	Focal Adhesion	0.6	0.048
rap1b	Focal Adhesion	0.6	0.044
sos1	Focal Adhesion	0.56	0.047
htr2a	Gap Junction	0.3	0.027
map3k2	Gap Junction	0.46	0.024
tuba1b	Gap Junction	1.59	0.008
cltc	Gap Junction	0.66	0.009
gjb2	Gap Junction	0.56	0.026
gjb5	Gap Junction	1.91	0.035
bax	Pathways in Cancer	1.56	0.009
ccdc6	Pathways in Cancer	0.55	0.027
cdkn1a	Pathways in Cancer	1.85	0.001
cdkn2b	Pathways in Cancer	1.74	0.045
chuk	Pathways in Cancer	0.57	0.003
egln2	Pathways in Cancer	1.52	0.028
hif1a	Pathways in Cancer	0.59	0.029
pml	Pathways in Cancer	1.73	0.042
ptgs2	Pathways in Cancer	0.55	0.017
rb1	Pathways in Cancer	0.53	0.045
runx1	Pathways in Cancer	0.65	0.036
smad2	Pathways in Cancer	0.66	0.043
tgfbr1	Pathways in Cancer	0.5	0.015
tpm3	Pathways in Cancer	0.45	0.003
bdkrb2	Regulation of Actin Cytoskeleton	0.59	0.045
nckap1	Regulation of Actin Cytoskeleton	0.41	0.013
mapre1	Regulation of Actin Cytoskeleton	0.65	0.027
nebl	Regulation of Actin Cytoskeleton	0.23	0.040
apoe	Small GTPase Mediated Signaling	0.38	0.010
cdc42bpa	Small GTPase Mediated Signaling	0.57	0.010

Gene	Pathway	fold change	p value
fgd4	Small GTPase Mediated Signaling	0.53	0.031
grap	Small GTPase Mediated Signaling	0.52	0.028
cdk8	TGF_beta signaling	0.62	0.034
rbl1	TGF_beta signaling	0.63	0.025
skil	TGF_beta signaling	0.56	0.02
usp9x	TGF_beta signaling	0.53	0.019
xpo1	TGF_beta signaling	0.54	0.035
id3	TGF_beta signaling	1.92	0.045

In the end we selected 10 genes whose expression change seemed to agree with our phenotype and the published literature for validation (Table 12).

Table 12. Genes selected for validation based on the algorithm.

Gene	miRNA pair	Pathway	fold change (Δ/Δ vs. WT)	p value	Information from Literature
Itga7		Cell Adhesion	1.78	0.025	Mediates migration and invasion on laminin isoforms (56)
Pten		Cell Adhesion	0.6	0.048	PTEN deletion promotes Breast Cancer Progression and Poor Prognosis (57)
Cdh2		EMT	0.66	0.042	DNp63 promotes N-Cadherin, N-Cadherin could be a marker of metastasis in Breast CA (58)
Tgfbr3	**mmu-miR-193b-5p**	EMT	2.45	0.034	Increased levels in TNBC, regulates polarity in luminal cells, mislocalization promotes EMT, migration, invasion & proliferation (59)
Nrip1	**mmu-miR-33-3p**	Estrogen Response	0.44	0.043	regulator of Estrogen signaling and oncogenic pathways, role in breast cancer cell growth, inhibits Wnt/Beta Catenin pathway, increased in tumors (60, 61)
Cdkn1A		Pathways in Cancer	1.85	0.001	Increased in breast cancer tissues, correlates with tumor size, dedifferentiation, lymph node mets, and shorter disease free survival, cytoplasmic expression in hyperplastic foci (62)
Hif1A		Pathways in Cancer	0.59	0.029	Expression associated with metastatic high grade breast cancers, expressed during early mammary gland development prior to polarization, promotes angiogenesis through VEGF release (63)
Igfbp5	**mmu-miR-193b-5p**	IGF signaling	2.45	0.002	Can inhibit IGF activity, regulates proliferation and cell death in mammary gland development (64)
Cald1		EMT	0.58	0.038	Down in human Mammary Stem Cell signature (65)
Cnp		Cell-Cell Signaling	1.70	0.043	Up in human Mammary Stem Cell signature (65)

Two particularly interesting genes that came up were Nuclear receptor binding protein 1 (Nrip1) and Insulin Growth Factor Binding Protein 5 (Igfbp5). These genes are involved in estrogen receptor (ER) signaling and insulin growth factor (IGF) signaling, respectively, two pathways that closely intertwine and are essential in mammary gland development (60, 61, 64). Moreover, these pathways are also involved in processes such as cell proliferation and apoptosis, which could have potential implications in the context of cancer. Some genes also came up in the functional pair analysis and their microRNA partner was noted. We designed SYBR Green RT-PCR primers for 8 of these genes and Taqman RT-PCR probes for the remaining two that we could not find working SYBR green primers for and proceeded to validate the genes.

We used fresh ΔNp63$^{\Delta/\Delta}$ RNA obtained from a pool of 3 mice for the validation. The RT-PCR validated the sequencing results for all 10 genes selected (Figure 58).

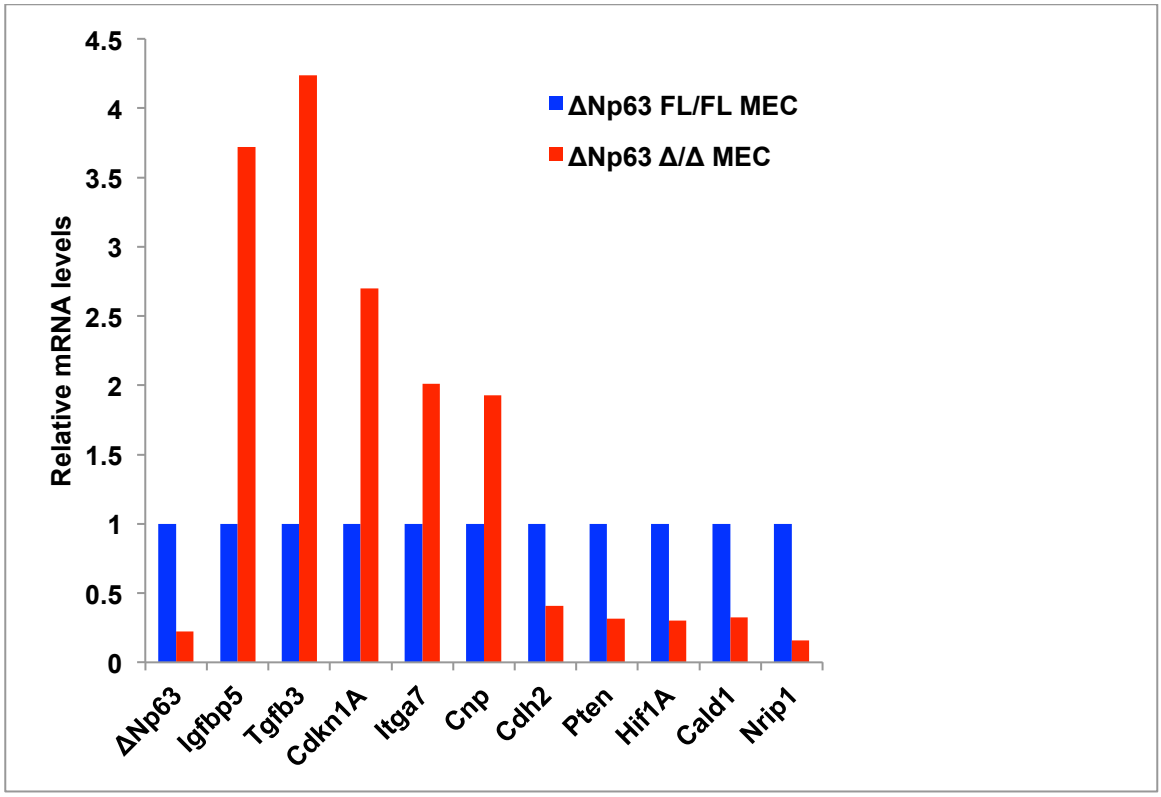

Figure 58. qRT PCR results for validation of selected genes. We were able to validate the expression of all the 10 selected genes. ΔNp63 FL/FL MEC = $\Delta Np63^{fl/fl}$ mammary epithelial cell RNA ΔNp63 Δ/Δ MEC = $\Delta Np63^{\Delta/\Delta}$ mammary epithelial cell RNA.

In the case of microRNAs, we ran all the 34 differentially expressed microRNAs through our algorithm, focusing first on the ones that came up in the functional pair analysis. In the end we selected 9 microRNAs whose expression change seemed to agree with our phenotype and the published literature for validation (Table 13).

Table 13. microRNAs selected for validation based on the algorithm.

microRNA	Fold Change	p-value	Oncogene vs. TS	Literature
mmu-mir-592-5p	5.13	0.005	Oncogene	Overexpressed in metastases vs. primary lung adenocarcinomas (66); increase correlates with poor prognosis in colorectal cancer (67)
mmu-mir-150-5p	2.94	0.006	Oncogene	Overexpressed in breast cancer patients of all subtypes (68); promotes Breast Cancer growth (69); promotes prostate CSCs (70)
mmu-mir-33-3p	2.20	0.034	Oncogene & TS	targets p53 (71); targets HIF1a (72); knockouts are obese due to higher SREBP1 (73)
mmu-mir-146b-5p	1.63	0.050	Oncogene & TS	targets BRCA1 (74) and inhibits migration and invasion *in vitro* (75)
mmu-mir-10b-5p	1.60	0.030	Oncogene	Promotes migration and invasion (Ma, Nature, 2007) (76)
mmu-mir-147-5p	0.35	0.001	Tumor suppressor	induces Mesenchymal to Epithelial Transition (MET) (77)
mmu-mir-193b-5p	0.34	0.043	Tumor suppressor	Promotes Breast Cancer progression (78)
mmu-mir-205-3p	0.29	0.003		ΔNp63 target inhibiting EMT (17)
mmu-mir-147-3p	0.05	0.002	Tumor suppressor	induces MET (77)

We designed Taqman RT-PCR probes for all the microRNAs proceeded to validate their expression. We used the same fresh $\Delta Np63^{\Delta/\Delta}$ RNA used for the gene validation. The RT-PCR validated the sequencing results for all 9 selected microRNAs (Figure 59).

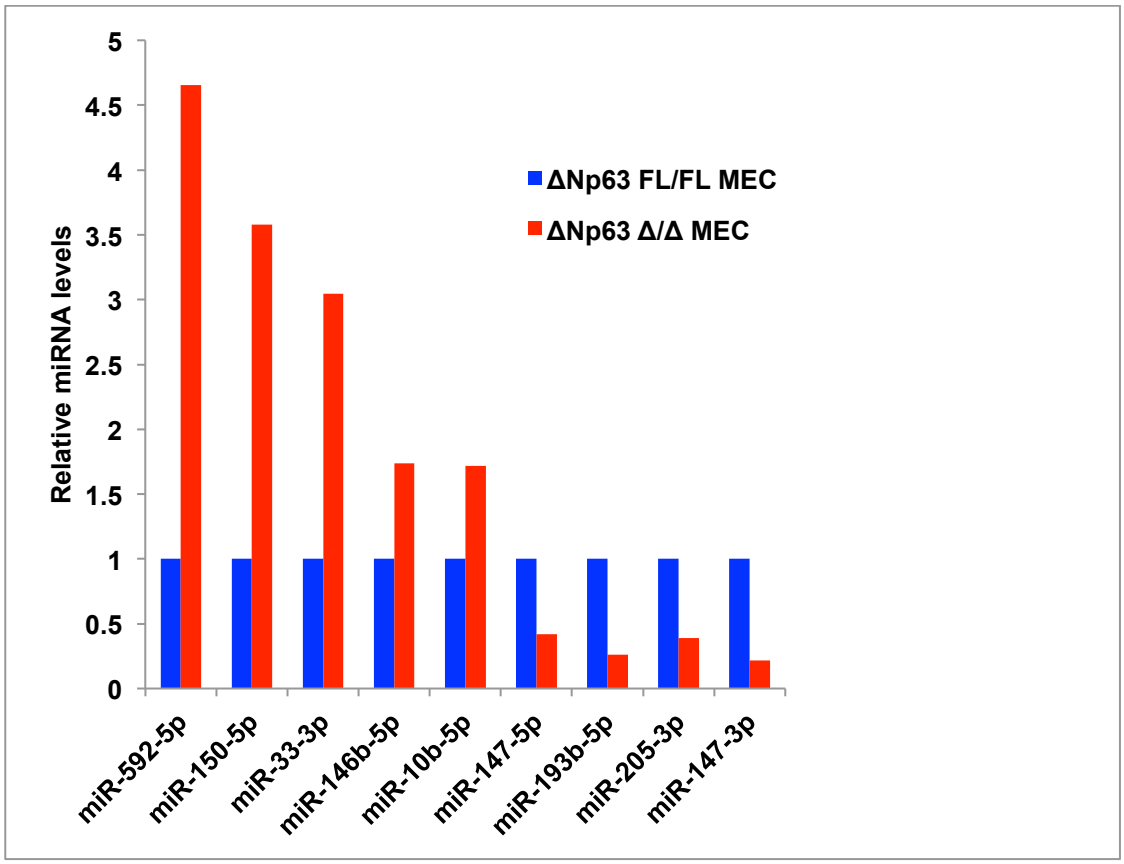

Figure 59. qRT PCR results for validation of selected microRNAs. We were able to validate the expression of all the 9 selected microRNAs. ΔNp63 FL/FL MEC = ΔNp63$^{fl/fl}$ mammary epithelial cell RNA ΔNp63 Δ/Δ MEC = ΔNp63$^{\Delta/\Delta}$ mammary epithelial cell RNA.

Currently, we have identified a second set of genes for validation, this time focusing on the ER signaling and IGF signaling pathways since they are among the most important in mammary gland development and breast cancer.

After validation of these genes and microRNAs with RT-PCR, our next step was to develop a system to test whether alterations in these validated genes can rescue the phenotypes observed in the *in vivo* experiments. Although it would be ideal to test these genes and microRNAs *in vivo*, we chose to start with an *in vitro* embedded 3D culture. An embedded 3D culture system gives us the advantages of a fast turnaround since the

cultures would be grown for 2 weeks while at the same time giving us information regarding the relationship and organization of mammary epithelial cells structures.

To set up the 3D cultures, we modified the protocol for 3D culture of normal and malignant mammary epithelial cells previously published (21). We isolated ΔNp63$^{fl/fl}$, Rosa$^{M/M}$ mammary epithelial cells and infected them to induce recombination as previously mentioned. During the final steps of the infection procedure, we coated chamber slides with 40 µl of GFR matrigel and set to dry in a 37° C incubator for 15 to 30 minutes, being careful not to over dry the slides. Once the infection was complete, the cells were counted and resuspended directly in matrigel at a concentration of 667 cells per µl. 150 µl of the cell mix was added to each well, so that there would be 100,000 cells per well. The slides were then placed for another 15 to 30 minutes in the 37° C incubator to polymerize the matrigel after which 200 µl of mammoshpere growth media were added. Media was replaced every other day for the two-week duration of the culture. After two weeks, the cultures were imaged using a fluorescent microscope (Figure 60) to assess for differences in size and number.

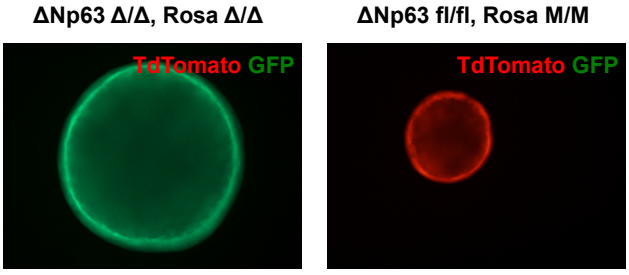

Figure 60. Representative fluorescent images from the 13th day of 3D culture.

We found that there were a significantly lower number of ΔNp63 knockout spheres when compared to wild type (Figure 61).

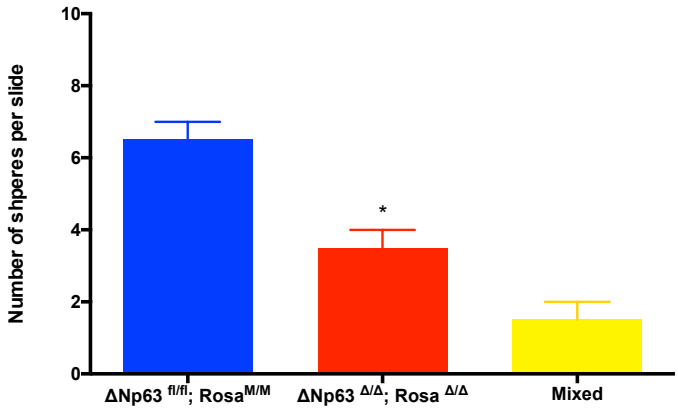

Figure 61. Number of spheres per slide at the 13th day of 3D Culture. Mixed glands had contributions from both recombined and unrecombined cells. There was significantly less number of spheres for the ΔNp63$^{Δ/Δ}$, Rosa$^{Δ/Δ}$ condition, p = 0.05, n = 2

However, the ΔNp63 knockout spheres were also significantly larger, which could be a sign that knocking out ΔNp63 results in increased proliferation (Figure 62). We attempted to stain the spheres with Ki67 to assess proliferation directly but unfortunately the spheres were lost while performing the washes in the immunofluorescence protocol.

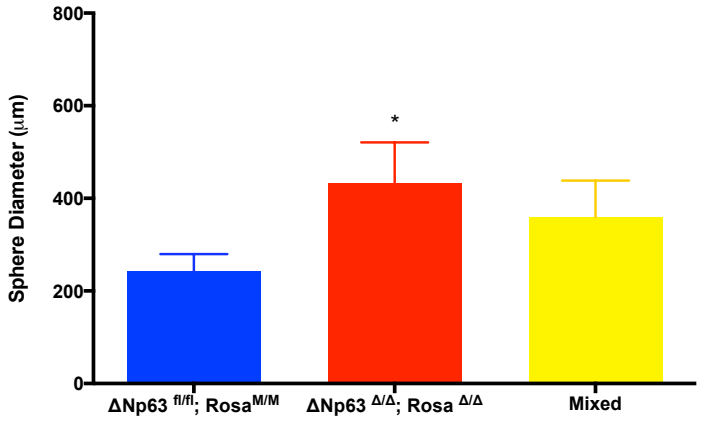

Figure 62. Average sphere diameter for each condition at the 13th day of 3D Culture. Mixed glands had contributions from both recombined and unrecombined cells. The diameter of the ΔNp63$^{Δ/Δ}$, Rosa$^{Δ/Δ}$ condition spheres was significantly larger, p = 0.03, n = 2

Finally, we performed immunofluorescence staining on these spheres to determine whether there were other phenotypic characteristics that correlated with what we observed *in vivo*. We stained the spheres with SMA to evaluate the basal layer and saw that, similarly to what we observed *in vivo,* the ΔNp63 knockout spheres had reduced expression when compared to the wild type: Some of the spheres did not have any SMA expression whatsoever while others had discontinuous expression only in a small population (Figure 63). We were not able to determine whether these changes were significant because only three spheres survived the staining protocol.

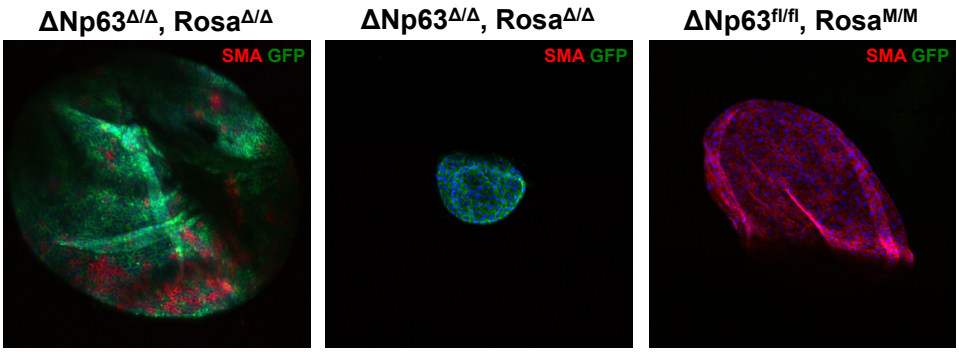

Figure 63. SMA staining to evaluate the basal layer of 3D cultures. Spheres were fixed and stained after 13 days in culture. GFP stains for cells that underwent recombination and lost ΔNp63 expression. SMA (red), GFP (green), confocal image, 10x.

This *in vitro* phenotype was similar to what we observed in the *in vivo* transplantations where there were less ΔNp63 ducts but the resulting ducts had increased number of layers and increased proliferation. We believe that the phenotype observed *in vitro* and the similarities to the *in vivo* observations are evidence that the 3D culture system could a viable alternative to examine whether altering any of the validated genes rescues the ΔNp63 knockout mammary development defects. This was only a pilot experiment and more tests need to be done to determine if the expression changes observed are significant,

but it is a promising start. Our next step would also include optimizing the fixation and staining protocol so that we can recover more spheres.

5.4. Attempted development of a new breast cancer tumor model.

As mentioned before, our goal with this part of the project was to understand the role of ΔNp63 in mammary tumors since ΔNp63 has been previously connected to breast cancer and since mammary tumors were the most common tumor type in our own, $\Delta Np63^{+/-}$ mice. We fist sought to understand its role in mammary gland development to have a base to build upon its role in tumor development but eventually our goal was to study ΔNp63 in a tumor context. To this end, we attempted to develop a mammary gland tumor model using conditional knockout mice and selectively knocking out in the mammary gland ΔNp63, TAp63, BRCA1, a known tumor suppressor in breast cancer that has previously been tied with ΔNp63 (53, 74, 79-81), or a combination of these genes using intraductal injection of adenoviral Cre. We were able to successfully inject the mice, 15 per condition, and confirm that the injections were successful and that recombination had taken place at both the luminal an basal layers of the mammary ducts (Figure 64, Appendix Table 4). We aged these mice for up to 2 years while monitoring for the development of tumors.

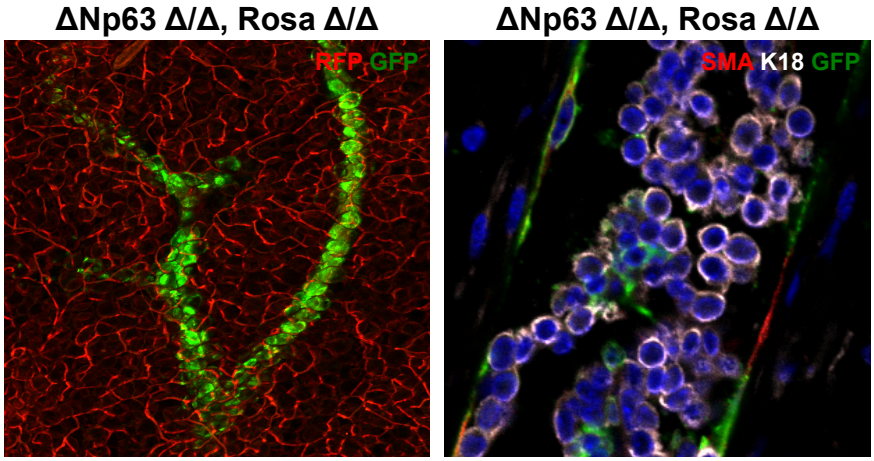

Figure 64. Confocal microscopy image and immunofluorescence staining showing successful intraductal injection and recombination to knockout ΔNp63. Left: 10x Confocal image of whole mammary gland RFP (red), GFP (green). Right: 40x Immunofluorescence staining for SMA (red) K18 (white), and GFP (green).

Unfortunately, none of the mice developed tumors throughout the duration of the experiment. Upon harvesting the glands and analyzing the hematoxylin and eosin sections, no changes such as hyperplasia or ductal disorganization that could be suggestive of potential tumor development were observed. We collected and processed the tissues for all the injected mice and continue to analyze them looking for minor changes that might not have been evident at first glance. In the future, this experiment could be modified and repeated by crossing our conditional knockout mice with a known breast cancer tumor model with high penetrance to evaluate how lack of ΔNp63 modulates the development and progression of tumors.

In summary, using the strength of *in vivo* models, primary cell culture methods, sequencing, and bioinformatics, we have increased our understanding of the pathways regulated by ΔNp63 in the mammary gland. Our main finding was that loss of ΔNp63 in mammary epithelial cells led to impaired mammary gland growth and disorganization of the ductal structure in spite of increased proliferation. Sequencing analysis gave us a broader picture of the mechanism for the observed phenotype, and we were able to confirm

alterations in EMT, ER signaling, IGF signaling, and cytoskeleton organization pathways among others. The next step will be to tie the sequencing findings to the observed phenotype and to this end we developed a 3D Culture system that appears in part to recapitulate what was observed *in vivo.* The 3D culture system still needs to be characterized further and optimized but it is a good start. All the pathways validated from the sequencing can also be linked to cancer, which would bridge our findings to the tumor phenotype observed in $\Delta Np63^{+/-}$ mice. We are currently following up on these leads.

Chapter 6

Chapter 6: Discussion

6.1 Discussion and Future Directions

Treatment of cancer remains one of our generations most pressing health issues. Our aim with this project was to address this by focusing on the basics and improving our understanding of the mechanisms of cancer development and progression. Understanding the basics is the key to developing new, more effective ways to treat this horrible disease. We focused on ΔNp63, a member of the p53 family of transcription factors that had been previously linked to various tumor types. Many of the previous research done on ΔNp63 was done on cancer cell lines, which provide valuable information but come with inherent limitations. The relationships and mechanisms discovered *in vitro* are done so in isolation, and there is no guarantee that these relationships will hold up in more complex systems. Is it to this end that we sought to use the various ΔNp63 mouse models we developed in house to address questions regarding its functions in both physiological and pathological contexts.

We began with a tumor cohort study using $\Delta Np63^{+/-}$ mice to obtain a broad idea regarding the role of ΔNp63 in cancer. In this study we found indisputable evidence that differences in ΔNp63 expression affect tumor development. ΔNp63 expression changes can both modulate the tumor spectrum in known genetic background such as $p53^{-/-}$, as well as tumor initiation in the case where ΔNp63 heterozygosity was the sole genetic alteration. More work needs to be done to determine if the increased propensity for tumors in the $\Delta Np63^{+/-}$ mice. Loss of heterozygosity is an option, although immunohistochemistry showed that at least some of the tumors retain ΔNp63 expression. Another option could be that ΔNp63 heterozygosity leads to genetic instability. To test this we could do karyotyping or comparative genomic hybridization to check if $\Delta Np63^{+/-}$ mice exhibit any abnormalities. Our analysis also demonstrated that ΔNp63 potentially modulates tumor progression as well,

evidenced by the increased aggressiveness and metastases observed in tumors developed on a ΔNp63$^{+/-}$ background.

With this evidence in hand, our next step was to try to understand the mechanisms through which ΔNp63 was modulating cancer. We began by characterizing the ΔNp63 knockout phenotype using primary keratinocytes directly harvested from ΔNp63$^{-/-}$ embryos. Previous research had shown that ΔNp63 loss leads to multipotency (8), but we demonstrated that it also jumpstarts an EMT program that results in increased invasion and migration. After establishing the EMT *in vitro*, we developed an *in vivo* wound healing mouse model that allowed us to study EMT and migration within the complex biological context of a living organism. With this model we found that ΔNp63 also regulates EMT *in vivo* and its loss promotes a transition into a mesenchymal phenotype that is potentially different from the typical EMT that occurs during wound healing and is unable to fully reepithelialize the wound site. Delving further into the mechanism of this phenotype, we found that ΔNp63 suppression of Twist1 and Lef1 through regulation of miR-98 and miR-34a, respectively, leads to the EMT observed. These transcription factors are not commonly involved in the EMT observed in traditional wound healing and we saw evidence of this as well in our system. We think that what is happening is that when ΔNp63 is lost, epithelial cells transition fully into a mesenchymal phenotype and become more invasive and migratory but they have poor directionality and little communication with their surrounding cells making the collective migration that is required for proper wound reepithelialization impossible to do. We also theorize that the cells could also be unable to revert back to an epithelial phenotype unless ΔNp63 expression was restored. The experiments to test this were beyond the scope of this project and were currently underway at the time of this writing. This contrasts with what happens in the control wounds, where the epidermal cells undergo a partial EMT program that is both transient and reversible, which allows them to migrate collectively to close the wound gap and restore the epidermal layer. We believe that a similar phenomenon could be

what causes ΔNp63$^{+/-}$ mouse tumors to be more aggressive and metastatic and saw immunohistochemical evidence that this could be the case: both Twist1 and Lef1 have reciprocal relationships to ΔNp63 expression in tumors and their corresponding mets. However, we still need to check for levels of miR-98 and miR-34a in the tumor samples, which could be done using fluorescence in situ hybridization. An alternative approach, could be to design a new tumor cohort experiment and collect pieces of the developing tumors and normal tissues could be flash frozen to extract RNA and protein. The RNA extracted could be sequenced to determine how ΔNp63 heterozygosity affects gene expression in the tumors and how it compares to normal tissues. The protein extracted could be used to study ΔNp63 induced changes at the protein level and how these could modulate tumor development, one area we were unable to test with our project. Finally, based on our data there is potential for miR-98 and miR-34a to be used as drug targets to attempt to stop metastatic progression, something that will be explored further.

The final part of this project concerned focusing on a specific tumor type to understand the role of ΔNp63 in its development and progression. We chose breast cancer since mammary adenocarcinoma was the most common tumor type observed in the ΔNp63$^{+/-}$ mouse model. We also theorized that the similarities between keratinocytes and mammary epithelial cells could mean that some of the same pathways could be regulated by ΔNp63 in both tissue types. Combing through the literature we found that ΔNp63 can be used as a biomarker for breast cancer in the clinic but when it comes to its function in breast cancer, there conflicting information detailing its role as both a tumor suppressor and an oncogene. Our own mouse data suggests that ΔNp63 could be functioning as a tumor suppressor, at least in some cases, but a lot of questions remained. We determined that part of the controversy regarding ΔNp63's role in breast cancer is due to gaps in knowledge about the roles of ΔNp63 in mammary development. Therefore, we decided to tackle the

subject of mammary development and how the role that ΔNp63 plays in it could clue us into its role in breast cancer.

Our data show that ΔNp63 loss impairs mammary ductal growth in spite of increased proliferation. The ducts that do grow out have an aberrant structure with multiple luminal layers and a disorganized basal layer. However, we were unable to fully explain the observed phenotype by staining the collected tissue samples, which led us to take a step back and try a different approach: sequencing the ΔNp63 knockout mammary epithelial cells to obtain a broader picture of expression changes due to ΔNp63 loss. We sequenced both ΔNp63 knockout mRNA and microRNA and saw that ΔNp63 loss significantly affected a complex network of pathways. Combining bioinformatics tools and our experimental data with information already available in the literature, we narrowed down the list of pathways, genes, and microRNAs to a more manageable number, and were able to validate the expression of all the candidates we tested. These candidates are involved in pathways such as EMT, ER signaling, cell polarity, and IGF signaling among others that could help explain our *in vivo* phenotype. Moreover, all of these pathways can potentially contribute to cancer as well, giving us an idea of ΔNp63's role in tumorigenesis. When comparing the these sequencing results with the previously published keratinocyte sequencing (8), we saw very little overlap. This shows that even though keratinocytes and mammary epithelial cells are related, ΔNp63 appears to regulate different sets of genes although the underlying pathways affected could be similar. This was partially observed in our staining, where we saw E-cadherin expression in the absence of ΔNp63 was reduced in the skin but unaffected in the mammary tissue. In the future, it would be interesting to compare the pathways affected in the keratinocytes and the pathways affected in the mammary epithelial cells further to see if there are any commonalities despite different genes being regulated.

We also developed a 3D culture system that appears to partially recapitulate the observed *in vivo* phenotype and, after further optimization, could be used to screen

validated targets from the sequencing data to better understand the mechanisms involved. This system could also be used to test some of the genes and microRNAs affected in the skin to explore whether there is a link between the phenotypes observed in these different tissues despite the sequencing results. The complete analysis and understanding of these sequencing results was beyond the scope of this project but this was an important first step. Further work is already underway to validate more targets and correlate our findings with human disease. With the information and understanding we obtain from these analyses, we will potentially be able to identify new targets and develop new therapies to treat cancer.

Finally we attempted to develop a new breast cancer mouse model using our conditional knockout mice and the intraductal injection process. Although our system appeared to work and recombination was successful, none of the mice developed tumors. This could suggest that ΔNp63 might not be able to promote tumor development by itself. The phenotypes observed in the $\Delta Np63^{+/-}$ mice could be due to ΔNp63's role as a modulator of tumor development, rather than a role a tumor initiator itself. To test this we would need to develop a new tumor study where we could cross ΔNp63 conditional knockout mice with a known breast cancer mouse model with high penetrance and assess how the absence of ΔNp63 modulates the development of tumors in terms of latency, aggressiveness and metastasis. Development of these models could be instrumental to test new therapeutic alternatives to treat cancer.

6.2 Final Thoughts

Finally, I wish to comment on the state of cancer research. Cancer remains one the main healthcare challenges of our lifetime. Despite considerable advances in cancer research, considerable hurdles remain to cure or even treat many tumor types. One of the main problems with cancer research is lack of communication between the research and clinical worlds. This leads to promising basic research that never moves beyond the bench

and drug development that does not take into account the nuances of the pathways that are being targeted. The end result is drugs that have a temporary benefit at best, or do not work as expected as worst. We cannot lose track that the reason we are doing this work is to help patients that are very sick. We owe it to them to make sure that we communicate better with one another, focus on projects with the potential to help patients, and that we properly research the mechanisms and pathways that we wish to target to allow the development of better drugs. Working together we will be able to make a difference and improve the way of life of millions of patients that depend on us.

Appendices

Appendix Table 1. Full list of significant differentially expressed genes from ΔNp63 mammary epithelial cell sequencing.

Gene ID	Biotype	Gene Name	Fold Change	p-value
ENSMUSG00000028188	protein_coding	Spata1	0.472455825	0.041877971
ENSMUSG00000069833	protein_coding	Ahnak	0.605783484	0.021056628
ENSMUSG00000028232	protein_coding	Tmem68	0.634606614	0.040179051
ENSMUSG00000087579	processed_ transcript	1500017E21Rik	0.29553544	0.006544033
ENSMUSG00000021583	protein_coding	Erap1	0.518710693	0.002234346
ENSMUSG00000006179	protein_coding	Prss16	2.202511234	0.025198551
ENSMUSG00000017723	protein_coding	Wfdc2	1.738558092	0.043126708
ENSMUSG00000025261	protein_coding	Huwe1	0.624111383	0.015531721
ENSMUSG00000031007	protein_coding	Atp6ap2	0.603174767	0.000303827
ENSMUSG00000034981	protein_coding	Parm1	0.576371239	0.004920375
ENSMUSG00000021635	protein_coding	Rad17	0.577321858	0.041677894
ENSMUSG00000087299	antisense	Gm12953	1.753327953	0.010372194
ENSMUSG00000044098	protein_coding	Rsbn1	0.436976541	0.018532493
ENSMUSG00000024943	protein_coding	Smc5	0.500974202	0.049479922
ENSMUSG00000051726	protein_coding	Kcnf1	119.1649248	0.002734457
ENSMUSG00000005610	protein_coding	Eif4g2	0.631982918	0.007883431
ENSMUSG00000081382	pseudogene	Rpl18-ps1	1.594876517	0.00793618
ENSMUSG00000022016	protein_coding	Akap11	0.600856307	0.042616279
ENSMUSG00000022018	protein_coding	Rgcc	2.318630937	0.049511908
ENSMUSG00000013646	protein_coding	Sh3bp5l	1.542964965	0.000445407
ENSMUSG00000052395	protein_coding	Rft1	1.828739046	0.002142806
ENSMUSG00000021733	protein_coding	Slc4a7	0.538404911	0.01364106
ENSMUSG00000039826	protein_coding	Trub2	2.003370131	0.035002903
ENSMUSG00000020063	protein_coding	Sirt1	0.552006525	0.047009325
ENSMUSG00000023004	protein_coding	Tuba1b	1.591759209	0.008350581
ENSMUSG00000026037	protein_coding	Orc2	0.592943004	0.046452867
ENSMUSG00000022358	protein_coding	Fbxo32	0.471599166	0.006052285
ENSMUSG00000034863	protein_coding	Ano8	1.649437359	0.01581636
ENSMUSG00000032420	protein_coding	Nt5e	0.618070253	0.026981946
ENSMUSG00000032423	protein_coding	Syncrip	0.586870077	0.019169812
ENSMUSG00000084824	antisense	Gm16344	0.499211937	0.023499996
ENSMUSG00000032301	protein_coding	Psma4	0.583369	0.043621786
ENSMUSG00000057454	protein_coding	Lypd3	1.681614233	0.039381724
ENSMUSG00000055320	protein_coding	Tead1	0.611123102	0.024296811
ENSMUSG00000036138	protein_coding	Acaa1a	1.715144911	0.012419495
ENSMUSG00000097327	pseudogene	E030030I06Rik	3.188553648	0.032721832

ENSMUSG00000029675	protein_coding	Eln	2.416634196	0.001085099
ENSMUSG00000038146	protein_coding	Notch3	2.425236741	0.000162539
ENSMUSG00000052214	protein_coding	Opa3	1.590558472	0.015832973
ENSMUSG00000071303	pseudogene	Rps8-ps1	1.558377855	0.022651824
ENSMUSG00000018286	protein_coding	Psmb6	1.551019769	0.041936645
ENSMUSG00000040928	protein_coding	S100pbp	0.564723107	0.028777518
ENSMUSG00000034121	protein_coding	Mks1	1.63901773	0.006355588
ENSMUSG00000034126	protein_coding	Pomt2	1.663827573	0.009721017
ENSMUSG00000035299	protein_coding	Mid1	0.560906396	0.033314475
ENSMUSG00000035293	protein_coding	G2e3	0.530503306	0.035584166
ENSMUSG00000078898	protein_coding	Gm4723	0.585575653	0.013833798
ENSMUSG00000074269	protein_coding	2410076I21Rik	0.082959346	0.000964462
ENSMUSG00000002944	protein_coding	Cd36	5.799925095	0.028715181
ENSMUSG00000066705	protein_coding	Fxyd6	0.284057768	0.001216221
ENSMUSG00000095463	protein_coding	Entpd4	1.86992647	0.016055019
ENSMUSG00000018040	protein_coding	Rrp7a	1.686064613	0.027236159
ENSMUSG00000053411	protein_coding	Cbx7	0.305713468	0.01061678
ENSMUSG00000040774	protein_coding	Cept1	0.483439484	0.040340229
ENSMUSG00000020921	protein_coding	Tmem101	1.891424096	0.019458113
ENSMUSG00000020928	protein_coding	Higd1b	5.874945774	0.034821525
ENSMUSG00000022788	protein_coding	Fgd4	0.534045811	0.030901835
ENSMUSG00000035505	protein_coding	Cox18	1.678836033	0.003616389
ENSMUSG00000020496	protein_coding	Rnf187	1.569657205	0.022706106
ENSMUSG00000059316	protein_coding	Slc27a4	2.832553527	0.015654845
ENSMUSG00000003038	protein_coding	Hmgn2	0.59596679	0.007289198
ENSMUSG00000054648	protein_coding	Zfp869	0.607726426	0.032456769
ENSMUSG00000071072	protein_coding	Ptges3	0.597147513	0.041639585
ENSMUSG00000071076	protein_coding	Jund	1.594640394	0.008677286
ENSMUSG00000023087	protein_coding	Ccrn4l	0.524742733	0.029995533
ENSMUSG00000087298	pseudogene	Gm9392	0.561941963	0.019289891
ENSMUSG00000031785	protein_coding	Gpr56	0.607713274	0.006566207
ENSMUSG00000031781	protein_coding	Ciapin1	2.260305286	0.007918667
ENSMUSG00000034259	protein_coding	Exosc4	1.889073875	0.014903473
ENSMUSG00000030291	protein_coding	Med21	0.598905373	0.044286093
ENSMUSG00000042298	protein_coding	Ttc19	0.603860948	0.038630241
ENSMUSG00000016253	protein_coding	Nelfcd	1.618820153	0.015305079
ENSMUSG00000002718	protein_coding	Cse1l	0.532414904	0.030982208
ENSMUSG00000093470	lincRNA	Gm20645	0.507222015	0.00024287
ENSMUSG00000025466	protein_coding	Fuom	1.889634684	0.012743902
ENSMUSG00000039236	protein_coding	Isg20	1.84282661	0.027850607
ENSMUSG00000096370	protein_coding	Gm21992	1.96053221	0.039214344
ENSMUSG00000074547	pseudogene	Gm10712	1.569945052	0.00748323
ENSMUSG00000046341	pseudogene	Gm11223	1.769934884	0.040091033

ENSMUSG00000029287	protein_coding	Tgfbr3	2.447606559	0.033676054
ENSMUSG00000028461	protein_coding	Ccdc107	1.579033726	0.007541431
ENSMUSG00000044258	protein_coding	Ctla2a	0.549759275	0.025869865
ENSMUSG00000057551	protein_coding	Zfp317	0.530981957	0.006439666
ENSMUSG00000055415	protein_coding	Atp10b	0.45325734	0.034852354
ENSMUSG00000007613	protein_coding	Tgfbr1	0.504364491	0.014690112
ENSMUSG00000007617	protein_coding	Homer1	0.518758828	0.018319242
ENSMUSG00000003549	protein_coding	Ercc1	3.320154461	0.011401933
ENSMUSG00000017421	protein_coding	Zfp207	0.661994247	0.012342569
ENSMUSG00000003545	protein_coding	Fosb	1.893676432	0.023445044
ENSMUSG00000031371	protein_coding	Haus7	1.582184715	0.019957416
ENSMUSG00000031373	protein_coding	Car5b	2.640286802	0.025844549
ENSMUSG00000053641	protein_coding	Dennd4a	0.64240839	0.001012295
ENSMUSG00000020413	protein_coding	Hus1	0.356022826	0.047124709
ENSMUSG00000020415	protein_coding	Pttg1	5.527931432	0.001208261
ENSMUSG00000062906	protein_coding	Hdac10	1.82104402	0.032986587
ENSMUSG00000052485	protein_coding	Tmem171	1.745715349	0.041565185
ENSMUSG00000035397	protein_coding	Klf16	1.662621384	0.027217771
ENSMUSG00000058254	protein_coding	Tspan7	1.553022873	0.017356824
ENSMUSG00000001946	protein_coding	Esam	3.312602883	0.044819171
ENSMUSG00000067336	protein_coding	Bmpr2	0.551270724	0.011446605
ENSMUSG00000087439	antisense	Gm15788	0.309619022	0.033141156
ENSMUSG00000038576	protein_coding	Susd4	1.80007631	0.018610801
ENSMUSG00000030704	protein_coding	Rab6a	0.621686665	0.006471361
ENSMUSG00000029073	protein_coding	Gltpd1	1.6354198	0.007491142
ENSMUSG00000022570	protein_coding	Tsta3	1.662621983	0.037102249
ENSMUSG00000020590	protein_coding	Snx13	0.498116186	0.046758874
ENSMUSG00000028032	protein_coding	Papss1	1.664489128	0.026689271
ENSMUSG00000032393	protein_coding	Dpp8	0.656352594	0.049741888
ENSMUSG00000026667	protein_coding	Uhmk1	0.542674605	0.006682865
ENSMUSG00000029635	protein_coding	Cdk8	0.623972342	0.033703681
ENSMUSG00000029633	pseudogene	Gm5578	0.549980501	0.029034057
ENSMUSG00000042408	protein_coding	Zmym6	0.466444526	0.023679426
ENSMUSG00000017697	protein_coding	Ada	1.75016077	0.043883273
ENSMUSG00000041846	protein_coding	Smek1	0.635772088	0.022791033
ENSMUSG00000031843	protein_coding	Mphosph6	0.656715901	0.013073606
ENSMUSG00000056260	protein_coding	Lrif1	0.536706484	0.019044787
ENSMUSG00000083833	pseudogene	Gm13841	3.043333404	0.000848782
ENSMUSG00000076609	IG_C_gene	Igkc	0	0.012069204
ENSMUSG00000092541	protein_coding	Gm20537	0.109145703	0.003265004
ENSMUSG00000037857	protein_coding	Nufip2	0.625077653	0.027930941
ENSMUSG00000037580	protein_coding	Gch1	1.536817969	0.004678558
ENSMUSG00000091775	protein_coding	Gm16494	Inf	0.038817118

ENSMUSG00000020810	protein_coding	Cygb	3.211574037	0.04224035
ENSMUSG00000031861	protein_coding	Lpar2	1.61130149	0.003543204
ENSMUSG00000039470	protein_coding	Zdhhc2	0.553419493	0.00368451
ENSMUSG00000048490	protein_coding	Nrip1	0.44016962	0.042622078
ENSMUSG00000042647	protein_coding	Acad12	2.546329803	0.025684514
ENSMUSG00000024121	protein_coding	Atp6v0c	1.597492898	0.044636953
ENSMUSG00000081911	pseudogene	Mrps36-ps2	1.96583267	0.0244778
ENSMUSG00000024870	protein_coding	Rab1b	1.642416738	0.034948983
ENSMUSG00000041939	protein_coding	Mvk	1.642357685	0.003113777
ENSMUSG00000026434	protein_coding	Nucks1	0.601634926	0.010765334
ENSMUSG00000094622	protein_coding	Gm3055	0.321052124	0.044943295
ENSMUSG00000026127	protein_coding	Imp4	1.556651483	0.004179514
ENSMUSG00000043252	protein_coding	Tmem64	0.646949871	0.01140988
ENSMUSG00000025255	protein_coding	Zfhx4	0.437326188	0.014317485
ENSMUSG00000019039	protein_coding	Dalrd3	1.682832793	0.005086043
ENSMUSG00000033671	protein_coding	Cep350	0.516968513	0.028241129
ENSMUSG00000003528	protein_coding	Slc25a1	1.545702543	0.034822183
ENSMUSG00000003527	protein_coding	Dgcr14	1.540668364	0.048146673
ENSMUSG00000050002	protein_coding	Idnk	1.63964968	0.038783904
ENSMUSG00000098374	protein_coding	RNF8	1.554783342	0.040731083
ENSMUSG00000081355	pseudogene	Gm15264	6.496217328	0.001576894
ENSMUSG00000064339	Mt_rRNA	mt-Rnr2	0.424828347	0.002065595
ENSMUSG00000054065	protein_coding	Pkp3	1.562244527	0.038213068
ENSMUSG00000041354	protein_coding	Rgl2	1.893787392	0.009598832
ENSMUSG00000056579	processed_ transcript	Tug1	0.655246389	0.04843102
ENSMUSG00000022066	protein_coding	Gm21685	1.886095064	0.015159655
ENSMUSG00000032245	protein_coding	Cln6	1.681281243	0.016336121
ENSMUSG00000038250	protein_coding	Usp38	0.584297943	0.015206379
ENSMUSG00000028743	protein_coding	Akr7a5	2.049469888	0.005544379
ENSMUSG00000028744	protein_coding	Pqlc2	1.935435511	0.000318236
ENSMUSG00000087006	lincRNA	Gm13889	4.05997505	0.013462978
ENSMUSG00000039126	protein_coding	Prune2	1.690277817	0.012820535
ENSMUSG00000086755	lincRNA	Gm11216	0.031375848	0.008308377
ENSMUSG00000070394	protein_coding	Tmem256	1.500423581	0.015324512
ENSMUSG00000033192	protein_coding	Lpcat2	0.569708261	0.006305498
ENSMUSG00000000253	protein_coding	Gmpr	2.518285846	0.008839893
ENSMUSG00000027356	protein_coding	Fermt1	0.517331106	0.015331695
ENSMUSG00000027353	protein_coding	Mcm8	0.521522649	0.014366969
ENSMUSG00000048379	protein_coding	Socs4	0.523594742	0.018142494
ENSMUSG00000030423	protein_coding	Pop4	0.651352208	0.039780501
ENSMUSG00000023075	protein_coding	Akirin1	0.661226571	0.006755183
ENSMUSG00000026004	protein_coding	Kansl1l	0.490056267	0.021226223

ENSMUSG00000089961	antisense	Gm16567	0.513930448	0.017783118
ENSMUSG00000006215	protein_coding	Zbtb17	1.68275631	0.040081993
ENSMUSG00000024098	protein_coding	Twsg1	0.611453076	0.020390133
ENSMUSG00000030246	protein_coding	Ldhb	2.135588229	0.009446349
ENSMUSG00000024542	protein_coding	Cep192	0.552182542	0.026569039
ENSMUSG00000030243	protein_coding	Recql	0.579936848	0.02149551
ENSMUSG00000001768	protein_coding	Rin2	0.444510978	0.030682235
ENSMUSG00000020898	protein_coding	Ctc1	1.548102901	0.048507538
ENSMUSG00000020893	protein_coding	Per1	1.9274878	0.008148585
ENSMUSG00000096953	protein_coding	Gm26571	2.171228186	0.048710204
ENSMUSG00000023277	protein_coding	Twf2	1.685391626	0.041363508
ENSMUSG00000092243	protein_coding	Gm7030	2.396045374	0.028464235
ENSMUSG00000087639	antisense	Gm15512	2.700840819	0.029523614
ENSMUSG00000040957	protein_coding	Cables1	2.592957318	0.021057192
ENSMUSG00000070565	protein_coding	Rasal2	0.64170823	0.008175748
ENSMUSG00000021109	protein_coding	Hif1a	0.591358879	0.02870421
ENSMUSG00000046442	protein_coding	Ppm1e	0.453751938	0.025135566
ENSMUSG00000042569	protein_coding	Dhrs7b	1.829519151	0.044580457
ENSMUSG00000095308	protein_coding	Gm5619	1.502354646	0.021137584
ENSMUSG00000049047	protein_coding	Armcx3	0.624060341	0.000835137
ENSMUSG00000041143	protein_coding	Tmco4	1.503371087	0.042836468
ENSMUSG00000055360	protein_coding	Prl2c5	0.290821441	0.024363475
ENSMUSG00000057858	protein_coding	D19Ertd737e	0.506872438	0.048041058
ENSMUSG00000095432	protein_coding	Zfp748	0.453745744	0.002129303
ENSMUSG00000036022	protein_coding	Fam122b	0.58955641	0.046263263
ENSMUSG00000061286	protein_coding	Exosc5	2.461440306	0.031727193
ENSMUSG00000043019	protein_coding	Edem3	0.560807953	0.041096367
ENSMUSG00000039531	protein_coding	Zufsp	0.297028988	0.005385881
ENSMUSG00000029186	protein_coding	Pi4k2b	0.662751432	0.0099982
ENSMUSG00000070960	pseudogene	Gm10307	2.130056701	0.028646626
ENSMUSG00000028583	protein_coding	Pdpn	13.13064474	0.017272484
ENSMUSG00000086846	pseudogene	Gm13642	0.589901968	0.011224696
ENSMUSG00000024939	protein_coding	Fam89b	1.562046018	0.024687747
ENSMUSG00000085738	pseudogene	Gm12335	0.475786377	0.024105868
ENSMUSG00000029840	protein_coding	Mtpn	0.641339783	0.019034084
ENSMUSG00000017057	protein_coding	Il13ra1	0.559344483	0.040017046
ENSMUSG00000000605	protein_coding	Clcn4-2	0.658807886	0.011997355
ENSMUSG00000090124	protein_coding	Ugt1a7c	0.379842643	0.032100616
ENSMUSG00000055660	protein_coding	Mettl4	0.429891616	0.00317559
ENSMUSG00000036528	protein_coding	Ppfibp2	0.653667151	0.043512093
ENSMUSG00000038056	protein_coding	Kmt2c	0.560546487	0.024044108
ENSMUSG00000038055	protein_coding	Dexi	1.676980358	0.006161848
ENSMUSG00000042462	protein_coding	Dctpp1	1.729226263	0.034858594

ENSMUSG00000042460	protein_coding	C1galt1	0.534340477	0.033146981
ENSMUSG00000035184	protein_coding	Fam124a	0.312229892	0.041305808
ENSMUSG00000035181	protein_coding	Heatr5a	0.483465068	0.024595294
ENSMUSG00000045767	protein_coding	B230219D22Rik	0.58937083	0.032528607
ENSMUSG00000007872	protein_coding	Id3	1.924589251	0.045400314
ENSMUSG00000000884	protein_coding	Gnb1l	2.286614094	0.022959758
ENSMUSG00000082789	pseudogene	Gm13284	0.01636126	3.64E-05
ENSMUSG00000026321	protein_coding	Tnfrsf11a	0.44643151	0.034633406
ENSMUSG00000002107	protein_coding	Celf2	0.539341384	0.03688282
ENSMUSG00000033306	protein_coding	Lpp	0.597660856	0.013189944
ENSMUSG00000062931	protein_coding	Zfp938	0.436758329	0.049936273
ENSMUSG00000054302	protein_coding	Eapp	0.553404521	0.023795201
ENSMUSG00000086480	antisense	Gm15287	0.201720792	0.024157669
ENSMUSG00000096252	pseudogene	Tes3-ps	0.500057136	0.02760951
ENSMUSG00000082280	pseudogene	Gm7901	2.443944047	0.034844239
ENSMUSG00000050373	protein_coding	Snx21	2.004251126	0.002101766
ENSMUSG00000091971	protein_coding	Hspa1a	1.893906685	0.005716001
ENSMUSG00000021553	protein_coding	Slc28a3	0.359169352	0.008202105
ENSMUSG00000060586	protein_coding	H2-Eb1	6.978752804	0.017213769
ENSMUSG00000026123	protein_coding	Plekhb2	1.793793953	0.006138812
ENSMUSG00000026126	protein_coding	Ptpn18	1.738582223	0.002443326
ENSMUSG00000025746	protein_coding	Il6	0.313681396	0.044160689
ENSMUSG00000029346	protein_coding	Srrd	1.57464499	0.040440244
ENSMUSG00000087371	antisense	Gm15541	1.783693271	0.029258811
ENSMUSG00000087370	protein_coding	Tmem170b	0.453982939	0.019846471
ENSMUSG00000081434	pseudogene	Gm14165	0.283676252	0.023710597
ENSMUSG00000005150	protein_coding	Wdr83	1.980759896	0.001494418
ENSMUSG00000058586	protein_coding	Serhl	1.752098058	0.020945297
ENSMUSG00000082423	pseudogene	Gm15148	0	0.036729895
ENSMUSG00000022201	protein_coding	Zfr	0.552534117	0.022670725
ENSMUSG00000036792	protein_coding	Mbd5	0.556609333	0.046785334
ENSMUSG00000025862	protein_coding	Stag2	0.558350372	0.032142329
ENSMUSG00000025137	protein_coding	Pcyt2	1.690949882	0.000540522
ENSMUSG00000032000	protein_coding	Birc3	0.457527479	0.045185159
ENSMUSG00000032006	protein_coding	Pdgfd	0.406929776	0.043786902
ENSMUSG00000023994	protein_coding	Nfya	0.665190787	0.009541107
ENSMUSG00000053702	protein_coding	Nebl	0.238611221	0.040229187
ENSMUSG00000030513	protein_coding	Pcsk6	1.822191685	0.034647208
ENSMUSG00000072640	protein_coding	Lyrm9	1.717409646	0.033211343
ENSMUSG00000083111	pseudogene	Gm14421	0.290502469	0.047787634
ENSMUSG00000019433	protein_coding	Gipc1	1.808713618	0.007379183
ENSMUSG00000001334	protein_coding	Fndc5	2.074308876	0.02554256
ENSMUSG00000051169	protein_coding	Rpusd3	1.849541563	0.031255822

ENSMUSG00000059668	protein_coding	Krt4	1.746639562	0.024552624
ENSMUSG00000070583	protein_coding	Fv1	0.333308012	0.011490331
ENSMUSG00000002257	protein_coding	Def6	1.758233689	0.002685983
ENSMUSG00000036613	protein_coding	Tssc1	1.534166465	0.036412453
ENSMUSG00000038508	protein_coding	Gdf15	2.196644166	0.016025478
ENSMUSG00000030753	protein_coding	Prkrir	0.539865958	0.000492156
ENSMUSG00000037253	protein_coding	Mex3c	0.511949606	0.013919599
ENSMUSG00000096795	protein_coding	Zfp433	0.26894548	0.041043873
ENSMUSG00000063320	protein_coding	1190007I07Rik	0.443793363	0.023247762
ENSMUSG00000039361	protein_coding	Picalm	0.583368133	0.009313534
ENSMUSG00000020676	protein_coding	Ccl11	2.930877629	0.035366477
ENSMUSG00000030055	protein_coding	Rab43	1.625962683	0.010666509
ENSMUSG00000042978	protein_coding	Sbk1	1.716827934	0.01617083
ENSMUSG00000004655	protein_coding	Aqp1	3.525975716	0.014111082
ENSMUSG00000082946	pseudogene	Gm12177	0.262780633	0.010908693
ENSMUSG00000079084	protein_coding	Ccdc82	0.432441404	0.026447207
ENSMUSG00000040128	protein_coding	Pnrc1	0.623115429	0.005769393
ENSMUSG00000040123	protein_coding	Zmym5	0.513028674	0.043967249
ENSMUSG00000043131	protein_coding	Mob1a	0.610345109	0.005041739
ENSMUSG00000042742	protein_coding	B630005N14Rik	0.530202532	0.04437797
ENSMUSG00000046441	protein_coding	Cmtr2	0.63073934	0.028304116
ENSMUSG00000005057	protein_coding	Sh2b2	1.894385036	0.00936593
ENSMUSG00000046603	protein_coding	Tcaim	0.531465926	0.021646222
ENSMUSG00000074876	processed_ transcript	Spata5l1	0.515552075	0.036958289
ENSMUSG00000039449	protein_coding	Prpf18	0.648983367	0.012367334
ENSMUSG00000089804	antisense	Gm16136	0.553445179	0.04599459
ENSMUSG00000042694	protein_coding	Obfc1	1.512072158	0.012585792
ENSMUSG00000032717	protein_coding	Mdfi	1.676223026	0.004569167
ENSMUSG00000074890	protein_coding	Lcmt2	1.553789491	0.015536782
ENSMUSG00000087519	processed_ transcript	AV039307	0.255410914	0.009609801
ENSMUSG00000091562	processed_ transcript	Gm9581	0.493021644	0.030269022
ENSMUSG00000031383	protein_coding	Dusp9	1.520733003	0.033297111
ENSMUSG00000041440	protein_coding	Gk5	0.600015447	0.020230106
ENSMUSG00000060152	protein_coding	Pop5	1.949752321	0.022392121
ENSMUSG00000038902	protein_coding	Pogz	0.635732267	0.032979442
ENSMUSG00000019951	protein_coding	Uhrf1bp1l	0.639202939	0.009512865
ENSMUSG00000045165	protein_coding	AI467606	0.131853449	0.001240041
ENSMUSG00000032998	protein_coding	Foxj3	0.532356926	0.02789832
ENSMUSG00000034032	protein_coding	Rpap1	1.776584413	0.009243439
ENSMUSG00000026930	protein_coding	Gpsm1	1.701154048	0.019456288

ENSMUSG00000025507	protein_coding	Lrdd	1.752556322	0.013331686
ENSMUSG00000006057	protein_coding	Atp5g1	1.608009486	0.017442356
ENSMUSG00000032527	protein_coding	Pccb	1.636067822	0.034246556
ENSMUSG00000024304	protein_coding	Cdh2	0.662908043	0.042328941
ENSMUSG00000024301	protein_coding	Kifc5b	1.583823437	0.031137258
ENSMUSG00000044033	protein_coding	Ccdc141	0.381950703	0.041291349
ENSMUSG00000059555	protein_coding	Tor4a	1.587657746	0.013594321
ENSMUSG00000050786	protein_coding	Ccdc126	0.618042546	0.028248167
ENSMUSG00000095869	pseudogene	Ppp1r2-ps6	0.39489571	0.024838673
ENSMUSG00000094403	miRNA	Mir692-2a	109527.9132	0.000464519
ENSMUSG00000083788	pseudogene	Gm11499	0.15733781	0.025981936
ENSMUSG00000002031	protein_coding	Ift46	0.55016284	0.047482003
ENSMUSG00000078441	protein_coding	Scamp4	1.518633039	0.04416554
ENSMUSG00000096718	protein_coding	Zfp781	0.317360833	0.046890746
ENSMUSG00000038502	protein_coding	Ptov1	1.672227691	0.001750895
ENSMUSG00000000308	protein_coding	Ckmt1	2.745226296	0.026547468
ENSMUSG00000029022	protein_coding	Miip	1.546875224	0.013039115
ENSMUSG00000028771	protein_coding	Ptpn12	0.610988004	0.034705957
ENSMUSG00000052331	protein_coding	Ankrd44	0.610029847	0.002895737
ENSMUSG00000037940	protein_coding	Inpp4b	0.391552929	0.034490497
ENSMUSG00000086784	protein_coding	Isoc2a	2.007065916	0.037309566
ENSMUSG00000074994	protein_coding	Qser1	0.637385674	0.043933501
ENSMUSG00000027324	protein_coding	Rpusd2	1.823756365	0.046071907
ENSMUSG00000027327	protein_coding	1700037H04Rik	1.824716269	0.029849264
ENSMUSG00000078897	protein_coding	Gm4724	0.534646801	0.042107855
ENSMUSG00000083011	pseudogene	Gm12816	2.71254239	0.011660565
ENSMUSG00000083013	pseudogene	Gm12978	0.009700559	0.000294424
ENSMUSG00000096472	protein_coding	Cdkn2d	1.596452184	0.042337316
ENSMUSG00000085334	processed_ transcript	Gm12940	0.455700683	0.002203986
ENSMUSG00000029710	protein_coding	Ephb4	1.588965514	0.028420689
ENSMUSG00000021803	protein_coding	Cdhr1	20.55814452	0.000485121
ENSMUSG00000076431	protein_coding	Sox4	0.598221944	0.026205497
ENSMUSG00000096699	pseudogene	Rps19-ps4	2.254298912	0.031668579
ENSMUSG00000011831	protein_coding	Evi5	0.554630757	0.045675853
ENSMUSG00000020738	protein_coding	Sumo2	0.662681701	0.047947539
ENSMUSG00000087598	protein_coding	Zfp111	0.630123887	0.020992185
ENSMUSG00000049511	protein_coding	Htr1b	0.414574567	0.034483944
ENSMUSG00000027288	protein_coding	Zfp106	0.369184889	0.001587085
ENSMUSG00000027287	protein_coding	Snap23	0.490215215	0.000693647
ENSMUSG00000024889	protein_coding	Rce1	1.5823102	0.021044105
ENSMUSG00000024885	protein_coding	Aldh3b1	1.750035844	0.004412469
ENSMUSG00000026484	protein_coding	Rnf2	0.53853128	0.02727312

ENSMUSG00000003808	protein_coding	Farsa	1.857734909	0.01052692
ENSMUSG00000040795	protein_coding	Iqcc	1.800693684	0.036236699
ENSMUSG00000053253	protein_coding	Ndfip2	0.585203624	0.001242445
ENSMUSG00000001604	protein_coding	Tcea3	0.471751461	0.023098759
ENSMUSG00000080950	pseudogene	Gm7278	33.43135683	0.018978525
ENSMUSG00000031391	protein_coding	L1cam	1.812041923	0.001984365
ENSMUSG00000031399	protein_coding	Fam3a	1.734755028	0.006955007
ENSMUSG00000029409	protein_coding	U90926	0.106372938	0.003407241
ENSMUSG00000007908	protein_coding	Hmgcll1	0.59436741	0.007684991
ENSMUSG00000024383	protein_coding	Map3k2	0.460815406	0.023691552
ENSMUSG00000075268	pseudogene	Gm10819	1.620609272	0.012984021
ENSMUSG00000002343	protein_coding	Armc6	2.422763981	0.024044154
ENSMUSG00000040550	protein_coding	Otud6b	0.56615291	0.038516707
ENSMUSG00000006651	protein_coding	Aplp1	2.228061928	0.033327094
ENSMUSG00000097445	lincRNA	Gm26631	0.632454188	0.047969487
ENSMUSG00000041324	protein_coding	Inhba	0.603390588	0.030629725
ENSMUSG00000067608	protein_coding	Pcna-ps2	2.08944811	0.038438293
ENSMUSG00000021711	protein_coding	Trappc13	0.653478988	0.013422922
ENSMUSG00000032890	protein_coding	Rims3	2.301198339	0.03831195
ENSMUSG00000039841	protein_coding	Zfp800	0.465183372	0.017904793
ENSMUSG00000037443	protein_coding	Cep85	0.238009157	0.03743226
ENSMUSG00000030498	protein_coding	Gas2	0.620998162	0.04721987
ENSMUSG00000030232	protein_coding	Aebp2	0.475432843	0.021424197
ENSMUSG00000006262	protein_coding	Mob1b	0.501188099	0.045866341
ENSMUSG00000079559	protein_coding	Gm684	0.225310375	0.042248346
ENSMUSG00000027598	protein_coding	Itch	0.590096175	0.018913868
ENSMUSG00000098117	lincRNA	Gm26958	0.137529698	0.004809897
ENSMUSG00000017677	protein_coding	Wsb1	0.654717342	0.020672017
ENSMUSG00000047084	protein_coding	Ngrn	0.508208419	0.020711815
ENSMUSG00000015749	protein_coding	Anp32e	0.526343883	0.021634835
ENSMUSG00000022177	protein_coding	Haus4	1.680886329	0.014964766
ENSMUSG00000038127	protein_coding	Ccdc50	0.580551264	0.012011417
ENSMUSG00000035992	protein_coding	Fnip1	0.539716422	0.027884681
ENSMUSG00000069892	protein_coding	9930111J21Rik2	0.418653259	0.034593337
ENSMUSG00000069893	protein_coding	9930111J21Rik1	0.404536108	0.01790283
ENSMUSG00000032171	protein_coding	Pin1	1.556323422	0.023731741
ENSMUSG00000097415	lincRNA	AU020206	0.426762705	0.022276609
ENSMUSG00000022952	protein_coding	Runx1	0.654105054	0.036141833
ENSMUSG00000032235	protein_coding	Narg2	0.374348529	0.020836912
ENSMUSG00000040242	protein_coding	Fgfr1op2	0.516876429	0.011760408
ENSMUSG00000056665	protein_coding	Them6	2.601974128	0.003352479

ENSMUSG00000081467	pseudogene	Gm13337	108.9311319	0.000936578
ENSMUSG00000020948	protein_coding	Klhl28	0.395981181	0.00593541
ENSMUSG00000069237	protein_coding	C78339	0.511028426	0.010262974
ENSMUSG00000066357	protein_coding	Wdr6	1.66814587	0.009363024
ENSMUSG00000063802	protein_coding	Hspbp1	1.541079843	0.047867896
ENSMUSG00000066553	pseudogene	Gm6969	22.03590255	4.30E-08
ENSMUSG00000066554	pseudogene	Gm10167	0.036755795	5.67E-05
ENSMUSG00000031591	protein_coding	Asah1	0.538553032	0.026160244
ENSMUSG00000038085	protein_coding	Cnbd2	0.29914734	0.035024787
ENSMUSG00000032487	protein_coding	Ptgs2	0.547692242	0.017391348
ENSMUSG00000027510	protein_coding	Rbm38	1.959572102	0.008416916
ENSMUSG00000074925	protein_coding	Ptar1	0.639562719	0.017372349
ENSMUSG00000098975	antisense	RP23-103I12.3	2.119282395	0.016501254
ENSMUSG00000040616	protein_coding	Tmem51	1.528157623	0.028573307
ENSMUSG00000026393	protein_coding	Nek7	0.661721878	0.039092085
ENSMUSG00000026390	protein_coding	Marco	0.117536602	0.021662937
ENSMUSG00000085622	antisense	3110056K07Rik	0.493085729	0.009302643
ENSMUSG00000098196	lincRNA	Gm26964	0.372023061	0.003305174
ENSMUSG00000083669	pseudogene	Gm10169	1.560254117	0.0272904
ENSMUSG00000053801	protein_coding	Grwd1	1.691079196	0.012022654
ENSMUSG00000052812	protein_coding	Atad2b	0.431891749	0.045323245
ENSMUSG00000020253	protein_coding	Ppm1m	1.680237971	0.033064219
ENSMUSG00000070003	protein_coding	Ssbp4	1.955547828	0.037309489
ENSMUSG00000020877	protein_coding	Scrn2	1.91849139	0.042952118
ENSMUSG00000072082	protein_coding	Ccnf	1.504347771	0.023149616
ENSMUSG00000030177	protein_coding	Ccdc77	0.595234836	0.000396543
ENSMUSG00000031807	protein_coding	Pgls	1.752534117	0.034019262
ENSMUSG00000031805	protein_coding	Jak3	1.917352794	0.009298532
ENSMUSG00000038766	protein_coding	Gabpb2	0.540479199	0.048131323
ENSMUSG00000035278	protein_coding	Plekhj1	1.600777722	0.005208514
ENSMUSG00000024143	protein_coding	Rhoq	0.612825111	0.023096127
ENSMUSG00000079610	protein_coding	Ankrd39	1.533323427	0.016272917
ENSMUSG00000040423	protein_coding	Rc3h1	0.574901508	0.03775095
ENSMUSG00000089715	protein_coding	Cbx6	0.511597608	0.012819981
ENSMUSG00000061273	protein_coding	Mmgt1	0.609826782	0.013271966
ENSMUSG00000045886	protein_coding	Gm9803	1.695806544	0.031993079
ENSMUSG00000037722	protein_coding	Gnpnat1	0.625930671	0.01258129
ENSMUSG00000037096	pseudogene	Gm9762	0.588251254	0.006193787
ENSMUSG00000038371	protein_coding	Sbf2	0.615266113	0.009175873
ENSMUSG00000052137	protein_coding	Rbm12b2	0.464737026	0.042586819
ENSMUSG00000038957	protein_coding	Edc3	1.505809055	0.022208005
ENSMUSG00000025188	protein_coding	Hps1	1.607658352	0.02033568
ENSMUSG00000019988	protein_coding	Nedd1	0.610937162	0.028784594

ENSMUSG00000018585	protein_coding	Atox1	1.823316011	0.02465084
ENSMUSG00000053774	protein_coding	Ubxn7	0.560518865	0.049522672
ENSMUSG00000063767	protein_coding	S100a7a	5.119740905	0.001330727
ENSMUSG00000083166	pseudogene	Gm8648	0.425548051	0.006783951
ENSMUSG00000004837	protein_coding	Grap	0.524439574	0.027583597
ENSMUSG00000087262	pseudogene	Gm15250	0.605288118	0.021357232
ENSMUSG00000040323	pseudogene	Gm15429	1.663397562	0.04354089
ENSMUSG00000040322	protein_coding	Slc25a24	0.627170843	0.043418769
ENSMUSG00000040321	protein_coding	Zfp770	0.452932199	0.027316115
ENSMUSG00000024339	protein_coding	Tap2	1.575016057	0.037313843
ENSMUSG00000040584	protein_coding	Abcb1a	0.590904171	0.017349115
ENSMUSG00000038552	protein_coding	Fndc4	2.263538954	0.031518836
ENSMUSG00000037119	protein_coding	D15Ertd621e	0.59949196	0.026598809
ENSMUSG00000001588	protein_coding	Acap1	7.069779859	0.048810922
ENSMUSG00000021265	protein_coding	Slc25a29	2.370957536	0.020109407
ENSMUSG00000093030	miRNA	Gm23632	10.80647877	0.049123738
ENSMUSG00000025026	protein_coding	Add3	0.588786574	0.036725093
ENSMUSG00000072955	protein_coding	Tmsb15l	0.325408509	0.049244181
ENSMUSG00000037938	protein_coding	Chchd5	1.782279255	0.012102135
ENSMUSG00000024640	protein_coding	Psat1	0.608874666	0.047826645
ENSMUSG00000040875	protein_coding	Osbpl10	2.193422593	0.003398753
ENSMUSG00000034216	protein_coding	Vps18	1.624386988	0.023662545
ENSMUSG00000074634	protein_coding	Gm7120	0.424434318	0.015994748
ENSMUSG00000091639	pseudogene	Gm3756	0.183582383	0.007533816
ENSMUSG00000068699	protein_coding	Flnc	1.50948869	0.046673342
ENSMUSG00000082935	pseudogene	Gm7658	6.234993608	0.001369039
ENSMUSG00000086949	antisense	Gm13066	2.522429924	0.00122581
ENSMUSG00000082062	pseudogene	Ftl2	1.644226275	0.042843197
ENSMUSG00000098702	antisense	RP24-390G17.1	23.85238469	0.004737752
ENSMUSG00000066613	protein_coding	Zfp932	0.405424249	0.027145483
ENSMUSG00000021831	protein_coding	Ero1l	0.617332382	0.014960295
ENSMUSG00000013833	protein_coding	Med16	1.614656031	0.028558976
ENSMUSG00000033488	protein_coding	BC026585	2.49799187	0.012666533
ENSMUSG00000033487	protein_coding	Fndc3a	0.585537189	0.01172785
ENSMUSG00000072772	protein_coding	Grcc10	1.573030816	0.012158994
ENSMUSG00000048701	protein_coding	Ccdc6	0.546019833	0.026724007
ENSMUSG00000039199	protein_coding	Zdhhc1	2.421318988	0.013509191
ENSMUSG00000036944	protein_coding	Tmem71	0.59265673	0.015006955
ENSMUSG00000028228	protein_coding	Cpne3	0.600196955	0.024431197
ENSMUSG00000018217	protein_coding	Pmp22	0.589151678	0.029710916
ENSMUSG00000024856	protein_coding	Cdk2ap2	1.658862001	0.002603952
ENSMUSG00000024851	protein_coding	Pitpnm1	2.012406677	0.007147619
ENSMUSG00000004788	protein_coding	Eif2b2	1.515346291	0.012918407

ENSMUSG00000025666	protein_coding	Tmem47	0.55787648	0.039587415
ENSMUSG00000006143	protein_coding	Upk3bl	2.494742976	0.008367456
ENSMUSG00000078867	protein_coding	Gm14418	0.402544626	0.00595818
ENSMUSG00000015468	protein_coding	Notch4	1.687545852	0.016021203
ENSMUSG00000078864	protein_coding	Gm14322	0.367771292	0.003648135
ENSMUSG00000040297	protein_coding	Suco	0.559978829	0.027013401
ENSMUSG00000047213	protein_coding	Ythdf3	0.575314846	0.025975526
ENSMUSG00000066798	protein_coding	Zbtb6	0.569705156	0.04631645
ENSMUSG00000036036	protein_coding	Zfp57	2.381994172	0.018827867
ENSMUSG00000026219	protein_coding	Trip12	0.635494101	0.023795254
ENSMUSG00000026211	protein_coding	Obsl1	2.296905536	0.024789131
ENSMUSG00000038646	protein_coding	Fam103a1	0.652743194	0.014952152
ENSMUSG00000031697	protein_coding	Orc6	0.540789445	0.024799821
ENSMUSG00000026960	protein_coding	Arl6ip6	0.605161316	0.032548889
ENSMUSG00000025730	protein_coding	Rab40c	1.890872833	0.028928967
ENSMUSG00000025732	protein_coding	Fam195a	1.766001647	0.049410968
ENSMUSG00000044080	protein_coding	S100a1	2.134233789	0.001357455
ENSMUSG00000024958	protein_coding	Gpr137	1.784598827	0.047717793
ENSMUSG00000082536	pseudogene	Gm13456	0.370070275	0.005394736
ENSMUSG00000002043	protein_coding	Trappc6a	1.766360565	0.034774206
ENSMUSG00000081378	pseudogene	Rps13-ps4	0.552519022	0.005630097
ENSMUSG00000079297	pseudogene	Gm2223	0.623940712	0.00644037
ENSMUSG00000028636	protein_coding	Ppcs	1.768855398	0.020643799
ENSMUSG00000041378	protein_coding	Cldn5	5.63718825	0.017110426
ENSMUSG00000057604	protein_coding	Lmcd1	1.999902111	0.045230014
ENSMUSG00000052384	protein_coding	Nrros	2.689206368	0.002201829
ENSMUSG00000023845	protein_coding	Lnpep	0.523767045	0.011379734
ENSMUSG00000035868	protein_coding	3110052M02Rik	0.34796894	0.001045491
ENSMUSG00000018604	protein_coding	Tbx3	0.476587344	0.006233764
ENSMUSG00000020092	protein_coding	Pald1	1.653826194	0.030796993
ENSMUSG00000037410	protein_coding	Tbc1d2b	1.728630407	0.036307938
ENSMUSG00000027957	protein_coding	Slc35a3	0.602810798	0.010931225
ENSMUSG00000079509	protein_coding	Zfx	0.551187866	0.04042717
ENSMUSG00000041570	protein_coding	Camsap2	0.61025551	0.020904107
ENSMUSG00000024563	protein_coding	Smad2	0.658189451	0.042512907
ENSMUSG00000081232	pseudogene	Gm14373	0.422986647	0.028811071
ENSMUSG00000064023	protein_coding	Klk8	2.600634541	0.019594924
ENSMUSG00000083563	pseudogene	Gm13340	0.52373412	0.023071733
ENSMUSG00000019428	protein_coding	Fkbp8	1.531400074	0.044859606
ENSMUSG00000067058	pseudogene	Rps15a-ps5	0.190141732	0.001181036
ENSMUSG00000038175	protein_coding	Mylip	0.572448018	0.037060523
ENSMUSG00000026721	protein_coding	Rabgap1l	0.577741323	0.047799704

ENSMUSG00000026180	protein_coding	Cxcr2	2.144033679	0.019928542
ENSMUSG00000026185	protein_coding	Igfbp5	2.454006564	0.002363209
ENSMUSG00000074064	protein_coding	Mlycd	2.460151505	0.02649814
ENSMUSG00000074063	protein_coding	Osgin1	1.553494557	0.009026394
ENSMUSG00000034480	protein_coding	Diap2	0.616986862	0.030485718
ENSMUSG00000083360	pseudogene	Gm13105	0.402290263	0.042383536
ENSMUSG00000042508	protein_coding	Dmtf1	0.502177721	0.005967863
ENSMUSG00000002416	protein_coding	Ndufb2	1.922825125	0.010510371
ENSMUSG00000035754	protein_coding	Wdr18	1.621405435	0.039648685
ENSMUSG00000050192	protein_coding	Eif5a2	0.454175382	0.003814343
ENSMUSG00000024241	protein_coding	Sos1	0.555009532	0.046975207
ENSMUSG00000050440	protein_coding	Hamp	26.60458793	0.043977087
ENSMUSG00000051319	lincRNA	1500011K16Rik	1.616757594	0.002581542
ENSMUSG00000029221	protein_coding	Slc30a9	0.639326001	0.036389041
ENSMUSG00000020937	protein_coding	Plcd3	1.967587976	0.021348457
ENSMUSG00000031070	protein_coding	Mrgprf	4.872164936	0.019769659
ENSMUSG00000022420	protein_coding	Dnal4	1.904669973	0.001312389
ENSMUSG00000036860	protein_coding	Mrpl55	0.626023915	0.028775025
ENSMUSG00000036863	protein_coding	Syde2	0.413550231	0.010684988
ENSMUSG00000020153	protein_coding	Ndufs7	1.588462456	0.036136851
ENSMUSG00000048807	protein_coding	Slc35e4	1.685561722	0.017723695
ENSMUSG00000080873	pseudogene	Rpl30-ps3	0.459039951	0.004827473
ENSMUSG00000029823	protein_coding	Luc7l2	0.64343085	0.02516138
ENSMUSG00000084403	pseudogene	Rps15a-ps8	0.003613855	0.004147457
ENSMUSG00000074746	protein_coding	Pdzd8	0.640342491	0.045109135
ENSMUSG00000046096	protein_coding	BC030336	0.615612078	0.011179904
ENSMUSG00000036199	protein_coding	Ndufa13	1.516045544	0.016234552
ENSMUSG00000041046	protein_coding	Ramp3	3.445091761	0.003472542
ENSMUSG00000040026	protein_coding	Saa3	0.230487981	0.047762837
ENSMUSG00000025533	protein_coding	Asl	1.718695911	0.030634088
ENSMUSG00000020019	protein_coding	Ntn4	0.184878858	0.007025107
ENSMUSG00000071064	protein_coding	Zfp827	0.613105925	0.043898869
ENSMUSG00000001918	protein_coding	Slc1a5	0.169131584	0.014626492
ENSMUSG00000038072	protein_coding	Galnt11	2.491781136	0.015242846
ENSMUSG00000032846	protein_coding	Zswim6	0.66203639	0.024670393
ENSMUSG00000031791	protein_coding	Tmem38a	1.772410682	0.027482662
ENSMUSG00000024072	protein_coding	Yipf4	0.525857538	0.04732503
ENSMUSG00000058793	protein_coding	Cds2	1.814505757	0.034839924
ENSMUSG00000058799	protein_coding	Nap1l1	0.621832182	0.037361578
ENSMUSG00000080932	pseudogene	Gm10224	1.514284559	0.026637011
ENSMUSG00000025348	protein_coding	Itga7	1.781308593	0.025162249
ENSMUSG00000026343	protein_coding	Gpr39	2.139499836	0.014457375
ENSMUSG00000017607	protein_coding	Tns4	3.763402828	0.040886593

ENSMUSG00000097517	lincRNA	Gm26695	3.784526803	0.047957228
ENSMUSG00000050359	protein_coding	Sprr1a	11.70003154	0.000353093
ENSMUSG00000066362	pseudogene	Rps13-ps1	0.225167759	0.000954158
ENSMUSG00000033454	protein_coding	Zbtb1	0.462217615	0.038113713
ENSMUSG00000026103	protein_coding	Gls	0.554418044	0.021274978
ENSMUSG00000026107	protein_coding	Nabp1	0.57618357	0.008506457
ENSMUSG00000034158	protein_coding	Lrrc58	0.611278583	0.001597601
ENSMUSG00000046352	protein_coding	Gjb2	0.557117126	0.026310494
ENSMUSG00000035206	protein_coding	Sppl2b	1.82516413	0.005808559
ENSMUSG00000028414	protein_coding	Fktn	0.66258497	0.048621703
ENSMUSG00000044864	protein_coding	Ankrd50	0.594761972	0.004743906
ENSMUSG00000032263	protein_coding	Bckdhb	2.601726488	0.018362498
ENSMUSG00000047749	protein_coding	Zc3hav1l	0.555848866	0.030060568
ENSMUSG00000027778	protein_coding	Ift80	0.567034714	0.02454636
ENSMUSG00000009575	protein_coding	Cbx5	0.415540109	0.018128189
ENSMUSG00000083449	pseudogene	Gm13487	0.330127246	0.019524932
ENSMUSG00000017418	protein_coding	Arl5b	0.536484548	0.035421966
ENSMUSG00000001627	protein_coding	Ifrd1	0.545357533	0.040568343
ENSMUSG00000001622	protein_coding	Csn3	2.197619552	0.032630839
ENSMUSG00000040936	protein_coding	Ulk4	0.660925211	0.015073817
ENSMUSG00000038347	protein_coding	Tcte2	0.397652076	0.019450131
ENSMUSG00000025153	protein_coding	Fasn	1.562243346	0.020443691
ENSMUSG00000028382	protein_coding	Ptbp3	0.548878756	0.021117074
ENSMUSG00000028381	protein_coding	Ugcg	0.660169253	0.025436994
ENSMUSG00000032060	protein_coding	Cryab	1.921432695	0.043961191
ENSMUSG00000032932	protein_coding	Hspa13	0.632934389	0.016700038
ENSMUSG00000027170	protein_coding	Eif3m	0.540826118	0.004082667
ENSMUSG00000020380	protein_coding	Rad50	0.589717492	0.026822773
ENSMUSG00000027177	protein_coding	Hipk3	0.560928037	0.030676817
ENSMUSG00000075470	protein_coding	Alg10b	0.521367265	0.011369406
ENSMUSG00000045095	protein_coding	Magi1	0.452073444	0.018833045
ENSMUSG00000024360	protein_coding	Etf1	0.639378183	0.03210856
ENSMUSG00000032293	protein_coding	Ireb2	0.585830587	0.04123814
ENSMUSG00000041954	protein_coding	Tnfrsf18	2.578586599	0.045586529
ENSMUSG00000050105	protein_coding	Grrp1	2.843356343	0.026716115
ENSMUSG00000053522	protein_coding	Lgals7	0.1788679	0.00748083
ENSMUSG00000036639	protein_coding	Nudt1	1.560365836	0.028119741
ENSMUSG00000014158	protein_coding	Trpv4	1.525617579	0.000886373
ENSMUSG00000059900	protein_coding	Tmem40	1.895600558	0.01560518
ENSMUSG00000001018	protein_coding	Snapin	0.567553108	0.000938649
ENSMUSG00000048142	protein_coding	Nat8l	2.097245572	0.013384303
ENSMUSG00000048149	pseudogene	Gm12663	2.855430274	0.007648168
ENSMUSG00000035757	protein_coding	Selo	1.532606527	0.034972686

ENSMUSG00000070372	protein_coding	Capza1	0.452063813	0.001636534
ENSMUSG00000037242	protein_coding	Clic4	0.599951543	0.01138256
ENSMUSG00000033166	protein_coding	Dis3	0.65146902	0.033516246
ENSMUSG00000058873	pseudogene	Gm5582	0.509768654	0.029282419
ENSMUSG00000063317	protein_coding	Usp31	0.606305694	0.006597809
ENSMUSG00000031168	protein_coding	Ebp	1.750396619	0.047211739
ENSMUSG00000040102	protein_coding	Klhl42	0.614804533	0.01967469
ENSMUSG00000032320	protein_coding	Rcn2	0.640028745	0.004439556
ENSMUSG00000053935	protein_coding	Atf7ip	0.618701275	0.006545699
ENSMUSG00000099083	protein_coding	ATF7	0.664798443	0.008642771
ENSMUSG00000033364	protein_coding	Usp37	0.650130912	0.032235673
ENSMUSG00000021867	protein_coding	Tmem254b	2.463116548	0.000932675
ENSMUSG00000021866	protein_coding	Anxa11	1.516008351	0.047368472
ENSMUSG00000038481	protein_coding	Cdk19	0.628348274	0.016575832
ENSMUSG00000038736	protein_coding	Nudcd1	0.648551273	0.038495341
ENSMUSG00000049421	protein_coding	Zfp260	0.657289933	0.018258304
ENSMUSG00000034731	protein_coding	Dgkh	0.613011228	0.005195604
ENSMUSG00000029545	protein_coding	Acads	1.649076516	0.042923008
ENSMUSG00000044573	protein_coding	Acp1	0.492291915	0.041665596
ENSMUSG00000024790	protein_coding	Sac3d1	1.590120912	0.03955599
ENSMUSG00000026798	protein_coding	Coq4	2.113637724	0.005665277
ENSMUSG00000040472	protein_coding	Rabggta	1.558977863	0.041070517
ENSMUSG00000026420	protein_coding	Il24	2.023176924	0.049953766
ENSMUSG00000047126	protein_coding	Cltc	0.657652115	0.009448229
ENSMUSG00000040280	protein_coding	Ndufa4l2	10.86606157	0.02239018
ENSMUSG00000040738	protein_coding	Ints8	0.603875594	0.024750937
ENSMUSG00000023973	protein_coding	Cnpy3	1.686785508	0.042880822
ENSMUSG00000019978	protein_coding	Epb4.1l2	0.625429917	0.031484301
ENSMUSG00000020300	protein_coding	Cpeb4	0.541888288	0.018902855
ENSMUSG00000060279	protein_coding	Ap2a1	1.539820889	0.038730129
ENSMUSG00000073422	protein_coding	H2-Ke6	1.57626821	0.017783389
ENSMUSG00000035365	protein_coding	Parpbp	0.605043475	0.021836914
ENSMUSG00000042046	protein_coding	Dstyk	0.599981717	0.03251959
ENSMUSG00000004885	protein_coding	Crabp2	3.103088998	0.009723583
ENSMUSG00000034947	protein_coding	Tmem106a	1.525295312	0.007040652
ENSMUSG00000086563	lincRNA	Gm14136	Inf	0.00941344
ENSMUSG00000042446	protein_coding	Zmym4	0.608787514	0.009631223
ENSMUSG00000046027	protein_coding	Stard5	1.567273225	0.001971542
ENSMUSG00000064264	protein_coding	Zfp428	1.640952873	0.00880763
ENSMUSG00000079733	protein_coding	Tmem181b-ps	1.749382791	0.004745081
ENSMUSG00000032554	protein_coding	Trf	2.010036909	0.040613458
ENSMUSG00000041346	protein_coding	Wrap53	1.657074404	0.011802092
ENSMUSG00000029134	protein_coding	Plb1	0.375739168	0.048017021

ENSMUSG00000062078	protein_coding	Qk	0.561327129	0.027727813
ENSMUSG00000062075	protein_coding	Lmnb2	1.566428562	0.027466604
ENSMUSG00000037965	protein_coding	Zc3h7a	0.610066654	0.022517579
ENSMUSG00000092843	miRNA	Gm24332	6.755100677	0.02763102
ENSMUSG00000038880	protein_coding	Mrps34	1.578400573	0.000122236
ENSMUSG00000038886	protein_coding	Man2a2	1.708450786	0.002079582
ENSMUSG00000039130	protein_coding	Zc3hc1	1.790104735	0.035528689
ENSMUSG00000021775	protein_coding	Nr1d2	0.643862139	0.0276718
ENSMUSG00000027341	protein_coding	Tmem230	1.60661557	0.014369784
ENSMUSG00000027962	protein_coding	Vcam1	0.575857695	0.047009155
ENSMUSG00000027966	protein_coding	Col11a1	0.511616696	0.000688923
ENSMUSG00000006782	protein_coding	Cnp	1.697691941	0.043312977
ENSMUSG00000024084	protein_coding	Qpct	0.586769104	0.002071726
ENSMUSG00000024085	protein_coding	Man2a1	0.608487579	0.041604083
ENSMUSG00000040187	protein_coding	Arntl2	0.453052285	0.001199534
ENSMUSG00000091903	protein_coding	Gm6460	0.309340117	0.00636746
ENSMUSG00000071713	protein_coding	Csf2rb	1.55805555	0.014071302
ENSMUSG00000002222	protein_coding	Rmnd5a	0.544440738	0.014277838
ENSMUSG00000042632	protein_coding	Pla2g6	1.649447975	0.036332138
ENSMUSG00000032116	protein_coding	Stt3a	0.631305306	0.01763453
ENSMUSG00000006423	protein_coding	C330007P06Rik	0.633623218	0.043530701
ENSMUSG00000003824	protein_coding	Syce2	0.574644788	0.007276386
ENSMUSG00000062758	protein_coding	Gm16477	1.51138572	0.022934373
ENSMUSG00000036707	protein_coding	Cab39	0.621938474	0.045774122
ENSMUSG00000034674	protein_coding	Tdg	0.565344405	0.019480229
ENSMUSG00000012640	protein_coding	Zfp715	0.569664662	0.016588167
ENSMUSG00000020102	protein_coding	Slc16a7	0.627445217	0.043770776
ENSMUSG00000044328	protein_coding	Trp53i13	2.019302933	0.027203362
ENSMUSG00000096035	protein_coding	Gm1045	20.30932724	0.018323196
ENSMUSG00000001542	protein_coding	Ell2	0.579223248	0.049483972
ENSMUSG00000097340	lincRNA	Gm26617	0.522090502	0.047778542
ENSMUSG00000093378	processed_ transcript	Gm20663	0.234892267	0.049241013
ENSMUSG00000052688	protein_coding	5430435G22Rik	0.4267864	0.001541776
ENSMUSG00000052681	protein_coding	Rap1b	0.602991461	0.044148063
ENSMUSG00000020023	protein_coding	Tmcc3	0.665988518	0.04162493
ENSMUSG00000096474	pseudogene	Gm5561	9.959146487	0.033524
ENSMUSG00000026070	protein_coding	Il18r1	0.49534495	0.01884274
ENSMUSG00000069633	protein_coding	Pex11g	1.603759511	0.00708513
ENSMUSG00000038024	protein_coding	Dennd4c	0.571513454	0.032383302
ENSMUSG00000046229	protein_coding	Scand1	1.70857322	0.047963871
ENSMUSG00000043618	pseudogene	Eif5al3-ps	8.610470981	0.001302018
ENSMUSG00000071856	protein_coding	Mcc	0.594416317	0.041096591

ENSMUSG00000027068	protein_coding	Dhrs9	3.076354279	0.013643543
ENSMUSG00000093954	protein_coding	Gm21464	2.131742596	0.02032976
ENSMUSG00000081262	pseudogene	Gm12261	0.393437798	0.049719669
ENSMUSG00000029638	protein_coding	Glcci1	0.560604526	0.036339921
ENSMUSG00000037622	protein_coding	Wdtc1	1.740732654	0.036625759
ENSMUSG00000022159	protein_coding	Rab2b	0.327779534	0.002255357
ENSMUSG00000097616	lincRNA	1110019D14Rik	0.272607682	0.002515544
ENSMUSG00000036990	protein_coding	Otud4	0.567061898	0.035075035
ENSMUSG00000057751	protein_coding	Megf6	2.5606622	0.047094981
ENSMUSG00000020794	protein_coding	Ube2g1	0.617855984	0.035715476
ENSMUSG00000095918	protein_coding	Gm5861	0.232086096	0.000665245
ENSMUSG00000022948	protein_coding	Setd4	2.827430583	0.004062675
ENSMUSG00000021549	protein_coding	Rasa1	0.494831183	0.024269809
ENSMUSG00000068744	protein_coding	Psrc1	2.109906934	0.009881815
ENSMUSG00000042447	protein_coding	Mios	0.552123085	0.025027283
ENSMUSG00000071649	protein_coding	B3gat3	1.636908049	0.011683071
ENSMUSG00000046380	protein_coding	Jrk	3.035724282	0.008282536
ENSMUSG00000029376	protein_coding	Mthfd2l	0.607562666	0.021100699
ENSMUSG00000035781	protein_coding	R3hdm4	1.553029116	0.017532594
ENSMUSG00000000085	protein_coding	Scmh1	1.696400118	0.03408686
ENSMUSG00000027428	protein_coding	Rbbp9	0.52514201	0.017917635
ENSMUSG00000027420	protein_coding	Bfsp1	2.444156418	0.03507797
ENSMUSG00000079671	protein_coding	2610203C22Rik	3.269099494	0.02911373
ENSMUSG00000032252	protein_coding	Glce	0.61572884	0.028562998
ENSMUSG00000016487	protein_coding	Ppfibp1	0.521654985	0.002216466
ENSMUSG00000074811	protein_coding	Hps6	1.975722459	0.011954522
ENSMUSG00000048772	protein_coding	Tmem53	1.703490957	0.047724561
ENSMUSG00000020962	protein_coding	Gtf2a1	0.574634846	0.012474706
ENSMUSG00000031333	protein_coding	Abcb7	0.553401492	0.029505749
ENSMUSG00000029176	protein_coding	Anapc4	0.599563299	0.027980969
ENSMUSG00000020189	protein_coding	Osbpl8	0.467358373	0.029875836
ENSMUSG00000049811	protein_coding	Fam161a	1.978484138	0.02363679
ENSMUSG00000003500	protein_coding	Impdh1	1.5176624	0.030805085
ENSMUSG00000008167	protein_coding	Fbxw9	2.750124757	0.007462882
ENSMUSG00000058126	protein_coding	Tpm3-rs7	3.912056151	0.005518293
ENSMUSG00000050730	protein_coding	Arhgap42	0.55327596	0.035280538
ENSMUSG00000041966	protein_coding	Dcaf17	0.541437944	0.002592881
ENSMUSG00000056380	protein_coding	Gpr50	0.524514787	0.004071757
ENSMUSG00000020015	protein_coding	Cdk17	0.580506301	0.018682438
ENSMUSG00000033216	protein_coding	Eefsec	1.584093906	0.015013896
ENSMUSG00000033213	protein_coding	AA467197	0.032359702	0.000840947
ENSMUSG00000021282	protein_coding	Eif5	0.611251402	0.044089134
ENSMUSG00000022533	protein_coding	Atp13a3	0.4413868	0.025007185

ENSMUSG00000029703	protein_coding	Lrwd1	1.671008693	0.008080527
ENSMUSG00000033792	protein_coding	Atp7a	0.358580393	0.040082221
ENSMUSG00000026623	protein_coding	Lpgat1	0.586494996	0.008659463
ENSMUSG00000008822	protein_coding	Acyp1	0.431262133	0.008463602
ENSMUSG00000059842	protein_coding	Zfp341	1.862726159	0.041963553
ENSMUSG00000000489	protein_coding	Pdgfb	0.407684733	0.034093697
ENSMUSG00000025429	protein_coding	Pstpip2	0.48730891	0.006567473
ENSMUSG00000020594	protein_coding	Pum2	0.624706591	0.000917313
ENSMUSG00000019843	protein_coding	Fyn	0.64374936	0.019141257
ENSMUSG00000021893	protein_coding	Capn7	0.472603393	0.039442637
ENSMUSG00000020859	protein_coding	Spag9	0.617471641	0.016707864
ENSMUSG00000097062	lincRNA	Gm17586	1.818298325	0.036976209
ENSMUSG00000037235	protein_coding	Mxd4	1.982317457	0.008191117
ENSMUSG00000042688	protein_coding	Mapk6	0.602251908	0.033523648
ENSMUSG00000025986	protein_coding	Slc39a10	0.544516876	0.010260615
ENSMUSG00000021070	protein_coding	Bdkrb2	0.588549209	0.045336497
ENSMUSG00000042357	protein_coding	Gjb5	1.912324908	0.035470397
ENSMUSG00000024298	protein_coding	Zfp871	0.433221401	0.017477192
ENSMUSG00000040447	protein_coding	Spns2	1.717687082	0.033774103
ENSMUSG00000023066	protein_coding	Rttn	0.630762816	0.032798906
ENSMUSG00000092626	processed_ transcript	9130230N09Rik	0.102819546	0.028051926
ENSMUSG00000097667	lincRNA	Gm26764	1.931931948	0.032436814
ENSMUSG00000041459	protein_coding	Tardbp	0.644454845	0.007502981
ENSMUSG00000022749	protein_coding	Tbc1d23	0.629498849	0.031690386
ENSMUSG00000022748	protein_coding	Cmss1	1.635826652	0.021428721
ENSMUSG00000039046	protein_coding	Usp6nl	0.595720931	0.022966067
ENSMUSG00000023909	protein_coding	Paqr4	1.808379059	0.036167379
ENSMUSG00000068394	protein_coding	Cep152	0.595367511	0.04674816
ENSMUSG00000027104	protein_coding	Atf2	0.534011746	0.02961546
ENSMUSG00000054226	protein_coding	Tprkb	0.641924242	0.005042828
ENSMUSG00000031982	protein_coding	Arv1	1.739995734	0.00702993
ENSMUSG00000071451	protein_coding	Psmg4	1.521449329	0.00358729
ENSMUSG00000046791	protein_coding	2410016O06Rik	1.604034131	0.040484919
ENSMUSG00000032519	protein_coding	Slc25a38	2.078530622	0.02896989
ENSMUSG00000032513	protein_coding	Gorasp1	1.501634385	0.002273309
ENSMUSG00000024319	protein_coding	Vps52	1.77700724	0.030300397
ENSMUSG00000027660	protein_coding	Skil	0.562991626	0.019816422
ENSMUSG00000027665	protein_coding	Pik3ca	0.556006033	0.046725679
ENSMUSG00000080893	pseudogene	Gm15920	3.329451872	0.001866435
ENSMUSG00000066026	protein_coding	Dhrs3	0.42126141	0.006707634
ENSMUSG00000067869	pseudogene	Tcea1-ps1	0.61188929	0.003990117
ENSMUSG00000055041	protein_coding	Commd5	1.994958702	0.021541837

ENSMUSG00000056537	protein_coding	Rlim	0.566267673	0.03513402
ENSMUSG00000056536	protein_coding	Pign	0.465969951	0.007792368
ENSMUSG00000028788	protein_coding	Ptp4a2	0.522140265	0.00942461
ENSMUSG00000029787	protein_coding	Avl9	0.54422798	0.045814995
ENSMUSG00000038217	protein_coding	Tlcd2	2.195785124	0.006056916
ENSMUSG00000038212	protein_coding	Hiatl1	0.565379038	0.010671249
ENSMUSG00000059013	protein_coding	Sh2d3c	2.26021758	0.046617112
ENSMUSG00000021469	protein_coding	Msx2	1.704818785	0.025767489
ENSMUSG00000040818	protein_coding	Dennd6a	0.621424201	0.044725047
ENSMUSG00000024576	protein_coding	Csnk1a1	0.592128904	0.016343516
ENSMUSG00000038618	protein_coding	Rassf7	1.698539804	0.009202144
ENSMUSG00000083022	pseudogene	Rps15a-ps6	1.905567442	0.006512515
ENSMUSG00000035142	protein_coding	Nubpl	0.508419128	0.03107837
ENSMUSG00000041801	protein_coding	Phlda3	1.769092523	0.039076464
ENSMUSG00000092586	protein_coding	Ly6g6c	4.931792699	0.031405244
ENSMUSG00000014852	protein_coding	Adamts13	0.479416241	0.028574611
ENSMUSG00000013858	protein_coding	Tmem259	1.544762194	0.042700736
ENSMUSG00000096112	miRNA	Gm26269	0.194496943	0.017627162
ENSMUSG00000033319	protein_coding	Fem1c	0.561337042	0.03478019
ENSMUSG00000002279	protein_coding	Lmf1	2.5518365	0.005493752
ENSMUSG00000039789	protein_coding	Zfp597	0.412966457	0.045581786
ENSMUSG00000096910	protein_coding	Zfp955b	0.574874811	0.042850721
ENSMUSG00000069355	protein_coding	Gm5152	0.199457596	0.040522425
ENSMUSG00000029598	protein_coding	Plbd2	1.563149543	0.009421308
ENSMUSG00000020747	protein_coding	2310067B10Rik	1.506404986	0.022189048
ENSMUSG00000028248	protein_coding	Sfrs18	0.623953781	0.024051284
ENSMUSG00000028249	protein_coding	Sdcbp	0.602909423	0.046473142
ENSMUSG00000028860	protein_coding	Sytl1	3.307043619	0.005175533
ENSMUSG00000005410	protein_coding	Mcm5	1.5297627	0.037344354
ENSMUSG00000085525	lincRNA	Gm13166	0.210586702	0.048361702
ENSMUSG00000049130	protein_coding	C5ar1	0.400038727	0.013466643
ENSMUSG00000040767	protein_coding	Snrnp25	1.611005433	0.010778404
ENSMUSG00000049606	protein_coding	Zfp644	0.466232415	0.041225018
ENSMUSG00000054733	protein_coding	Msra	1.855622598	0.009046315
ENSMUSG00000071722	protein_coding	Spin4	0.587047842	0.028245829
ENSMUSG00000049686	protein_coding	Orai1	1.595570166	0.005297773
ENSMUSG00000026941	protein_coding	Mamdc4	0.077538712	0.00462729
ENSMUSG00000070923	protein_coding	Klhl9	0.519563046	0.00647932
ENSMUSG00000048087	protein_coding	Gm4737	2.841606308	0.003094814
ENSMUSG00000034997	protein_coding	Htr2a	0.303893821	0.02697941
ENSMUSG00000032598	protein_coding	Nckipsd	1.552735389	0.022431858
ENSMUSG00000005609	protein_coding	Ctr9	0.610224257	0.038562232
ENSMUSG00000040564	protein_coding	Apoc1	31.91678282	0.032235077

ENSMUSG00000001774	protein_coding	Chordc1	0.543084801	0.028861652
ENSMUSG00000026535	protein_coding	Ifi202b	0.182144664	0.040710162
ENSMUSG00000008730	protein_coding	Hipk1	0.614960221	0.036928296
ENSMUSG00000095362	protein_coding	Gm14325	0.423249692	0.005261555
ENSMUSG00000023262	protein_coding	Acy1	1.875925947	0.036007075
ENSMUSG00000017548	protein_coding	Suz12	0.439325915	0.017685216
ENSMUSG00000032372	protein_coding	Plscr2	0.465437962	0.003728918
ENSMUSG00000094800	pseudogene	Gm9780	3.868203132	0.04534847
ENSMUSG00000060032	protein_coding	H2afj	1.824065191	0.016463544
ENSMUSG00000020072	protein_coding	Pbld1	1.756117846	0.017563027
ENSMUSG00000027931	protein_coding	Npr1	2.244509675	0.045923479
ENSMUSG00000003444	protein_coding	Med29	1.643206221	0.000445627
ENSMUSG00000041889	protein_coding	Shisa4	1.836188215	0.02200698
ENSMUSG00000016534	protein_coding	Lamp2	0.632999734	0.039799243
ENSMUSG00000015750	protein_coding	Aph1a	1.724461169	0.023318924
ENSMUSG00000067071	protein_coding	Hes6	1.618374351	0.032215261
ENSMUSG00000054836	protein_coding	Elp6	1.781488848	0.009491016
ENSMUSG00000050335	protein_coding	Lgals3	1.693794927	0.032049679
ENSMUSG00000028134	protein_coding	Ptbp2	0.629997435	0.009940437
ENSMUSG00000039285	protein_coding	Azi2	0.660203708	0.015208211
ENSMUSG00000071337	protein_coding	Tia1	0.538103901	0.001576022
ENSMUSG00000087679	lincRNA	C330006A16Rik	1.535142511	0.042499297
ENSMUSG00000060096	pseudogene	Amd-ps3	0.497749548	0.020186751
ENSMUSG00000062300	protein_coding	Pvrl2	1.653978188	0.005183557
ENSMUSG00000073802	protein_coding	Cdkn2b	1.743520244	0.044923735
ENSMUSG00000078881	protein_coding	Gm14434	0.447025974	0.047385363
ENSMUSG00000000296	protein_coding	Tpd52l1	1.852580096	0.000360929
ENSMUSG00000044562	protein_coding	Rasip1	2.793545545	0.003504755
ENSMUSG00000091549	pseudogene	Gm6548	0.32132922	0.006116913
ENSMUSG00000020956	protein_coding	Dtd2	0.250081588	0.003896093
ENSMUSG00000072568	protein_coding	Fam84b	0.595704775	0.019342032
ENSMUSG00000037007	protein_coding	Zfp113	0.499323957	0.045815923
ENSMUSG00000029142	protein_coding	Mrpl33	0.582602332	0.047262289
ENSMUSG00000025790	protein_coding	Slco3a1	0.563146785	0.005572137
ENSMUSG00000027479	protein_coding	Mapre1	0.652418749	0.02736103
ENSMUSG00000018570	protein_coding	2810408A11Rik	2.788337863	0.009628796
ENSMUSG00000033068	protein_coding	Entpd6	1.602319699	0.038939433
ENSMUSG00000033065	protein_coding	Pfkm	1.608433687	0.038348577
ENSMUSG00000005686	protein_coding	Ampd3	1.586980187	0.033718263
ENSMUSG00000079492	protein_coding	Gm11127	1.852767729	0.031375007
ENSMUSG00000081883	pseudogene	Gm15574	0.468311428	0.036787234
ENSMUSG00000041935	protein_coding	AW549877	0.465816508	0.018309843
ENSMUSG00000017831	protein_coding	Rab5a	0.567434449	0.015220874

ENSMUSG00000019139	protein_coding	Isyna1	1.612100214	0.005203616
ENSMUSG00000094627	pseudogene	Gm10182	2.598121447	0.001100664
ENSMUSG00000030793	protein_coding	Pycard	2.651036582	0.021337393
ENSMUSG00000039323	protein_coding	Igfbp2	0.581965732	0.038193534
ENSMUSG00000032496	protein_coding	Ltf	3.144732106	0.034571338
ENSMUSG00000042115	protein_coding	Klhdc8a	1.60492632	0.036966268
ENSMUSG00000024050	protein_coding	Wiz	0.618594836	0.038985125
ENSMUSG00000043333	protein_coding	Rhbdl2	0.662194309	0.011525936
ENSMUSG00000026361	protein_coding	Cdc73	0.64991766	0.01075973
ENSMUSG00000085636	processed_ transcript	Gm11769	1.563748913	0.015129021
ENSMUSG00000098183	lincRNA	Gm27010	2.197818944	0.013952069
ENSMUSG00000046133	protein_coding	C130073F10Rik	5.163510434	0.025935525
ENSMUSG00000053870	protein_coding	Fpgt	0.648090956	0.048965677
ENSMUSG00000022105	protein_coding	Rb1	0.527900605	0.045347757
ENSMUSG00000051469	protein_coding	Zfp191	0.521468138	0.003998962
ENSMUSG00000039201	protein_coding	Tbc1d25	1.551942441	0.038045066
ENSMUSG00000068264	protein_coding	Ap5s1	1.749299622	0.030778389
ENSMUSG00000019813	protein_coding	Cep57l1	0.59770529	0.022350113
ENSMUSG00000074553	pseudogene	Gm10713	0.350502898	0.00080409
ENSMUSG00000003271	protein_coding	Sult2b1	0.325743572	0.030789165
ENSMUSG00000026832	protein_coding	Cytip	0.352764449	0.016493262
ENSMUSG00000011254	protein_coding	Thg1l	1.532014079	0.008241575
ENSMUSG00000029385	protein_coding	Ccng2	0.624910968	0.025406896
ENSMUSG00000029386	protein_coding	Tctn2	1.591020073	0.001223878
ENSMUSG00000048799	protein_coding	Cep120	0.647877083	0.011499377
ENSMUSG00000028470	protein_coding	Hint2	1.549855326	0.010076254
ENSMUSG00000006356	protein_coding	Crip2	1.788287615	0.004755242
ENSMUSG00000031722	protein_coding	Hp	0.285739086	0.030595236
ENSMUSG00000059412	protein_coding	Fxyd2	0.263166152	0.023468476
ENSMUSG00000082399	pseudogene	Gm14036	2.421009801	0.020452543
ENSMUSG00000080700	pseudogene	Gm15981	2.05606493	0.035910832
ENSMUSG00000028671	protein_coding	Gale	1.652211323	0.014801419
ENSMUSG00000053291	protein_coding	Rab4b	1.576067519	0.049552101
ENSMUSG00000032952	protein_coding	Ap4b1	0.457986175	0.006323345
ENSMUSG00000072680	protein_coding	Tmem254c	2.360950718	0.001267783
ENSMUSG00000073158	protein_coding	9030624G23Rik	0.579047284	0.016930962
ENSMUSG00000034926	protein_coding	Dhcr24	1.679114266	0.019712591
ENSMUSG00000006095	protein_coding	Tbcb	1.585585018	0.037573639
ENSMUSG00000040339	protein_coding	Fam102b	0.652505564	0.025587021
ENSMUSG00000079418	protein_coding	Atg4a	0.634520413	0.02649739
ENSMUSG00000040596	protein_coding	Pogk	0.612823318	0.03194595
ENSMUSG00000051034	protein_coding	Zfp11	0.414151402	0.023715455

ENSMUSG00000047648	protein_coding	Fbxo30	0.555158772	0.020697807
ENSMUSG00000008384	protein_coding	Sertad1	1.853086453	0.048443888
ENSMUSG00000014956	protein_coding	Ppp1cb	0.527161623	0.007339326
ENSMUSG00000067855	protein_coding	Speer3	0.381767611	0.033265963
ENSMUSG00000018846	protein_coding	Pank3	0.536333584	0.007263979
ENSMUSG00000001039	protein_coding	B9d1	3.101518152	0.001555207
ENSMUSG00000039630	protein_coding	Hnrnpu	0.62664303	0.048761419
ENSMUSG00000023348	protein_coding	Trip6	1.563730196	0.015623765
ENSMUSG00000037295	protein_coding	Ldlrap1	1.668791832	0.02370703
ENSMUSG00000021185	protein_coding	9030617O03Rik	1.585598639	0.00964419
ENSMUSG00000020634	protein_coding	Ubxn2a	0.574291967	0.013112298
ENSMUSG00000039195	protein_coding	1110008P14Rik	1.868338645	0.032828431
ENSMUSG00000030452	protein_coding	Nipa2	0.617582265	0.021180787
ENSMUSG00000026094	protein_coding	Stk17b	0.603057808	0.029764061
ENSMUSG00000003346	protein_coding	Abhd17a	1.731779929	0.048384248
ENSMUSG00000074649	processed_ transcript	BC029722	1.668129535	0.024639041
ENSMUSG00000028945	protein_coding	Rheb	0.624983506	0.018303443
ENSMUSG00000042410	protein_coding	Agps	0.611201927	0.011975019
ENSMUSG00000002767	protein_coding	Mrpl2	1.837266507	0.032881762
ENSMUSG00000002769	protein_coding	Gnmt	4.554205096	0.002605721
ENSMUSG00000044712	protein_coding	Slc38a6	0.537518547	0.029358257
ENSMUSG00000038650	protein_coding	Rnh1	1.570247118	0.038871754
ENSMUSG00000097815	lincRNA	Gm26809	0.386813463	0.03557972
ENSMUSG00000097811	lincRNA	2810425M01Rik	1.696189626	0.023046173
ENSMUSG00000060216	protein_coding	Arrb2	1.974383358	0.019837214
ENSMUSG00000013822	protein_coding	Elof1	1.587147607	0.004538205
ENSMUSG00000048930	protein_coding	Tada3	1.612175973	0.002898239
ENSMUSG00000089847	protein_coding	Timm10b	1.763751396	0.020031725
ENSMUSG00000021027	protein_coding	Ralgapa1	0.563662089	0.043777203
ENSMUSG00000021020	protein_coding	Srp54c	0.58807848	0.043668216
ENSMUSG00000029569	protein_coding	Tmem168	0.593256163	0.013938104
ENSMUSG00000027463	protein_coding	Slc52a3	0.196533655	0.001473219
ENSMUSG00000027466	protein_coding	Rbck1	1.66745494	0.00431521
ENSMUSG00000024845	processed_ transcript	Tmem134	1.630402809	0.006064439
ENSMUSG00000097554	lincRNA	Gm26825	0.043691414	0.013185276
ENSMUSG00000047141	protein_coding	Zfp654	0.549597516	0.015590252
ENSMUSG00000017707	protein_coding	Serinc3	0.607329063	0.04228069
ENSMUSG00000078872	protein_coding	Gm14401	0.176067652	0.034239938
ENSMUSG00000041483	protein_coding	Zfp281	0.617145015	0.027395363
ENSMUSG00000041482	protein_coding	Piezo2	0.53588872	0.015956128

ENSMUSG00000051502	protein_coding	Ufsp1	1.93305344	0.009088212
ENSMUSG00000023953	protein_coding	Polh	0.560271628	0.022097628
ENSMUSG00000023951	protein_coding	Vegfa	0.328724622	0.032836391
ENSMUSG00000091105	pseudogene	Gm5633	0.26900409	0.029307959
ENSMUSG00000019261	protein_coding	Map1s	1.672212661	0.029085932
ENSMUSG00000066415	protein_coding	Msl2	0.630513733	0.017507099
ENSMUSG00000020362	protein_coding	Cnot6	0.522764342	0.017669428
ENSMUSG00000064127	protein_coding	Med14	0.578076244	0.017768419
ENSMUSG00000030088	protein_coding	Aldh1l1	2.729800361	0.037375434
ENSMUSG00000073405	pseudogene	C920025E04Rik	1.893071857	0.017209276
ENSMUSG00000039737	protein_coding	Prkrip1	1.521302451	0.026308508
ENSMUSG00000045039	protein_coding	Megf8	1.876089766	0.01340271
ENSMUSG00000025723	protein_coding	Nmb	2.217008685	0.015469058
ENSMUSG00000086503	lincRNA	Xist	0.560918575	0.015728824
ENSMUSG00000027610	protein_coding	Gss	1.811032701	0.013279965
ENSMUSG00000027612	protein_coding	Mmp24	2.477574305	0.017117707
ENSMUSG00000086320	lincRNA	Gm12840	0.406054233	0.04091855
ENSMUSG00000040511	protein_coding	Pvr	0.65871058	0.022092243
ENSMUSG00000061527	protein_coding	Krt5	0.205620679	0.014177178
ENSMUSG00000047166	pseudogene	Tigd5	1.687267933	0.004920095
ENSMUSG00000031292	protein_coding	Cdkl5	0.454968409	0.041648597
ENSMUSG00000066235	protein_coding	Pomgnt2	1.783462979	0.035283338
ENSMUSG00000013663	protein_coding	Pten	0.600416421	0.048258865
ENSMUSG00000063659	protein_coding	Zbtb18	0.596290674	0.032603639
ENSMUSG00000027363	protein_coding	Usp8	0.612179797	0.024455176
ENSMUSG00000027940	protein_coding	Tpm3	0.454015667	0.002644191
ENSMUSG00000031765	protein_coding	Mt1	7.809953605	0.02223719
ENSMUSG00000023067	protein_coding	Cdkn1a	1.850254253	0.00125138
ENSMUSG00000023064	protein_coding	Sncg	3.812064493	0.015175913
ENSMUSG00000032549	protein_coding	Rab6b	20.54612313	0.040240608
ENSMUSG00000042496	protein_coding	Prdm10	0.479444289	0.020831944
ENSMUSG00000059895	protein_coding	Ptp4a3	1.7617956	0.001266217
ENSMUSG00000032449	protein_coding	Slc25a36	0.567108255	0.029880569
ENSMUSG00000027002	protein_coding	Nckap1	0.405758753	0.013074163
ENSMUSG00000000811	protein_coding	Txnrd3	1.639138485	0.02057612
ENSMUSG00000051285	protein_coding	Pcmtd1	0.573215094	0.026672899
ENSMUSG00000053626	protein_coding	Tll1	0.413717368	0.017215891
ENSMUSG00000036114	protein_coding	Rpp25l	1.823658391	0.047599114
ENSMUSG00000061517	protein_coding	Sox21	0.330191454	0.01663781
ENSMUSG00000030613	protein_coding	Ccdc90b	0.664625912	0.000195356
ENSMUSG00000039481	protein_coding	Nrtn	1.63133367	0.028647582
ENSMUSG00000093106	miRNA	Gm25534	Inf	0.005749115
ENSMUSG00000022602	protein_coding	Arc	3.259089843	0.012706523

ENSMUSG00000071362	protein_coding	Gm10330	0.283943211	0.004375132
ENSMUSG00000005447	protein_coding	Pafah1b3	1.528617212	0.009010685
ENSMUSG00000020290	protein_coding	Xpo1	0.538304665	0.034975053
ENSMUSG00000026197	protein_coding	Zfand2b	1.949078948	0.014616655
ENSMUSG00000083392	pseudogene	Gm6335	0.475573456	0.028602722
ENSMUSG00000042510	protein_coding	AA986860	1.614400395	0.02490333
ENSMUSG00000036093	protein_coding	Arl5a	0.397099313	0.009913208
ENSMUSG00000037058	protein_coding	Paip2	0.576636317	0.025968238
ENSMUSG00000020905	protein_coding	Usp43	1.879753103	0.038382427
ENSMUSG00000092171	lincRNA	4833427F10Rik	0.265145399	0.049949581
ENSMUSG00000092178	processed_ transcript	Gm3912	0.077207769	0.006624867
ENSMUSG00000021690	protein_coding	Jmy	0.635508217	0.038771513
ENSMUSG00000029447	protein_coding	Cct6a	0.552320618	0.030956834
ENSMUSG00000035521	protein_coding	Gnptg	1.730644637	0.011737275
ENSMUSG00000094114	protein_coding	Gm21967	0.426248878	0.049928266
ENSMUSG00000095648	protein_coding	Gm2004	0.129555049	0.019864824
ENSMUSG00000094843	pseudogene	Ppp1r2-ps1	0.333933483	0.01846604
ENSMUSG00000041058	protein_coding	Wwp1	0.653107369	0.019071356
ENSMUSG00000060380	lincRNA	C030014I23Rik	2.79346844	0.010819733
ENSMUSG00000018387	protein_coding	Shroom1	1.862621214	0.048792427
ENSMUSG00000022899	protein_coding	Slc15a2	1.638353832	0.019295388
ENSMUSG00000036686	protein_coding	Cc2d1a	1.74829115	0.026589778
ENSMUSG00000039886	protein_coding	Tmem120a	1.677274618	0.017324074
ENSMUSG00000073563	protein_coding	Csnk1g3	0.548449373	0.005283863
ENSMUSG00000029761	protein_coding	Cald1	0.57647206	0.038410177
ENSMUSG00000029767	protein_coding	Calu	0.64117141	0.003153042
ENSMUSG00000039385	protein_coding	Cdh6	0.437351372	0.041493165
ENSMUSG00000042275	protein_coding	Pelo	1.808187688	0.015494618
ENSMUSG00000040653	protein_coding	Ppp1r14c	1.971962715	0.027989518
ENSMUSG00000027087	protein_coding	Itgav	0.568198287	0.005786716
ENSMUSG00000029016	protein_coding	Clcn6	0.491937619	0.027396023
ENSMUSG00000026358	protein_coding	Rgs1	0.283573942	0.029000812
ENSMUSG00000026356	protein_coding	Dars	0.58285015	0.03657611
ENSMUSG00000037487	protein_coding	Ubr5	0.643020737	0.040869698
ENSMUSG00000046169	protein_coding	Adamts6	0.421649824	0.001088982
ENSMUSG00000081249	pseudogene	Gm11517	0.026336932	0.004385111
ENSMUSG00000002799	protein_coding	Jag2	2.71307953	0.036315477
ENSMUSG00000000420	protein_coding	Galnt1	0.639011409	0.024373685
ENSMUSG00000035958	protein_coding	Tdp2	0.61648261	0.042860094
ENSMUSG00000035954	protein_coding	Dock4	0.532052727	0.02616129
ENSMUSG00000022914	protein_coding	Brwd1	0.584139388	0.043430363
ENSMUSG00000018199	protein_coding	Trove2	0.559794241	0.038549925

ENSMUSG00000019820	protein_coding	Utrn	0.600802769	0.042168737
ENSMUSG00000020219	protein_coding	Timm13	1.680833753	0.041464671
ENSMUSG00000037568	protein_coding	Vash2	0.615568818	0.017915792
ENSMUSG00000003228	protein_coding	Grk5	1.620807191	0.00015314
ENSMUSG00000028403	protein_coding	Zdhhc21	0.547307442	0.028617049
ENSMUSG00000030752	protein_coding	Kdm8	1.928514841	0.049120586
ENSMUSG00000079659	protein_coding	Tmem243	0.589837775	0.013501231
ENSMUSG00000028737	protein_coding	Aldh4a1	1.750711014	0.019550816
ENSMUSG00000043192	protein_coding	Gm1840	1.98095656	0.03166322
ENSMUSG00000058594	protein_coding	Fbxo18	1.532357752	0.025850375
ENSMUSG00000084104	pseudogene	Gm13578	0.583639719	0.001758668
ENSMUSG00000016756	protein_coding	Cmah	0.251508735	0.024801332
ENSMUSG00000053470	protein_coding	Kdm3a	0.631560581	0.015760971
ENSMUSG00000017400	protein_coding	Stac2	4.551533794	0.004578225
ENSMUSG00000001630	protein_coding	Stk38l	0.492032643	0.005922575
ENSMUSG00000074489	protein_coding	Bglap3	0.467384877	0.033869858
ENSMUSG00000074482	pseudogene	Gm16589	0.618567522	0.012103981
ENSMUSG00000069274	protein_coding	Hist1h4f	0.276548516	0.018071471
ENSMUSG00000045316	protein_coding	Fahd1	0.43097975	0.015124601
ENSMUSG00000001348	protein_coding	Acp5	1.545333061	0.039181206
ENSMUSG00000040097	protein_coding	Flywch1	1.764119086	0.03514826
ENSMUSG00000002083	protein_coding	Bbc3	1.796509586	0.022910554
ENSMUSG00000017307	protein_coding	Acot8	1.528539902	0.021747406
ENSMUSG00000061062	protein_coding	Gm10093	2.042305497	0.009150115
ENSMUSG00000038517	protein_coding	Tbkbp1	1.931043897	0.023468961
ENSMUSG00000097230	lincRNA	Gm26853	0.395886545	0.003503577
ENSMUSG00000072476	protein_coding	Gm9008	0.404676695	0.009580745
ENSMUSG00000058709	protein_coding	Egln2	1.522389552	0.027641391
ENSMUSG00000033170	protein_coding	Card10	1.740540203	0.00665837
ENSMUSG00000026603	protein_coding	Smyd2	1.544885283	0.006305327
ENSMUSG00000085666	pseudogene	Gm9855	2.799184558	0.020561662
ENSMUSG00000024548	protein_coding	Setbp1	0.468125553	0.029657292
ENSMUSG00000045427	protein_coding	Hnrnph2	0.638493583	0.012907176
ENSMUSG00000042428	protein_coding	Mgat3	0.443384425	0.041041431
ENSMUSG00000078949	protein_coding	R3hdml	15.36390745	0.037273373
ENSMUSG00000028988	protein_coding	Ctnnbip1	1.707325626	0.003578325
ENSMUSG00000036775	protein_coding	Decr2	2.084985121	0.015550277
ENSMUSG00000078954	protein_coding	Arhgap8	1.940868576	0.048787625
ENSMUSG00000075600	protein_coding	Zc3h3	1.655506309	0.019149933
ENSMUSG00000097006	lincRNA	9530082P21Rik	1.988957145	0.027608364
ENSMUSG00000027828	protein_coding	Ssr3	0.559812716	0.03262528
ENSMUSG00000031841	protein_coding	Cdh13	2.623839479	0.016535559
ENSMUSG00000039450	protein_coding	Dcxr	2.613737899	0.003379623

ENSMUSG00000034729	protein_coding	Mrps10	1.521301461	0.009407525
ENSMUSG00000034724	protein_coding	Cnot6l	0.594119798	0.019072615
ENSMUSG00000031010	protein_coding	Usp9x	0.525897108	0.018950496
ENSMUSG00000029535	protein_coding	Triap1	1.518138473	0.024025892
ENSMUSG00000045636	protein_coding	Mtus1	0.562199357	0.042441836
ENSMUSG00000032030	protein_coding	Cul5	0.498466575	0.036480449
ENSMUSG00000024811	protein_coding	Tnks2	0.596813122	0.049979691
ENSMUSG00000026411	protein_coding	Tmem9	1.761232284	0.002919916
ENSMUSG00000064254	protein_coding	Ethe1	1.973672	0.005227515
ENSMUSG00000032590	protein_coding	Apeh	1.578306506	0.028216007
ENSMUSG00000041471	protein_coding	Fam35a	0.542985057	0.028537035
ENSMUSG00000022761	protein_coding	Lztr1	1.524369153	0.019948986
ENSMUSG00000025235	protein_coding	Bbs4	0.6479654	0.020806967
ENSMUSG00000052794	protein_coding	1700030K09Rik	1.579993724	0.041762061
ENSMUSG00000023150	protein_coding	Ivns1abp	0.565446751	0.047913153
ENSMUSG00000026921	protein_coding	Egfl7	2.139297605	0.004922047
ENSMUSG00000026922	protein_coding	Agpat2	1.659315314	0.040900656
ENSMUSG00000034686	protein_coding	Prr7	2.607776356	0.020441657
ENSMUSG00000028568	protein_coding	Btf3l4	0.614017098	0.04809021
ENSMUSG00000028550	protein_coding	Atg4c	0.477633421	0.029731708
ENSMUSG00000044950	protein_coding	Pwwp2a	0.574682242	0.041070251
ENSMUSG00000045394	protein_coding	Epcam	0.571735063	0.041406516
ENSMUSG00000030264	protein_coding	Thumpd3	0.644950072	0.034286419
ENSMUSG00000027641	protein_coding	Rbl1	0.625519056	0.025174162
ENSMUSG00000004319	protein_coding	Clcn3	0.640285183	0.034890364
ENSMUSG00000004317	protein_coding	Clcn5	0.603364099	0.048951699
ENSMUSG00000057329	protein_coding	Bcl2	0.602976154	0.047719079
ENSMUSG00000061576	protein_coding	Dpp6	0.008092109	0.002704636
ENSMUSG00000003873	protein_coding	Bax	1.562348006	0.009209187
ENSMUSG00000021222	protein_coding	Dcaf4	1.697952875	0.001116249
ENSMUSG00000029019	protein_coding	Nppb	7.123407204	0.013880181
ENSMUSG00000025064	protein_coding	Col17a1	0.26793373	0.004624325
ENSMUSG00000092853	miRNA	Gm25959	7.858725482	0.044683948
ENSMUSG00000032333	protein_coding	Stoml1	1.657403004	0.005676848
ENSMUSG00000071256	protein_coding	Zfp213	2.876163828	0.0058256
ENSMUSG00000046185	protein_coding	Zfp84	0.651244665	0.006943714
ENSMUSG00000021767	protein_coding	Kat6b	0.438783557	0.032117413
ENSMUSG00000022867	protein_coding	Usp25	0.561589282	0.040469053
ENSMUSG00000040836	protein_coding	Gpr161	0.631745519	0.04937103
ENSMUSG00000047037	protein_coding	Nipa1	0.575376924	0.008914411
ENSMUSG00000073664	protein_coding	Nbeal1	0.436996246	0.03723263
ENSMUSG00000009640	protein_coding	Dmap1	1.618594377	0.035471946
ENSMUSG00000094497	pseudogene	Gm8210	1.77028596	0.002014653

ENSMUSG00000035125	protein_coding	Gcfc2	0.34047822	0.002687169
ENSMUSG00000004931	protein_coding	Apba3	1.620589147	0.046104134
ENSMUSG00000055228	protein_coding	Zfp935	0.547562457	0.047981192
ENSMUSG00000091243	protein_coding	Vgll3	0.655253573	0.046862174
ENSMUSG00000037349	protein_coding	Nudt22	2.103233075	0.010641194
ENSMUSG00000096979	lincRNA	Gm26880	0.269738513	0.008332728
ENSMUSG00000063894	protein_coding	Zkscan8	0.467006613	0.035372498
ENSMUSG00000025921	protein_coding	Rdh10	0.551226552	0.003066761
ENSMUSG00000063253	protein_coding	Scoc	0.57468781	0.019582502
ENSMUSG00000032109	protein_coding	Nlrx1	2.035014421	0.00907513
ENSMUSG00000043991	protein_coding	Pura	0.622773063	0.021306615
ENSMUSG00000074800	pseudogene	Gm4149	1.836979137	0.00716657
ENSMUSG00000026491	protein_coding	Ahctf1	0.613658405	0.036582566
ENSMUSG00000026490	protein_coding	Cdc42bpa	0.572253283	0.010039558
ENSMUSG00000081619	pseudogene	Gm13351	0.292181717	0.01182391
ENSMUSG00000003299	protein_coding	Mrpl4	1.516753869	0.049009427
ENSMUSG00000002459	protein_coding	Rgs20	0.607884341	0.012320372
ENSMUSG00000017776	protein_coding	Crk	0.661084024	0.01052634
ENSMUSG00000002985	protein_coding	Apoe	0.379074798	0.010035223
ENSMUSG00000078821	lincRNA	Gm17414	0.049486826	0.000197494
ENSMUSG00000058388	protein_coding	Phtf1	0.608940943	0.02396119
ENSMUSG00000016918	protein_coding	Sulf1	0.542395304	0.028959191
ENSMUSG00000056124	protein_coding	B4galt6	0.506144391	0.017488736
ENSMUSG00000061118	protein_coding	Dnajc30	1.747237975	0.024983991
ENSMUSG00000071748	protein_coding	Gm14698	0.456730454	0.014406508
ENSMUSG00000033526	protein_coding	Ppip5k1	1.816087365	0.033047918
ENSMUSG00000037060	protein_coding	Prkcdbp	1.658414918	0.038587011
ENSMUSG00000002580	protein_coding	Mien1	1.538701111	0.01664508
ENSMUSG00000022280	protein_coding	Rnf19a	0.644924084	0.039831005
ENSMUSG00000086869	pseudogene	Gm7809	4.960487418	0.000583134
ENSMUSG00000020115	protein_coding	Tbk1	0.615149641	0.04882086
ENSMUSG00000033955	protein_coding	Tnks1bp1	1.597371055	0.022164285
ENSMUSG00000024911	protein_coding	Fibp	1.771700679	0.039318958
ENSMUSG00000004393	protein_coding	Ddx56	1.691762235	0.043159935
ENSMUSG00000045103	protein_coding	Dmd	0.573632867	0.008422676
ENSMUSG00000003623	protein_coding	Crot	0.567576108	0.017373089
ENSMUSG00000064358	protein_coding	mt-Co3	0.542445116	0.041807312
ENSMUSG00000046056	protein_coding	Sbsn	2.521675578	0.002058536
ENSMUSG00000083716	pseudogene	Gm13436	1.566684446	0.010745051
ENSMUSG00000045503	protein_coding	Sys1	2.03438643	0.002503947
ENSMUSG00000015542	protein_coding	Nat9	1.710516342	0.017675017
ENSMUSG00000081824	pseudogene	BC002163	2.436936491	0.042770147
ENSMUSG00000035828	protein_coding	Pim3	1.677331606	0.020241111

ENSMUSG00000054693	protein_coding	Adam10	0.528088749	0.022528567
ENSMUSG00000019158	protein_coding	Tmem160	2.019262707	0.017336311
ENSMUSG00000033752	protein_coding	Mnd1	0.576917483	0.047705285
ENSMUSG00000036504	protein_coding	Phpt1	1.865156461	0.007380722
ENSMUSG00000027913	protein_coding	Crct1	0.381762374	0.006080593
ENSMUSG00000027919	protein_coding	Lce1g	2.067120763	0.024796821
ENSMUSG00000003423	protein_coding	Pih1d1	1.89077127	0.013967157
ENSMUSG00000022360	protein_coding	Atad2	0.516166355	0.047061194
ENSMUSG00000089906	pseudogene	Gm6428	0.310791261	0.000920662
ENSMUSG00000071847	protein_coding	Apcdd1	2.94022336	0.040458064
ENSMUSG00000084349	pseudogene	Rpl3-ps1	2.295211169	0.00215209
ENSMUSG00000083693	pseudogene	Gm11971	0	0.009057883
ENSMUSG00000050310	protein_coding	Rictor	0.580767847	0.041797131
ENSMUSG00000036986	protein_coding	Pml	1.725378578	0.042214831
ENSMUSG00000013483	protein_coding	Card14	5.93931509	0.025586349
ENSMUSG00000053137	protein_coding	Mapk11	1.814876364	0.001156896
ENSMUSG00000071671	pseudogene	Gm10343	0.463770127	0.049479965
ENSMUSG00000034112	protein_coding	Atp2c2	3.897580949	0.049636188
ENSMUSG00000021111	protein_coding	Papola	0.55166473	0.034483292
ENSMUSG00000075376	protein_coding	Rc3h2	0.515125506	0.013760957
ENSMUSG00000078532	protein_coding	Nkain1	1.606796332	0.016060272
ENSMUSG00000024205	pseudogene	Rpl36-ps2	2.233103518	0.048795351
ENSMUSG00000024201	protein_coding	Kdm4b	1.550891383	0.035166033
ENSMUSG00000051355	protein_coding	Commd1	1.527294392	0.030815184
ENSMUSG00000084131	pseudogene	Rpl3-ps2	3.115192572	0.000425883
ENSMUSG00000020646	protein_coding	Mboat2	1.685465021	0.012047287
ENSMUSG00000062729	protein_coding	Ppox	1.589616763	0.043847979
ENSMUSG00000036046	protein_coding	5031439G07Rik	1.539592942	0.016504527
ENSMUSG00000031309	protein_coding	Rps6ka3	0.615630174	0.037298992
ENSMUSG00000036820	protein_coding	Amdhd2	2.724640067	0.032384479
ENSMUSG00000035559	protein_coding	Mpv17l2	1.870133745	0.003109812
ENSMUSG00000028344	protein_coding	Invs	1.570105467	0.008480728
ENSMUSG00000087153	protein_coding	Gm6483	0.526447267	0.025921561
ENSMUSG00000026594	protein_coding	Ralgps2	0.476612433	0.040861447
ENSMUSG00000059363	protein_coding	Fxn	1.525995068	0.001151467
ENSMUSG00000058979	protein_coding	Cecr5	1.842565442	0.000297831
ENSMUSG00000032419	protein_coding	Tbx18	0.582283966	0.03736789
ENSMUSG00000078700	processed_ transcript	D030028A08Rik	0.66604986	0.025329078
ENSMUSG00000040356	protein_coding	Skiv2l	1.85364927	0.028927653
ENSMUSG00000015134	protein_coding	Aldh1a3	0.489670225	0.012303698
ENSMUSG00000059647	protein_coding	Gm10068	0.545540493	0.042263
ENSMUSG00000002763	protein_coding	Pex6	2.011553439	0.047632297

ENSMUSG00000054612	protein_coding	Mgmt	2.726530816	0.007911592
ENSMUSG00000054619	protein_coding	Mettl7a1	2.197793868	0.021393489
ENSMUSG00000021908	protein_coding	Gm6768	0.630203201	0.014594438
ENSMUSG00000096111	antisense	Gm21917	11.30215077	0.008973939
ENSMUSG00000002504	protein_coding	Slc9a3r2	1.602555742	0.018585621
ENSMUSG00000097799	lincRNA	Gm26899	0.48278542	0.017962358
ENSMUSG00000048186	protein_coding	Bend7	0.327901148	0.032694006
ENSMUSG00000070867	protein_coding	Trabd2b	4.151481304	0.019421865
ENSMUSG00000027562	protein_coding	Car2	1.542097413	0.037503657
ENSMUSG00000058756	protein_coding	Thra	1.544876737	0.035455638
ENSMUSG00000026389	protein_coding	Steap3	4.472553157	0.030488637
ENSMUSG00000045464	processed_ transcript	2810002D19Rik	0.386991556	0.002149833
ENSMUSG00000050395	protein_coding	Tnfsf15	0.54898252	0.043693556
ENSMUSG00000066324	protein_coding	Impad1	0.543717128	0.005016898
ENSMUSG00000040146	protein_coding	Rgl3	1.678414517	0.040715547
ENSMUSG00000025383	protein_coding	Il23a	0.551504887	0.014221498
ENSMUSG00000065007	snRNA	Gm26324	0.238446536	0.013364667
ENSMUSG00000068205	protein_coding	Macrod2	2.237467439	0.003597434
ENSMUSG00000036282	protein_coding	Naa30	0.577829005	0.008986332
ENSMUSG00000019877	protein_coding	Serinc1	0.636764678	0.018113228
ENSMUSG00000033411	protein_coding	Ctdspl2	0.505556125	0.043359307
ENSMUSG00000029455	protein_coding	Aldh2	1.925473483	0.003243171
ENSMUSG00000020841	protein_coding	Cpd	0.528535741	0.011092889
ENSMUSG00000031813	protein_coding	Mvb12a	1.639903313	0.02276326
ENSMUSG00000038776	protein_coding	Ephx1	2.068691631	0.001522857
ENSMUSG00000037103	protein_coding	Dcaf15	1.643004667	0.037124744
ENSMUSG00000026854	protein_coding	Usp20	2.331723262	0.019483425
ENSMUSG00000026857	protein_coding	Ntmt1	1.682175926	0.008261139
ENSMUSG00000028458	protein_coding	Tesk1	1.818426583	0.002538414
ENSMUSG00000024177	protein_coding	Nme4	2.989725021	0.018994918
ENSMUSG00000024283	protein_coding	Wac	0.517212884	0.04609735
ENSMUSG00000037347	protein_coding	Chst7	2.183886616	0.001658215
ENSMUSG00000079889	pseudogene	Gm11951	1.815044583	0.033483976
ENSMUSG00000030800	protein_coding	Prss8	1.63908558	0.001447105
ENSMUSG00000046876	protein_coding	Atxn1	0.538652437	0.012274478
ENSMUSG00000089728	pseudogene	Clec2f	0.033706317	0.021012635
ENSMUSG00000080268	protein_coding	Brms1	1.765578846	0.004336203
ENSMUSG00000054178	protein_coding	Gm9938	0.513216404	0.01933479
ENSMUSG00000041426	protein_coding	Hibch	0.585693817	0.023554865
ENSMUSG00000044221	protein_coding	Grsf1	0.655334396	0.034561099
ENSMUSG00000057886	pseudogene	Gm6984	0.617337493	0.014058381
ENSMUSG00000020441	protein_coding	2310033P09Rik	1.944344499	0.011967008

ENSMUSG00000072676	protein_coding	Tmem254a	2.461426564	0.000923034
ENSMUSG00000025199	protein_coding	Chuk	0.57429642	0.003193736
ENSMUSG00000040152	protein_coding	Thbs1	0.512699917	0.0119707
ENSMUSG00000027132	protein_coding	Katnbl1	0.526026733	0.021084073
ENSMUSG00000031996	protein_coding	Aplp2	0.629781241	0.049422184
ENSMUSG00000074476	protein_coding	Spc24	1.528700184	0.031072191
ENSMUSG00000096990	lincRNA	Gm26790	0.665161004	0.049656286
ENSMUSG00000050063	protein_coding	Klk6	9.12322023	0.036512392
ENSMUSG00000028556	protein_coding	Dock7	0.552743654	0.044418442
ENSMUSG00000028557	protein_coding	Rnf11	0.644850279	0.01343588
ENSMUSG00000044903	protein_coding	Psg22	0.02499172	0.004715722
ENSMUSG00000021824	protein_coding	Ap3m1	0.65891095	0.001976924
ENSMUSG00000031536	protein_coding	Polb	0.589940901	0.009795764
ENSMUSG00000041992	protein_coding	Rapgef5	0.446020896	0.04261956
ENSMUSG00000002379	protein_coding	Ndufa11	1.91593878	0.034565813
ENSMUSG00000009470	protein_coding	Tnpo1	0.635088713	0.008989953
ENSMUSG00000079478	protein_coding	Sssca1	1.633498172	0.013918415
ENSMUSG00000036676	protein_coding	Tmtc3	0.559425305	0.041991738
ENSMUSG00000066839	protein_coding	Ecsit	1.735985348	0.035442878
ENSMUSG00000039617	pseudogene	Gm7488	1.508918498	0.036329087
ENSMUSG00000073371	protein_coding	Gm6594	Inf	0.005970766
ENSMUSG00000022096	protein_coding	Hr	1.672874715	0.045429004
ENSMUSG00000035615	protein_coding	Frmpd1	3.314162469	0.025385086
ENSMUSG00000038225	protein_coding	Ccdc111	0.457447925	0.001253138
ENSMUSG00000025016	protein_coding	Tm9sf3	0.640281438	0.003152915
ENSMUSG00000069972	pseudogene	Rps13-ps2	1.651121538	0.010855534
ENSMUSG00000032344	protein_coding	Mb21d1	0.640716582	0.03559247
ENSMUSG00000025326	protein_coding	Ube3a	0.547450583	0.042483166
ENSMUSG00000036333	protein_coding	Kidins220	0.536100826	0.021236955
ENSMUSG00000025321	protein_coding	Itgb8	0.361039369	0.042292357
ENSMUSG00000030471	protein_coding	Zdhhc13	0.656372381	0.037662702
ENSMUSG00000058835	protein_coding	Abi1	0.577207469	0.017875298
ENSMUSG00000058833	protein_coding	2810428I15Rik	1.809916671	0.011767505
ENSMUSG00000095710	protein_coding	Gm8871	0.241006001	0.004872404
ENSMUSG00000074625	protein_coding	Arhgap40	2.334272343	0.027567813
ENSMUSG00000035150	protein_coding	Eif2s3x	0.646540372	0.029968824
ENSMUSG00000042474	protein_coding	Faim3	2.902236599	0.044848416
ENSMUSG00000042473	protein_coding	Tbc1d8b	0.582300706	0.03380968
ENSMUSG00000033400	protein_coding	Agl	0.613117776	0.010644586
ENSMUSG00000041815	protein_coding	Poldip3	1.520244881	0.022856749
ENSMUSG00000051223	protein_coding	Bzw1	0.585272261	0.048840942
ENSMUSG00000037808	protein_coding	Fam76b	0.530448892	0.035618295
ENSMUSG00000005043	protein_coding	Sgsh	1.617234264	0.045359134

ENSMUSG00000056018	protein_coding	1700008F21Rik	0.145923421	0.046485597

Appendix Table 2. Full list of differentially expressed microRNAs from ΔNp63 knockout mammary epithelial cell sequencing

microRNA ID	Fold Change	p-value
mmu-let-7g-3p	1.70273553	0.047364148
mmu-mir-10b-5p	1.596353876	0.030040532
mmu-mir-139-5p	1.855381713	0.001236052
mmu-mir-146b-5p	1.626768239	0.049534176
mmu-mir-147-3p	0.047710952	0.002332487
mmu-mir-147-5p	0.345098365	0.000641297
mmu-mir-150-5p	2.935659555	0.006295063
mmu-mir-155-3p	0.50809615	0.022448719
mmu-mir-193b-5p	0.338982469	0.043209234
mmu-mir-195a-3p	1.849994583	0.020074576
mmu-mir-1964-3p	0.14643117	0.006620285
mmu-mir-205-3p	0.285544892	0.003235674
mmu-mir-3084-3p	0.279531617	0.040482324
mmu-mir-33-3p	2.204620123	0.034053163
mmu-mir-3473b	2.142942477	0.00992017
mmu-mir-3473d	0.601101691	0.049275803
mmu-mir-3473e	3.370262119	0.015960721
mmu-mir-34c-3p	1.560740508	0.040299379
mmu-mir-451a	4.071961653	0.038340711
mmu-mir-466a-3p	2.681149719	0.038634707
mmu-mir-466b-3p	2.546483484	0.039292175
mmu-mir-466c-3p	2.546483484	0.039292175
mmu-mir-466e-3p	2.681149719	0.038634707
mmu-mir-466p-3p	2.546483484	0.039292175
mmu-mir-592-5p	5.125489635	0.00458933
mmu-mir-6390	0.494557626	0.016550889
mmu-mir-6406	2.407306678	0.004896486
mmu-mir-6414	2.172543327	0.041848263
mmu-mir-668-3p	3.19129028	0.008358401
mmu-mir-672-5p	2.41882197	0.007673931
mmu-mir-7047-5p	2.142989094	0.038206719
mmu-mir-7086-5p	0.606363359	0.004926464
mmu-mir-712-5p	0.625737496	0.037626281
mmu-mir-879-5p	0.411254017	0.004801053

Appendix Table 3. Functional Pair Analysis results for ΔNp63 mammary epithelial cell sequencing

microRNA up, gene down:

microRNA	Gene	p-value
mmu-let-7g-3p	EDEM3	2.32E-23
mmu-let-7g-3p	SMAD2	2.32E-23
mmu-let-7g-3p	CPEB4	2.32E-23
mmu-let-7g-3p	CLCN5	2.32E-23
mmu-let-7g-3p	DMD	2.32E-23
mmu-let-7g-3p	LPGAT1	2.32E-23
mmu-let-7g-3p	CEP120	2.32E-23
mmu-let-7g-3p	SULF1	2.32E-23
mmu-let-7g-3p	CNOT6L	2.32E-23
mmu-let-7g-3p	FBXO32	2.32E-23
mmu-let-7g-3p	BRWD1	2.32E-23
mmu-let-7g-3p	CPD	2.32E-23
mmu-let-7g-3p	ARL5A	2.32E-23
mmu-let-7g-3p	COL11A1	2.32E-23
mmu-let-7g-3p	SYNCRIP	2.32E-23
mmu-let-7g-3p	UTRN	2.32E-23
mmu-let-7g-3p	FNIP1	2.32E-23
mmu-let-7g-3p	NIPA1	2.32E-23
mmu-let-7g-3p	FAM84B	2.32E-23
mmu-let-7g-3p	RPS6KA3	2.32E-23
mmu-let-7g-3p	CALU	2.32E-23
mmu-let-7g-3p	TGFBR1	2.32E-23
mmu-let-7g-3p	NAP1L1	2.32E-23
mmu-let-7g-3p	PTP4A2	2.32E-23
mmu-let-7g-3p	EIF4G2	2.32E-23
mmu-let-7g-3p	ATF7	2.32E-23
mmu-let-7g-3p	ERO1L	2.32E-23
mmu-let-7g-3p	PARM1	2.32E-23
mmu-let-7g-3p	IL6	2.32E-23
mmu-let-7g-3p	POGZ	2.32E-23
mmu-let-7g-3p	NAA30	2.32E-23
mmu-let-7g-3p	ATAD2B	2.32E-23
mmu-let-7g-3p	MGAT3	2.32E-23
mmu-let-7g-3p	CRCT1	2.32E-23
mmu-let-7g-3p	THBS1	2.32E-23
mmu-let-7g-3p	SNAP23	2.32E-23
mmu-let-7g-3p	ITGB8	2.32E-23

mmu-let-7g-3p	USP38	2.32E-23
mmu-let-7g-3p	LAMP2	2.32E-23
mmu-let-7g-3p	MTPN	2.32E-23
mmu-let-7g-3p	ARL6IP6	2.32E-23
mmu-let-7g-3p	PDGFB	2.32E-23
mmu-let-7g-3p	YTHDF3	2.32E-23
mmu-let-7g-3p	RICTOR	2.32E-23
mmu-let-7g-3p	SOCS4	2.32E-23
mmu-let-7g-3p	CCDC141	2.32E-23
mmu-let-7g-3p	MTUS1	2.32E-23
mmu-let-7g-3p	MAPK6	2.32E-23
mmu-let-7g-3p	SLC4A7	2.32E-23
mmu-let-7g-3p	GALNT1	2.32E-23
mmu-let-7g-3p	FAM103A1	2.32E-23
mmu-let-7g-3p	CBX5	2.32E-23
mmu-let-7g-3p	SLC25A24	2.32E-23
mmu-let-7g-3p	TMTC3	2.32E-23
mmu-let-7g-3p	AHCTF1	2.32E-23
mmu-let-7g-3p	RDH10	2.32E-23
mmu-let-7g-3p	CHUK	2.32E-23
mmu-let-7g-3p	MAP3K2	2.32E-23
mmu-let-7g-3p	BZW1	2.32E-23
mmu-let-7g-3p	VGLL3	2.32E-23
mmu-let-7g-3p	RB1	2.32E-23
mmu-let-7g-3p	GK5	2.32E-23
mmu-let-7g-3p	VASH2	2.32E-23
mmu-let-7g-3p	C1GALT1	2.32E-23
mmu-let-7g-3p	PTAR1	2.32E-23
mmu-let-7g-3p	BTF3L4	2.32E-23
mmu-let-7g-3p	FNDC3A	2.32E-23
mmu-let-7g-3p	TIA1	2.32E-23
mmu-miR-10b-5p	SMAD2	4.54E-10
mmu-miR-10b-5p	CLCN5	4.54E-10
mmu-miR-10b-5p	RLIM	4.54E-10
mmu-miR-10b-5p	NUFIP2	4.54E-10
mmu-miR-10b-5p	FBXO30	4.54E-10
mmu-miR-10b-5p	BRWD1	4.54E-10
mmu-miR-10b-5p	CRK	4.54E-10
mmu-miR-10b-5p	PIK3CA	4.54E-10
mmu-miR-10b-5p	PTP4A2	4.54E-10
mmu-miR-10b-5p	UBXN7	4.54E-10
mmu-miR-10b-5p	CNOT6	4.54E-10
mmu-miR-10b-5p	ITGB8	4.54E-10

mmu-miR-10b-5p	ZDHHC21	4.54E-10
mmu-miR-10b-5p	TMEM170B	4.54E-10
mmu-miR-10b-5p	GALNT1	4.54E-10
mmu-miR-10b-5p	CBX5	4.54E-10
mmu-miR-10b-5p	CELF2	4.54E-10
mmu-miR-10b-5p	MAP3K2	4.54E-10
mmu-miR-10b-5p	USP25	4.54E-10
mmu-miR-10b-5p	MAPRE1	4.54E-10
mmu-miR-10b-5p	SPAG9	4.54E-10
mmu-miR-10b-5p	CEP350	4.54E-10
mmu-miR-150-5p	NR1D2	0.00132779
mmu-miR-150-5p	CPD	0.00132779
mmu-miR-150-5p	RC3H1	0.00132779
mmu-miR-150-5p	TM9SF3	0.00132779
mmu-miR-150-5p	CALU	0.00132779
mmu-miR-150-5p	ETF1	0.00132779
mmu-miR-150-5p	HNRNPU	0.00132779
mmu-miR-150-5p	TEAD1	0.00132779
mmu-miR-150-5p	LRRC58	0.00132779
mmu-miR-150-5p	AEBP2	0.00132779
mmu-miR-150-5p	TPM3	0.00132779
mmu-miR-150-5p	PTBP2	0.00132779
mmu-miR-195a-3p	DENND4A	2.84E-18
mmu-miR-195a-3p	CLCN5	2.84E-18
mmu-miR-195a-3p	SLC39A10	2.84E-18
mmu-miR-195a-3p	EVI5	2.84E-18
mmu-miR-195a-3p	RLIM	2.84E-18
mmu-miR-195a-3p	CDK17	2.84E-18
mmu-miR-195a-3p	CNOT6L	2.84E-18
mmu-miR-195a-3p	EIF5A2	2.84E-18
mmu-miR-195a-3p	NUFIP2	2.84E-18
mmu-miR-195a-3p	ATP13A3	2.84E-18
mmu-miR-195a-3p	ATP7A	2.84E-18
mmu-miR-195a-3p	CCDC6	2.84E-18
mmu-miR-195a-3p	CHORDC1	2.84E-18
mmu-miR-195a-3p	BCL2	2.84E-18
mmu-miR-195a-3p	HTR2A	2.84E-18
mmu-miR-195a-3p	SFRS18	2.84E-18
mmu-miR-195a-3p	CPD	2.84E-18
mmu-miR-195a-3p	ARL5B	2.84E-18
mmu-miR-195a-3p	DMTF1	2.84E-18
mmu-miR-195a-3p	USP9X	2.84E-18
mmu-miR-195a-3p	WSB1	2.84E-18

mmu-miR-195a-3p	RPS6KA3	2.84E-18
mmu-miR-195a-3p	CALU	2.84E-18
mmu-miR-195a-3p	FAM122B	2.84E-18
mmu-miR-195a-3p	SKIL	2.84E-18
mmu-miR-195a-3p	RSBN1	2.84E-18
mmu-miR-195a-3p	EIF4G2	2.84E-18
mmu-miR-195a-3p	CAB39	2.84E-18
mmu-miR-195a-3p	PARM1	2.84E-18
mmu-miR-195a-3p	WWP1	2.84E-18
mmu-miR-195a-3p	PI4K2B	2.84E-18
mmu-miR-195a-3p	USP31	2.84E-18
mmu-miR-195a-3p	PURA	2.84E-18
mmu-miR-195a-3p	SCOC	2.84E-18
mmu-miR-195a-3p	CCDC126	2.84E-18
mmu-miR-195a-3p	LAMP2	2.84E-18
mmu-miR-195a-3p	SYDE2	2.84E-18
mmu-miR-195a-3p	TEAD1	2.84E-18
mmu-miR-195a-3p	RICTOR	2.84E-18
mmu-miR-195a-3p	PPM1E	2.84E-18
mmu-miR-195a-3p	LRRC58	2.84E-18
mmu-miR-195a-3p	GLCE	2.84E-18
mmu-miR-195a-3p	AEBP2	2.84E-18
mmu-miR-195a-3p	TNPO1	2.84E-18
mmu-miR-195a-3p	POP4	2.84E-18
mmu-miR-195a-3p	SLC4A7	2.84E-18
mmu-miR-195a-3p	TMEM170B	2.84E-18
mmu-miR-195a-3p	LPP	2.84E-18
mmu-miR-195a-3p	GALNT1	2.84E-18
mmu-miR-195a-3p	ZFHX4	2.84E-18
mmu-miR-195a-3p	CBX5	2.84E-18
mmu-miR-195a-3p	SUZ12	2.84E-18
mmu-miR-195a-3p	SNX13	2.84E-18
mmu-miR-195a-3p	G2E3	2.84E-18
mmu-miR-195a-3p	NEBL	2.84E-18
mmu-miR-195a-3p	ELL2	2.84E-18
mmu-miR-195a-3p	SOS1	2.84E-18
mmu-miR-195a-3p	STK38L	2.84E-18
mmu-miR-195a-3p	VEGFA	2.84E-18
mmu-miR-195a-3p	OTUD4	2.84E-18
mmu-miR-195a-3p	AKAP11	2.84E-18
mmu-miR-195a-3p	USP25	2.84E-18
mmu-miR-195a-3p	MAPRE1	2.84E-18
mmu-miR-195a-3p	TLL1	2.84E-18

mmu-miR-195a-3p	CEP350	2.84E-18
mmu-miR-195a-3p	UHMK1	2.84E-18
mmu-miR-33-3p	SMAD2	4.64E-12
mmu-miR-33-3p	RLIM	4.64E-12
mmu-miR-33-3p	CDK19	4.64E-12
mmu-miR-33-3p	HIPK1	4.64E-12
mmu-miR-33-3p	NUFIP2	4.64E-12
mmu-miR-33-3p	TM9SF3	4.64E-12
mmu-miR-33-3p	AGPS	4.64E-12
mmu-miR-33-3p	NIPA1	4.64E-12
mmu-miR-33-3p	TGFBR1	4.64E-12
mmu-miR-33-3p	CDK8	4.64E-12
mmu-miR-33-3p	NAA30	4.64E-12
mmu-miR-33-3p	CROT	4.64E-12
mmu-miR-33-3p	SYDE2	4.64E-12
mmu-miR-33-3p	PDGFD	4.64E-12
mmu-miR-33-3p	YTHDF3	4.64E-12
mmu-miR-33-3p	RMND5A	4.64E-12
mmu-miR-33-3p	UBR5	4.64E-12
mmu-miR-33-3p	NRIP1	4.64E-12
mmu-miR-33-3p	CDC42BPA	4.64E-12
mmu-miR-33-3p	TPM3	4.64E-12
mmu-miR-33-3p	SPIN4	4.64E-12
mmu-miR-33-3p	ZFHX4	4.64E-12
mmu-miR-33-3p	CELF2	4.64E-12
mmu-miR-33-3p	ELL2	4.64E-12
mmu-miR-33-3p	CDH6	4.64E-12
mmu-miR-33-3p	GLCCI1	4.64E-12
mmu-miR-33-3p	MAPRE1	4.64E-12
mmu-miR-33-3p	ANKRD44	4.64E-12
mmu-miR-33-3p	PANK3	4.64E-12
mmu-miR-33-3p	CEP350	4.64E-12
mmu-miR-451a	CAB39	0.004330218
mmu-miR-451a	MEX3C	0.004330218
mmu-miR-451a	AEBP2	0.004330218

microRNA down, gene up:

MicroRNA	Gene	p-value
mmu-miR-155-3p	CSF2RB	0.781083842
mmu-miR-155-3p	ARRB2	0.781083842
mmu-miR-155-3p	VPS18	0.781083842
mmu-miR-155-3p	USP43	0.781083842
mmu-miR-193b-5p	IGFBP5	0.25893452
mmu-miR-193b-5p	TGFBR3	0.25893452
mmu-miR-193b-5p	RFT1	0.25893452
mmu-miR-205-3p	DHCR24	0.57570751
mmu-miR-205-3p	WDTC1	0.57570751
mmu-miR-205-3p	SCMH1	0.57570751
mmu-miR-205-3p	CNP	0.57570751

Appendix Table 4. List of Intraductally Injected Mice. The list includes additional genotypes that were injected from other projects in our lab.

Mouse number	Genotype	DOB	Weight (g)	Surgery Date	Right	Left	Comments
G503	ΔNp63 fl/fl, Rosa M/M	10/21/13	18	12/4/13	Empty	Cre	
G504	ΔNp63 fl/fl, Rosa M/M	10/21/13	20	12/4/13	Empty	Cre	
G521	ΔNp63 fl/fl, Rosa M/M	10/23/13	18	12/4/13	Cre	Cre (fat pad)	Sacrificed 6 weeks after injection to assess recombination
G522	ΔNp63 fl/fl, Rosa M/M	10/23/13	20	12/4/13	Cre	Cre (fat pad)	Sacrificed 6 weeks after injection to assess recombination
G523	ΔNp63 fl/fl, Rosa M/M	10/23/13	18	12/4/13	Cre	Cre (fat pad)	Had to inject additional anesthesia (50 ul)/ Sacrificed 6 weeks after injection to assess recombination
G524	ΔNp63 fl/fl, Rosa M/M	10/23/13	20	12/4/13	Empty	Cre	Euthanized - abdominal wall perforation
N480	Dicer fl/fl, Rosa M/M	12/26/13	23	2/18/14	Cre	Empty	
N481	Dicer fl/fl, Rosa M/M	12/26/13	19	2/18/14	Cre	Empty	
N484	Dicer fl/fl, Rosa M/M	12/26/13	23	2/18/14	Cre	Empty	
N485	Dicer fl/fl, Rosa M/M	12/26/13	20	2/18/14	Cre	Empty	
N491	Dicer fl/fl, Rosa M/M	12/26/13	21	2/18/14	Cre (fat pad)	Cre	
W208	TAp63 fl/fl, Rosa M/M	2/24/14	23.1	4/22/14	Cre (fat pad)	Cre	
W209	TAp63 fl/fl, Rosa M/M	2/24/14	21.9	4/22/14	Cre	Empty	
W210	TAp63 fl/fl, Rosa M/M	2/24/14	21.4	4/22/14	Cre	Empty	
W211	TAp63 fl/fl, Rosa M/M	2/24/14	18.7	4/22/14	Cre	Empty	
W212	TAp63 fl/fl, Rosa M/M	2/24/14	20.2	4/22/14	Cre	Empty	Found dead on 6/30/14. No tumors found on necropsy

W213	TAp63 fl/fl, Rosa M/M	2/24/14	16.7	4/22/14	Cre	Empty	Euthanized - abdominal wall perforation
W222	TAp63 fl/fl, Rosa M/M	2/25/14	19.7	4/22/14	Cre	Empty	
W223	TAp63 fl/fl, Rosa M/M	2/25/14	21.5	4/22/14	Cre	Empty	
N728	BRCA1 fl/fl, Rosa M/M	8/7/14	21.5	10/2/14	Cre	Empty	
N730	BRCA1 fl/fl, Rosa M/M	8/7/14	19.7	10/2/14	Cre	Empty	Found dead on 1/6/15. No tumors found on necropsy
N729	BRCA1 fl/fl, Rosa M/M	8/7/14	22.2	10/2/14	Cre	Empty	
G1017	ΔNp63 fl/fl, BRCA1 fl/fl, Rosa M/M	8/20/14	22	10/2/14	Cre	Empty	
G1018	ΔNp63 fl/fl, BRCA1 fl/fl, Rosa M/M	8/20/14	19.05	10/2/14	Cre	Empty	tag off
no tag	ΔNp63 fl/fl, BRCA1 fl/fl, Rosa M/M	8/20/14	14.55	10/2/14			too small - could not get needle into ducts - euthanized
N731	BRCA1 fl/fl, Rosa M/M	8/7/14	21.5	10/3/14	Cre	Empty	
N732	BRCA1 fl/fl, Rosa M/M	8/7/14	19.8	10/3/14	Cre	Empty	
N733	BRCA1 fl/fl, Rosa M/M	8/7/14	19.9	10/3/14	Cre	Empty	
G1019	TAp63 fl/fl, BRCA1 fl/fl, Rosa M/M	8/22/14	24.13	10/7/14	Cre	Empty	Did not wake up from anesthesia
G1020	TAp63 fl/fl, BRCA1 fl/fl, Rosa M/M	8/22/14	20.79	10/7/14	Cre (fat pad)	Cre	Did not wake up from anesthesia
G1021	TAp63 fl/fl, BRCA1 fl/fl, Rosa M/M	8/22/14	21.54	10/7/14	Cre	Empty	Did not wake up from anesthesia
no tag	TAp63 fl/fl, BRCA1 fl/fl, Rosa M/M	8/22/14	20.82	10/7/14			Died immediately after anesthesia injection
no tag	TAp63 fl/fl, Rosa M/M	8/24/14	18.73	10/7/14			too small - could not get needle into ducts - euthanized
G1022	TAp63 fl/fl, Rosa M/M	8/24/14	22.24	10/13/14	Cre	Cre (fat	Right injection into nipple but

						pad)	no branching visible
G1023	TAp63 fl/fl, Rosa M/M	8/24/14	21.68	10/13/14	Cre	Empty	
G1024	ΔNp63 fl/fl, Rosa M/M	9/1/14	21.24	10/13/14	Cre	Empty	
G1025	ΔNp63 fl/fl, Rosa M/M	9/1/14	21.12	10/13/14	Cre	Empty	
no tag	ΔNp63 fl/fl, Rosa M/M	9/1/14	19.19	10/13/14			too small - could not get needle into ducts - euthanized
G1026	ΔNp63 fl/fl, Rosa M/M	9/1/14	20.29	10/13/14			too small - surgery postponed one week
G1027	ΔNp63 fl/fl, Rosa M/M	9/1/14	19.52	10/13/14			too small - surgery postponed one week
N739	Dicer fl/fl, Rosa M/M	8/12/14	21.57	10/14/14	Cre (fat pad)	Cre	
N742	Dicer fl/fl, Rosa M/M	8/12/14	19.76	10/14/14	Cre	Empty	Did not wake up from anesthesia
N740	Dicer fl/fl, Rosa M/M	8/12/14	23.28	10/14/14			Died immediately after anesthesia injection
N738	Dicer fl/fl, Rosa M/M	8/12/14	20.48	10/14/14	Cre	Empty	
G1026	ΔNp63 fl/fl, Rosa M/M	9/1/14	21.84	10/23/14	Cre	Empty	
G1027	ΔNp63 fl/fl, Rosa M/M	9/1/14	20.13	10/23/14			too small - surgery postponed one week
G1028	ΔNp63 fl/fl, BRCA1 fl/fl, Rosa M/M	9/9/14	20.63	10/23/14	Cre	Empty	
G1029	ΔNp63 fl/fl, BRCA1 fl/fl, Rosa M/M	9/9/14	20.6	10/23/14	Cre	Empty	Had to inject additional anesthesia (50 ul)
G1043	TAp63 fl/fl, BRCA1 fl/fl, Rosa M/M	9/15/14	22.78	10/28/14	Cre	Empty	Did not wake up from anesthesia
G1044	TAp63 fl/fl, BRCA1 fl/fl, Rosa M/M	9/15/14	22.84	10/28/14	Cre	Empty	Did not wake up from anesthesia
G1027	ΔNp63 fl/fl, Rosa M/M	9/1/14	20.09	10/28/14			Died immediately

							after anesthesia injection
no tag	ΔNp63 fl/fl, Rosa M/M	9/1/14	20.3	10/28/14			Died immediately after anesthesia injection
G1045	ΔNp63 fl/fl, Rosa M/M	9/1/14	19.5	10/28/14	Cre	Empty	Did not wake up from anesthesia
G1046	ΔNp63 fl/fl, Rosa M/M	9/1/14	16.78	10/28/14	Cre (fat pad)	Cre	
G1047	ΔNp63 fl/fl, BRCA1 fl/fl, Rosa M/M	9/1/14	20.15	10/28/14	Cre	Empty	Found dead on 11/29/14, cachexia
G1048	ΔNp63 fl/fl, BRCA1 fl/fl, Rosa M/M	9/1/14	18.26	10/28/14	Cre	Cre (fat pad)	Did not wake up from anesthesia
N760	Dicer fl/fl, Rosa M/M	9/4/14	19.33	10/31/14	Cre	Empty	
N762	Dicer fl/fl, Rosa M/M	9/4/14	21.3	10/31/14	Cre	Empty	
N763	Dicer fl/fl, Rosa M/M	9/4/14	18.68	10/31/14	Cre	Empty	
N758	Dicer fl/fl, Rosa M/M	9/4/14	20.43	10/31/14	Cre	Empty	
N759	Dicer fl/fl, Rosa M/M	9/4/14	19.7	10/31/14	Cre (fat pad)	Cre	
N753	Dicer fl/fl, BRCA1 fl/fl, Rosa M/M	9/2/14	19.11	10/31/14	Cre	Empty	
N754	Dicer fl/fl, BRCA1 fl/fl, Rosa M/M	9/2/14	18.43	10/31/14	Cre	Empty (fat pad)	
N752	Dicer fl/fl, BRCA1 fl/fl, Rosa M/M	9/2/14	17.17	10/31/14	Cre (fat pad)	Cre	
N755	Dicer fl/fl, BRCA1 fl/fl, Rosa M/M	9/2/14	20.49	10/31/14	Cre (fat pad)	Cre	
N756	Dicer fl/fl, BRCA1 fl/fl, Rosa M/M	9/2/14	18.6	10/31/14	Cre (fat pad)	Cre	
N757	Dicer fl/fl, BRCA1 fl/fl, Rosa M/M	9/2/14	17.16	10/31/14	Cre	Empty	
G1049	ΔNp63 fl/fl, BRCA1 fl/fl, Rosa M/M	9/9/14	20.28	10/31/14	Cre (fat pad)	Cre	Did not wake up from anesthesia
no tag	ΔNp63 fl/fl, BRCA1 fl/fl, Rosa M/M	9/9/14	19.3	10/31/14			too small - could not get needle into ducts -

							euthanized
G1050	ΔNp63 fl/fl, BRCA1 fl/fl, Rosa M/M	9/17/14	20.35	11/3/14	Cre (fat pad)	Cre	
no tag	ΔNp63 fl/fl, BRCA1 fl/fl, Rosa M/M	9/17/14	18.68	11/3/14			did not go under after administering anesthesia - surgery postponed
no tag	ΔNp63 fl/fl, BRCA1 fl/fl, Rosa M/M	9/17/14	18.17	11/3/14			too small - could not get needle into ducts - euthanized
G1051	ΔNp63 fl/fl, BRCA1 fl/fl, Rosa M/M	9/21/14	18.78	11/7/14	Cre (fat pad)	Cre	
G1052	ΔNp63 fl/fl, BRCA1 fl/fl, Rosa M/M	9/21/14	20.03	11/7/14	Cre	Empty	
G1053	ΔNp63 fl/fl, Rosa M/M	9/13/14	18.93	11/7/14	Cre	Empty	
G1054	ΔNp63 fl/fl, Rosa M/M	9/13/14	17.19	11/7/14	Cre (fat pad)	Cre	
no tag	ΔNp63 fl/fl, Rosa M/M	9/13/14	16.11	11/7/14			too small - could not get needle into ducts - euthanized
G1055	ΔNp63 fl/fl, Rosa M/M	9/19/14	18.4	11/11/14	Cre	Cre (fat pad)	
G1056	ΔNp63 fl/fl, Rosa M/M	9/19/14	18.1	11/11/14			too small - could not get needle into ducts - euthanized
G1057	ΔNp63 fl/fl, Rosa M/M	9/19/14	17.1	11/11/14	Cre	Cre (fat pad)	
G1058	ΔNp63 fl/fl, BRCA1 fl/fl, Rosa M/M	9/21/14	16.8	11/11/14	Cre (fat pad)	Cre	
G1059	ΔNp63 fl/fl, BRCA1 fl/fl, Rosa M/M	9/17/14	17.7	11/17/14	Cre	Empty	
G1060	ΔNp63 fl/fl, BRCA1 fl/fl, Rosa M/M	9/17/14	17.8	11/17/14	Cre (fat pad)	Cre (fat pad)	too small - could not get needle into ducts - euthanized
G1061	ΔNp63 fl/fl, BRCA1 fl/fl,	9/17/14	18.4	11/17/14	Cre	Empty	Had to inject additional

	Rosa M/M						anesthesia (80 ul)
no tag	ΔNp63 fl/fl, BRCA1 fl/fl, Rosa M/M	9/17/14	16.6	11/17/14	Cre (fat pad)	Cre (fat pad)	too small - could not get needle into ducts - euthanized
no tag	TAp63 fl/fl, Rosa M/M	9/26/14	16.9	11/17/14	Cre (fat pad)	Cre (fat pad)	too small - could not get needle into ducts - euthanized
G1062	TAp63 fl/fl, Rosa M/M	9/26/14	19.9	11/17/14	Cre	Cre (fat pad)	
no tag	TAp63 fl/fl, Rosa M/M	10/3/14	19.4	11/17/14	Cre (fat pad)	Cre (fat pad)	too small - could not get needle into ducts - euthanized
G1063	TAp63 fl/fl, Rosa M/M	10/3/14	20.6	11/17/14	Cre	Empty	
G1064	TAp63 fl/fl, Rosa M/M	10/2/14	18.9	11/17/14	Cre	Empty	
G1065	TAp63 fl/fl, Rosa M/M	10/2/14	20.1	11/21/14	Cre	Empty	
no tag	TAp63 fl/fl, Rosa M/M	10/2/14	17.5	11/21/14	Cre (fat pad)	Cre (fat pad)	too small - could not get needle into ducts - euthanized
G1066	TAp63 fl/fl, Rosa M/M	10/2/14	20.2	11/21/14	Cre	Empty (fat pad)	
N843	Dicer fl/fl, Rosa M/M	9/30/14	22.1	12/3/14	Cre	Empty	Did not wake up from anesthesia
N844	Dicer fl/fl, Rosa M/M	9/30/14	20.95	12/3/14	Cre	Empty	Did not wake up from anesthesia
N845	Dicer fl/fl, Rosa M/M	9/30/14	25.3	12/3/14	Cre	Empty	
G1067	TAp63 fl/fl, BRCA1 fl/fl, Rosa M/M	10/5/14	24.86	12/3/14	Cre	Empty	Did not wake up from anesthesia
G1068	TAp63 fl/fl, BRCA1 fl/fl, Rosa M/M	10/5/14	21.39	12/3/14	Cre	Empty	Did not wake up from anesthesia
G1069	TAp63 fl/fl, BRCA1 fl/fl, Rosa M/M	10/5/14	23.23	12/3/14	Cre	Empty	
G1070	TAp63 fl/fl, BRCA1 fl/fl, Rosa M/M	10/5/14	23.98	12/3/14	Cre	Empty	Did not wake up from anesthesia

no tag	TAp63 fl/fl, Rosa M/M	10/18/14	19.43	12/3/14			too small - surgery postponed one week
N846	BRCA1 fl/fl, Rosa M/M	10/1/14	21.7	12/5/14	Cre	Empty	
N847	BRCA1 fl/fl, Rosa M/M	10/1/14	19	12/5/14	Empty	Cre	
N785	BRCA1 fl/fl, Rosa M/M	10/5/14	24	12/5/14	Cre	Empty	
N787	BRCA1 fl/fl, Rosa M/M	10/5/14	26.2	12/5/14	Cre	Empty	
N788	BRCA1 fl/fl, Rosa M/M	10/5/14	22.2	12/5/14	Cre	Empty	
N789	BRCA1 fl/fl, Rosa M/M	10/5/14	23.1	12/5/14	Cre (fat pad)	Cre	Found dead after waking up from anesthesia
N790	BRCA1 fl/fl, Rosa M/M	10/5/14	21	12/5/14	Cre	Empty	
N791	BRCA1 fl/fl, Rosa M/M	10/5/14	22.4	12/5/14	Cre	Empty	
N792	BRCA1 fl/fl, Rosa M/M	10/5/14	23	12/5/14	Cre	Empty	
G1071	TAp63 fl/fl, Rosa M/M	10/18/14	20	12/17/14	Cre	Empty	
G1072	TAp63 fl/fl, Rosa M/M	10/18/14	19.5	12/17/14	Cre	Cre (fat pad)	
N804	BRCA1 fl/fl, Rosa M/M	10/13/14	25	12/17/14	Cre	Empty	
N809	Dicer fl/fl, Rosa M/M	10/18/14	20.8	12/17/14	Cre	Empty	
N810	Dicer fl/fl, Rosa M/M	10/18/14	20.5	12/17/14	Cre	Empty	Had to inject additional anesthesia (60 ul)
N813	Dicer fl/fl, BRCA1 fl/fl, Rosa M/M	10/20/14	18.7	12/17/14	Cre	Empty	
N814	Dicer fl/fl, BRCA1 fl/fl, Rosa M/M	10/20/14	16.4	12/17/14	Cre (fat pad)	Cre	
G1073	ΔNp63 fl/fl, Rosa M/M	10/24/14	19	12/17/14	Cre	Empty	
G1074	ΔNp63 fl/fl, Rosa M/M	10/24/14	19.5	12/17/14	Cre	Empty	
G1075	TAp63 fl/fl, BRCA1 fl/fl, Rosa M/M	10/26/14	19	12/17/14	Cre	Empty	
G1076	TAp63 fl/fl, BRCA1 fl/fl, Rosa M/M	10/26/14	23.1	12/17/14	Cre	Empty	
G1077	ΔNp63 fl/fl,	10/31/14	21.7	12/17/14	Cre	Empty	

	BRCA1 fl/fl, Rosa M/M						
G1078	ΔNp63 fl/fl, BRCA1 fl/fl, Rosa M/M	10/31/14	20	12/17/14	Cre (fat pad)	Cre	
G1079	ΔNp63 fl/fl, BRCA1 fl/fl, Rosa M/M	10/31/14	19.6	12/17/14	Cre	Empty	
N842	BRCA1 fl/fl, Rosa fl/fl	11/11/14	21.6	1/13/15	Cre	Empty	Did not wake up from anesthesia
G1080	ΔNp63 fl/fl, BRCA1 fl/fl, Rosa M/M	11/13/14	20.3	1/13/15	Cre	Empty	Did not wake up from anesthesia
G1081	ΔNp63 fl/fl, BRCA1 fl/fl, Rosa M/M	11/13/14	19	1/13/15	Cre	Empty	Had to inject additional anesthesia (50 ul)
no tag	ΔNp63 fl/fl, Rosa M/M	11/13/14	19.6	1/13/15			did not go under after administering anesthesia - surgery postponed
G1082	ΔNp63 fl/fl, Rosa M/M	11/13/14	20.2	1/13/15	Cre	Empty	
G1083	ΔNp63 fl/fl, Rosa M/M	11/13/14	18.3	1/13/15	Cre	Empty	
G1084	ΔNp63 fl/fl, Rosa M/M	11/13/14	21.3	1/13/15	Cre	Empty	
N853	Dicer fl/fl, BRCA1 fl/fl, Rosa M/M	11/14/14	20.6	1/13/15	Cre	Empty	
N854	Dicer fl/fl, BRCA1 fl/fl, Rosa M/M	11/14/14	20.1	1/13/15	Cre	Empty	
N855	Dicer fl/fl, BRCA1 fl/fl, Rosa M/M	11/14/14	18.9	1/13/15	Cre (fat pad)	Cre	
N856	Dicer fl/fl, BRCA1 fl/fl, Rosa M/M	11/14/14	18.4	1/13/15	Cre	Empty	
N857	Dicer fl/fl, BRCA1 fl/fl, Rosa M/M	11/14/14	19.1	1/13/15	Cre	Empty	
N858	Dicer fl/fl, BRCA1 fl/fl, Rosa M/M	11/17/14	17.5	1/13/15	Cre	Empty	
N860	Dicer fl/fl, BRCA1 fl/fl, Rosa M/M	11/17/14	17.5	1/13/15	Cre	Empty	
N903	TAp73 fl/fl TdT	11/17/14	22.5	1/21/15	Cre	Empty	
D324	TAp73 fl/fl	11/24/14	16.7	1/21/15	Cre	Empty	

	TdT						
D326	TAp73 fl/fl TdT	11/24/14	18.2	1/21/15	Cre	Empty	
G1085	TAp63 fl/fl, BRCA1 fl/fl, Rosa M/M	11/18/14	23.6	1/21/15	Cre	Empty	Did not wake up from anesthesia
G1086	TAp63 fl/fl, BRCA1 fl/fl, Rosa M/M	11/18/14	20.9	1/21/15	Cre	Empty	Did not wake up from anesthesia
W1378	p53 LSL/+, Rosa M/M	11/19/14	21.6	1/21/15	Cre	Empty	
W1379	p53 LSL/+, Rosa M/M	11/19/14	18.9	1/21/15	Cre	Empty	
W1380	p53 LSL/+, Rosa M/M	11/19/14	23.5	1/21/15	Cre	Empty	
W1381	p53 LSL/+, Rosa M/M	11/19/14	20.1	1/21/15	Cre	Empty	Did not wake up from anesthesia
W1382	p53 LSL/+, Rosa M/M	11/19/14	17.1	1/21/15	Cre	Empty	Did not wake up from anesthesia
D346	TAp73 fl/fl TdT	12/7/14	22.5	2/3/15	Cre	Empty	
D347	TAp73 fl/fl TdT	12/7/14	16.7	2/3/15	Cre	Empty	
D348	TAp73 fl/fl TdT	12/7/14	18.2	2/3/15	Cre	Empty	
D359	TAp73 fl/fl TdT	12/15/14	17.4	2/6/15	Cre	Empty	
G1096	ΔNp63 fl/fl, BRCA1 fl/fl, Rosa M/M	12/23/14	22.1	2/6/15	Cre	Empty	Had to inject additional anesthesia (50 ul)
N862	BRCA1 fl/fl, Rosa M/M	12/27/14	19.3	2/6/15	Cre	Empty	
N879	Dicer fl/+, Rosa M/M	12/27/14	26.2	3/3/15	Cre	Empty	
N880	Dicer fl/+, Rosa M/M	12/27/14	24.7	3/3/15	Cre	Empty	
N881	p53 LSL/+, Dicer fl/+, Rosa M/M	12/27/14	22.4	3/3/15	Cre	Empty (fat pad)	Did not wake up from anesthesia
N882	p53 LSL/+, Dicer fl/+, Rosa M/M	12/27/14	20.9	3/3/15	Cre	Empty	
N883	p53 LSL/+, Dicer fl/+, Rosa M/M	12/27/14	17	3/3/15	Cre	Empty	
N884	p53 LSL/+, Dicer fl/fl, Rosa M/M	12/27/14	22.8	3/3/15	Cre	Empty	
D398	TAp73 fl/fl TdT	1/5/15	20.5	3/3/15	Cre	Empty	

D399	TAp73 fl/fl TdT	1/5/15	17.1	3/3/15	Cre	Empty	
D400	TAp73 fl/fl TdT	1/5/15	13.6	3/3/15			too small - could not get needle into ducts - euthanized
D405	TAp73 fl/fl TdT	1/14/15	18	3/3/15	Cre	Empty	
D407	TAp73 fl/fl TdT	1/14/15	18.7	3/3/15	Cre	Empty	
W1615	p53 LSL/+, Rosa M/M	2/2/15	20	4/1/15	Cre	Empty	Did not wake up from anesthesia
W1616	p53 LSL/+, Rosa M/M	2/2/15	20.2	4/1/15	Cre	Empty	Did not wake up from anesthesia
N923	Dicer fl/+, Rosa M/M	2/5/15	21.5	4/1/15	Cre	Empty	Did not wake up from anesthesia
N925	Dicer fl/+, Rosa M/M	2/5/15	23.3	4/1/15	Cre	Empty	Did not wake up from anesthesia
N926	Dicer fl/+, Rosa M/M	2/5/15	20	4/1/15	Cre	Empty	
N960	Dicer fl/+, Rosa M/M	2/5/15	16.9	4/1/15	Cre	Empty	
N961	Dicer fl/+, Rosa M/M	2/5/15	19.4	4/1/15	Cre	Empty	
N927	p53 LSL/+, Dicer fl/+, Rosa M/M	2/6/15	21.8	4/1/15	Cre	Empty	
N929	p53 LSL/+, Dicer fl/+, Rosa M/M	2/6/15	24.3	4/1/15	Cre	Empty	
N930	p53 LSL/+, Dicer fl/fl, Rosa M/M	2/6/15	21	4/1/15	Cre	Empty (fat pad)	
N962	TAp63 fl/fl, Rosa M/M	2/6/15	19.9	4/1/15	Cre	Empty	Sacrificed 1 week after injection to assess recombination in TEB
N963	TAp63 fl/fl, Rosa M/M	2/6/15	21.7	4/1/15	Cre	Empty	Did not wake up from anesthesia
W1694	p53 LSL/+, Rosa M/M	2/24/15	20.9	4/28/15	Cre	Empty	
W1695	p53 LSL/+, Rosa M/M	2/24/15	16.3	4/28/15	Cre	Empty	
W1696	p53 LSL/+, Rosa M/M	2/24/15	22.4	4/28/15	Cre	Empty	
N952	Dicer fl/+,	3/2/15	17.8	4/28/15	Cre	Empty	

	Rosa M/M						
N953	Dicer fl/+, Rosa M/M	3/2/15	20.1	4/28/15	Cre	Empty	
N951	Dicer fl/+, Rosa M/M	3/2/15	19.4	4/28/15	Cre	Empty (fat pad)	
N954	Dicer fl/+, Rosa M/M	3/2/15	19.4	4/28/15	Cre	Empty	
N956	Dicer fl/+, Rosa M/M	3/2/15	21.5	4/28/15	Cre	Empty	
N957	Dicer fl/+, Rosa M/M	3/2/15	21.2	4/28/15	Cre	Empty	
D493	TAp73 fl/fl TdT	3/4/15	18.7	4/28/15	Cre	Empty	Did not wake up from anesthesia
D492	TAp73 fl/fl TdT	3/4/15	18.9	4/28/15	Cre	Empty	Did not wake up from anesthesia
D491	TAp73 fl/fl TdT	3/4/15	18.2	4/28/15	Cre	Empty	Did not wake up from anesthesia
G1189	TAp63 fl/fl, BRCA1 fl/fl, Rosa M/M	3/4/15	22.1	4/28/15	Cre	Empty	Did not wake up from anesthesia
G1190	TAp63 fl/fl, BRCA1 fl/fl, Rosa M/M	3/4/15	22.7	4/28/15	Cre	Empty	Did not wake up from anesthesia
G1191	TAp63 fl/fl, BRCA1 fl/fl, Rosa M/M	3/4/15	23.2	4/28/15	Cre	Empty	Did not wake up from anesthesia
N958	p53 LSL/+, Dicer fl/+, Rosa M/M	3/10/15	25.1	5/5/15	Cre	Empty	Did not wake up from anesthesia
N992	p53 LSL/+, Dicer fl/+, Rosa M/M	3/10/15	18.3	5/5/15	Cre	Empty	
N993	p53 LSL/+, Dicer fl/+, Rosa M/M	3/10/15	18.4	5/5/15	Cre	Empty	
N964	Dicer fl/+, Rosa M/M	3/16/15	18.7	5/5/15	Cre	Empty	
N965	Dicer fl/+, Rosa M/M	3/16/15	18.2	5/5/15	Cre	Empty	
N969	Dicer fl/+, Rosa M/M	3/16/15	20.6	5/5/15	Cre	Empty	
N970	Dicer fl/+, BRCA1 fl/fl, Rosa M/M	3/25/15	19.1	5/27/15	Cre	Empty	
N971	Dicer fl/+, BRCA1 fl/fl, Rosa M/M	3/25/15	21.2	5/27/15	Cre	Empty	
N972	Dicer fl/+, BRCA1 fl/fl, Rosa M/M	3/25/15	20.1	5/27/15	Cre	Empty	

N994	Dicer fl/+, Rosa M/M	4/18/15	22.9	6/19/15	Cre	Empty	
N1009	p53 LSL/+, Rosa M/M	4/23/15	21.8	6/19/15	Cre	Empty	
W1868	p53 LSL/+, Rosa M/M	4/21/15	17.9	6/19/15	Cre	Empty	
W1869	p53 LSL/+, Rosa M/M	4/21/15	16.8	6/19/15	Cre	Empty	
W1870	p53 LSL/+, Rosa M/M	4/21/15	17.6	6/19/15	Cre	Empty	
W1871	p53 LSL/+, Rosa M/M	4/21/15	18.7	6/19/15	Cre	Empty	
N1005	p53 LSL/+, Dicer fl/+, Rosa M/M	4/23/15	20.7	6/19/15	Cre	Empty	
N1008	p53 LSL/+, Dicer fl/+, Rosa M/M	4/23/15	20.9	6/19/15	Cre	Empty	
N998	Dicer fl/+, BRCA1 fl/fl, Rosa M/M	4/21/15	23.8	6/23/15	Cre	Empty	
N999	Dicer fl/+, BRCA1 fl/fl, Rosa M/M	4/21/15	18.8	6/23/15	Cre	Empty	
N1000	Dicer fl/+, BRCA1 fl/fl, Rosa M/M	4/21/15	21.6	6/23/15	Cre	Empty	
N1001	Dicer fl/+, BRCA1 fl/fl, Rosa M/M	4/21/15	20.7	6/29/15	Cre	Empty	
N1002	Dicer fl/+, BRCA1 fl/fl, Rosa M/M	4/21/15	20.7	6/29/15	Cre	Empty	
N1003	Dicer fl/+, BRCA1 fl/fl, Rosa M/M	4/21/15	24.4	6/29/15	Cre	Empty	
N1026	p53 LSL/+, Dicer fl/+, Rosa M/M	5/20/15	20	7/14/15	Cre	Empty	
N1024	p53 LSL/+, Dicer fl/fl, Rosa M/M	5/20/15	19.5	7/14/15	Cre	Empty	
N1025	p53 LSL/+, Dicer fl/fl, Rosa M/M	5/20/15	20.7	7/14/15	Cre	Empty	
D581	TAp73 fl/fl TdT	5/26/15	20.1	7/14/15	Cre	Empty	
F8623	TAp73 fl/fl TdT	5/26/15	18.7	7/14/15	Cre	Empty	
D583	TAp73 fl/fl TdT	5/26/15	19.4	7/14/15	Cre	Empty	
D584	TAp73 fl/fl TdT	5/26/15	20.4	7/14/15	Cre	Empty	
N1093	p53 LSL/+,	6/24/15	19.9	8/11/15	Cre	Empty	

	Dicer fl/+, Rosa M/M						
N1104	p53 LSL/+, Dicer fl/+, Rosa M/M	6/24/15	19.5	8/11/15	Cre	Empty	
N1099	p53 LSL/+, Dicer fl/fl, Rosa M/M	6/26/15	20.1	8/11/15	Cre	Empty	
N1100	p53 LSL/+, Dicer fl/fl, Rosa M/M	6/26/15	19.9	8/11/15	Cre	Empty	
N1101	p53 LSL/+, Dicer fl/fl, Rosa M/M	6/26/15	19.2	8/11/15	Cre (fat pad)	Cre	
N1105	p53 LSL/+, Dicer fl/fl, Rosa M/M	6/23/15	18.2	8/11/15	Cre	Empty	
N1114	Dicer fl/+, BRCA1 fl/fl, Rosa M/M	6/28/15	21	8/27/15	Cre	Empty	
N1115	Dicer fl/+, BRCA1 fl/fl, Rosa M/M	6/28/15	18.5	8/27/15	Cre	Empty	
N1116	Dicer fl/+, BRCA1 fl/fl, Rosa M/M	6/28/15	19.2	8/27/15	Cre	Empty (fat pad)	
N1127	p53 LSL/+, Dicer fl/fl, Rosa M/M	7/20/15		9/10/15	Cre	Empty	
N1129	p53 LSL/+, Dicer fl/fl, Rosa M/M	7/24/15		9/10/15	Cre	Empty	
N1131	p53 LSL/+, Dicer fl/fl, Rosa M/M	7/24/15		9/10/15	Cre	Empty	
N1128	p53 LSL/+, Dicer fl/+, Rosa M/M	7/24/15		9/10/15	Cre	Empty	
N1068	Dicer fl/+, BRCA1 fl/fl, Rosa M/M	6/8/15		8/5/15	Cre	Empty	
N1069	Dicer fl/+, BRCA1 fl/fl, Rosa M/M	6/8/15		8/5/15	Cre	Empty	

Bibliography

1. Siegel, R. L., K. D. Miller, and A. Jemal. 2016. Cancer statistics, 2016. *CA Cancer J Clin* 66: 7-30.
2. Fidler, I. J. 2011. The biology of cancer metastasis. *Semin Cancer Biol* 21: 71.
3. Talmadge, J. E., and I. J. Fidler. 2010. AACR centennial series: the biology of cancer metastasis: historical perspective. *Cancer Res* 70: 5649-5669.
4. Hanahan, D., and R. A. Weinberg. 2011. Hallmarks of cancer: the next generation. *Cell* 144: 646-674.
5. Hanahan, D., and R. A. Weinberg. 2000. The hallmarks of cancer. *Cell* 100: 57-70.
6. Su, X., D. Chakravarti, and E. R. Flores. 2013. p63 steps into the limelight: crucial roles in the suppression of tumorigenesis and metastasis. *Nat Rev Cancer* 13: 136-143.
7. Flores, E. R., S. Sengupta, J. B. Miller, J. J. Newman, R. Bronson, D. Crowley, A. Yang, F. McKeon, and T. Jacks. 2005. Tumor predisposition in mice mutant for p63 and p73: evidence for broader tumor suppressor functions for the p53 family. *Cancer Cell* 7: 363-373.
8. Chakravarti, D., X. Su, M. S. Cho, N. H. Bui, C. Coarfa, A. Venkatanarayan, A. L. Benham, R. E. Flores Gonzalez, J. Alana, W. Xiao, M. L. Leung, H. Vin, I. L. Chan, A. Aquino, N. Muller, H. Wang, A. J. Cooney, J. Parker-Thornburg, K. Y. Tsai, P. H. Gunaratne, and E. R. Flores. 2014. Induced multipotency in adult keratinocytes through down-regulation of DeltaNp63 or DGCR8. *Proc Natl Acad Sci U S A* 111: E572-581.
9. Su, X., D. Chakravarti, M. S. Cho, L. Liu, Y. J. Gi, Y. L. Lin, M. L. Leung, A. El-Naggar, C. J. Creighton, M. B. Suraokar, I. Wistuba, and E. R. Flores. 2010. TAp63

suppresses metastasis through coordinate regulation of Dicer and miRNAs. *Nature* 467: 986-990.

10. Su, X., and E. R. Flores. 2009. TAp63: The fountain of youth. *Aging (Albany NY)* 1: 866-869.

11. Su, X., Y. J. Gi, D. Chakravarti, I. L. Chan, A. Zhang, X. Xia, K. Y. Tsai, and E. R. Flores. 2012. TAp63 is a master transcriptional regulator of lipid and glucose metabolism. *Cell Metab* 16: 511-525.

12. Su, X., M. Paris, Y. J. Gi, K. Y. Tsai, M. S. Cho, Y. L. Lin, J. A. Biernaskie, S. Sinha, C. Prives, L. H. Pevny, F. D. Miller, and E. R. Flores. 2009. TAp63 prevents premature aging by promoting adult stem cell maintenance. *Cell Stem Cell* 5: 64-75.

13. Venkatanarayan, A., P. Raulji, W. Norton, D. Chakravarti, C. Coarfa, X. Su, S. K. Sandur, M. S. Ramirez, J. Lee, C. V. Kingsley, E. F. Sananikone, K. Rajapakshe, K. Naff, J. Parker-Thornburg, J. A. Bankson, K. Y. Tsai, P. H. Gunaratne, and E. R. Flores. 2015. IAPP-driven metabolic reprogramming induces regression of p53-deficient tumours in vivo. *Nature* 517: 626-630.

14. Bergholz, J., and Z. X. Xiao. 2012. Role of p63 in Development, Tumorigenesis and Cancer Progression. *Cancer Microenviron* 5: 311-322.

15. Yao, J. Y., and J. K. Chen. 2012. Roles of p63 in epidermal development and tumorigenesis. *Biomed J* 35: 457-463.

16. Goto, Y., S. Kawano, R. Matsubara, T. Kiyosue, M. Hirano, T. Jinno, Y. Maruse, T. Toyoshima, R. Kitamura, H. Tanaka, K. Oobu, and S. Nakamura. 2014. Possible involvement of DeltaNp63 downregulation in the invasion and metastasis of oral squamous cell carcinoma via induction of a mesenchymal phenotype. *Clin Exp Metastasis* 31: 293-306.

17. Tran, M. N., W. Choi, M. F. Wszolek, N. Navai, I. L. Lee, G. Nitti, S. Wen, E. R. Flores, A. Siefker-Radtke, B. Czerniak, C. Dinney, M. Barton, and D. J. McConkey.

2013. The p63 protein isoform DeltaNp63alpha inhibits epithelial-mesenchymal transition in human bladder cancer cells: role of MIR-205. *J Biol Chem* 288: 3275-3288.

18. Tucci, P., M. Agostini, F. Grespi, E. K. Markert, A. Terrinoni, K. H. Vousden, P. A. Muller, V. Dotsch, S. Kehrloesser, B. S. Sayan, G. Giaccone, S. W. Lowe, N. Takahashi, P. Vandenabeele, R. A. Knight, A. J. Levine, and G. Melino. 2012. Loss of p63 and its microRNA-205 target results in enhanced cell migration and metastasis in prostate cancer. *Proc Natl Acad Sci U S A* 109: 15312-15317.
19. Zhou, Y., Q. Xu, B. Ling, W. Xiao, and P. Liu. 2011. Reduced expression of DeltaNup63alpha in cervical squamous cell carcinoma. *Clin Invest Med* 34: E184-191.
20. Zhang, Y., W. Yan, and X. Chen. 2014. P63 regulates tubular formation via epithelial-to-mesenchymal transition. *Oncogene* 33: 1548-1557.
21. Lee, G. Y., P. A. Kenny, E. H. Lee, and M. J. Bissell. 2007. Three-dimensional culture models of normal and malignant breast epithelial cells. *Nat Methods* 4: 359-365.
22. Acloque, H., M. S. Adams, K. Fishwick, M. Bronner-Fraser, and M. A. Nieto. 2009. Epithelial-mesenchymal transitions: the importance of changing cell state in development and disease. *J Clin Invest* 119: 1438-1449.
23. Kalluri, R. 2009. EMT: when epithelial cells decide to become mesenchymal-like cells. *J Clin Invest* 119: 1417-1419.
24. Kalluri, R., and R. A. Weinberg. 2009. The basics of epithelial-mesenchymal transition. *J Clin Invest* 119: 1420-1428.
25. Mani, S. A., W. Guo, M. J. Liao, E. N. Eaton, A. Ayyanan, A. Y. Zhou, M. Brooks, F. Reinhard, C. C. Zhang, M. Shipitsin, L. L. Campbell, K. Polyak, C. Brisken, J. Yang,

and R. A. Weinberg. 2008. The epithelial-mesenchymal transition generates cells with properties of stem cells. *Cell* 133: 704-715.

26. Thiery, J. P., H. Acloque, R. Y. Huang, and M. A. Nieto. 2009. Epithelial-mesenchymal transitions in development and disease. *Cell* 139: 871-890.

27. Zeisberg, M., and E. G. Neilson. 2009. Biomarkers for epithelial-mesenchymal transitions. *J Clin Invest* 119: 1429-1437.

28. Hollier, B. G., K. Evans, and S. A. Mani. 2009. The epithelial-to-mesenchymal transition and cancer stem cells: a coalition against cancer therapies. *J Mammary Gland Biol Neoplasia* 14: 29-43.

29. Hudson, L. G., K. M. Newkirk, H. L. Chandler, C. Choi, S. L. Fossey, A. E. Parent, and D. F. Kusewitt. 2009. Cutaneous wound reepithelialization is compromised in mice lacking functional Slug (Snai2). *J Dermatol Sci* 56: 19-26.

30. Savagner, P., and V. Arnoux. 2009. [Epithelio-mesenchymal transition and cutaneous wound healing]. *Bull Acad Natl Med* 193: 1981-1991; discussion 1992.

31. Thiery, J. P. 2002. Epithelial-mesenchymal transitions in tumour progression. *Nat Rev Cancer* 2: 442-454.

32. Weber, C. E., N. Y. Li, P. Y. Wai, and P. C. Kuo. 2012. Epithelial-mesenchymal transition, TGF-beta, and osteopontin in wound healing and tissue remodeling after injury. *J Burn Care Res* 33: 311-318.

33. Noszczyk, B. H., and S. T. Majewski. 2001. p63 expression during normal cutaneous wound healing in humans. *Plast Reconstr Surg* 108: 1242-1247; discussion 1248-1250.

34. Arwert, E. N., E. Hoste, and F. M. Watt. 2012. Epithelial stem cells, wound healing and cancer. *Nat Rev Cancer* 12: 170-180.

35. Broughton, G., 2nd, J. E. Janis, and C. E. Attinger. 2006. Wound healing: an overview. *Plast Reconstr Surg* 117: 1e-S-32e-S.

36. Broughton, G., 2nd, J. E. Janis, and C. E. Attinger. 2006. The basic science of wound healing. *Plast Reconstr Surg* 117: 12S-34S.

37. Dvorak, H. F. 2015. Tumors: wounds that do not heal-redux. *Cancer Immunol Res* 3: 1-11.

38. Dvorak, H. F. 1986. Tumors: wounds that do not heal. Similarities between tumor stroma generation and wound healing. *N Engl J Med* 315: 1650-1659.

39. Shaw, T. J., and P. Martin. 2009. Wound repair at a glance. *J Cell Sci* 122: 3209-3213.

40. Velnar, T., T. Bailey, and V. Smrkolj. 2009. The wound healing process: an overview of the cellular and molecular mechanisms. *J Int Med Res* 37: 1528-1542.

41. Arnoux, V., C. Come, D. Kusewitt, L. Hudson, and P. Savagner. 2005. Cutaneous Wound Reepithelialization: A Partial and Reversible EMT. In *Rise and Fall of Epithelial Phenotype: Concepts of Epithelial-Mesenchymal Transition*. P. Savagner, ed. Kluwer Academic/Plenum Publisers. 111-134.

42. Kusewitt, D. F., C. Choi, K. M. Newkirk, P. Leroy, Y. Li, M. G. Chavez, and L. G. Hudson. 2009. Slug/Snai2 is a downstream mediator of epidermal growth factor receptor-stimulated reepithelialization. *J Invest Dermatol* 129: 491-495.

43. Savagner, P., D. F. Kusewitt, E. A. Carver, F. Magnino, C. Choi, T. Gridley, and L. G. Hudson. 2005. Developmental transcription factor slug is required for effective re-epithelialization by adult keratinocytes. *J Cell Physiol* 202: 858-866.

44. Yan, C., W. A. Grimm, W. L. Garner, L. Qin, T. Travis, N. Tan, and Y. P. Han. 2010. Epithelial to mesenchymal transition in human skin wound healing is induced by tumor necrosis factor-alpha through bone morphogenic protein-2. *Am J Pathol* 176: 2247-2258.

45. Muzumdar, M. D., B. Tasic, K. Miyamichi, L. Li, and L. Luo. 2007. A global double-fluorescent Cre reporter mouse. *Genesis* 45: 593-605.

46. Vasioukhin, V., L. Degenstein, B. Wise, and E. Fuchs. 1999. The magical touch: genome targeting in epidermal stem cells induced by tamoxifen application to mouse skin. *Proc Natl Acad Sci U S A* 96: 8551-8556.

47. Reis-Filho, J. S., F. Milanezi, I. Amendoeira, A. Albergaria, and F. C. Schmitt. 2002. p63 Staining of myoepithelial cells in breast fine needle aspirates: a study of its role in differentiating in situ from invasive ductal carcinomas of the breast. *J Clin Pathol* 55: 936-939.

48. Reis-Filho, J. S., F. Milanezi, I. Amendoeira, A. Albergaria, and F. C. Schmitt. 2003. Distribution of p63, a novel myoepithelial marker, in fine-needle aspiration biopsies of the breast: an analysis of 82 samples. *Cancer* 99: 172-179.

49. Sailer, V., C. Luders, W. Kuhn, V. Pelzer, and G. Kristiansen. 2015. Immunostaining of Np63 (using the p40 antibody) is equal to that of p63 and CK5/6 in high-grade ductal carcinoma in situ of the breast. *Virchows Arch* 467: 67-70.

50. Chakrabarti, R., Y. Wei, J. Hwang, X. Hang, M. Andres Blanco, A. Choudhury, B. Tiede, R. A. Romano, C. DeCoste, L. Mercatali, T. Ibrahim, D. Amadori, N. Kannan, C. J. Eaves, S. Sinha, and Y. Kang. 2014. DeltaNp63 promotes stem cell activity in mammary gland development and basal-like breast cancer by enhancing Fzd7 expression and Wnt signalling. *Nat Cell Biol* 16: 1004-1015, 1001-1013.

51. Orzol, P., M. Nekulova, J. Holcakova, P. Muller, B. Vojtesek, and P. J. Coates. 2016. Erratum to: DeltaNp63 regulates cell proliferation, differentiation, adhesion, and migration in the BL2 subtype of basal-like breast cancer. *Tumour Biol*.

52. Orzol, P., M. Nekulova, J. Holcakova, P. Muller, B. Votesek, and P. J. Coates. 2016. DeltaNp63 regulates cell proliferation, differentiation, adhesion, and migration in the BL2 subtype of basal-like breast cancer. *Tumour Biol*.

53. Buckley, N. E., S. J. Conlon, K. Jirstrom, E. W. Kay, N. T. Crawford, A. O'Grady, K. Sheehan, S. S. Mc Dade, C. W. Wang, D. J. McCance, P. G. Johnston, R. D.

Kennedy, D. P. Harkin, and P. B. Mullan. 2011. The DeltaNp63 proteins are key allies of BRCA1 in the prevention of basal-like breast cancer. *Cancer Res* 71: 1933-1944.

54. Leong, C. O., N. Vidnovic, M. P. DeYoung, D. Sgroi, and L. W. Ellisen. 2007. The p63/p73 network mediates chemosensitivity to cisplatin in a biologically defined subset of primary breast cancers. *J Clin Invest* 117: 1370-1380.

55. Forster, N., S. V. Saladi, M. van Bragt, M. E. Sfondouris, F. E. Jones, Z. Li, and L. W. Ellisen. 2014. Basal cell signaling by p63 controls luminal progenitor function and lactation via NRG1. *Dev Cell* 28: 147-160.

56. Yao, C. C., B. L. Ziober, R. M. Squillace, and R. H. Kramer. 1996. Alpha7 integrin mediates cell adhesion and migration on specific laminin isoforms. *J Biol Chem* 271: 25598-25603.

57. Lebok, P., V. Kopperschmidt, M. Kluth, C. Hube-Magg, C. Ozden, T. B, K. Hussein, A. Mittenzwei, A. Lebeau, I. Witzel, L. Wolber, S. Mahner, F. Janicke, S. Geist, P. Paluchowski, C. Wilke, U. Heilenkotter, R. Simon, G. Sauter, L. Terracciano, R. Krech, A. von d Assen, V. Muller, and E. Burandt. 2015. Partial PTEN deletion is linked to poor prognosis in breast cancer. *BMC Cancer* 15: 963.

58. Dang, T. T., M. A. Esparza, E. A. Maine, J. M. Westcott, and G. W. Pearson. 2015. DeltaNp63alpha Promotes Breast Cancer Cell Motility through the Selective Activation of Components of the Epithelial-to-Mesenchymal Transition Program. *Cancer Res* 75: 3925-3935.

59. Meyer, A. E., C. E. Gatza, T. How, M. Starr, A. B. Nixon, and G. C. Blobe. 2014. Role of TGF-beta receptor III localization in polarity and breast cancer progression. *Mol Biol Cell* 25: 2291-2304.

60. Ghoussaini, M., O. Fletcher, K. Michailidou, C. Turnbull, M. K. Schmidt, E. Dicks, J. Dennis, Q. Wang, M. K. Humphreys, C. Luccarini, C. Baynes, D. Conroy, M.

Maranian, S. Ahmed, K. Driver, N. Johnson, N. Orr, I. dos Santos Silva, Q. Waisfisz, H. Meijers-Heijboer, A. G. Uitterlinden, F. Rivadeneira, B. Netherlands Collaborative Group on Hereditary, C. Ovarian, P. Hall, K. Czene, A. Irwanto, J. Liu, H. Nevanlinna, K. Aittomaki, C. Blomqvist, A. Meindl, R. K. Schmutzler, B. Muller-Myhsok, P. Lichtner, J. Chang-Claude, R. Hein, S. Nickels, D. Flesch-Janys, H. Tsimiklis, E. Makalic, D. Schmidt, M. Bui, J. L. Hopper, C. Apicella, D. J. Park, M. Southey, D. J. Hunter, S. J. Chanock, A. Broeks, S. Verhoef, F. B. Hogervorst, P. A. Fasching, M. P. Lux, M. W. Beckmann, A. B. Ekici, E. Sawyer, I. Tomlinson, M. Kerin, F. Marme, A. Schneeweiss, C. Sohn, B. Burwinkel, P. Guenel, T. Truong, E. Cordina-Duverger, F. Menegaux, S. E. Bojesen, B. G. Nordestgaard, S. F. Nielsen, H. Flyger, R. L. Milne, M. R. Alonso, A. Gonzalez-Neira, J. Benitez, H. Anton-Culver, A. Ziogas, L. Bernstein, C. C. Dur, H. Brenner, H. Muller, V. Arndt, C. Stegmaier, S. Familial Breast Cancer, C. Justenhoven, H. Brauch, T. Bruning, N. Gene Environment Interaction of Breast Cancer in Germany, S. Wang-Gohrke, U. Eilber, T. Dork, P. Schurmann, M. Bremer, P. Hillemanns, N. V. Bogdanova, N. N. Antonenkova, Y. I. Rogov, J. H. Karstens, M. Bermisheva, D. Prokofieva, E. Khusnutdinova, A. Lindblom, S. Margolin, A. Mannermaa, V. Kataja, V. M. Kosma, J. M. Hartikainen, D. Lambrechts, B. T. Yesilyurt, G. Floris, K. Leunen, S. Manoukian, B. Bonanni, S. Fortuzzi, P. Peterlongo, F. J. Couch, X. Wang, K. Stevens, A. Lee, G. G. Giles, L. Baglietto, G. Severi, C. McLean, G. G. Alnaes, V. Kristensen, A. L. Borrensen-Dale, E. M. John, A. Miron, R. Winqvist, K. Pylkas, A. Jukkola-Vuorinen, S. Kauppila, I. L. Andrulis, G. Glendon, A. M. Mulligan, P. Devilee, C. J. van Asperen, R. A. Tollenaar, C. Seynaeve, J. D. Figueroa, M. Garcia-Closas, L. Brinton, J. Lissowska, M. J. Hooning, A. Hollestelle, R. A. Oldenburg, A. M. van den Ouweland, A. Cox, M. W. Reed, M. Shah, A. Jakubowska, J. Lubinski, K. Jaworska, K. Durda, M. Jones, M. Schoemaker, A. Ashworth, A. Swerdlow, J. Beesley, X.

Chen, I. kConFab, G. Australian Ovarian Cancer Study, K. R. Muir, A. Lophatananon, S. Rattanamongkongul, A. Chaiwerawattana, D. Kang, K. Y. Yoo, D. Y. Noh, C. Y. Shen, J. C. Yu, P. E. Wu, C. N. Hsiung, A. Perkins, R. Swann, L. Velentzis, D. M. Eccles, W. J. Tapper, S. M. Gerty, N. J. Graham, B. A. Ponder, G. Chenevix-Trench, P. D. Pharoah, M. Lathrop, A. M. Dunning, N. Rahman, J. Peto, and D. F. Easton. 2012. Genome-wide association analysis identifies three new breast cancer susceptibility loci. *Nat Genet* 44: 312-318.

61. Aziz, M. H., X. Chen, Q. Zhang, C. DeFrain, J. Osland, Y. Luo, X. Shi, and R. Yuan. 2015. Suppressing NRIP1 inhibits growth of breast cancer cells in vitro and in vivo. *Oncotarget* 6: 39714-39724.

62. Tafuri, L. S., G. F. Rocha, and H. Gobbi. 2006. Cell cycle related proteins in hyperplasia of usual type in breast specimens of patients with and without breast cancer. *BMC Cell Biol* 7: 29.

63. Shi, Y. H., L. Bingle, L. H. Gong, Y. X. Wang, K. P. Corke, and W. G. Fang. 2007. Basic FGF augments hypoxia induced HIF-1-alpha expression and VEGF release in T47D breast cancer cells. *Pathology* 39: 396-400.

64. Tripathi, G., D. A. Salih, A. C. Drozd, R. A. Cosgrove, L. J. Cobb, and J. M. Pell. 2009. IGF-independent effects of insulin-like growth factor binding protein-5 (Igfbp5) in vivo. *FASEB J* 23: 2616-2626.

65. Ben-Porath, I., M. W. Thomson, V. J. Carey, R. Ge, G. W. Bell, A. Regev, and R. A. Weinberg. 2008. An embryonic stem cell-like gene expression signature in poorly differentiated aggressive human tumors. *Nat Genet* 40: 499-507.

66. Kim, J., N. J. Lim, S. G. Jang, H. K. Kim, and G. K. Lee. 2014. miR-592 and miR-552 can distinguish between primary lung adenocarcinoma and colorectal cancer metastases in the lung. *Anticancer Res* 34: 2297-2302.

67. Liu, M., Q. Zhi, W. Wang, Q. Zhang, T. Fang, and Q. Ma. 2015. Up-regulation of miR-592 correlates with tumor progression and poor prognosis in patients with colorectal cancer. *Biomed Pharmacother* 69: 214-220.

68. Sakurai, M., M. Masuda, Y. Miki, H. Hirakawa, T. Suzuki, and H. Sasano. 2015. Correlation of miRNA expression profiling in surgical pathology materials, with Ki-67, HER2, ER and PR in breast cancer patients. *Int J Biol Markers* 30: e190-199.

69. Huang, S., Y. Chen, W. Wu, N. Ouyang, J. Chen, H. Li, X. Liu, F. Su, L. Lin, and Y. Yao. 2013. miR-150 promotes human breast cancer growth and malignant behavior by targeting the pro-apoptotic purinergic P2X7 receptor. *PLoS One* 8: e80707.

70. Liu, D. Z., H. Y. Zhang, X. L. Long, S. L. Zou, X. Y. Zhang, G. Y. Han, and Z. G. Cui. 2015. MIR-150 promotes prostate cancer stem cell development via suppressing p27Kip1. *Eur Rev Med Pharmacol Sci* 19: 4344-4352.

71. Herrera-Merchan, A., C. Cerrato, G. Luengo, O. Dominguez, M. A. Piris, M. Serrano, and S. Gonzalez. 2010. miR-33-mediated downregulation of p53 controls hematopoietic stem cell self-renewal. *Cell Cycle* 9: 3277-3285.

72. Zhou, J., D. Xu, H. Xie, J. Tang, R. Liu, J. Li, S. Wang, X. Chen, J. Su, X. Zhou, K. Xia, Q. He, J. Chen, W. Xiong, P. Cao, and K. Cao. 2015. miR-33a functions as a tumor suppressor in melanoma by targeting HIF-1alpha. *Cancer Biol Ther* 16: 846-855.

73. Horie, T., T. Nishino, O. Baba, Y. Kuwabara, T. Nakao, M. Nishiga, S. Usami, M. Izuhara, N. Sowa, N. Yahagi, H. Shimano, S. Matsumura, K. Inoue, H. Marusawa, T. Nakamura, K. Hasegawa, N. Kume, M. Yokode, T. Kita, T. Kimura, and K. Ono. 2013. MicroRNA-33 regulates sterol regulatory element-binding protein 1 expression in mice. *Nat Commun* 4: 2883.

74. Garcia, A. I., M. Buisson, P. Bertrand, R. Rimokh, E. Rouleau, B. S. Lopez, R. Lidereau, I. Mikaelian, and S. Mazoyer. 2011. Down-regulation of BRCA1 expression

by miR-146a and miR-146b-5p in triple negative sporadic breast cancers. *EMBO Mol Med* 3: 279-290.

75. Hurst, D. R., M. D. Edmonds, G. K. Scott, C. C. Benz, K. S. Vaidya, and D. R. Welch. 2009. Breast cancer metastasis suppressor 1 up-regulates miR-146, which suppresses breast cancer metastasis. *Cancer Res* 69: 1279-1283.

76. Ma, L., J. Teruya-Feldstein, and R. A. Weinberg. 2007. Tumour invasion and metastasis initiated by microRNA-10b in breast cancer. *Nature* 449: 682-688.

77. Lee, C. G., S. McCarthy, M. Gruidl, C. Timme, and T. J. Yeatman. 2014. MicroRNA-147 induces a mesenchymal-to-epithelial transition (MET) and reverses EGFR inhibitor resistance. *PLoS One* 9: e84597.

78. Yang, Z., M. He, K. Wang, G. Sun, L. Tang, and Z. Xu. 2014. Tumor suppressive microRNA-193b promotes breast cancer progression via targeting DNAJC13 and RAB22A. *Int J Clin Exp Pathol* 7: 7563-7570.

79. Brodie, S. G., and C. X. Deng. 2001. BRCA1-associated tumorigenesis: what have we learned from knockout mice? *Trends Genet* 17: S18-22.

80. Brodie, S. G., X. Xu, W. Qiao, W. M. Li, L. Cao, and C. X. Deng. 2001. Multiple genetic changes are associated with mammary tumorigenesis in Brca1 conditional knockout mice. *Oncogene* 20: 7514-7523.

81. Diaz-Cruz, E. S., M. C. Cabrera, R. Nakles, B. H. Rutstein, and P. A. Furth. 2010. BRCA1 deficient mouse models to study pathogenesis and therapy of triple negative breast cancer. *Breast Dis* 32: 85-97.

Vita

Ramón Edgardo Flores González was born on February 25, 1983 in San Juan, Puerto Rico. His parents María Noelia González Muñiz and Ramón Edgardo Flores Ríos always fostered a spirit of discovery in him so he became interested in science at an early age. Ramón attended the Colegio San José High School in Rio Piedras, Puerto Rico. He has a Bachelor's in Science in Chemical Engineering from the Massachusetts Institute of Technology in Cambridge, Massachusetts, a Master's in Engineering in Biomedical Engineering from Cornell University in Ithaca, New York, and a Medical Doctorate from the University of Puerto Rico Medical School, in San Juan, Puerto Rico. He pursued a Doctorate of Philosophy from the University of Texas and MD Anderson Cancer Center Graduate School of Biomedical Sciences under the guidance of Elsa R. Flores, Ph.D. After completing his doctorate, Ramón will be starting a Neurology Residency at the Jackson Memorial Hospital in Miami, Florida. His ultimate goal is to combine his engineering, scientific, and medical backgrounds to develop new treatments for chronic diseases and improve the quality of life of many patients.